

https://dspace.org/

Peptidoglycan amidation enzymes in Mycobacterium tuberculosis are new drug targets for Tuberculosis treatment and development of a novel TB vaccine

Shaku, Moagi Tube

2024

https://hdl.handle.net/10539/37589

Downloaded from a DSpace repository. https://dspace.org/

Peptidoglycan amidation enzymes in *Mycobacterium tuberculosis* are new drug targets for Tuberculosis treatment and development of a novel TB vaccine



Moagi Tube Shaku

A thesis submitted to the Faculty of Health Sciences, University of the Witwatersrand, Johannesburg, in fulfilment of the requirements for the degree of Doctor of Philosophy.

Johannesburg, 2023

Declaration

I, Moagi Tube Shaku, declare that this thesis is my own work. It is being submitted for the degree of Doctor of Philosophy at the University of the Witwatersrand, Johannesburg. It has not been submitted before for any other degree or examination at any other university.

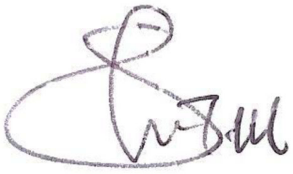

……

Moagi Tube Shaku

Signed on 15th day of June in 2023

Presentations from this study

5TH South Africa Tuberculosis conference (2018). Poster presentation: Peptidoglycan amidation enzymes are novel drug targets.

Pathred 2019 congress: Oral presentation: Breaching the barrier: targeting cell wall enzymes in *Mycobacterium tuberculosis* for development of novel TB drugs. Award received: Honorable mention.

SAMRC-Early Career Scientist Convention 2019: Oral presentation: Breaching the barrier: targeting cell wall enzymes in *Mycobacterium tuberculosis* for development of novel TB drugs.

SAMRC-Early Career Scientist Convention 2020: Oral presentation: Breaching the barrier: targeting cell wall enzymes in *Mycobacterium tuberculosis* for development of novel TB drugs.

Publications during this study

Editorial: Shaku, M.T. and Kana, B.D., 2018**.** Tuberculosis: Breaking down walls. Elife, 7, p.e42033.

Book chapter: Shaku, M., Ealand, C., Matlhabe, O., Lala, R. and Kana, B.D., 2020. Peptidoglycan biosynthesis and remodeling revisited. Advances in Applied Microbiology, 112, pp.67-103.

Review: Shaku, M., Ealand, C. and Kana, B.D., 2020**.** Cell surface biosynthesis and remodeling pathways in mycobacteria reveal new drug targets**.** Frontiers in Cellular and Infection Microbiology, 10, p.603382.

Research articles

Manuscript in preparation: Shaku, M.T., Pires, M., VanNieuwenhze, M., Dhar, N., and Kana, B.D., 2023. Amidation of glutamate in mycobacterial peptidoglycan is essential for cross-linking

Manuscript in preparation: Shaku, M.T., Um, P., Pires, M., Bishai, W.R., and Kana, B.D., 2023. A Novel CRISPRi based BCG vaccine targeting the NOD-1 pathway induces protection against *Mycobacterium tuberculosis* infection in mice.

Acknowledgments

I am very grateful to everyone who has trained and supported me throughout this work. First, I would like to thank my supervisor Professor Bavesh Kana, whose endless academic and personal support has kept me going. I have been privileged to train in his lab and for the support from all former and current members of our lab, especially my PhD peers. I would also like to thank Dr Neeraj Dhar and the McKinney lab at the École polytechnique fédérale de Lausanne (EPFL) in Switzerland for hosting me in 2018 to perform experiments for the initial part of this work.

I would also like to thank Professor William Bishai and the Bishai lab members for hosting me at the Centre of Tuberculosis at Johns Hopkins University (JHU) School of Medicine in 2021 to perform experiments for the second part of this work. I particularly thank Peter Um of the Bishai lab for assisting with my experiments and training during my visit at JHU.

I am grateful for the financial support I received from the Wits University post-graduate research office, South African Medical Research Council (SAMRC) and the Fulbright program (USA). During this work I aslo had an opportunity to join the Global Stop TB partnership Working Group on New TB vaccines (WGNV) as a communications intern. This allowed me to perform TB vaccine advocacy work, and for this I would like to thank Jennifer Woolley of the WGNV for granting me with the opportunity.

Finally, I would like to thank my family, my late Father who always motivated me to give my best for this work. To my Mother, I will forever be thankful for all the love and support you always provide and to my siblings; I hope I've made you proud. Lastly, I would like to thank my partner and daughter (Bokang) for always being there for me and for all the support. Thank you.

List of figures

Figure #	Figure name	Page #
Figure 1.1.	Global estimated TB incidence rates, 2021.	20
Figure 1.2.	History of TB drug discovery and development of treatment regimens.	22
Figure 1.3.	Periplasmic cell wall biosynthesis pathways of the mycobacterial cell wall.	25
Figure 1.4.	Cytoplasmic cell wall biosynthesis pathways of the mycobacterial cell wall.	26
Figure 2.1.	Allelic replacement by homologous recombination.	53
Figure 3.1.	Peptidoglycan biosynthesis in mycobacteria and peptidoglycan monomer (lipid II) amidation by the MurT-GatD complex.	56
Figure 3.2.	Schematic of the CRISPRi mechanism in bacteria.	59
Figure 3.3.	Schematic of the M-PFC assay.	60
Figure 3.4.	Superimposition of Mtb MurT and *E. coli* Mpl.	64
Figure 3.5.	Chemical structures of TetraFL-1 and TetraFL-2 PG stem peptide mimics.	65
Figure 3.6.	Amidated peptidoglycan stem peptide mimics are incorporated into the mycobacterial cell wall.	66
Figure 3.7.	Labeling of Mtb with TetraFL-1, TetraFL-2 and PentaFL overtime to assess the rate of probe incorporation.	68
Figure 3.8.	Restriction profile of plasmid pMV306H+MurT-GFP.	69
Figure 3.9.	Restriction profile of plasmid pTweety+mRFP-GatD.	69
Figure 3.10.	MurT-GFP and mRFP-GatD localize at cell poles.	70
Figure 3.11.	pUAB400+MurT restriction profile.	71
Figure 3.12.	pUAB300+GatD restriction profile.	72
Figure 3.13.	M-PFC assay for MurT-GatD interactions.	72
Figure 3.14.	Mycobacterial cell growth involves sidewall of maturing PG.	73
Figure 3.15.	MurT-GFP co-localizes with mature PG.	74

Figure 3.16.	Knockout of *murT* from a *M. smegmatis* strain with a second episomal copy of *murT*.	75
Figure 3.17.	Restriction profile of plasmid PLR962+MSMEG_6276sgRNA.	76
Figure 3.18.	Labeling of mc^2155::CRISPRi-MurT-GatD (without CRISPRi activation) with FDAAs.	76
Figure 3.19.	Depletion of MurT and GatD reduces cell growth.	77
Figure 3.20.	Schematic for incorporation of Alk-DADA or monopeptide probes (TADA/HADA) during PG biosynthesis in mycobacteria.	78
Figure 3.21.	MurT-GatD depletion causes perturbed PG remodeling.	79
Figure 3.22.	AFM cell wall stiffness images of mc^2155::CRISPRi-MurT-GatD.	80
Figure 3.23.	MurT-GatD depletion causes increased cell wall permeability.	81
Figure 3.24.	MurT-GatD depletion causes increased sensitivity to lysozyme.	81
Figure 3.25.	Depletion of MurT and GatD causes reduced PG amidation.	82
Figure 3.26.	Secondary structure of PknB.	83
Figure 3.27.	Restriction profile of plasmid pFLAGEM+PknB.	84
Figure 3.28.	Growth of the mc^2155::CRISPRi-MurT-GatD+PknB-FLAG strain in increasing ATc concentration.	84
Figure 3.29.	Reduced MurT-GatD activity affects PknB activity.	85
Figure 3.30.	Secondary structure of mRFP-PknB.	85
Figure 3.31.	Restriction of plasmid pMV306H+mRFP-pknB.	86
Figure 3.32.	MurT-GatD depletion causes mis-localization of mRFP-PknB.	86
Figure 3.33.	Time-lapse microscopic analysis of amoxicilin (AMX) and clavulanate (CLV) treated MurT-GatD depletion strain cells with/without CRISPRi activation.	88
Figure 3.34.	Essentiality of GatD/CobQ2 in PG biosynthesis or Vitamin B_{12} biosynthesis.	89
Figure 3.35.	Growth curve of mc^2155::CRISPRi-MurT-GatD in vitamin B_{12}.	90
Figure 3.36.	Proposed model for the role of MurT and GatD during PG biosynthesis and cell growth in mycobacteria.	93

Figure 4.1.	Genetic organization of the ESX-1 secretion system.	103
Figure 4.2.	Time-line showing the key events of recombinant BCG vaccine development since the development of the BCG vaccine in 1921.	107
Figure 4.3.	Immune responses induced by BCG vaccination at the site of injection, lymph nodes and peripheral blood.	109
Figure 4.4.	Targets of the host immune system for new TB vaccine candidates.	110
Figure 4.5.	Restriction profile of plasmid PLR965+Mb3739 sgRNA.	119
Figure 4.6.	Phenotypic characterization of rBCG::iE-DAP.	120
Figure 4.7.	Transmission electron microscopy and phenotypic characterization of rBCG::iE-DAP.	121
Figure 4.8.	rBCG::iE-DAP enhances the Mtb H37Rv killing ability of macrophages derived from trained U937 monocytes.	123
Figure 4.9.	Survival of rBCG-CRISPRi-MurT-GatD in IFNγ activated BMDMs and analysis of pro-inflammatory cytokine release.	124
Figure 4.10.	rBCG::iE-DAP activation *in vitro* and in mice-aerosol infections with doxycycline.	126
Figure 4.11.	Efficacy of 1 mg/kg/day dose of doxycycline for CRISPRi activation.	127
Figure 4.12.	Analysis of rBCG::iE-DAP strain attenuation.	128
Figure 4.13.	Efficacy of rBCG::iE-DAP in comparison to standard WT BCG for protection against Mtb H37Rv infection in mice.	130
Figure 4.14.	Histopathological analysis of lung samples.	132
Figure 5.1.	The MurT-GatD complex is a new drug target and a target for development of a new TB vaccine.	146

List of tables

Table 1.1.	A list of drug targets in the mycobacterial cell wall biosynthesis pathways with compounds showing inhibitory activity of Mtb growth. Compounds without proven *in-vitro* data were excluded.	26, 27
Table 2.1.	Parameters used for designing primers through Primer3.	43
Table 4.1.	A list of recombinant BCG vaccines.	104
Table A1.	List of plasmids created and/or used in this study.	140
Table A2.	List of strains generated with CRISPRi, target genes, PAM sequences and sgRNA targeting sequences.	141
Table A3.	List of bacterial strains created and/or used in this study.	141, 142

Abbreviations

AIDS:	Acquired immunodeficiency syndrome
AMK:	Amikacin
AMs:	Alveolar macrophages
ART:	Anti-retroviral therapy
ATc:	Anhydrotetracycline
BMDMs:	Bone marrow derived macrophages
BAL:	Broncho-alveolar lavage
BCG:	Bacillus Calmette–Guérin
BDQ:	Bedaquiline
BPaL:	Bedaquiline, pretonamid and linezolid
BTZs:	Benzothiazinones
CAP:	Capreomycin
CRISPRi:	Clustered regularly interspaced short palindromic repeats interference
CFU:	Colony forming units
CTAB:	Cetyltrimethylammonium bromide
DMSO:	Dimethyl sulfoxide
dNTPs:	Deoxynucleoside triphosphates
DOTS:	Directly observed treatment short course
Dox:	Doxycycline
DPA:	Decaprenylphosphoryl-D-arabinose
DR-TB:	Drug-resistant TB
DS-TB:	Drug-susceptible TB
EDTA:	Ethylenediaminetetraacetic acid
EMB:	Ethambutol
EPM:	Ertapenem
ETM:	Ethionamide
FAS:	Fatty acid synthase
FBS:	Fetal bovine serum

FDAAs:	Fluorescent D-alanine amino acids
GatD:	Glutamine amidotransferase-like protein D
Glc*N*Ac:	*N*-acetylglucosamine
HCl:	Hydrochloric acid
HIV:	Human immunodeficiency virus
Hyg:	Hygromycin
HSCs:	Hematopoietic stem cells
INH:	Isoniazid
IV:	Intravenous
KAN:	Kanamycin
LA:	Luria-Bertani agar
LAM:	Lipoarabinomannans
LB:	Luria-Bertani broth
LDTs:	L,D-transpeptidases
LM:	Lipomannans
LPS:	Lipopolysaccharide
LZD:	Linezolid
Mtb:	*Mycobacterium tuberculosis*
MDR-TB:	Multi-drug resistant TB
MDP:	Murein dipeptide
meso-DAP:	*meso*-diaminopimelate
MIC:	Minimum inhibitory concentration
MOX:	Moxifloxacin
MurT:	Murein amidotransferase
NADA:	3-[(7-Nitro-2,1,3-benzoxadiazol-4-yl)amino]-D-alanine hydrochloride
PAM:	Protospacer adjacent motif
PAS:	Para-aminosalicylic acid
PBS:	Phosphate buffered saline
PBPs:	Penicillin-binding proteins
PDIM:	Phthiocerol dimycocerosate

PG:	Peptidoglycan
PIM:	Phosphatidylinositol monomannoside
PknB:	Protein kinase B
PPM:	Polyprenyl-phosphate-based mannose
PRRs:	Pathogen recognition receptors
PTM:	Pretonamid
PZA:	Pyrazinamide
PPD:	Purified protein derivative
rBCG:	Recombinant Bacillus Calmette–Guérin
RIF:	Rifampicin
RFP:	Rifapentine
Rpfs:	Resuscitation promoting factors
SDS:	Sodium dodecyl sulfate
SEDS:	Shape, elongation, division and sporulation proteins
SM:	Streptomycin
sgRNA:	Short-guide ribonucleic acid
STPKs:	Serine/threonine protein kinases
TAMRA:	Tetramethylrhodamine
TADA:	Tetramethylrhodamine-D-alanine
TB:	Tuberculosis
TLM:	Thiolactomycin
TMMs:	Trehalose monomycolates
TDMs:	Trehalose dimycolates
$VitB_{12}$:	Vitamin B_{12}
WHO:	World health organization
XDR-TB:	Extensively-drug resistant TB

Abstract

Mycobacteria assemble a complex cell wall with cross-linked peptidoglycan (PG) playing an essential role for maintenance of cell wall integrity and tolerance of osmotic pressure. In previous work, it was demonstrated that various hydrolytic enzymes are required to remodel PG during essential processes such as cell elongation and septal hydrolysis. In this thesis work, we explore the chemistry associated with PG cross-linking, specifically the requirement for amidation of the D-glutamate residue found in PG precursors. In *Mycobacterium smegmatis*, an experimental surrogate for *Mycobacterium tuberculosis* (Mtb), we confirm the essentiality of D-glutamate amidation in PG cross-linking by labeling cells with synthetic fluorescent PG probes that require amidated side chains for stable incorporation. We also use CRISPRi targeted knockdown of genes encoding the MurT-GatD complex, previously implicated in D-glutamate amidation in other bacterial species, and demonstrate that these genes are essential for mycobacterial growth. We show that MurT-GFP co-localizes with mRFP-GatD at the cell poles and septum, which are the sites of cell wall synthesis in mycobacteria and that these enzymes interact to form the PG amidation complex. Furthermore, time-lapse microscopic analysis of MurT-GFP localization in fluorescent D-amino acid (FDAA) - labeled mycobacterial cells during growth demonstrated co-localization with maturing PG, suggestive of a role for PG amidation during cell wall remodeling and repair. Depletion of MurT and GatD caused reduced PG cross-linking and increased sensitivity to lysozyme and β-lactam antibiotics. Cell growth cessation was found to be the result of a shutdown of PG biosynthesis mediated by the serine/threonine protein kinase B (PknB) which senses uncross-linked PG. Collectively, the first component of this work in *M. smegmatis* demonstrates the importance of D-glutamate amidation in mycobacterial PG precursors. We further exploit this enzyme complex in the second part of the dissertation to develop a novel CRISPRi-based recombinant BCG (rBCG) vaccine named rBCG::iE-DAP. This rBCG vaccine is based on the depletion of MurT-GatD, which results in reduced PG side chain amidation. As amidation masks detection of PG by the NOD1 pathogen recognition receptor, we postulate that this novel recombinant BCG will facilitate enhanced immunity against TB disease. As expected, the recombinant BCG induced increased immune activation and protection against Mtb infection in a mouse model of TB infection. This work

highlights the MurT-GatD complex as a novel drug target and as a target for development of a next generation TB vaccine targeting innate immune responses against Mtb infection.

Contents

Declaration ii

Presentations from this study 3

Publications during this study 4

Acknowledgments 5

List of figures 6

List of tables 9

Abbreviations 10

Abstract 13

CHAPTER 1 19

(Tuberculosis literature review and cell wall associated drug targets) 19

1.1. Introduction 20

CHAPTER 2 39

(General methods) 39

2.1. General methods 40

CHAPTER 3: 54

(Amidation of glutamate in mycobacterial peptidoglycan is essential for cell wall cross-linking) 54

3.1. Introduction 55

3.2. Hypothesis 58

3.3. Aims 58

3.4. Objectives 58

3.5. Methods 59

3.5. Results 64

3.5.1. Identification of the mycobacterial MurT-GatD homologs 64

3.5.2. MurT-GFP and mRFP-GatD localize at sites of PG biosynthesis 68

3.5.3. MurT interacts with GatD to form the MurT-GatD amidotransferase complex. 71

3.5.4. MurT-GFP co-localizes with maturing peptidoglycan during cell growth 73

3.5.5. MurT and GatD are required for PG amidation and cell growth in mycobacteria 74

3.5.6. PG cross-linking in mycobacteria requires amidation of D-glutamate in lipid II 77

3.5.7. PknB regulates cell growth in response to PG amidation 82

3.5.8. PknB localization is perturbed in MurT-GatD depleted cells 85

3.5.9. MurT-GatD depletion causes sensitivity to β-lactam antibiotics 87

3.5.10. Essentiality of GatD is associated with a role in vitamin B_{12} biosynthesis 87

3.6. Discussion 91

3.7. Appendices 96

CHAPTER 4 102

(A Novel CRISPRi based BCG vaccine targeting the NOD-1 pathway induces protection against *Mycobacterium tuberculosis* infection in mice) 102

4.1. Introduction 103

4.2. BCG induced correlates of protection against TB infection beyond T helper-1 responses 108

4.3. Role of CD8+T cells in BCG induced immunity 108

4.4. Role of Th17 responses in BCG induced immunity 110

4.5. Role of Natural Killer cells in BCG induced immunity 111

4.6. Role of humoral anti-TB immunity in BCG induced immunity 112

4.7. Role of BCG induced trained innate immunity against Mtb infection 113

4.8. Hypothesis 115

4.9. Aim 115

4.10. Objectives 115

4.11. Materials and Methods 116

4.11.1.1. Growth conditions for *E. coli* DH5α and derivative strains 116

4.11.1.2. Growth conditions for Mycobacterial and derivative strains 116

4.12. Results 120

4.12.1. Generation of rBCG::iE-DAP 120

4.12.2. rBCG::iE-DAP *in vitro* trained macrophages control Mtb H37Rv growth 123

4.12.3. rBCG::iE-DAP is responsive to anhydrotetracycline activation and causes increased TNFα expression in BMDMs 125

4.12.4. rBCG::iE-DAP activation *in vitro* and in mice-aerosol infections with doxycyline 126

4.12.5. Analysis of rBCG::iE-DAP attenuation in SCID mice 129

4.12.6. rBCG::iE-DAP induces better protection against *Mycobacterium tuberculosis* infection in mice compared to WT BCG 130

4.12.7. Histopathological analysis of lung pathology after vaccination with rBCG::iE-DAP+Dox compared to WT BCG post Mtb Infection 132

4.13. Discussion 134

4.14. Appendices 138

CHAPTER 5 146

(Summary: Conclusion, limitations and future studies) 146

5.1. Conclusion 147

5.2. Limitations 148

5.3. Future studies 148

References 149

CHAPTER 1

(Tuberculosis literature review and cell wall associated drug targets)

1.1. Introduction

1.1.1. Etiology of TB

Mycobacterium tuberculosis (Mtb) is the causative agent of Tuberculosis (TB), a communicable disease that remains the leading cause of death from an infectious disease worldwide accounting for nearly 1.5 million deaths annually (1). Despite the availability of a TB vaccine (the Bacille Calmette Guérin [BCG] vaccine) and antibiotics, Mtb has infected approximately a quarter of the global population and continues to cause nearly 10.4 million new infections annually with the highest incidence of the disease found in sub-Saharan Africa (Fig. 1.1) (1). The emergence and global spread of drug-resistant TB (DR-TB), currently amounting to ~500 000 cases per annum, and co-infection with the human immunodeficiency virus (HIV) further complicates the global control of the disease (1, 2). Moreover, the COVID-19 pandemic has affected TB control programs worldwide, causing the first increase in TB related mortality in over a decade (3).

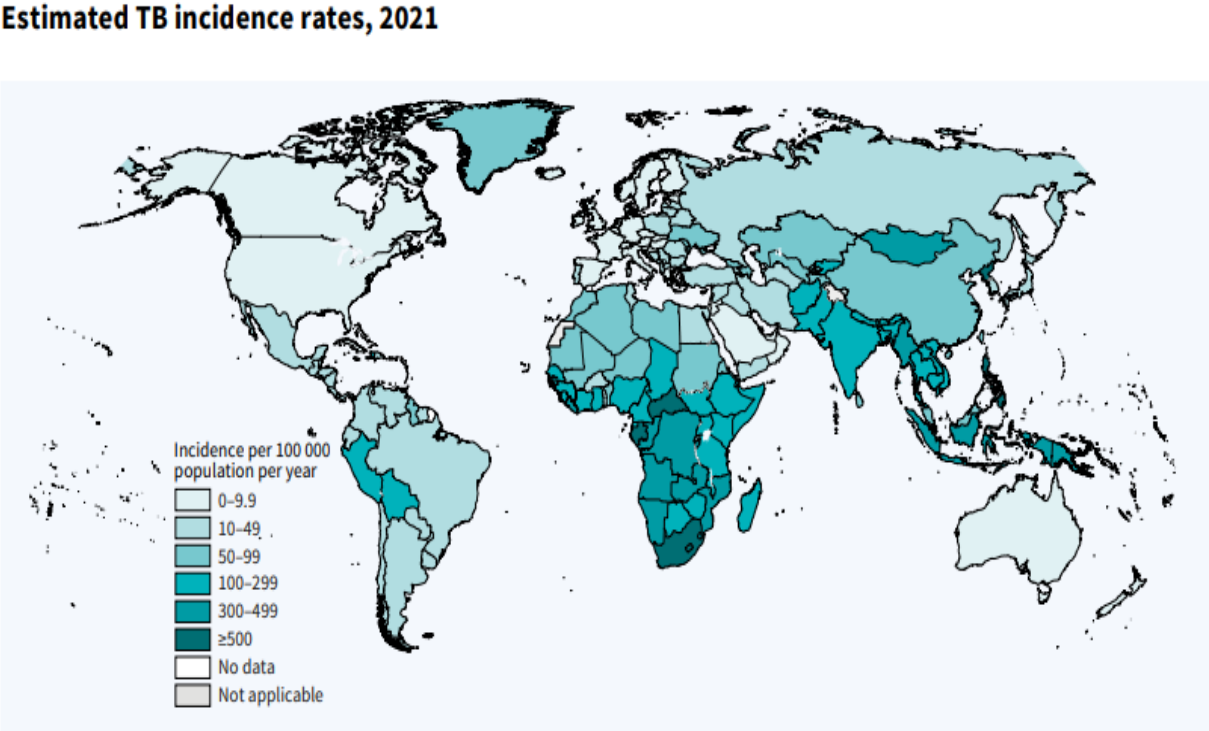

Figure 1.1. **Global estimated TB incidence rates, 2021**. Sub-Saharan Africa has the most severe TB incidence relative to population (1).

TB infection is acquired through inhalation of transmitted aerosols containing Mtb from an infected individual and it primarily affects the lungs although the infection can spread to other organs causing extrapulmonary TB (4). In the lungs alveolar macrophages (AMs) recognize and phagocytose Mtb in an attempt to eliminate the infection (4, 5). Paradoxically, macrophages serve as the preferred niche for Mtb replication (6). Mtb has evolved to evade and resist the human immune system mainly through counteracting the antimicrobial response of the alveolar macrophage (7, 8). Notably, Mtb possesses a variety of immunomodulatory mechanisms that facilitate persistence during immune assault. For example, Mtb massively manipulates macrophage responses by selectively activating macrophage pathogen recognition receptors (PRRs) which favor bacterial survival or by arresting phagosome maturation with cell wall lipids such as phosphatidylinositol mannosides, trehalose dimycolates, lipoarabinomannan (LAM) and sulfoglycolipids (7, 9). Mtb also expresses a variety of virulence proteins such as NdkA, SapM and PknG which inhibit lysosomal trafficking pathways or virulence proteins such as ESAT6-CFP10 which facilitate phagolysosomal escape (9). Furthermore, Mtb uses cell wall associated lipids to recruit more growth permissive macrophages to the site of infection and subsequent processes involve killing of AMs, infection of recruited cells and propagation of infection resulting in the aggregation of the immune cells at the site of infection, causing the formation of a granuloma – the pathological hallmark of TB infection (10, 11).

As the disease progresses, adaptive immunity is induced resulting in development of a mature granuloma characterized by the presence of T and B cells at the periphery of the granuloma forming a lymphocytic cuff enclosing the macrophage rich center (11). Combat within the granuloma between Mtb and immune cells results in characteristic regions of necrotic material accumulating as a result of the death of infected host cells (10). The necrotic lesions lead to the formation of what is known as the caseum – characterized by extensive cellular degradation. In some cases the caseum undergoes liquefaction and cavitation occurs when a liquefying granuloma fuses with an adjacent airway facilitating spread of Mtb released from dying cells through the respiratory system to another susceptible host via expectorated Mtb-containing aerosols (10).

1.1.2. History of TB treatment

Chemotherapeutic treatment of TB is complex; requiring (I) long term use of multiple antibiotics with severe side effects, (II) involving regimens that are difficult to manage leading to compliance issues. At the core of this challenge is the remarkable ability of Mtb to tolerate antibiotic exposure and to develop drug resistance (12). The current regimen for treatment of drug-susceptible or resistant TB (DS-TB/DR-TB) is a result of decades of research and clinical trials to develop an effective combination therapy administered for over a period of up to 6 months for DS-TB or 24 months for DR-TB with standard therapy or 6 months with newly discovered regimens such as the BPaL regimen (Fig. 1.2) (12, 13).

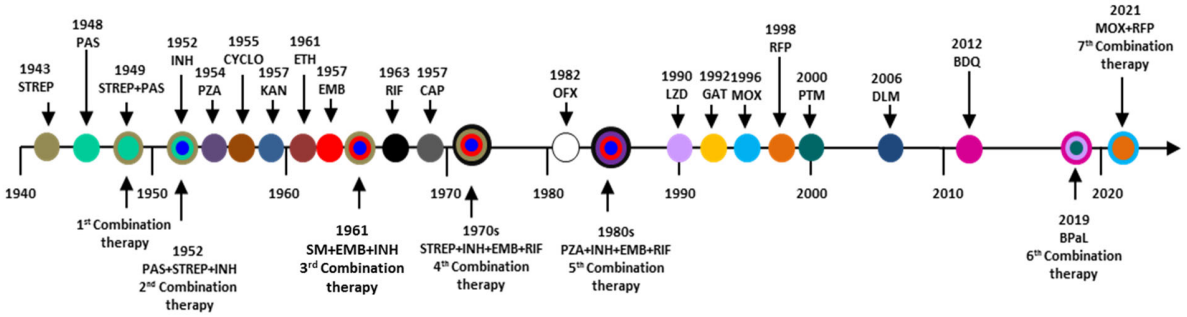

Figure 1.2. **History of TB drug discovery and development of treatment regimens**. Shown is the time-line for TB-drug development with key points when combinatorial therapy was introduced. The different drugs are represented by the colored circles (overlayed colored circles represent combination therapy). STREP: Streptomycin, PAS: para-aminosalicylic acid, INH: Isoniazid, PZA: Pyrazinamide, CYCLO: Cycloserine, KAN: Kanamycin, ETH: Ethionamide, EMB: Ethambutol, RIF: Rifampicin, CAP: Capreomyin, OFX: Ofloxacin, LZD: Lineozilid, GAT: Gatifloxacin, MOX: Moxifloxacin, RFP: Rifapentine, PTM: Pretonamid, DLM: Delamanid, BDQ: Bedaquiline. Drugs that are in early-phases of development or with no human proof-of-concept data are not shown. This figure was adapted from Ma et al. 2010 (14).

The discovery and use of streptomycin (SM) in 1943 as a TB antibiotic heralded the use of chemotherapy for TB treatment (Fig. 1.2). However, the development of resistance to SM was documented in ~70% of SM treated patients and in addition, SM induced nerve toxicity was also documented (15). These issues spurred the need for a renewed effort for the search for new antibiotics. SM was subsequently used together with para-aminosalicylic acid (PAS), which was discovered in 1948 and shown to reduce symptoms of renal TB, TB meningitis and TB enteritis (16). The SM/PAS combination showed improved efficacy than either drug alone, and resulted in the establishment of the first combination therapy for TB (Fig. 1.2) (14). In 1952, Isoniazid (INH) was shown to be safe and effective as a treatment for TB, however, INH resistance was

rapidly documented in 70% of cases after 3 months of therapy (17). INH was introduced to the SM/PAS regimen in an attempt to improve treatment and to curb further development of drug resistance (Fig. 1.2). The SM/PAS/INH therapy resulted in cure rates of up to 90-95%, however, this combination treatment required up to 24 months of continued therapy to achieve this durable cure (17). In 1961, Ethambutol (EMB) was discovered during a random screen of compounds able to kill Mtb *in vitro* (18). PAS was replaced with EMB (Fig. 1.2), as EMB was better tolerated than PAS and the SM/EMB/INH therapy was shown to reduce the duration of therapy from 24 to 18 months (17). During the early 1960s, rifampicin (RIF, a modified form of rifamycin [discovered in 1957]) was shown to be safe and effective when added to the triple therapy (SM/EMB/INH) reducing the treatment duration down to 8-9 months (17). Finally, addition of pyrazinamide (PZA, discovered in 1952) to EMB/INH/RIF to replace SM (Fig. 1.2), owing to the ability of PZA to accelerate the required time to achieve culture negativity to 6 months, resulted in development of the current regimen for DS-TB (14, 17). This regimen involves treatment with all 4 drugs for 2 months (i.e. the intensive phase of treatment) followed by treatment with RIF and INH for 4 months (i.e. the continuation phase of treatment). To combat the issue of non-compliance to treatment, in 1995 the World Health Organization (WHO) endorsed the Directly Observed Treatment, Short course (DOTS) which has improved the cure rate for DS-TB (19).

Recently, a 4-month daily DS-TB treatment regimen with an optimized rifapentine (RFP) dose and moxifloxacin (MOX) was shown to be as safe and effective as the 6-months standard (Fig. 1.2) (20). Despite this success of combinatorial therapy, DR-TB continues to increase and requires extensive treatment periods, using drugs associated with severe side effects (1). Treatment of multi-drug resistant TB (MDR-TB, defined as resistance to at least INH and RIF) is complicated with patients receiving up to 7 drugs including a second-line injectable drug (amikacin [AMK], capreomycin [CAP] or kanamycin [KAN]) while extensively-drug resistant TB (XDR-TB, defined as MDR-TB additionally resistant to any fluoroquinolone drug and at least one injectable drug) has few treatment options (21, 22). However, recent clinical trials with novel treatment shortening regimens to treat DR-TB have yielded positive results in the past few years (23). For example, the BPaL all-oral regimen involving the use of new drugs (bedaquiline

[BDQ] and pretonamid [PTM[, with linezolid [LZD]), yielded favorable treatment outcomes in 90% of XDR-TB patients or complicated-MDR-TB patients after 6 months of treatment while previously the standard treatment regimen for XDR-TB only yielded ~50% cure rates at 24 months of treatments of treatment (13, 24).

As coinfection with HIV is the leading contributing factor for the increased TB burden, particularly in sub-Saharan Africa (1), new treatment regimens that are developed need to consider HIV-TB co-infected individuals given the potential of adverse drug-drug interactions causing toxicities that can be avoided (25). For example, treatment with BDQ is associated with prolonged QT interval (26), therefore the known inhibitory effects of anti-retroviral therapy (ART) on the BDQ metabolizing isoenzyme cytochrome P450 3A4 (27), might increase BDQ concentrations in patients on ART potentially causing toxicity. Considering these factors, there is an urgent need for development of new drugs with novel modes of action, which would shorten the duration of treatment, with limited ART interaction properties, reduce the daily pill burden, and are effective against DR-TB. Based on previous research (28), the mycobacterial cell wall remains an interesting target for identification and validation of novel drug targets as the current anti-TB drug regimen for DS-TB involves cell wall targeting drugs such as INH and EMB, which disrupt the protective mycobacterial cell wall increasing the efficacy of non-cell wall targeting drugs.

1.1.3. The mycobacterial cell wall

Mycobacteria assemble a unique and complex cell wall composed of three distinct layers, namely: mycolic acids, anchored by the arabinogalactan layer which is covalently attached to the peptidoglycan (PG) layer (Fig 1.3) (29). Lipid, glycan and peptide precursors of the mycobacterial cell wall are vital for biosynthesis of this macromolecule. The diverse biosynthesis pathways for the cell wall precursors and the enzymes required for incorporation of the precursors into the cell wall are the most widely exploited targets for anti-TB drugs (30).

1.1.3.1. Glycolipid and mycolic acids biosynthesis and potential targets

Among the bacterial species, the actinobacteria are distinguished by the presence of a mycolic acid layer (Fig 1.3) (29). The mycolic acids are attached to the arabinogalactan layer and are mainly long chain α-alkyl-β-hydroxy fatty acids composed of a meromycolate carbon $(C)_{42}$-C_{62} chain and a long saturated C_{24}-C_{36} α-chain. The outer cell envelope is also composed of free fatty acids such as trehalose mono/di-mycolates, diacyltrehalose and polyacyltrehalose, PDIM, sulfoglycolipids and glucose monomycolates. The glycolipids, phosphatidyl-myo-inositol mannosides, lipomannans (LM), LAM and mannosylated LAMs are attached to the cell membrane or to other layers of the cell wall. The mycolic acids and related lipids are important for cell wall integrity and also contribute to the pathogenicity of Mtb during infection (29). They also comprise a substantive permeability barrier for drugs and small molecules. Considering the important features of the mycolic acids and related lipids, the enzymes involved in their biosynthesis have been identified as potential drug targets. For example, INH and diarylcoumarin compounds in preclinical development inhibit mycolic acid biosynthesis (see below).

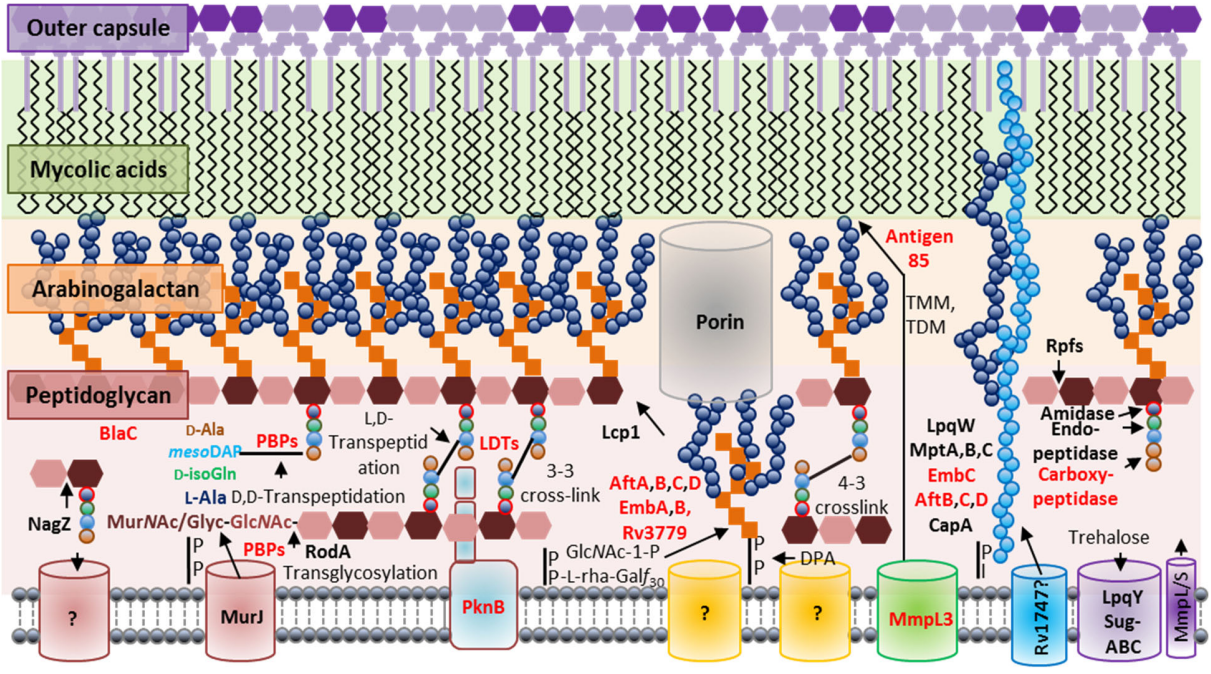

Figure 1.3. **Periplasmic cell wall biosynthesis pathways of the mycobacterial cell wall.** Shown is the periplasmic cell wall biosynthesis pathways for the different components of the mycobacterial cell wall (peptidoglycan [PG], arabinogalactan, mycolic acids and glycolipids). The validated enzymes and potential drug targets in the mycobacterial cell wall are shown in red font. PG hydrolases, required for PG remodeling during cell growth are also shown.

1.1.3.2. Biosynthesis of glycolipids and drug targets in the pathway

Glycolipids are essential for mycobacterial growth and their biosynthesis is initiated in the cytoplasm (Fig 1.4, blue section). PimA and PimB, the α-mannopyranosyl transferases, transfer mannosyl residues from donor GDP-mannopyranose to the second and sixth positions of the inositol moiety of phosphatidylinositol to form phosphatidylinositol monomannoside (PIM_1) and PIM_2, respectively (29). PIM_1 is acylated by Rv2611c before formation of PIM_2 and subsequent to formation of PIM_2, the C_3 position of the myo-inositol ring of PIM_2 is acylated by an unknown acyl transferase to form Ac_1/Ac_2PIM_3.

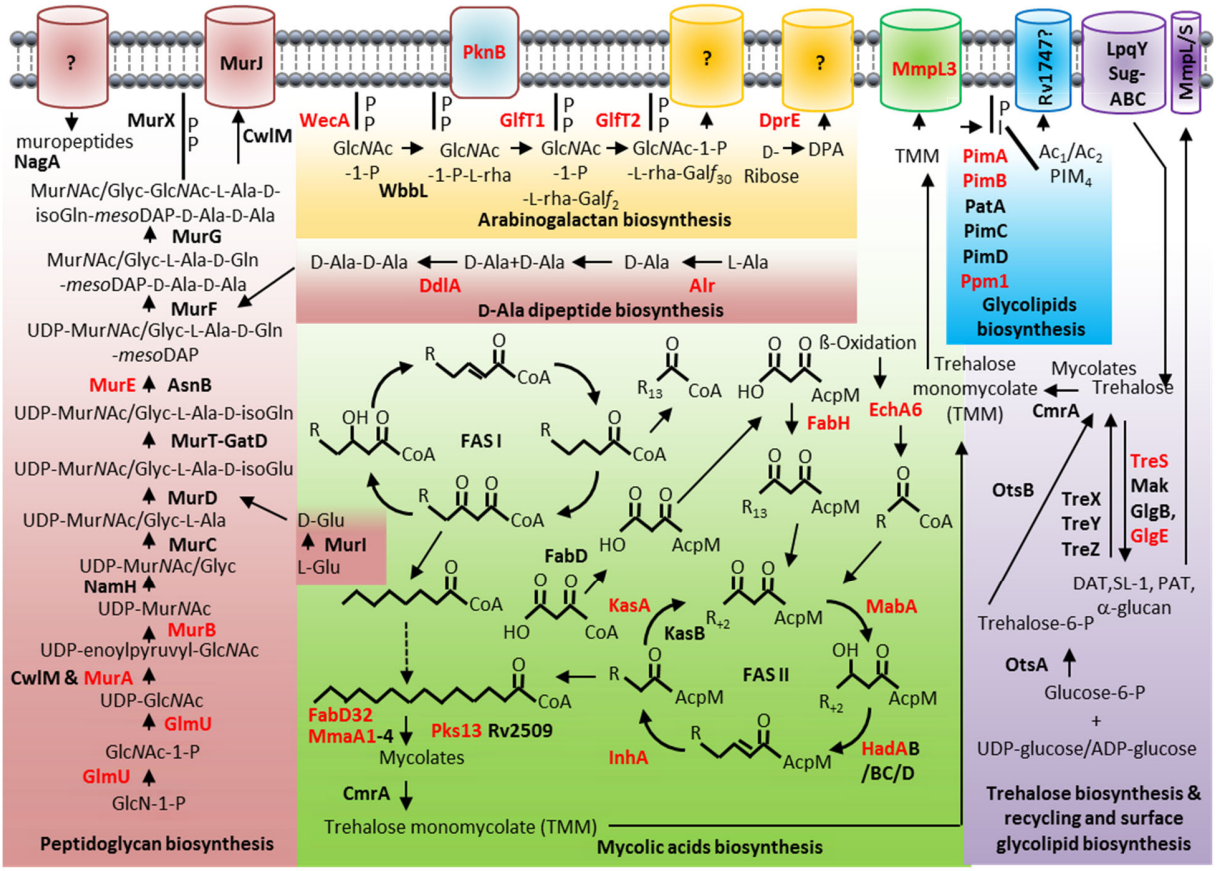

Figure 1.4. **Cytoplasmic cell wall biosynthesis pathways of the mycobacterial cell wall.** Shown is the cytoplasmic cell wall biosynthesis pathways for the different components of the mycobacterial cell wall (peptidoglycan [PG], arabinogalactan, mycolic acids and glycolipids). The vaildated cytoplasmic enzymes and potential cytoplasmic drug targets are shown in red font. Membrane channels involved in PG recycling, GlcNAc-1-P-L-rha-Galf_{30}-, DPA-, Ac_1/Ac_2PIM_4-, and surface glycolipid translocation remain to be identified (depicted by "?")(31).

Table 1.1. **A list of drug targets in the mycobacterial cell wall biosynthesis pathways with compounds showing inhibitory activity of Mtb growth**. Compounds without proven *in-vitro* data were excluded.

Drug target	Drug	Effect	Ref
GlmU	4-aminoquinazolines (compounds HMP-05 and HMP-15), 2 phenylbenzofurans, arylamines, arylsufonamides, diterpenoids (TPSA and 2-amino-2,3-dideoxy-3-fluoro-α-d-glucopyranosyl phosphate)	Inhibit PG precursor biosynthesis	(32, 33)
MurA	Fosfomycin analogs, peptidomimetic compounds and sulfonoxyanthranilic acid derivatives	Inhibit PG precursor biosynthesis	(34-36)
MurB	Sulfadoxine, pyrimethamine, piperazine derivatives and chloropicolinate amides	Inhibit PG precursor biosynthesis	(37)
MurE	Glucosamine uridine analogs	Inhibit PG precursor biosynthesis	(38)
PBPs	Moenomycin, beta-lactams, carbapenems and cephalosporins	Inhibit PG cross-linking	(39)
Alr	D-cycloserine	Inhibits PG precursor biosynthesis	(40, 41)
DdlA	D-cycloserine	Inhibits PG precursor biosynthesis	(41)
BlaC	Clavulanate, diazabicycloctanones, avibactam and sulbactam	Inhibit BlaC beta-lactamase activity	(39)
LDTs	Carbapenems and cephalosporins	Inhibit PG cross-linking	(42, 43)
PknB	5-substituted pyrimidine analogs	Inhibit PknB signaling	(44)
Carboxypeptidases	Meropenem	Inhibits PG remodeling	(45)
MurJ	Humimycins	Block translocation of Lipid II to the periplasm and inhibit PG biosynthesis	(46)
MurX/MraY	Capuramycin, capuramycin analogs (compound UT-01320), tunicamycin, compound SQ 641, compound X-J99620886, muramycin D2, caprazamycin and liposidomycin	Inhibit PG precursor biosynthesis	(47, 48)
WecA	Tunicamycin, compound X-J99620886 and compound CPZEN-45	Inhibit Arabinogalactan precursor biosynthesis	(48)
GlfT1 & 2	UDP-Galf derivatives	Inhibit arabinogalactan precursor biosynthesis	(29)
DprE	>15 (compounds are listed in Degiacomi et al., 2020)	Inhibit arabinogalactan precursor biosynthesis	(49)
AftA,B,C,D	DPA analogs	Inhibit periplasmic arabinogalactan biosynthesis	(29)
EmbA,B,C	Ethambutol	Inhibit periplasmic arabinogalactan biosynthesis	(50)
FabH	Thiolactomycin analogs, platensimycin, platencin, thiazole and pyrazol-benzimidazole amide derivatives	Inhibit mycolic acid biosynthesis	(33, 51)
MabA	Anthranilic acid analogs	Inhibit mycolic acid biosynthesis	(52)
HadA	Thiacetazone and thiocarlide	Inhibit mycolic acid biosynthesis	(53)

InhA	Isoniazid, ethionamide, triclosan, diazaborines (compound AN12855), 2-(o-tolyloxy)-5-hexylphenols (compound PT70), 4-hydroxy-2-pyridines (compounds NITD-916 and NITD-113), pyridomycin, pyrrolidine, carboxamides, pyrroles, acetamides, thiadiazoles, triazoles and thiadiazole-based compounds (e.g. compound GSK693)	Inhibit mycolic acid biosynthesis	(33, 54-56)
KasA, KasB	Cerulenin, plastensimycin, TLM and compound GSK3011724A	Inhibit mycolic acid biosynthesis	(29, 57)
FabD32	Diarylcoumarin	Inhibits mycolic acid biosynthesis	(29)
MmaA1	Compound 3-(2-morpholinoacetamido)-N-(1,4-dihydro-4-oxoquinazolin-6-yl)benzamide	Inhibits mycolic acid biosynthesis	(58)
Pks13	Benzofurans (TAM16), coumestants, thiophene compounds and β-lactones (EZ120)	Inhibit mycolic acid biosynthesis	(59-61)
EchA6	THPPs (Tetrahydropyrazo [1,5-a]pyrimidine-3-carboxamides)	Inhibit mycolic acid biosynthesis	(62)
MmpL3	Compound SQ109 (a 1,2-ethylenediamine), compound C215 (a benzimidazole derivative), compounds NITD-304 & NITD-349 (indole-2-carboxamides), compound TBL-140 (a diphenylether-modified adamantyl 1,2-diamine), THPPs (Tetrahydropyrazo [1,5-a]pyrimidine-3-carboxamides), SPIRO analogs (N-benzyl-6',7'-dihydrospiro[piperidine-4,4'-thieno[3,2-c]pyran] analogs), compound E11 (an acetamide analog), compound AU1235 (an adamantyl urea), compound BM212 (a 1,5-diarylpyrrole derivative) or BM635, compound HC2091 (a N-[2-(4-chlorophenyl)ethyl]-4-thiophen-2-yloxane-4-carboxamide) and compound PIPD1 (a piperidinol-containing molecule)	Block translocation of mycolic acids to the periplasm and inhibit periplasmic mycolic acid biosynthesis	(30, 63, 64)
Antigen 85	Compound I3-AG85, mannose-binding lectin (MBL) and ficolins, structural analogs of trehalose and arabinogalactan, β-isomer monocyclic enolphosphorus cycliphostin ($CyC_{8\beta}$) and cyclipostins	Inhibit mycolic acid biosythesis	(65-67)
Ppm1	Amphomycin	Inhibits glycolipid biosynthesis	(68)
TreS	α-glycoside analogs	Inhibit surface glycolipid biosynthesis	(69, 70)
GlgE	Maltose mimics: maltose-C-phosphonate (MCP) 13, 2-deoxy-2-fluoro-α-maltosyl fluoride and deoxy-2-2-difluoro-α-maltosyl fluoride	Inhibit surface glycolipid biosynthesis	(69-71)
MptA & MptB	prenyl-related photoactivatable probes	Inhibits LAM biosynthesis	(29)

PimC or PimD, facilitate another step of monosylation of Ac_1/Ac_2PIM_3 to form Ac_1/Ac_2PIM_4. Higher order glycolipids are synthesized in the periplasm subsequent to flipping of the precursor/anchor Ac_1/Ac_2PIM_4 to the cell wall by an unknown flippase (Fig. 1.3, blue section). Ppm1, a polyprenol monophosphomannose synthase, facilitates the synthesis of polyprenyl-phosphate-based mannose (PPM) – the essential substrate for higher order glycolipid biosynthesis in the periplasmic space. Monosylation of Ac_1/Ac_2PIM_4 by PimE and other unidentified GT-C glycosyltransferases results in the formation of Ac_1/Ac_2PIM_6. Ppm1 is a target of amphomycin (Table 1) (29).

LM and LAM biosynthesis is facilitated by periplasmic mannolyltransferases (MptA, MptB and MptC) which use Ac_1/Ac_2PIM_4 as the precursor/anchor for glycolipid biosynthesis (Fig 1.3, blue section). Extension of Ac_1/Ac_2PIM_4 with mannan or arabinomannan chains results in the formation of LM and LAM, respectively. MptA and MptB facilitate the synthesis of the mannan core of LM and LAM. MptC facilitates the transfer of monomannose side chains to form mature LM. The mannosyltransferases MptA and MptB are targets of recently discovered prenyl-related photoactivatable probes (Table 1).

Glycosylation of LM with ~50-80 α-D-arabinofuranosyl residues by EmbC, AftB, AftC and AftD using decaprenylphosphoryl-D-arabinose (DPA) results in the formation of mature LAM (Fig 1.3, blue section). CapA, a mannolyltrasferase, uses PPM as a substrate to add capping motifs in the form of mannosyl residues to LAM resulting in the formation of ManLAM. Further modifications to ManLAM are introduced by MptC, which adds more 1-4 mannosyl residues to the terminal mannosyl residue of ManLAM (29). EmbC, AftB and AftC are targets of EMB and DPA analogs (Table 1).

1.1.3.3. Biosynthesis of mycolic acids and drug targets in the pathway

Mycolic acid biosynthesis is initiated in the cytoplasm and involves two distinct pathways, the fatty acid synthase type I and II (FAS-I and FAS-II) pathways (Fig 1.4, green section) (72). FAS-I generates short chain fatty acyl-CoA esters that form the saturated C_{24} α-chain or are extended by the FAS-II to form the meromycolate C_{42}-C_{62} chain. FabD, the malonyl:AcpM transacylase

generates malonyl-AcpM, which is required for the elongation of the fatty acyl-CoA esters. FabH, the β-ketoacyl ACP synthase fuses the fatty acyl-CoA esters with malonyl-AcpM to form C_{16}-AcpM (29). Analogs of thiolactomycin (TLM) have been shown to possess *in vitro* inhibitory activity against FabH but no cell growth inhibition was observed (Table 1).

The FAS-II pathway uses the C_{16}-AcpM to generate the meromycolate C_{42}-C_{62} chain (Fig. 1.4, green section). Firstly, MabA, a β-ketoacyl-AcpM reductase facilitates the keto-reduction reaction of C_{16}-AcpM and this is followed by the activity of HadAB/BC, a β-hydroxyacyl-AcpM hydratase that facilitates the dehydration reaction. InhA, an enoyl-AcpM reductase facilitates the enoyl-reduction reaction. KasA and KasB, both complementary β-ketoacyl ACP synthases, replace the requirement of FabH in the successive cycles for elongation of the AcpM-bound acyl chain which extends by two carbons during each cycle, resulting in the formation the meromycolate C_{42}-C_{62} chain (29).

The long-chain meromycolate undergoes further modification, including a *cis*-/*trans*-cyclopropanation reaction and the addition of methoxy- and keto-groups before being incorporated into the cell wall (Fig. 1.4, green section). For this, FabD32, a fatty acyl-AMP ligase, activates the meromycolate chain and following this, Pks13, a polyketide synthase, fuses an α-alkyl-CoA ester with the activated meromycolate chain to generate an α-alkyl-β-keto-mycolic acid. Rv2509 facilitates the reduction of the α-alkyl-β-keto-mycolic acid to generate a mature mycolic acid (29).

MabA has been shown to be a target of pteleoellagic acid and HadA is a target of thiacetazone and thiocarlide antibiotics which were formerly used for TB treatment but discontinued due to high toxicity (Table 1). InhA is a target of the first-line TB drug INH and structural analogs such as ethionamide (ETM) which require prior activation by a catalase peroxidase (KatG) and a flavoprotein monooxygenase (EtaA), respectively (Table 1)(73, 74). InhA inhibitors, such as triclosan and a thiadiazole compound GSK693 which unlike INH and ETM do not require prior activation are currently under development (Table 1). KasA and KasB are targets of cerulenin, plastensimycin and TLM. KasA is also a target of GSK3011724A. FabD32 is a target of

diarylcoumarin. Pks13 is a target of thiophene compounds such as 2-aminothiophenes which inhibit the N-terminus acyl carrier protein domain of Pks13 (Table 1). Pks13 is also a target of benzofurans, coumestants and β-lactones (Table 1). Recently, the benzofuran compound TAM16, coumestan analogs and the β-lactone compound EZ120 have been shown to inhibit the thioesterase activity of Pks13 required for the condensation of the α-alkyl-CoA ester with the meromycolate chain (59, 61, 75).

The mature mycolic acids are transported from the cytoplasm to the cell wall through cell membrane embedded transporters (Fig. 1.4, green section). MmpL3, an inner membrane mycolic acid flippase has been shown to be essential for transportation of mycolic acids to the cell wall (64). Before transportation to the cell wall, the mature mycolic acids are first attached to trehalose by mycolyl-transferases to form trehalose monomycolates (TMMs) which are translocated by MmpL flippases (Fig. 1.4, green section) (72). The TMMs are attached to arabinogalactan by the mycolyltransferase antigen 85 complex (composed of the enzymes Ag85A, Ag85B and Ag85C). The TMMs can also be converted to trehalose dimycolates (TDMs) by the antigen 85 complex before being attached to arabinogalactan (72).

Several compounds including SQ109, C215, BM212 and AU1235 are shown to be MmpL3 inhibitors (Table 1). BM212, a 1,5-diarylpyrrole compound, has recently been shown to directly target MmpL3 (64). Ech6, a catalycally inactive enoyl-CoA hydratase required for shuttling fatty acyl-CoA esters into FAS-II for mycolic acid biosynthesis (see Fig. 1.4, green section) is a target of tetrahydropyrazo[1,5-a]pyrimidine-3-carboxamide (THPP) (Table 1). Ag85C is a target of the compound I3-AG85 causing inhibition of incorporation of mycolic acids into the mycobacterial cell wall (Table 1).

1.1.3.4. Arabinogalactan biosynthesis and potential targets

Arabinogalactan biosynthesis is initiated in the cytoplasm by WecA, a *N*-acetylglucosamine-1-phosphate (Glc*N*Ac-1-P) transferase, which transfers Glc*N*Ac-1-P to C_{50}-P resulting in the formation of C_{50}-P-P-Glc*N*Ac (Fig 1.4, orange section). WbbL, a rhamnosyltransferase facilitates the transfer of L-rhamnose to C_{50}-P-P-Glc*N*Ac using dTDP-L-rhamnose as a substrate to form

C_{50}-P-P-Glc*N*Ac-L-Rha, the linker unit for attachment of the galactan chain. GlfT1 and GlfT2, galactatofuranosyltransferases, facilitate the synthesis of the galactan chain. GlfT1 facilitates the addition of two Gal*f* residues to C_{50}-P-P-Glc*N*Ac-L-Rha to form C_{50}-P-P-Glc*N*Ac-L-Rha-Galf_2. Subsequently, GlfT2 adds β-D-galactofuranosyl (Gal*f*) residues to the growing chain resulting in the formation of a galactan chain with ~ 30 Gal*f* residues (C_{50}-P-P-Glc*N*Ac-L-Rha-Galf_{30}) (76).

The cell membrane linked galactan chain (C_{50}-P-P-Glc*N*Ac-L-Rha-Galf_{30}) is translocated to the periplasm by an unknown flippase where Ara*f* residues are added to the galactan chain from decaprenylphosphoryl-d-Ara*f* (DPA) as the donor (Fig 1.3, orange section). DPA is synthesized in the cytoplasm through a series of reactions involving the activity of the decaprenylphosphoribose-2'-epimerase (DprE) (29). Rv3789 (a transmembrane GtrA family protein) recruites AftA (77), which facilitates the addition of single Ara*f* residues from DPA to position C_5 of Gal*f* residues of the galactan chain (Fig. 1.3, orange section). EmbA and EmbB arabinosyltransferases, facilitate the extension of the Ara*f* residues and AftC along with AftD introduce α(1-3) branching with Ara*f* residues. The terminal and penultimate Ara*f* residues of the arabinogalactan chain serve as anchoring points for mycolic acids. The final steps of arabinogalactan biosynthesis involve the transfer of a D-Gal*N* residue to the inner arabinan units by Rv3779 and subsequent attachment of the arabinogalactan macromolecule to PG by Lcp1 (Fig. 1.3, orange section)(78).

WecA is a target of caprazamycin compounds such as CPZEN-45 (Table 1) (48). UDP-Gal*f* derivatives with various modifications inhibit GlfT1 and GlfT2 causing premature termination of arabinogalactan biosynthesis. DprE1 is a target of nitro-benzothiazinones (BTZs) and dinitrobenzamides (49). EmbA and EmbB are targets of EMB, a first-line TB drug (Table 1).

1.1.3.5. PG biosynthesis and potential targets

PG biosynthesis is initiated in the cytoplasm and the first committed step is the synthesis of UDP-Glc*N*Ac facilitated by GlmU (a UDP-*N*-acetylglucosamine pyrophosphorylase) (Fig 1.4, red section) (29). Firstly, GlmU transfers an acetyl group from acetyl-CoA to glucosamine-1-phosphate to produce Glc*N*Ac-1-P. Thereafter, GlmU transfers uridine-5'-monophosphate from

UTP to Glc*N*Ac-1-P to generate UDP-Glc*N*Ac. MurA, a UDP-*N*-acetylglucosamine 1-carboxyvinyltransferase and MurB, a UDP-*N*-acetylenolpyruvoylglucosamine reductase, are involved in the biosynthesis of UDP-Mur*N*Ac by addition of the enoylpyruvyl moiety of phosphoenoyl pyruvate, followed by reduction of a lactoyl ether moiety of UDP-enoylpyruvyl-Glc*N*Ac via NADPH to generate UDP-Mur*N*Ac (Fig. 1.4, red section). In actinomycetes, NamH - a UDP-*N*-acetylmuramic acid hydroxylase, facilitates the hydroxylation of UDP-Mur*N*Ac resulting in the formation of UDP-*N*-glycolylmuramic acid (UDP-Mur*N*Glyc) (Fig.1.4, red section). The hydroxylation modification of Mur*N*Ac is unique to actinomycetes and provides resistance to lysozyme (79).

A pentapeptide chain is then incorporated onto UDP-Mur*N*Ac or UDP-Mur*N*Glyc by successive addition of amino acid residues; L-alanine, D-glutamate, *meso*-diaminopimelate (*meso*-DAP) and D-alanyl-D-alanine by the Mur ligases C-F respectively, resulting in the formation of UDP-Mur*N*Ac/Glyc-L-Ala-D-Glu-*meso*-DAP-D-Ala-D-Ala (Fig 1.4, red section). The D-alanyl-D-alanine dipeptide is synthesized by the D-Ala: D-Ala ligase (Ddl) a target of D-cycloserine (a second line TB drug) (Table 1). MurX links the UDP-Mur*N*Ac/Glyc-L-Ala-D-Glu-*meso*-DAP-D-Ala-D-Ala to decaprenyl phosphate (C_{50}-P) resulting in the formation of lipid I (Fig. 1.4, red section). MurG, a glycosyltransferase, facilitates the transfer of Glc*N*Ac from UDP-Glc*N*Ac to Mur*N*Ac or Mur*N*Glyc of lipid I to generate lipid II (Fig. 1.4, red section). MurX is a target of capuramycin and related natural compounds including muramycin, caprazamycin and liposidomycin. MurG is inhibited by ramoplanin, a lipoglycodepsipeptide which binds lipid I preventing MurG synthesis of lipid II (Table 1).

The final stages of lipid II biosynthesis involve the modification of the pentapeptide stem including amidation of the α-carboxyl group of D-Glu by the MurT-GatD complex and the ε-carboxyl group of *meso*-DAP by AsnB to form amidated lipid II (Fig. 1.4, red section) (80, 81). Amidated lipid II is translocated to the cell wall by MurJ and is polymerized into PG by monofunctional and bifunctional penicillin-binding proteins (PBPs). In gram positive bacteria like *S. aureus* and *S. pneumoniae*, the D-Glu amidation modification (i.e. D-isoGln) is required

for PG cross-link formation, cell viability, beta-lactam antibiotic resistance and lysozyme resistance (82).

Once lipid II is amidated and translocated from the cytoplasm to the periplasm, the transglycosylase activity of PBPs and SEDS (Shape, Elongation, Division, and Sporulation) proteins facilitate the linking of the disaccharide component of lipid II to the existing PG glycan chains (Fig 1.3, red section). The D,D-transpeptidase activity of PBPs facilitates the formation of 3-4 cross-links between *meso*-DAP and D-Ala of adjacent pentapeptide chains. In mycobacteria, as the cell expands, L,D-transpeptidases (LDTs) and PG endopeptidases facilitate the remodeling of 3-4 crosslinks to 3-3 cross-links (83). The 3-3 cross-links further strengthen the PG sacculus and maintain cell shape (83). MurJ is a target of newly discovered antibiotics such as the humimycins. Ramoplanin, teixobactin, malacidin and nisin, bind periplasmic lipid II preventing polymerization into the cell wall by PBPs (Table 1). Glycopeptides, vancomycin and teicoplanin bind the D-Ala-D-Ala terminus of lipid II also preventing lipid II polymerization.

Fosfomycin targets MurA in Gram-negative bacteria (84). Mycobacterial MurA lacks a critical active site cysteine (replaced by aspartic acid [D117C]) required for fosfomycin binding (85). Consequently, Mtb MurA is resistant to fosfomycin. Molecular docking studies of MurB inhibitors on the Mtb MurB indicate the inhibitory potential for existing compounds such as 4-thiazolidinones against Mtb MurB (Table 1). Moenomycin inhibits the transglycosylase activity of PBPs. β-lactam antibiotics inhibit the transpeptidase activity of PBPs, and these are only effective when used together with beta-lactamase inhibitors like clavulanate, diazabicycloctanones, avibactam and sulbactam (39). In addition to expression of β-lactamases, mycobacteria express β-lactam insensitive LDTs required for 3-3 cross-link formation (83). However, recently, carbapenems have been shown to inactivate both the LDTs and PBPs and are poor substrates for the β-lactamase BlaC (86).

1.1.3.6. Regulation of PG biosynthesis and potential targets

Mtb expresses 11 serine/threonine protein kinases (STPKs) named PknA to PknL, which regulate various metabolic pathways through protein phosphorylation signaling (87). PknB and

PknG are the only essential STPKs for intracellular survival of Mtb. PknB regulates PG biosynthesis by localizing at sites of PG biosynthesis and binding non-cross-linked PG precursors (see Fig. 1.3, red section) and through phosphorylation of substrates like GlmU, CwlM, MurJ, RodA (a monofunctional PG transglycosylase) and PonA1 (a bifunctional PBP) (88). CwlM, a cytoplasmic amidase, exists in phosphorylated and non-phosphorylated forms in the cell. Phosphorylated CwlM activates MurA and also interacts with FhaA, a fork head associated protein required for regulating the amount of PG precursors translocated to the periplasm. Non-phosphorylated CwlM associates with non-phosphorylated MurJ and allows for lipid II translocation (89). Non-phosphorylated CwlM also interacts with other proteins including FtsZ (a tubulin-like protein required for synthesis and degradation of cell division septa), DnaA (chromosomal replication initiator protein) and Wag31 (a tropomyosin-like protein required for cell elongation). Phosphorylated MurJ interacts with FhaA inhibiting lipid II translocation (89). PknB phosphorylates RodA, a non-canonical PG transglycosylase required for linking lipid II to the PG glycan strand (90). Phosphorylation of PonA1 by PknB is required to regulate the PG transglycosylation activity of PonA1 (91). Kinase inhibitors against PknA and PknB have been developed and are bactericidal against Mtb (Table 1) (44).

1.1.3.7. PG remodeling and potential targets

Mycobacteria display distinct modes of cell growth and cell division in contrast to most rod-shaped bacteria (92). Mycobacteria insert nascent PG at the cell poles and cell division septum and the cells divide assymetrically-producing daughter cells of different cell sizes (92). The PG sacculus is constantly remodelled by various classes of PG hydrolases (resuscitation promoting factors [Rpfs], PG amidases, carboxypeptidases, NlpC/p60 endopeptidases and M23 peptidases) to allow for insertion of new PG percursors and cell division (Fig 1.3, red section) (93). Carboxypeptidases cleave-off the terminal D-Ala residue of lipid II to regulate PG biosynthesis and also cleave 4-3 PG cross-links to provide substrates for synthesis of 3-3 cross-links which strengthen the cell wall. In mycobacteria, the Rpfs, PG amidases, NlpC/p60 hydrolases and M23 peptidases have previously been shown to be important for cell division (92). Rpfs possess a catalytic domain similar to that of lysozyme and lytic transglycosylases - enzymes that cleave β-l,4-glycosidic bonds between Glc*N*Ac and Mur*N*Ac units of the PG glycan strands (Fig. 1.3, red

section) (93). The amidases cleave the amide bond connecting the PG cross-linking stem peptides to the glycan backbone (Fig. 1.3, red section) (94). The NlpC/p60 hydrolases cleave the bond between D-glutaminyl and *meso*-diaminopimelyl residues in the PG stem peptides and the M23 peptidases display a range of endopeptidase activities, cleaving various PG stem peptide linkages (Fig. 1.3, red section). The NlpC/p60 endopeptidases; RipA and RipB, are potential drug targets as they are collectively essential for cell viability and the PG amidase Ami1 has also been identified as a potential drug target required for cell division (95, 96). Regulators of the NlpC/p60 endopeptidase RipA (like MarP) and regulators of the PG amidase Ami3 (like HtrA) are also potential drug targets essential for cell growth (95, 97).

1.1.3.8. PG recycling, role in signal transduction and potential targets

During nutrient limitation Gram-negative and Gram positive bacteria have been shown to possess the ability to recycle PG material (i.e. muropeptides) released during growth (98). The muropeptides obtained are used as a carbon source, however, this process remains unclear for mycobacteria (99). *E. coli* recycles approximately 90% of the muropeptides, releasing only ~5% (100). Mycobacteria lack most known PG-recycling enzymes but have conserved two potential PG recycling enzymes – NagZ/LpqI (a β-*N*-acetylglucosaminidase) and NagA (a *N*-acetylglucosamine-6-phosphate deacetylase) (Fig. 1.3, red section) (99). Similarly to Rpfs, NagZ/LpqI is required for the cleavage of 1,6-glycodic bonds between Glc*N*Ac and Mur*N*Ac residues of muropeptides. It remains unknown whether mycobacteria can use Glc*N*Ac as a carbon source, however, D-lactate released from Mur*N*Ac during muropeptide recycling can be used as a carbon source (99). NagA catalyzes the deacetylation of *N*-acetylglucosamine-6-phosphate to glucosamine-6-phosphate which can be used for generation of fructose-6-phosphate for glycolysis or to produce UDP-Glc*N*Ac for PG biosynthesis (101). NagA has been identified as a a potential TB drug target (102). Muropeptides that are not recycled but released to the extracellular space can also serve as signaling molecules for resuscitation of dormant cells or can be detected by pathogen recognition receptors (PRRs, specifically NOD-1 and NOD-2) of the immune system during infection (103). Mtb expresses five resuscitation promoting factors (Rpfs) in a growth-phase dependent manner and the Rpfs are essential for resuscitation of Mtb from a state of quiescence (94).

In this work we further explore the role of PG amidation in mycobacterial PG biosynthesis and identify the enzymes required for PG amidation (MurT and GatD) as potential TB drug targets. We further exploit the PG amidation process in the *Mycobacterium bovis* BCG vaccine to develop a recombinant *Mycobacterium bovis* BCG vaccine re-engineered with a CRISPRi platform to activate the NOD-1 PRR to enhance BCG efficacy. The outline of the thesis is shown in the next page.

Chapter 1: Introduction to TB

Chapter 2: General methods

Chapter 3:

Glutamate amidation by the MurT-GatD complex during mycobacterial PG biosynthesis is required for cell growth and PG cross-linking.

Highlights

- Amidated probes confirm the importance of PG precursor amidation for PG cross-linking.
- MurT-GFP and mRFP-GatD localize at sites of PG biosynthesis.
- MurT interacts with GatD to form the MurT-GatD amidotransferase complex.
- MurT and GatD are required for PG amidation and cell growth in mycobacteria.
- PknB regulates cell growth in response to PG amidation.
- MurT-GatD depletion causes increased cell wall permeability and increased sensitivity to lysozyme.
- PknB regulates cell growth in response to PG amidation.
- MurT-GatD depletion causes sensitivity to β-lactam antibiotics.

Conclusion

- Mycobacterial MurT-GatD enzymes are attractive new targets for TB drug development.

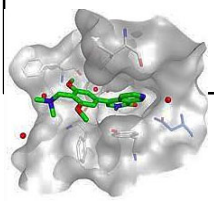

New Drug target

Chapter 4:

A novel CRISPRi based BCG vaccine targeting the NOD-1 pathway induces protection against Mtb infection in mice.

Highlights

- CRISPRi was used to generate a recombinant BCG strain.
- MurT-GatD depletion in *M. bovis* BCG causes cell wall defects associated with decreased PG cross-linking and reduced amidation.
- rBCG::iE-DAP is responsive to anhydrotetracycline activation and causes increased TNFα expression in BMDMs.
- rBCG::iE-DAP *in vitro* trained macrophages control Mtb H37Rv growth.
- rBCG::iE-DAP is responsive to activation *in vitro* and in mice-aerosol infections with doxycyline (Dox).
- rBCG::iE-DAP+Dox vaccination induces better protection against Mtb infection in mice compared to WT BCG.

Conclusion

- rBCG::iE-DAP provides a novel platform for development of a new TB vaccine

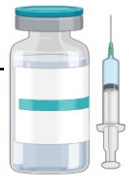

New Vaccine Candidate

Appendices & References

CHAPTER 2

(General methods)

2.1. General methods

2.1.1. Bacterial growth conditions

2.1.1.1. Growth conditions for *E. coli* DH5α and derivative strains

E. coli DH5α and derivative strains were grown in Luria-Bertani broth (LB) or on Luria-Bertani agar (LA) at 37°C with supplementation of the media with appropriate antibiotics. The antibiotic concentrations used were as follows: Kanamycin (Kan): 50 μg/ml and Hygromycin (Hyg): 200 μg/ml. Liquid cultures were grown at 37°C with shaking at 200 rpm.

2.1.1.2. Growth conditions for *M. smegmatis* mc^{2}155, Mtb H37Rv, *M. bovis* BCG and derivative strains

M. smegmatis mc^{2}155 and derivative strains were grown at 37°C in Middlebrook 7H9 broth supplemented with 0.2% glucose, 0.2% glycerol, 0.085% NaCl, 0.05% Tween 80 and appropriate antibiotics (hereafter referred to as only Middlebrook 7H9 broth) or on Middlebrook 7H10 agar supplemented with 0.5% glycerol, 0.2% glucose, 0.085% NaCl and appropriate antibiotics (hereafter referred to as only Middlebrook 7H10 agar). *M. bovis* BCG, Mtb H37Rv and the recombinant BCG::CRISPRi MurT-GatD strain were grown at 37°C in Middlebrook 7H9 broth supplemented with OADC (Oleic acid, Albumin, Dextrose, Catalase) enrichment, 0.5% glycerol, 0.05% Tween 80 and appropriate antibiotics (hereafter referred to as Middlebrook 7H9 broth) or on Middlebrook 7H11 agar supplemented with OADC enrichment and 0.5% glycerol and appropriate antibiotics. The antibiotics used for supplementation of the media were at the following concentrations: Kan: 25 μg/ml, Hyg: 50 μg/ml. Supplementation of media with ATc where stated was at determined concentrations and supplementation with vitamin B_{12} was at 10 μg/ml. Middlebrook 7H9 broth cultures were grown at 37°C with shaking at a100 rpm.

2.1.2. Phenotypic analysis of *Mycobacterium smegmatis* mc^{2}155 , Mtb H37Rv, *M. bovis* BCG and derivative strains

2.1.2.1. Growth rate analysis

The growth rates of the mutant strains in comparison to the wildtype and the genetically complemented strains were assessed by conducting three independent growth curve experiments with plating for colony formation unit (CFU/ml) determination. Briefly, the bacterial strains were

grown overnight at 37ºC with shaking at a 100 rpm in 5 ml of Middlebrook 7H9 broth, supplemented with appropriate antibiotics when necessary. Thereafter, the pre-culture of each strain was diluted to an OD_{600nm} of 0.01 in 50 ml of Middlebrook 7H9 broth, supplemented with appropriate antibiotics when necessary. The cultures were incubated at 37ºC with shaking at a 100 rpm and the growth rate was assessed by generating a scatter plot from data obtained by recording the OD_{600nm} of each culture and plating for CFU/ml on Middlebrook 7H10 agar at three hour intervals. The GraphPad Prism 6 software was used for statistical analysis (Student's *t*-test was conducted to compare the growth rate difference of the mutant strains in relation to the wildtype).

2.1.3. DNA extractions

2.1.3.1. *Mycobacterium smegmatis* mc^{2}155, Mtb H37Rv and *M. bovis* BCG chromosomal DNA extractions

2.1.3.1.1. Small scale chromosomal DNA extraction

The colony boil method was used for small scale chromosomal DNA extraction. Briefly, a single colony of wildtype bacteria or derivative strains was scraped from an agar plate and resuspended in 50 µl of distilled water (dH_2O). Subsequently, 50 µl of chloroform was added and mixed with the cells by vortexing. The mixture was then incubated at 65°C for 10 minutes. Thereafter, the sample was centrifuged at 12470 ×*g* for 5 minutes and the supernatant was transferred into a clean tube. For PCR, 5 µl of this sample was used as DNA template.

2.1.3.1.2. Large scale chromosomal DNA extraction

The Cetyltrimethylammonium bromide (CTAB) DNA extraction method was used for large scale chromosomal DNA extraction. Wildtype bacteria and derivative strains were grown at 37°C on Middlebrook 7H10 agar for 2 days. The cells were harvested by scraping from the agar plates and this was followed by resuspension of cells in 500 µl of Tris-EDTA (TE) buffer. The cells were incubated at 95°C for 20 minutes. Following the incubation, the cells were put on ice for 10 minutes. Thereafter, 50 µl of lysozyme (10 mg/ml) was added and the mixture was incubated at 37°C for an hour. Subsequently, 6 µl of proteinase K (10 mg/ml) and 70 µl of 10% SDS were added and the mixture was incubated at 65°C for an hour. Following this, 100 µl of

NaCl (5 M) and 80 µl of pre-warmed CTAB/NaCl (10% N-cetyl-N,N,N-trimethyl ammonium bromide, 4.1% NaCl dissolved in dH_2O) were added. The mixture was incubated at 65°C for 10 minutes. Thereafter, 750 µl of chloroform: Isoamyl alcohol solution (24:1 ratio) was added to the cells, which was mixed by inverting the tubes, followed by centrifugation at 12 470 ×*g* for 10 minutes. The top aqueous layer was transferred into a clean tube into which 450 µl of isopropanol was added. The DNA was precipitated by centrifugation at 12 470 ×*g* for 30 minutes. Thereafter, the supernatant was discarded and the pellet was washed with 1 ml of 70% ethanol by centrifugation at 12 470 ×*g* for 5 minutes and dried using an Epperndorf Concentrator 5301. The DNA pellet was resuspended in 50 µl of nuclease free water and quantified using the NanoDrop ND-1000 Spectrophotometer (Thermo Fisher Scientific). The DNA was stored at 4°C until further use.

2.1.3.2. Plasmid DNA extraction from *E. coli* DH5α

2.1.3.2.1. Small scale plasmid DNA extraction from *E. coli* DH5α

The alkaline lysis mini-preparation method was used for small scale plasmid DNA extraction. *E. coli* DH5α derivative strains carrying plasmids of interest were grown overnight at 37°C in 2 ml of LB media supplemented with appropriate antibiotics. Thereafter, the cells were harvested by centrifugation at 12 470 ×*g* for 5 minutes and resuspended in 80 µl of solution 1 (50 mM glucose, 25 mM Tris-HCl [pH 8] and 10 mM EDTA). Following this, 160 µl of solution 2 (1% SDS and 0.2 M NaOH) was added and mixed with the cells by inversion and incubated at room temperature for 5 minutes. Subsequently, 120 µl of solution 3 (3 M potassium acetate, 11.5% acetic acid) was added and mixed vigourously and incubated on ice for 5 minutes. The sample was then centrifuged at 12 470 ×*g* for 10 minutes and the supernatant was transferred into a clean tube. Following this, 3 µl of RNAse-A (10 mg/ml) was added to the supernatant and this mixture was incubated at 42°C for 15 minutes. Plasmid DNA was precipitated by addition of 600 µl of isopropanol and centrifugation at 12 470 ×*g* for 30 minutes. The supernatant was discarded and the pellet was washed with 1 ml of 70% ethanol and dried using an Epperndorf concentrator 5301. The plasmid DNA pellet was resuspended in 50 µl of nuclease free water and quantified

using the NanoDrop ND-1000 Spectrophotometer (Thermo Fisher Scientific). The DNA was stored at -20°C until further use.

2.1.3.2.2. Large scale plasmid DNA extraction from *E. coli* DH5α

The Nucleobond DNA extraction kit (Macherey-Nagel) was used for large scale plasmid DNA extraction following manufacturer's instructions. Briefly, *E. coli* DH5α strains carrying plasmids of interest were grown overnight at 37°C in 50 ml of LB media supplemented with appropriate antibiotics. The cells were harvested by centrifugation at 1180 ×*g* for 15 minutes. The supernatant was discarded and the pellet of cells was resuspended in 4 ml of Buffer S1 (50 mM Tris-HCl, 10 mM EDTA, 100 µg/ml RNase-A, pH 8.0) with subsequent addition of 4 ml of Buffer S2 (200 mM NaOH, 1% SDS). The sample was mixed by inversion and incubated at room temperature for 3 minutes. Thereafter, 4 ml of Buffer S3 (2.8 M KAc, pH 5.1) was added to the sample, mixed by inversion and incubated on ice for 5 minutes. The mixture was then centrifuged at 1180 ×*g* for 30 minutes. A nucleobond Ax100 column was equilibrated with 2.5 ml of Buffer N2 (100 mM Tris, 15% ethanol, 900 mM KCl, 0.15% Triton X-100, adjusted to pH 6.3 with H_3PO_4). This was followed by addition of the clarified supernatant through the column. Thereafter, 10 ml of Buffer N3 (100 mM Tris, 15% ethanol, 1.15 M KCl, adjusted to pH 6.3 with H_3PO_4) was used to wash the column. Following this, 5 ml of Buffer N5 (100 mM Tris, 15% ethanol, 1 M KCl, adjusted to pH 8.5 with H_3PO_4) was then used for elution of plasmid DNA from the column into a clean tube. The plasmid DNA was precipitated by addition of 3.5 ml of isopropanol to the sample and centrifugation of the mixture at 12 470 ×*g* for 30 minutes. The pellet was washed with 1 ml 70% ethanol. Thereafter, the supernatant was discarded and the pellet was dried using an Epperndorf concentrator 5301. The plasmid DNA pellet was resuspended in 50 µl of nuclease free water and quantified using the NanoDrop ND-1000 Spectrophotometer (Thermo Fisher Scientific). The DNA was stored at -20°C until further use.

As an alternative method for large scale plasmid purification, the small scale plasmid DNA extraction protocol described above (section 2.1.3.2.1) was up-scaled. Briefly, *E. coli* DH5α derivative strains carrying plasmids of interest were grown overnight at 37°C in 50 ml of LB media supplemented with appropriate antibiotics. The cells were harvested by centrifugation at

1180 ×*g* for 15 minutes. The supernatant was discarded and the pellet was resuspended in 0.8 ml of solution 1. Thereafter, 1.6 ml of solution 2 was added, mixed by inversion and incubated at room temperature for 10 minutes. After this, 1.2 ml of solution 3 was added, mixed with the cells and incubated on ice for 10 minutes. The sample was centrifuged at 1180 ×*g* for 30 minutes and 900 µl of the resultant supernatant was transferred into clean tubes. Following this, 3 µl of RNAse-A (10 mg/ml) was added to the samples and the samples were incubated at 42°C for 15 minutes. Plasmid DNA was precipitated by addition of 600 µl of isopropanol and centrifugation of the sample at 12 470 ×*g* for 30 minutes. The supernatant was discarded and the pellet was washed with 1 ml of 70% ethanol and dried using an Epperndorf concentrator 5301. The plasmid DNA pellet was resuspended in 50 µl of nuclease free water and quantified using the NanoDrop ND-1000 Spectrophotometer (Thermo Fisher Scientific). The DNA was stored at -20°C until further use.

2.1.4. DNA manipulations

2.1.4.1. DNA amplification

2.1.4.1.1. Designing PCR primers

The online software Primer3 (http://bioinfo.ut.ee/primer3/) was used to design PCR primers using the parameters indicated in Table 2.1.

Table 2.1. **Parameters used for designing primers through Primer3**.

	Size (bp)	Tm (°C)	% GC
Minimum	18	55	30
Optimum	21	60	50
Maximum	24	65	70

2.1.4.1.2. Polymerase Chain reaction (PCR)

2.1.4.1.2.1. Phusion High-Fidelity DNA polymerase reaction

The Phusion High-Fidelity DNA polymerase (Thermo Scientific) was used according to the manufacturer's instructions for PCR synthesis of DNA fragments used for cloning. Briefly, PCR reactions were conducted in a final volume of 50 µl by the addition of 5 µl 5× HF buffer, 8 µl of

dNTPs (0.2 mM each), 100 ng of DNA template, 2.5 µl of primers (1 mM each), 1 U of Phusion DNA polymerase, 3% of dimethyl sulfoxide (DMSO) and nuclease free dH_2O to make up the final volume. A thermo-cycler (Bio-Rad laboratories) was used to incubate the samples using the following parameters: 3 minutes of initial denaturation at 98°C, 35 cycles of 30 seconds of secondary denaturation at 98°C, 30 seconds of annealing at 65°C, 1 minute of extension at 72°C and 10 minutes of final extension at 72°C. PCR DNA products were visualized on a 1% agarose gel as indicated in section 2.1.4.4.

2.1.4.1.2.2. Roche Fast Start Taq DNA polymerase reaction

The Roche Fast Start Taq DNA polymerase (Roche Applied Science) was used according to the manufacturer's instructions for PCR confirmation of clones or *M. smegmatis* gene deletion mutants. Briefly, PCR reactions were conducted in a final volume of 50 µl by the addition of 5 µl of 10× Roche Fast Start Taq DNA polymerase buffer, 10 µl of GC buffer, 2.5 µl of primers, 100 ng of DNA template, 1 U of Roche Fast Start Taq DNA polymerase, 8 µl of dNTPs (0.2 mM each) and nuclease free dH_2O to make up the final volume. A thermo-cycler (Bio-Rad laboratories) was used to incubate the samples using the following parameters: 3 minutes of initial denaturation at 95°C, 35 cycles of 30 seconds of secondary denaturation at 95°C, 30 seconds of annealing at the recommended temperature for the primers, 1 minute of extension at 72°C and 10 minutes of final extension at 72°C. PCR DNA products were visualized on a 1% agarose gel as indicated in section 2.1.4.4.

2.1.4.2. DNA purification by sodium acetate precipitation

The sodium-acetate DNA precipitation protocol was used to remove contaminating proteins, salts and other impurities from extracted chromosomal DNA, plasmid DNA or PCR DNA products. Briefly, the volume of the DNA was adjusted to 100 µl with dH_2O and 10 µl of sodium acetate (3 M, pH 5.2) was added, and this was mixed. Thereafter, 390 µl of ice-cold 100% ethanol was added, the solution was mixed and centrifuged at 12 470 ×*g* for 15 minutes. The supernatant was discarded and the pellet was dried using an Epperndorf concentrator 5301 and resuspended in 50 µl of nuclease free water. The DNA was stored at 4°C.

2.1.4.3. Restriction digestions

Restriction digestions of plasmids used in this study were performed through the use of restriction enzymes purchased from Thermo Fisher Scientific, New England Biolabs (NEB) or Roche Applied Science (Roche). Restriction digests of plasmids and PCR products were performed following manufacturer's instructions. Briefly, restriction digestions were conducted in a final volume of 20 µl per reaction with the addition of 1 µg of plasmid or PCR DNA, 2 µl of a restriction enzyme specific buffer, 1 U of restriction enzyme, 2 µl of 100× BSA (Bovine serum albumin) when necessary. dH_2O was added to make up the final volume. The sample was incubated at 37°C for an hour, unless stated otherwise by the manufacturer's instructions. Thereafter, the restriction digestion reaction was terminated by heat inactivation at 65°C for 10 minutes unless stated otherwise by the manufacturer's instructions.

2.1.4.4. Agarose gel electrophoresis

Agarose gel electrophoresis was used for visualization of extracted chromosomal DNA, plasmid DNA or PCR DNA products. The DNA was run on 1% agarose gels prepared with 1× TAE buffer (40 mM Tris-acetate and 1 mM EDTA) and the addition of ethidium bromide to a final concentration of 0.5 µg/ml. Electrophoresis was performed in agarose gel electrophoresis tanks (Bio-Rad laboratories) containing 1× TAE buffer at 90 V for 45 minutes. DNA molecular weight markers were also loaded on the agarose gel for estimation of the molecular weight of the DNA sample analyzed. The DNA on the agarose gel was visualized using a SYNGENE G-Box system.

2.1.4.5. DNA fragment purification

The NucleoSpin PCR clean-up and gel extraction kit (Macherey-Nagel) was used according to the manufacturer's instructions for purification of PCR products or DNA fragments excised from an agarose gel. Briefly, the agarose gel slice containing the excised DNA fragment was solubilized by incubation at 50°C for 5 minutes and for both the solubilized gel slice or PCR product clean-up, 1 volume of sample was mixed with 2 volumes of buffer NTI. Thereafter, the sample was loaded into a NucleoSpin PCR clean-up column, which was inserted into a collection tube. For DNA binding, the sample was centrifuged for 30 seconds at 11 000 ×*g*. The flow-through in the collection tube was discarded and 700 µl of buffer NT3 was added into the

column, followed by centrifugation at 11 000 ×*g* for 30 seconds. The flow-through in the collection tube was discarded and the column was dried by centrifugation at 11 000 ×*g* for 1 minute. The DNA was eluted into a clean microcentrifuge tube by the addition of 20 µl of buffer NE into the column and centrifugation of the sample at 11 000 ×*g* for 1 minute. The DNA was stored at -20°C until further use.

2.1.4.6. Dephosphorylation and phosphorylation of DNA

Antarctic alkaline phosphatase (NEB) was used to remove phosphate groups at the 5' end of linearized plasmid DNA to prevent self-ligation according to the manufacturer's instructions. Dephosphorylation reactions were conducted in a final volume of 20 µl per reaction by the addition of 1 µg of linearized plasmid DNA, 1 U of antarctic alkaline phosphatase, 2 µl of antarctic alkaline phosphatase buffer (NEB) and dH_2O to make up the final volume. The sample was incubated at 37°C for an hour and the reaction was terminated by heat inactivation at 65°C for 20 minutes. T4 DNA kinase (NEB) was used for addition of phosphate groups to non-phosphorylated DNA fragments according to the manufacturer's instructions to enable cloning of the DNA fragments into dephosphorylated vectors. Phosphorylation reactions were conducted in a final volume of 20 µl per reaction by the addition of 1 µg of DNA, 1 U of T4 DNA kinase, 2 µl of T4 DNA kinase buffer (NEB) and dH_2O to make up the final volume. The sample was incubated at 37°C for an hour and the reaction was terminated by heat inactivation at 65°C for 20 minutes.

2.1.4.7. DNA ligation

T4 DNA ligase (NEB or Thermo Scientific) was used for ligation of PCR DNA fragments into plasmid DNA according to the manufacturer's instructions. Briefly, the ligation reaction was performed in a final volume of 20 µl per reaction by the addition of 50 ng of plasmid DNA, 2 µl of T4 DNA ligase buffer, 5 U of T4 DNA ligase, "x" amount (ng) of DNA insert (x - calculated using the formula indicated below) and dH_2O was added to make up the final volume. To optimize the ligation efficiency, 1:1, 2:1 and 1:2 molar ratios of vector to insert were used for ligations (the equation for determining the amounts of DNA is given below). The samples were incubated at room temperature for 20 minutes and the ligation reaction was terminated by heat

inactivation at 65°C for 10 minutes. The DNA ligation products were used to transform chemically competent *E. coli* DH5α cells as indicated in section 2.1.5.2.

$$\text{Amount of insert (ng)} = \frac{\text{Amount of vector (50 ng)} \times \text{Size of insert (bp)}}{\text{Size of vector (bp)}}$$

2.1.4.8. DNA sequencing

DNA sequencing was performed at the DNA sequencing Facility of Stellenbosch University. The BigDye Terminator v3.1 Cycle sequencing kit (Applied Biosystems) was used for DNA sequencing and the DNASTAR Software (DNASTAR) was used for analysis of the DNA sequencing data.

2.1.5. Bacterial transformations

2.1.5.1. Preparation of chemically competent *E. coli* DH5α cells

Chemically competent *E. coli* DH5α were prepared using the calcium chloride ($CaCl_2$) protocol. A single colony of *E. coli* DH5α was inoculated into 50 ml of LB and incubated overnight at 37°C with shaking at 100 rpm. Thereafter, 1 ml of the pre-culture was inoculated into 100 ml of LB and incubated at 37°C with shaking at 100 rpm for 2 hours. The cells were harvested by centrifugation at 1180 ×*g* for 5 minutes at 4°C. The supernatant was discarded and the cells were resuspended in 10 ml of cold $CaCl_2$ (0.1 M) and immediately placed on ice for 20 minutes. The cells were centrifuged as before, resuspended in 5 ml of cold $CaCl_2$ (0.1 M) and used immediately for transformations with plasmids.

2.1.5.2. Transformation of chemically competent *E. coli* DH5α cells

A 100 µl aliquot of chemically competent *E. coli* DH5α cells was mixed with plasmid DNA. The cells were incubated on ice for 15 minutes and transformed by heat shock at 42°C for 90 seconds. Subsequently, 200 µl of pre-warmed LB media was added and the cells were incubated at 37°C for an hour, with shaking at 100 rpm. Thereafter, the cells were plated on LA media supplemented with the appropriate antibiotic. The LA plates were incubated overnight at 37°C. Single colonies were picked and screening for positive clones was performed as described in sections 2.1.3.1.2, 2.1.4.3 and 2.1.4.4.

2.1.6. Preparation of electro-competent mycobacterial or derivative strains

Mycobacterial cells were inoculated into 50 ml of Middlebrook 7H9 broth and grown to an optical density $(OD)_{600nm}$ of 0.5-0.8. The cells were harvested by centrifugation at 1180 ×*g* for 10 minutes at 4°C. The supernatant was discarded and the cells were resuspended and washed in 10 ml of ice cold 10% glycerol and harvested as before. The washing step was repeated twice and the cells were resuspended in 2 ml of ice cold 10% glycerol and used immediately for transformation with plasmids as described below.

2.1.6.1. Electroporation of plasmids into mycobacterial cells

Approximately 1 µg of plasmid DNA was used to transform electro-competent Mycobacterial cells or derivative strains by mixing 300 µl of cells with the plasmid DNA and transferring the mixture into a pre-chilled 0.2 cm electroporation cuvette (Bio-Rad laboratories). The cells were incubated on ice for 15 minutes and the Bio-Rad Gene Pulser XCell^{TM} (Bio-Rad laboratores) system was used to perform plasmid DNA electroporations with the following parameters: voltage: 2500 V, time constant: 25 µF, resistance: 1000 Ω and distance: 0.2 cm. After electroporation, 800 µl of LB media was added to the electroporation cuvette and the cells were transferred into a clean tube and incubated at 37°C overnight. Thereafter, the cells were pelleted by centrifugation at 12470 ×*g* and the supernatant was discarded followed by the resuspension of the cells in 500 µl of Middlebrook 7H9 broth. The cells were inoculated onto Middlebrook 7H10 agar containing appropriate antibiotics and incubated at 37°C for 3-5 days.

2.1.7. Localization of proteins of interest

The localization of proteins of interest was achieved by cloning of the open reading frame (ORF) of the gene of interest without the stop codon into plasmids pMV306H-GFP and pTweety-mRFP to create a protein fusion with the rseGFP or mRFP, respectively. The primers for the synthesis of the relevant ORF were designed to allow C-terminal tagging of the protein of interest with the rseGFP or to allow N-terminal tagging with mRFP. The DNA ligation process was performed as indicated in section 2.1.4.7 and resulting plasmid constructs were sequenced as indicated in section 2.1.4.8. Thereafter, the plasmid constructs were electroporated into either wild type *M. smegmatis* or derivative strains according to the protocol outlined in section 2.1.6.1. The

resultant colonies were picked and grown in 5 ml of Middlebrook 7H9 broth supplemented with the appropriate antibiotic to an OD_{600nm} of 0.6. The cells were harvested by centrifugation at 12470 ×*g*. The supernatant was discarded and the pellet of cells was resuspended in 50 µl of Middlebrook 7H9 broth and 5 µl of the cells was mounted onto a slide with a 2% agarose pad. The slides were visualized with the Zeiss Observer Z1 inverted fluorescence microscope and the images taken were analyzed with the ZEN lite software (Zeiss). Any image manipulation (brightness, contrast etc.) was applied to the entire image.

2.1.8. Fluorescence microscopy

2.1.8.1. Fluorescent BODIPY-FL vancomycin staining

The Fluorescent BODIPY-FL vancomycin stain (Life Technologies) was used according to the manufacturer's instructions for analysis of PG synthesis in the mutant strains in comparison to the wildtype and complemented strains. The fluorescent vancomycin stain binds to the terminal dipeptide D-alanine-D-alanine found on the PG stem peptide periplasmic precursor lipid II and consequently indicates the sites of new PG synthesis. The bacterial strains were grown to an OD_{600nm} of 0.6 at 37°C with shaking at a 100 rpm in 5 ml of Middlebrook 7H9 broth supplemented with appropriate antibiotics when necessary. Subsequently, 2 ml of the cells were harvested by centrifugation at 12 470 ×*g* for 5 minutes and the supernatant was discarded followed by washing of the cells with 500 µl 0.01 M phosphate buffered saline (PBS), pH 7.4 and subsequent resuspension in 500 µl of 0.01 M PBS. Thereafter, 1.25 µl of vancomycin (200 µg/ml) and 2.5 µl of fluorescent BODIPY-FL vancomycin (100 µg) were added to the cells followed by incubation at 37°C with shaking for 1.5 hours. Following this, 500 µl of 0.01 M PBS was used to wash the cells three times, the cells were then resuspended in a 100 µl of 0.01 M PBS. For visualization, 5 µl of the cells was spotted on glass slides with 2% agarose pads. The slides were visualized with the Zeiss Observer Z1 inverted fluorescence microscope and the images taken were analyzed with the ZEN lite software (Zeiss) and Fiji software (ImageJ). Any image manipulation (brightness, contrast, etc.) was applied to the entire image.

2.1.8.2. Click chemistry D-alanine analog staining

The click chemistry technique was also used for *in vivo* labeling of sites of new PG synthesis. The technique involves the incubation of cells with an alkyne-functionalized D-alanine analog which is incorporated into the PG during cell wall biosynthesis. This alkyne-functionalized D-alanine analog probe was obtained as a gift from Dr Sloan Seigrist (University of Massachusetts Amherat). The alkyne-functionalized D-alanine was visualized by reactions with click chemistry probes. For this, 1 µl of 1 mM alkyne functionalized D-alanine was added to harvested cells grown to an OD_{600nm} of 0.6 and resuspended in 2 ml of Middlebrook 7H9 broth. The cells were incubated for 2 hours at 37°C with shaking at 100 rpm. Subsequently, the cells were washed three times with PBSTB buffer (1× PBS, 0.05% BSA and 0.01% Tween20) and fixed for 10 minutes in 1 ml of 2% formaldehyde diluted in 1× PBS. Thereafter, the cells were centrifuged at 12 470 ×*g* for 5 ml and the supernatant was discarded. The click chemistry reaction was conducted as follows: 920 µl of PBSTB buffer was used to resuspend the cells and 20 µl of $CuSO_4$ (50 mM), 20 µl of TBTA (tris-(benzyltriazolylmethyl) amine) (6.4 mM), 20 µl of sodium ascorbate (60 mM) and 20 µl of an Azido probe (1 mM diluted in DMSO) were added in the order stated to the cells and mixed gently. The cells were incubated at room temperature for 45 minutes and subsequently washed three times with 1× PBS. Thereafter, 5µl of the cells was spotted onto glass slides which were visualized with the Zeiss Observer Z1 inverted fluorescence microscope and the images taken were analyzed with the ZEN lite software (Zeiss) and the Fiji software (ImageJ). Any image manipulation (brightness, contrast etc.) was applied to the entire image.

2.1.8.3. Peptidoglycan staining with fluorescent D-Alanine amino acids (FDAAs) and fluorescent peptide mimics

The PG stains; FDAAs (TADA [TAMRA-D-Alanine] and HADA [HCC-D-Alanine]) and fluorescent peptide mimics (TetraFL-1 and TetraFL-2) provided by collaborators (Michael VanNieuwenhze [Indiana University Bloomington, USA] & Marcos Pires [Lehigh University, USA], respectively) were used to probe PG remodeling and biosynthesis during growth, respectively. Briefly, the cells were grown in 5 ml of Middlebrook 7H9 broth supplemented with appropriate antibiotics to an OD_{600nm} of 0.6 and harvested by centrifugation at 12 470 ×*g*. The

cells were then resuspended in 2 ml of Middlebrook 7H9 broth, 2 µl of the FDAA stain or 1 µl peptide mimic stain was added to the cells and incubated at 37°C for 20 minutes. Subsequently, the cells were washed twice with 1× PBS, harvested by centrifugation at 12 470 ×*g* and resuspended in 50 µl of 1× PBS. Thereafter, 5 µl of the cells was spotted onto glass slides which were visualized with the Nikon TI20 and the Fiji software (ImageJ). Any image manipulation (brightness, contrast etc.) was applied to the entire image.

2.1.9. Flow cytometric analysis of stained mycobacterial cells

Flow cytometry was used for analysis of the labeling pattern of *M. smegmatis* mc^2155, Mtb H37Rv and *M. bovis* BCG in comparison to the genetically modified strains. Cells were grown in 5 ml of Middlebrook 7H9 broth supplemented with appropriate antibiotics at 37°C with shaking to an OD_{600nm} of 0.6. Thereafter, 200 µl of labeled cell cultures were transferred to a 96 well plate (Thermo Scientific). The CytoFLEX flow cytometer (Beckman Coulter) was used for analysis of the labeled cells.

2.1.10. Protein structure prediction

I-TASSER (http://zhanglab.ccmb.med.umich.edu/I-TASSER/). The Iterative Threading ASSEmbly Refinement (I-TASSER) server is a protein threading and protein function prediction tool. This tool was used for the threading and functional prediction of the mycobacterial MurT 52,.

2.1.11. Protein structure super-imposition

The FATCAT (Flexible structure AlignmenT by Chaining Aligned fragment pairs allowing Twists) server (http://fatcat.sanfordburnham.org/fatcat/) is a protein structure comparison tool. This tool was used for the comparison of the tertiary structures of the identified proteins.

2.1.12. Two-step allelic exchange homologous recombination method for generation of *M. smegmatis* mutant strains

The two-step allelic exchange homologous recombination method (Fig. 2.1) (104), was used for gene deletion in *M. smegmatis* mc^2155. Briefly, a mutant allele of the gene of interest is generated by ligation of upstream and downstream regions of the gene. The mutant gene is cloned into a suicide

plasmid and the selectable marker genes *lacZ* and *sacB,* encoding beta-galactosidase and levansucrase, respectively, were excised from the plasmid pGOAL17 and cloned into the suicide plasmid carrying the mutant gene. The resultant plasmid construct was electroporated into *M. smegmatis* as described in section 2.1.6.1. The suicide plasmid integrates into the chromosome through either upstream or downstream regions of homology to generate a single cross-over (SCO) strain which is Kan-resistant and forms blue colonies on media supplemented with 2% Xgal (as a result of expression of *lacZ*). Thereafter, the SCO strain was grown to stationary phase in 5 ml of Middlebrook 7H9 broth supplemented with Kan (25 g/ml). Subsequently, a 100 µl aliquot of this SCO culture was inoculated into 5 ml of Middlebrook 7H9 broth without antibiotic supplementation and grown to stationary phase to allow for a second cross-over event resulting in knockout of the wildtype gene in some cells. The *sacB* marker allows for counter-selection on Middlebrook 7H10 supplemented with sucrose, resulting in the production of levans which are toxic to bacteria that have not released the suicide plasmid during growth in Middlebrook 7H9 broth without antibiotic supplementation. Cells in which a second cross-over event occurred form white colonies that survived on Middlebrook 7H10 agar supplemented with 5% sucrose and 2% X-gal. These colonies were picked, resuspended in 25 µl Middlebrook 7H9 broth and spotted onto Middlebrook 7H10 agar with or without Kan (25 g/ml) supplementation. Colonies that do not grow on media supplemented with Kan were screened using PCR to identify the mutants.

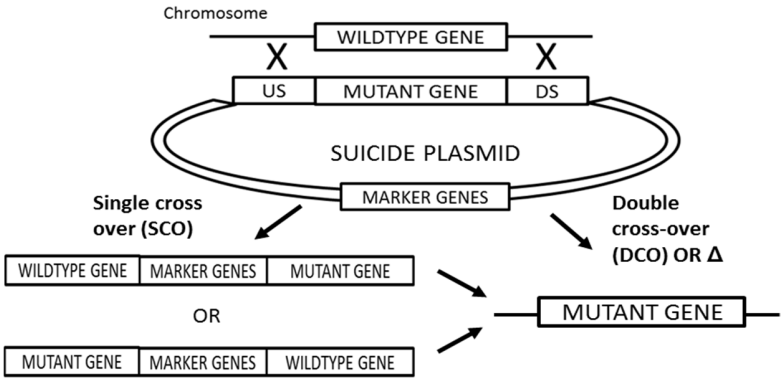

Figure 2.1. **Allelic replacement by homologous recombination**. Shown is how a suicide plasmid (i.e. non-replicating) carrying a mutated allele of the gene interest is introduced into the bacteria to facilitate homologous recombination which results in either single cross-overs (SCOs), where a single recombination event has occured or double cross-overs (DCOs) where two recombination events have occurred. SCOs carry both wild-type and mutated alleles of the gene of interest and marker genes found on the plasmid. DCOs will carry one copy of the gene of interest and no marker genes.

CHAPTER 3:

(Amidation of glutamate in mycobacterial peptidoglycan is essential for cell wall cross-linking)

3.1. Introduction

Peptidoglycan (PG) is a heteropolymer composed of glycan strands made up of alternating units of *N*-acetylglucosamine (Glc*N*Ac) linked to *N*-acetylmuramic acid (Mur*N*Ac) cross-linked by stem peptide attached to the lactyl moiety of Mur*N*Ac (105). PG biosynthesis is initiated in the bacterial cytoplasm, where the PG precursor lipid II is constructed by cytoplasmic PG biosynthesis enzymes as discussed in section 1.1.3.5. This involves introduction of several modifications on lipid II that enable transport to the periplasm and incorporation of lipid II into existing PG (Fig. 3.1). In mycobacteria, these modifications include hydroxylation of Mur*N*Ac to Mur*N*Glyc, amidation of the α-carboxyl group of D-glutamate in the pentapeptide stem of lipid II and the ε-carboxyl group of *meso*-DAP (106). These modifications are required for binding by periplasmic PG biosynthetic enzymes which incoroporate lipid II into PG through transglycosylation and transpeptidation reactions (105). The transpeptidation reactions form either 4-3 crosslinks (D-alanine-*meso*-DAP, by D,D-transpeptidases) or 3-3 crosslinks (*meso*-DAP-*meso*-DAP, by LDTs) between adjacent stem peptides (105). In mycobacteria, the 3-3 cross-links constitute the majority of PG cross-links and are required for the maintenance of cell wall integrity (107). The Mur*N*Ac residues are further modified by addition of an alpha-L-rhamnopyranose-(1-3)-alpha-D-NAG-(1-P) unit that links PG to arabinogalactan (105). Considering the requirement of lipid II pentapeptide stem amidation for incorporation lipid II into the existing PG, the enzymes required for PG amidation are attractive targets for TB drug development.

Recently, it was demonstrated that lack of lipid II amidation inhibits PG cross-linking by PG transpeptidases and sensitizes bacteria to β-lactam antibiotics, lysozyme and immunological detection during infection (108). Ldt_{FM} and Ldt_{MT2} of *E. faecium* and Mtb respectively, are not able to use PG stem peptide derivatives with non-amidated D-Glu and non-amidated *meso*-DAP as substrates for PG biosynthesis (108). We have recently demonstrated that synthetic PG stem peptide mimics with D-isoGlu amidation (D-isoGlu, when amidated forms D-isoGln) can be used to assay PG cross-linking in mycobacteria, highlighting the importance of D-isoGln in lipid II for PG cross-linking in mycobacteria (82). Furthermore, depletion of AsnB, a glutamate amidotransferase required for *meso*-DAP amidation in Mtb was shown to cause cell death as a

result of defective PG cross-linking (108). Similarly, LtsA functions as a *meso*-DAP amidotransferase in corynebacteria. Deletion of LtsA causes reduced PG cross-linking and

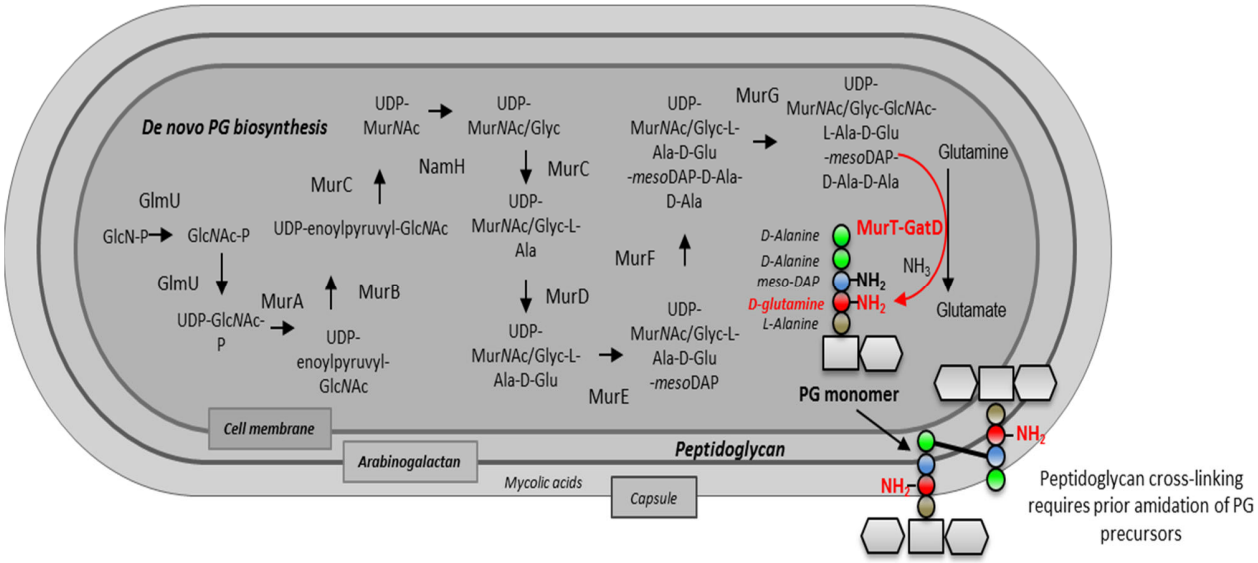

Figure 3.1. **Peptidoglycan biosynthesis in mycobacteria and peptidoglycan monomer (lipid II) amidation by the MurT-GatD complex**. Shown is the *de novo* PG biosynthesis process. Prior amidation of D-glutamate by the MurT-GatD complex (shown in **red** text) using glutamine as the substrate is required to enable PG cross-linking during PG biosynthesis.

amidation of D-glutamate was recently shown to be facilitated by the essential amidotransferase MurT-GatD complex in *Staphylococcus aureus* and *Streptococcus pneumoniae* (80, 109). The MurT-GatD complex catalyzes D-glutamate amidation using L-glutamine as an amine donor (110), resulting in the conversion of the L-glutamine substrate into D-glutamate and an amide group (NH_3) which is shuttled from the GatD glutaminase active site to the MurT amidotransferase active-site. Through an ATP-dependent reaction, MurT catalyzes lipid II amidation by transferring the NH_3 to the D-glutamate on the PG precursor lipid II, thus creating D-glutamine (Fig. 3.1) (110, 111).

In this chapter, we show that depletion of MurT and GatD in mycobacteria causes cell growth cessation due to decreased MurT-GatD function (i.e. reduced lipid II amidation) and consequent reduced PG cross-linking using the model organism *M. smegmatis* mc^2155.

With the use of fluorescent tetrapeptide probes (Amidated; Tetramethylrhodamine [TAMRA]-L-Ala-D-isoGln-L-lysine-D-Ala and non-amidated; TAMRA-L-Ala-D-Glu-L-lysine-D-Ala), we confirm that D-isoGln is required for probe incorporation into mycobacterial cells (112). We also show that, fluorescent protein tagged MurT (MurT-GFP) localizes at the cell poles and also at the cell division septum together with mRFP-GatD which interact as confirmed by a protein-protein interaction assay to form a PG amidation complex. Interestingly, through time-lapse microscopic analysis of MurT-GFP localization in FDAA labeled mycobacterial cells during cell growth, we find that MurT-GFP localizes with maturing PG, which is remodelled during cell growth by LDTs and strengthened by sidewall repair processes (83).

Depletion of MurT and GatD causes reduced PG cross-linking, growth cessation, increased sensitivity to glycopeptide and β-lactam antibiotics. Furthermore, we demonstrate that cell growth cessation as a result of MurT-GatD depletion is due to a coordinated shut-down of PG biosynthesis mediated by the serine/threonine protein kinase B (PknB) which senses uncross-linked PG and relays signals to stop PG biosynthesis by cytoplasmic PG biosynthesis enzymes. Considering this, we propose a model in which PG precursor amidation is required for PG polymerization and the level of PG cross-linking is surveyed by the essential serine/threonine protein kinase – PknB and resulting in a signaling cascade for regulation of cell growth. Collectively, these data add to the understanding of how mycobacteria synthesize PG and regulate cell growth and we identify the mycobacterial MurT-GatD complex as a new drug target.

The hypothesis, aims and objectives of this chapter are outlined below.

3.2. Hypothesis

MurT and GatD are essential for PG cross-linking and cell growth in mycobacteria and inhibiting the expression thereof will cause inhibition of PG cross-linking, cessation of cell growth together with consequent effects on cell wall stability.

3.3. Aims

The aim of this section is to identify and characterize the enzymes required for D-Glutamate amidation during PG biosynthesis in mycobacteria and to document the phenotypic effects of inhibition of PG amidation in mycobacteria using the model organism *M. smegmatis* mc^2155.

3.4. Objectives

1. Bio-informatics analysis of the mycobacterial genome to identify putative MurT and GatD enzymes.
2. Construction of a CRISPRi based *M.smegmatis* mc^2155 MurT-GatD depletion strain.
3. Assess growth of the MurT-GatD depletion strain and derivative strains through single cell time-lapse microscopy.
4. Assess the importance of MurT-GatD mediated PG amidation for PG cross-linking.
5. Assess the localization of MurT-GFP and mRFP-GatD in live cells.
6. Assess the localization & phosphorylation state of PknB in MurT-GatD depleted cells
7. Assess the lysozyme and β-lactam antibiotic susceptibility of MurT-GatD depleted mycobacterial cells.

3.5. Methods

3.4.1. Construction of the *M. smegmatis* MurT-GatD depletion strain

The programmable mycobacterial CRISPRi system for repression of gene transcription was used as previously described to investigate the role of the MurT-GatD amidotransferase complex in mycobacterial cell wall biosynthesis (113). Briefly, the CRISPRi system utilizes a catalytically-inactivated anhydrotetracycline (ATc) inducible dead endonuclease (dCas9) from *Streptococcus thermophiles* which is directed by a ATc inducible short-guide RNA (sgRNA) to specific target genes to prevent transcription initiation or elongation (Fig. 3.2) (113). A sgRNA targeting the promoter region of the *murT-gatD* (MSMEG_6276-MSMEG_6277) operon was synthesized by annealing two oligos listed in Table A1, which were cloned into BsmBI-digested CRISPRi vector PLJR962 in proximity to the dCas9 endonuclease handle to assemble the sgRNA. The protospacer adjacent motif (PAM) sequence and designed sgRNA used for CRISPRi are listed in Table A2 and shown in Appendix 3.1. The CRISPRi construct expresses the dCas9 endonuclease and contains the sgRNA backbone. The cloning of the annealed sgRNA oligos into the BsmBI-digested CRISPRi vector PLJR962 was performed as described in section 2.4.1.7 and the clone was amplified in *E. coli* as described in section 2.1.5.2. This plasmid was introduced into *M. smegmatis* mc^2155 as outlined in section 2.1.6.1.

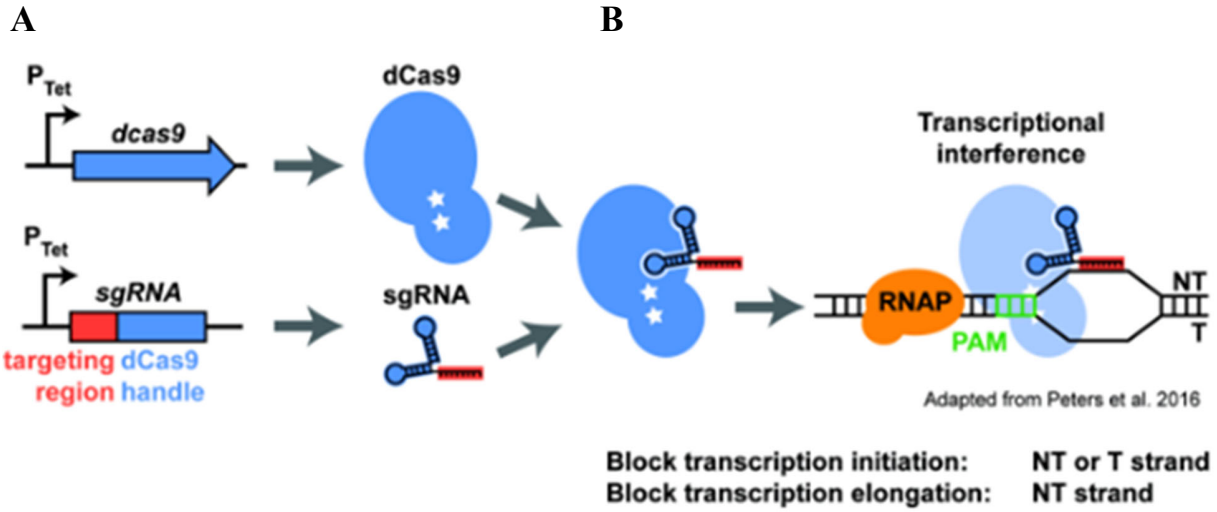

Figure 3.2. **Schematic of the CRISPRi mechanism in bacteria**. (A) Anhydrotetracycline (ATc)-inducible (P_{Tet}) dCas9 is directed to specific DNA targets by ATc-inducible sgRNA, which then prevents transcription initiation or elongation (B). RNAP: RNA polymerase; NT: non-template; T: template. This figure was taken from Rock et al. 2017 (113).

3.4.2. Construction of the *M. smegmatis* MurT-GFP and mRFP-GatD localization strain and the PknB phosphorylation reporter strain

A MurT-GFP fusion was constructed by cloning wildtype *murT* (MSMEG_6276) with 100 bp upstream of the gene (i.e. including the promoter region) into plasmid pMV306H-GFP for C-terminus tagging and the resulting plasmid (pMV306H+MurT-GFP) was electroporated into wildtype *M. smegmatis* mc^2155 as indicated in section 2.1.6.1. mRFP-GatD was constructed by cloning wildtype *gatD* (MSMEG_6277) into plasmid pTweety-mRFP for N-terminus tagging and the resulting plasmid (pTweety+mRFP-GatD) was electroporated into wildtype *M. smegmatis* mc^2155 as indicated in section 2.1.6.1.

3.4.3. Mycobacterial protein fragment complementation (M-PFC) system

The mycobacterial protein fragment complementation (M-PFC) system (114) was used as previously described to test the interaction of the predicted potential interacting partners for a protein of interest (Fig. 3.3).

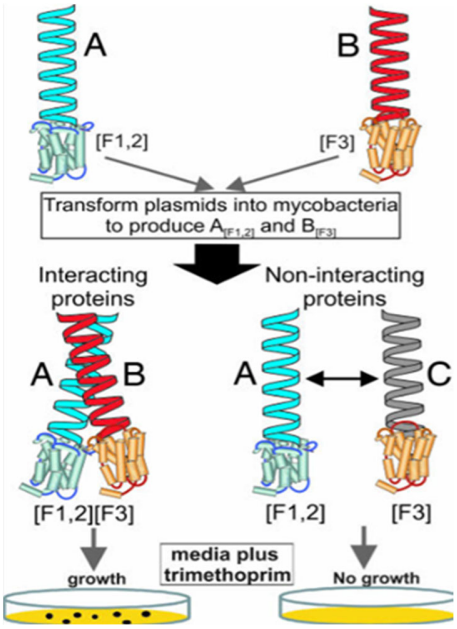

Figure 3.3. **Schematic of the M-PFC assay**. Interacting proteins A and B are fused to complementary mDHFR fragments F[1,2] and F[3]. Cotransformation of AF[1,2] and BF[3] fusions in mycobacteria results in the functional reconstitution of mDHFR activity and subsequent growth on TRIM plates, whereas proteins that do not interact (A and C) will not reconstitute F[1,2] and F[3] and will not allow transformants to survive on TRIM plates. This figure was taken from Singh et al. 2006 (114).

Briefly, the M-PFC system is based on the functional reconstitution of the two murine dihydrofolate reductase (mDHFR) domains, fused independently to two putative interacting proteins. The interaction between the two proteins of interest results in the reassembly of the two mDHFR domains into a functional enzyme, which confers resistance to Trimethoprim (Trim at 7.5 μg/ml) (Fig. 3.3). The ORFs of the genes of interest were cloned separately into plasmids pUAB400 and pUAB300. Thereafter, the plasmids were electroporated into wildtype *M. smegmatis* according to the protocol outlined in section 2.1.6.1. The resultant colonies were picked, resuspended in 50 μl of Middlebrook 7H9 broth, inoculated onto Middlebrook 7H10 agar supplemented with kan (25 g/ml), hyg (50 g/ml) and Trim (7.5 g/ml), and grown at 37ºC for 5-7 days. For MPFC system controls; the *M. smegmatis* mc^2155 derivative strain mc^2155::F[1,3]-RpfB+F[2]-RipA was used as a positive control based on proven interaction between MSMEG_5439 (RpfB) and MSMEG_3145 (RipA) (115) and the strain mc2::pUAB300+pUAB400 (plasmid only control) was used as a negative control.

3.4.4. Cell envelope labeling

Fluorogenic probes used in this study include (i) Tetramethylrhodamine (TAMRA)-3-amino-L-alanine-D-glutamine-L-lysine-D-alanine (TetraFL-1), (ii) TAMRA-3-amino-L-alanine-D-glutamate-L-lysine-D-alanine (TetraFL-2), (iii) 3-[(7-Nitro-2,1,3-benzoxadiazol-4-yl)amino]-D-alanine hydrochloride (NADA), (iv) TAMRA-D-Alanine (TADA), (v) HCC-D-Alanine (HADA), (vi) Alkyne-D-Alanine-D-Alanine (AlkDADA) and (vii) BODIPY-FL vancomycin. A 1 ml culture of mid-exponential wildtype *M. smegmatis* mc^2155 was labeled with 5 mM TetraFL-1 or TetraFL-2 for 30 minutes and analyzed for probe incorporation by flow cytometry and fluorescence microscopy. Similarly, *M. smegmatis* mc^2155 derivative strains grown to exponential phase were labeled with 500 μM TADA and HADA and analyzed for probe incorporation by fluorescence microscopy and time-lapse fluorescence microscopy as described in sections 2.1.8.3 and 3.4.5. For AlkDADA labeling, wildtype *M. smegmatis* mc^2155 derivative strains grown to exponential phase were labeled with 2 mM AlkDADA and the probe was detected by click chemistry as described in section 2.1.8.2 and analyzed by fluorescence microscopy. For labeling with BODIPY-FL vancomycin, 1 ml exponential cultures of *M. smegmatis* mc^2155 and derivative strains were labeled with BODIPY-FL vancomycin for 3 hours

and analyzed by fluorescence microscopy and flow cytometry for probe incorporation as described in sections 2.1.8.1 and 2.1.9.

3.4.5. Time-lapse-microscopy

M. smegmatis mc^2155 derivative strains were grown in microfluidic devices and time-lapse microscopy experiments were carried out as previously described (116). Briefly, the bacterial cultures were grown to exponential phase in ink-well bottles at 37 °C. Clumps of bacteria were removed by concentrating the cells 10-fold and filtering through a 5 µm filter. The bacteria were seeded into a microfluidic device and imaged on a Delta vision Personal DV imaging system (GE HealthCare Life Sciences) using a 100× objective (Olympus Plan Semi Apochromat, 1.3 NA). The images were acquired at 10 min intervals using a CoolSnap HQ2 camera. Middlebrook 7H9 medium with or without 200 ng/mL ATc and also supplemented with FDAAs was circulated through the device at a flow rate of 25 µl/min. Images were analyzed and processed using Softworx 4.1 (Applied Precision, GE HealthCare) or ImageJ v 1.47n.

3.4.6. Atomic force microscopy (AFM)

Atomic force microscopy was performed as previously described (117). Briefly, coverslips were prepared by mixing polydimethylsiloxane (PDMS) (Sylgard 184, Dow Corning) at a ratio of 15:1 (elastomer:curing agent). Air bubbles in the mixture were removed under negative pressure for 15 min. The PDMS mixture was dropped onto a 22 mm glass coverslip (VWR) and spin-coated at 8,000 r.p.m. (SUSS MicroTec LabSpin6) for 30 s. PDMS-coated coverslips were baked at 80°C for 10 min before use. A 3 ml aliquot of mid-exponential phase cell culture was filtered through a 0.5 mm pore size PVDF filter (Millipore) to remove cell clumps and concentrated into 200 ml final volume by pelleting cells (2,400g, 8 min). A 50 µl aliquot was deposited on the hydrophobic surface of a PDMS-coated coverslip and incubated for 20 min to increase the surface interactions between bacteria and coverslip. Bacteria were imaged by a Peak Force QNM with a Nanoscope 5 controller (Veeco Metrology) at a scan rate of 0.5 Hz and a maximum Z-range of 5 µm. ImageJ was used for extracting bacterial cell profiles.

3.4.7. Ethidium bromide (EtBr) diffusion assay to monitor cell permeability

The EtBr diffusion assay was performed as previously described (118). Briefly, *M. smegmatis* mc^2155 derivative strains were grown to an $OD_{600nm} = 0.6$. Cultures were centrifuged at 4500 rpm for 10 minutes, the supernatant was discarded and the pellet washed in PBS. Thereafter, the pellet was resuspended in Middlebrook 7H9 containing 0.4% glucose and the OD_{600nm} was adjusted to 0.4. 95 µl aliquots of bacterial suspension were placed into flat bottom, black 96-well plates followed by addition of EtBr to a final concentration of 10 µg/mL. Fluorescence was measured with an excitation and emission wavelength of 530 nm and 585 nm respectively, every 60 seconds for 60 minutes at 37 °C.

3.4.8. Peptidoglycan extraction

PG was extracted as previously described (96). Briefly, wildtype *M. smegmatis* mc^2155 was grown to OD_{600nm} of 2 and the cells were then harvested by centrifugation at 3500 ×*g* for 10 min and resuspended in phosphate-buffered saline (PBS, pH 7.2). The cells were then lysed with a French press (Constant Systems). Insoluble material was obtained by centrifugation at 4000 ×*g* for 30 min. The pellet was then resuspended in PBS containing 2% SDS and incubated at room temperature for 1 h, then in PBS containing 2 mg/ml proteinase K and 2% SDS at 37°C for 24h and finally in PBS containing 2% SDS at 90°C for 1 h. The extracted cell wall material was lyophilized, weighed and stored at 4°C until further use.

3.4.9. Quantitative real-time PCR (qPCR)

qPCR was performed using Sso Fast Evagreen Supermix (BioRad) as per manufacturer's instructions. Briefly, 20 µl reactions were set up, each containing 10 µl Evagreen Supermix, 0.75 µl forward primer (10 µM), 0.75 µl reverse primer (10 µM), 2 µl cDNA and nuclease-free water. All reactions were incubated in the CFX96 Real-Time PCR detection system (BioRad) using the following parameters: 98 °C for 2 min followed by 39 cycles consisting of three steps – 98 °C for 5 sec, 60 °C for 5 sec and 72 °C for 5 sec with SYBR Green quantification at the end of each cycle. Melt curve analysis was conducted from 65 °C with a gradual increase in 0.5 °C increments every 0.05 sec to 95 °C with SYBR Green quantification conducted continuously throughout this stage. The raw data was analyzed using the Biorad CFX Manager 3.0 Software (BioRad).

3.5. Results

3.5.1. Identification of the mycobacterial MurT-GatD homologs

MurT and GatD homologs in Gram-positive bacteria are required for PG amidation and PG cross-linking (80, 109). Recently, the mycobacterial MurT-GatD complex was identified and biochemically characterized (119). In Mtb, the genes Rv3712-Rv3713 encode for the mycobacterial MurT-GatD homologs, respectively. Rv3712 and Rv3713 are predicted to be essential for *in vitro* growth of Mtb by Himar1 transposon mutagenesis and sequencing (Tn-Seq) and are highly conserved among mycobacteria (120, 121). Further bio-informatics analysis was performed to predict the tertiary structure of the mycobacterial MurT homolog as described in sections 2.1.10 - 2.1.11 and the results indicated that the mycobacterial enzyme is similar to *E. coli* murein peptide ligase (Mpl), required for PG recycling (Fig. 3.4A). However, Rv3712 lacks a N-terminal UDP-Mur*N*Ac binding domain suggesting that Rv3712 is involved in PG amidation rather than PG recycling (Fig. 3.4B).

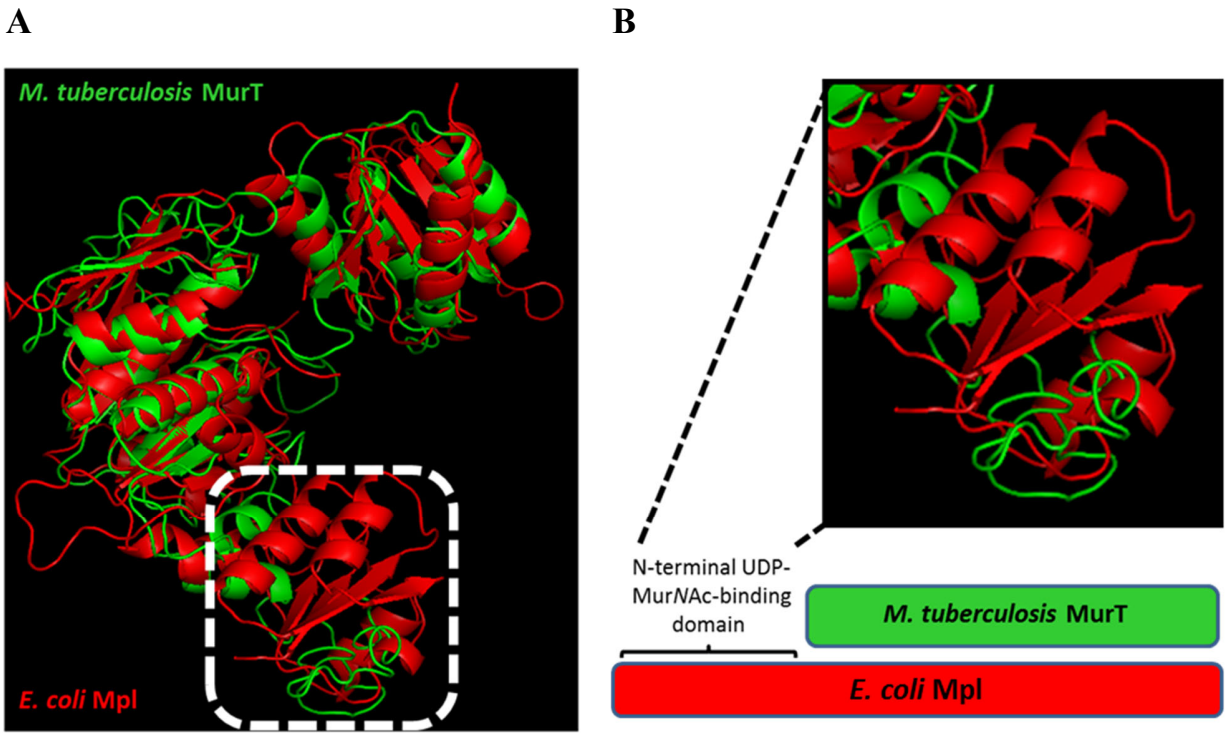

Figure 3.4. **Superimposition of Mtb MurT and *E. coli* Mpl**. (A) Full length protein superimposition of predicted Mtb MurT structure with predicted *E. coli* Mpl. (B) Mtb MurT lacks a UDP-Mur*N*Ac binding domain found in Mpl, a PG recycling enzyme.

To confirm *in vivo* that mycobacteria require PG amidation for PG cross-linking, a pair of fluorescent PG stem peptide mimics bearing either D-Glutamine (D-Gln) or D-Glutamate (D-Glu) at position 2 of a tetrapeptide probe (TetraFL-1 [amidated probe] and TetraFL-2 [non-amidated probe], respectively) were used to investigate the requirement of D-Glu amidation for PG cross-linking (Fig. 3.5) (82, 112). The approach involved adding these probes to growing mycobacterial cells. They should be incorporated into the PG through the activity of LDTs, if their chemical composition meets the requirement for the associated enzymes to recognize and incorporate them.

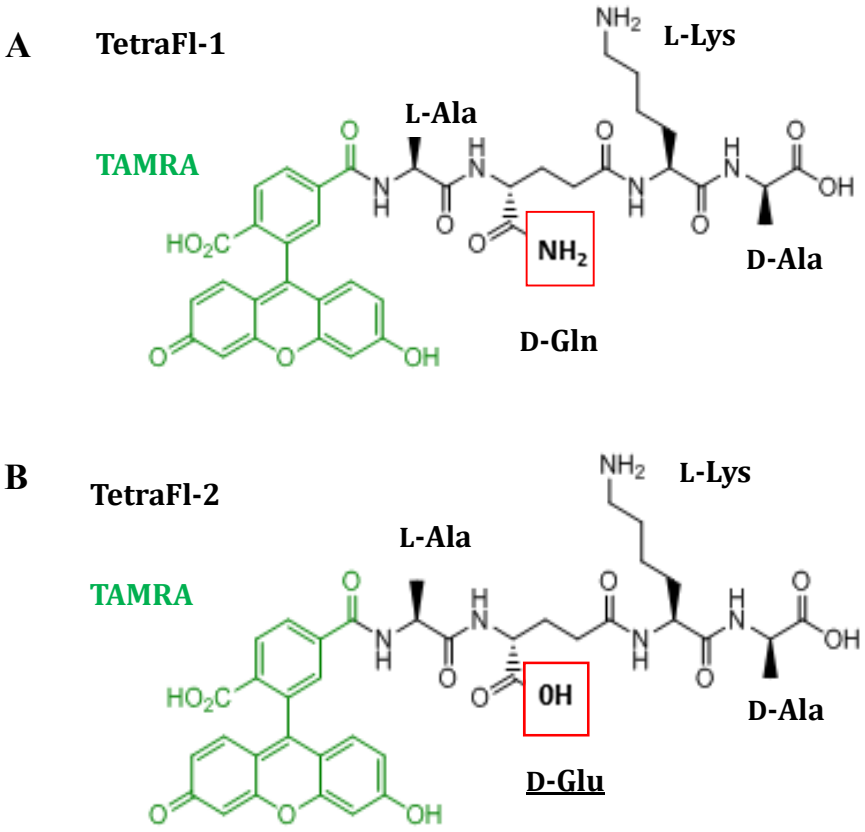

Figure 3.5. **Chemical structures of TetraFL-1 and TetraFL-2 PG stem peptide mimics. (**A) Shown is the chemical structure of Tetramethylrhodamine (TAMRA)-3-amino-L-alanine-D-glutamine-L-lysine-D-alanine (TetraFL-1). Red box shows the amide group of D-glutamine. (B) Shown is the chemical structure of Tetramethylrhodamine (TAMRA)-3-amino-L-alanine-D-glutamate-L-lysine-D-alanine (TetraFL-2). Red box shows the hydroxyl group of D-glutamate.

Microscopic analysis of cells labeled for 3 hours with these probes was performed and this demonstrated that D-Gln bearing tetrapeptide probes labeled *M. smegmatis* and Mtb cells, whilst the probe bearing D-Glu at position 2 was not incorporated (Fig. 3.6). Flow cytometry analysis of the labeled cells corrobarated the imaging results (Fig. 3.6). As some TetraFL-1 unlabeled Mtb cells were also observed (Fig. 3.6), probably due to the slow replication rate of Mtb because TetraFL-1 is incorporated into PG by LDTs during cell growth (82), we assessed labeling overtime from 30 minutes, 3 hours and 24 hours. We also included a pentapeptide probe (see appendix 3.2), which is incorporated into PG by PBPs, as a control. Microscopic analysis of the labeled Mtb cells revealed increased TetraFL-1 labeling with increasing time of labeling while the pentapeptide probe showed rapid incorporation into PG (Fig. 3.7A&C). Flow cytometry analysis of the labeled cells corrobarated the imaging results (Fig. 3.7B).

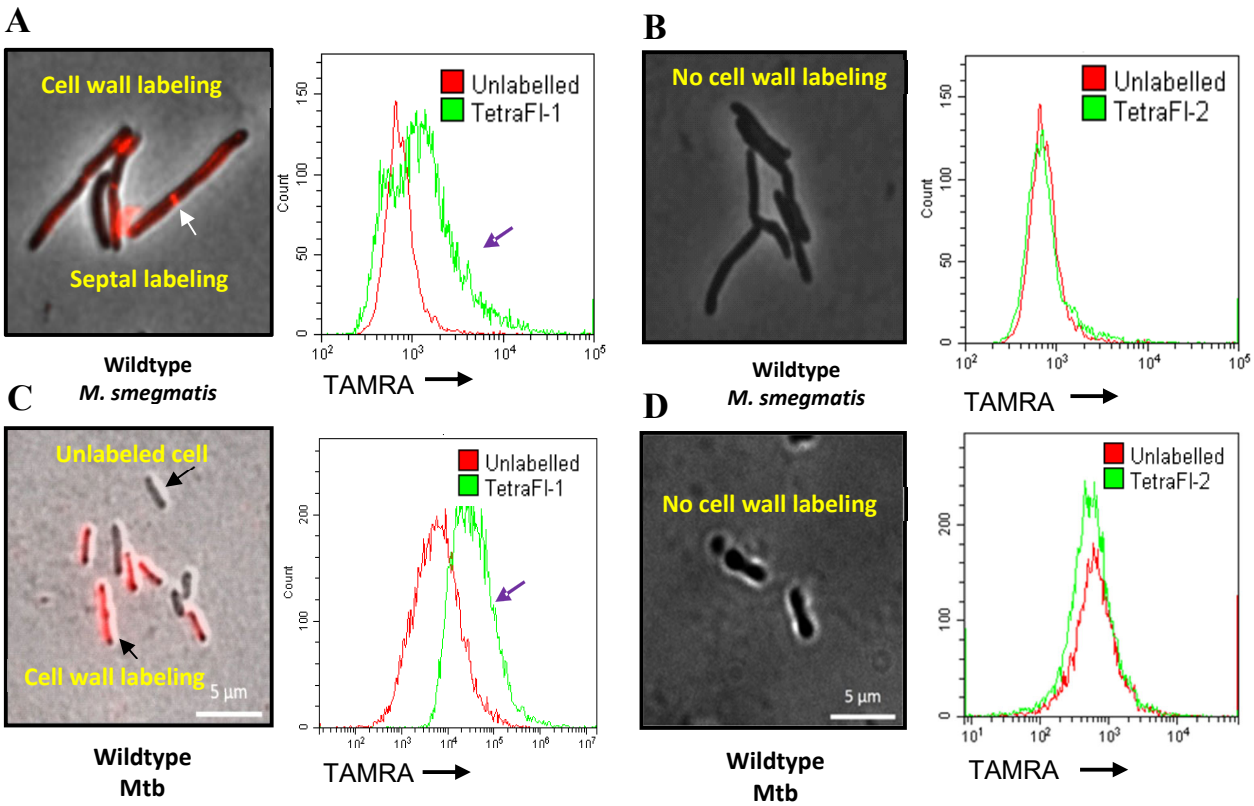

Figure 3.6. **Amidated peptidoglycan stem peptide mimics are incorporated into the mycobacterial cell wall.** (A&B) Micrographs and flow cytometry histographs of *M. smegmatis* mc^{2}155 and Mtb H37Rv labeled with the TetraFL-1 probe for 3 hours. The change in TAMRA fluorescence intensity during TetraFL-1 incorporation into PG is indicated by the purple arrow in the flow cytometry histograms. White arrow shows septal labeling with TetraFl-1. (C&D) Micrographs and flow cytometry histographs of *M. smegmatis* mc^{2}155 and Mtb H37Rv labeled with the TetraFL-2 probe for 3 hours. Cells did not label with TetraFL-2, indicating that the amidation at D-glutamine is required for probe incorporation.

Collectively, as the D-Glu bearing probe was not incorporated whilst the D-Gln was, these data confirmed that PG biosynthesis in mycobacteria requires prior D-Glu amidation (to create D-Gln) of PG precursors.

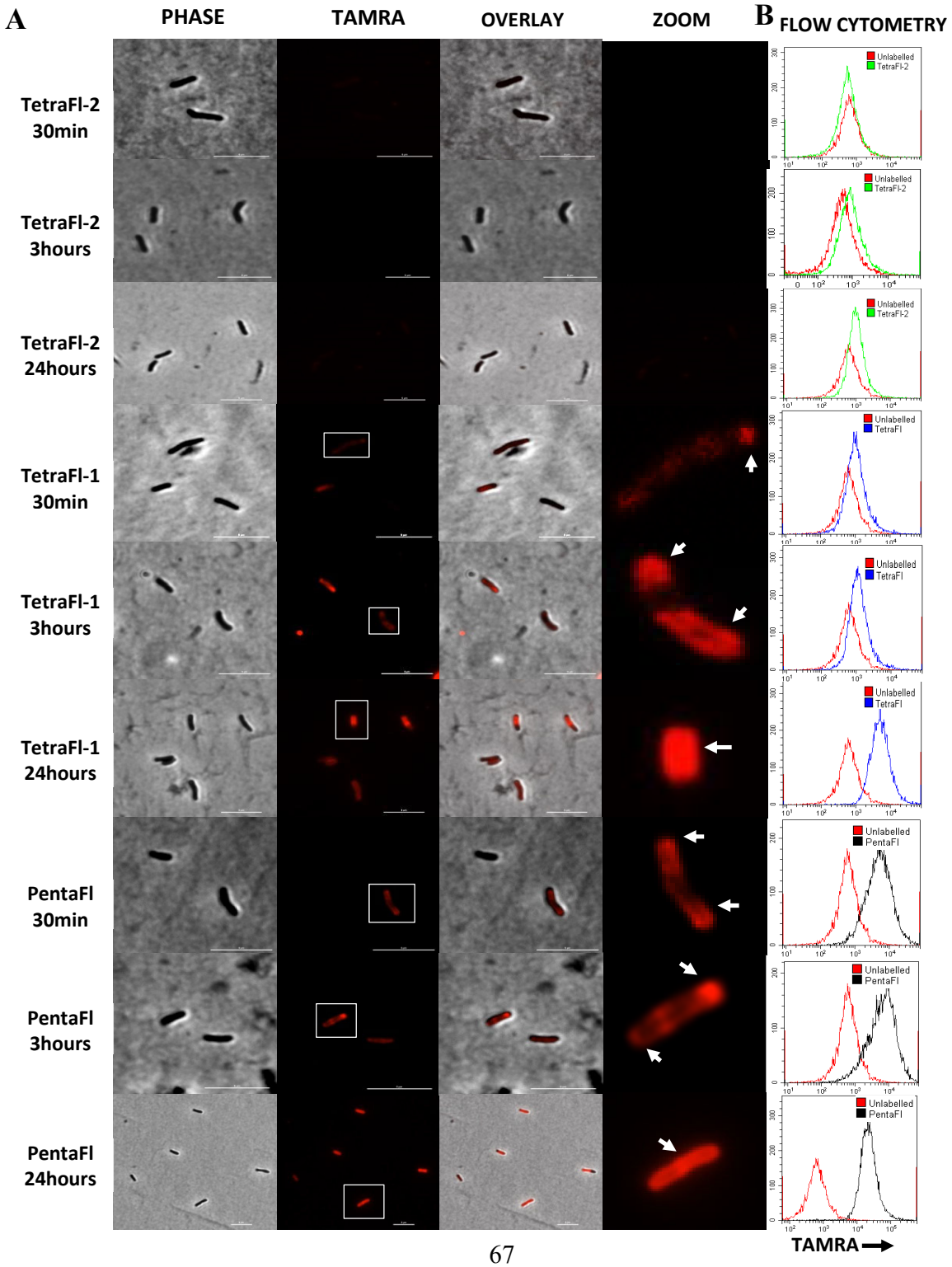

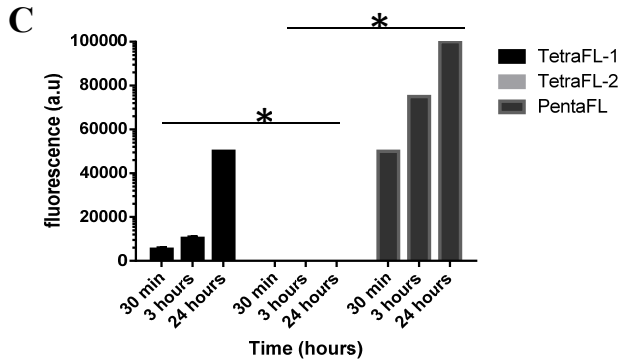

Figure 3.7. **Labeling of Mtb with TetraFL-1, TetraFL-2 and PentaFL over time to assess the rate of probe incorporation**. (A) Micrographs and flow cytometry histographs of Mtb H37Rv labeled with the TetraFL-1, TetraFL-2 and PentaFL probe for 30 min, 3 hours and 24 hours. (B) Flow cytometry histographs of MtbH37Rv labeled with the TetraFL-1, TetraFL-2 and PentaFL probe for 30 min, 3 hours and 24 hours. (C) Analysis of the fluorescence intensity of TetraFL-1, TetraFL-2 and PentaFL labeled cells. PentaFL probe is incorporated more rapidly than the TetraFl-1 probe. The student *t*-test was used to detect stastistical significance between labeled and unlabeled cells. * : p values of < 0.0001.

3.5.2. MurT-GFP and mRFP-GatD localize at sites of PG biosynthesis.

Given that the MurT-GatD bienzyme complex has been identified as essential for PG amidation in other organisms, we next analyzed the localization of MurT and GatD in mycobacteria as mycobacteria are known to spatially localize the major cell wall biosynthesis processes at the cell poles and septum (95, 122). Cell wall synthesis enzymes are recruited by DivIVA to the cell poles forming a complex of enzymes termed the elongosome, which facilitates polar cell wall synthesis (123). To investigate whether the MurT-GatD complex also localizes at sites of cell wall synthesis, we constructed an *M. smegmatis* strain, mc^{2}155::MurT-GFP+mRFP-GatD, by linking the native *murT* gene (MSMEG_6276) to GFP and native *gatD* gene (MSMEG_6277) to mRFP as indicated in section 2.1.7. Restriction profiling of the plasmid construct indicated the expected profile for the MurT-GFP construct and the mRFP-GatD construct (Fig. 3.8 & 3.9). The constructs were sequenced to confirm their integrity and then introduced into wildtype *M. smegmatis* mc^{2}155 as indicated in section 2.1.6.1 for generation of the MurT-GFP+mRFP-GatD localization strain and plasmids pMV306H-GFP and pTweety-mRFP were also introduced into wildtype *M. smegmatis* mc^{2}155 to create the GFP and mRFP only control strains, respectively. Microscopic analysis of the MurT-GFP+mRFP-GatD strain displayed that MurT-GFP and mRFP-GatD localize at the cell poles and the septum, the major sites of cell wall synthesis in mycobacteria while no localization was observed in the GFP-only or mRFP-only control strains (Fig. 3.10).

A

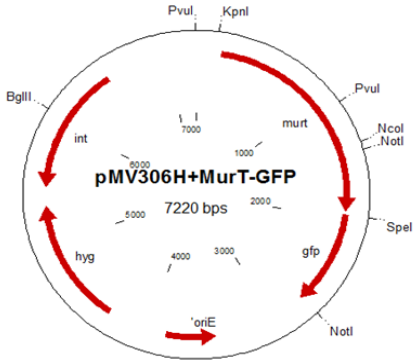

B

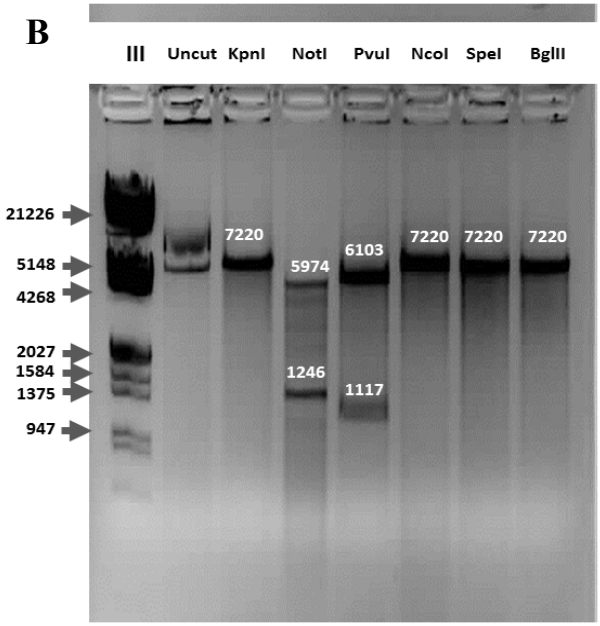

C

Restriction enzyme	Band sizes expected (bps)
KpnI	7220
NotI	5974, 1246
PvuI	6103, 1117
NcoI	7220
SpeI	7220
BglII	7220

Figure 3.8. **Restriction profile of plasmid pMV306H+MurT-GFP**. (A) Plasmid map of pMV306H+MurT-GFP. (B) Agarose gel showing the DNA bands sizes expected (labeled in base pairs [bps]). (C) Table indicating the restriction enzymes used for restriction analysis of pMV306H+MurT-GFP and the DNA band sizes expected. All expected band sizes were observed.

A

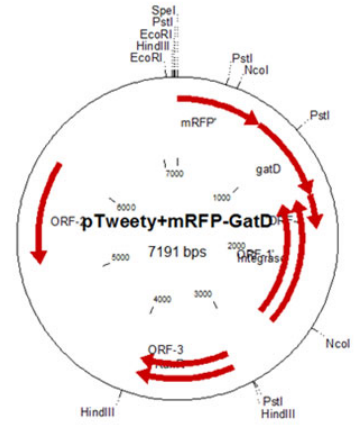

B

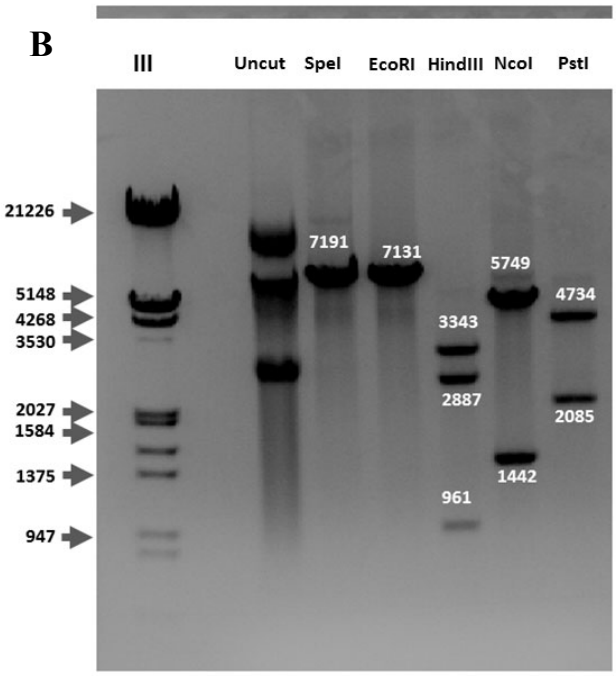

C

Restriction enzyme	Band sizes expected (bps)
SpeI	7191
EcoRI	7131, 60
HindIII	3343, 2887, 961
NcoI	5749, 1442
PstI	4734, 2085, 372

Figure 3.9. **Restriction profile of plasmid pTweety+mRFP-GatD**. (A) Plasmid map of pTweety+mRFP-GatD. (B) Agarose gel showing the DNA bands sizes expected (labeled in base pairs). (C) Table indicating the restriction enzymes used for restriction analysis of pTweety+mRFP-GatD and the DNA band sizes expected. All expected band sizes were observed.

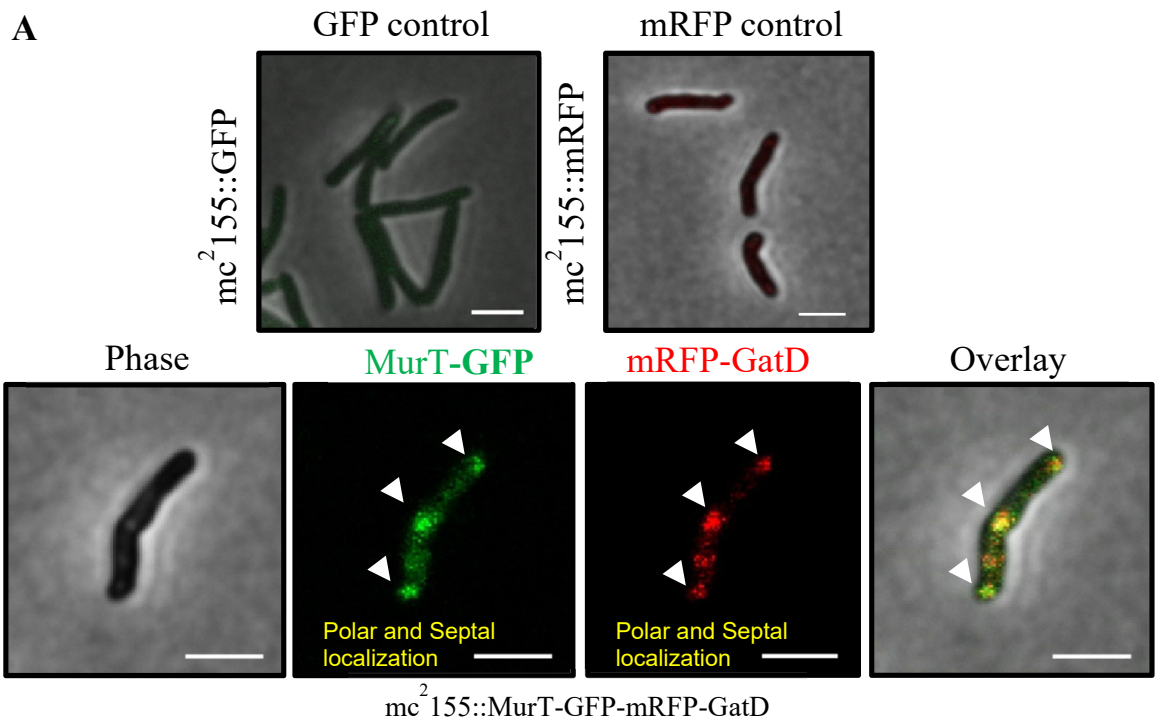

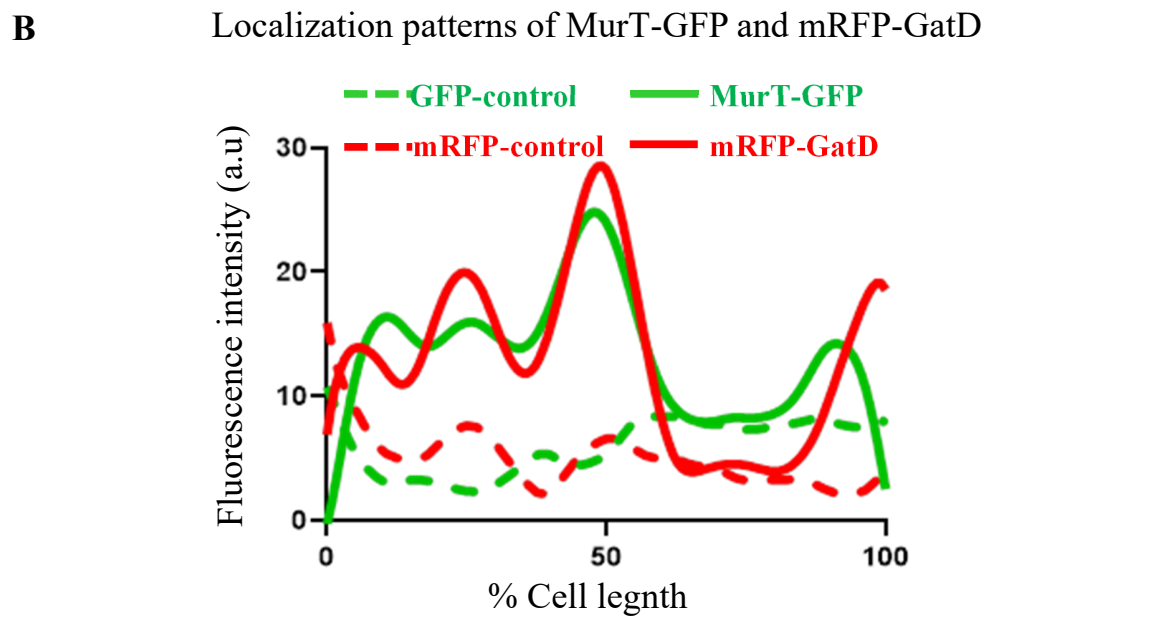

Figure 3.10. **MurT-GFP and mRFP-GatD localize at cell poles. (A)** Micrographs showing MurT-GFP and mRFP-GatD localization at the cell poles and septum. ~90%-95% (n=100) of cells displayed this localization pattern. (B) Localization patterns of MurT-GFP and mRFP-GatD in *M. smegmatis*.

3.5.3. MurT interacts with GatD to form the MurT-GatD amidotransferase complex.

To confirm the interaction of MurT and GatD in mycobacteria, the mycobacterial protein fragment complementation assay was used to further assay this interaction as described in section 3.4.3. MurT and GatD were both linked on the N-terminus to the F[1,3] and F[2] fragments of the murine dehydrofolate reductase, respectively. Restriction profiling of the plasmid constructs indicated the expected profiles (Fig. 3.11 and Fig. 3.12). The constructs were sequenced and then introduced into wildtype *M. smegmatis* mc^{2}155 as indicated in section 2.1.6.1. The interaction of F[1,3]-MurT and F[2]-GatD allowed the carrier strain (mc^{2}155::F[1,3]-MurT+F[2]-GatD) to grow on trimethroprim similar to a previously generated positive control strain (mc^{2}155:: F[1,3]-RpfB+F[2]-RipA) which shows growth in this assay due to RpfB and RipA interaction (115) at an MIC higher than that of a wildtype plasmids–only control strain (Fig. 3.13)**.** This data confirms that mycobacterial MurT and GatD interact to form the PG amidation amidotransferase complex.

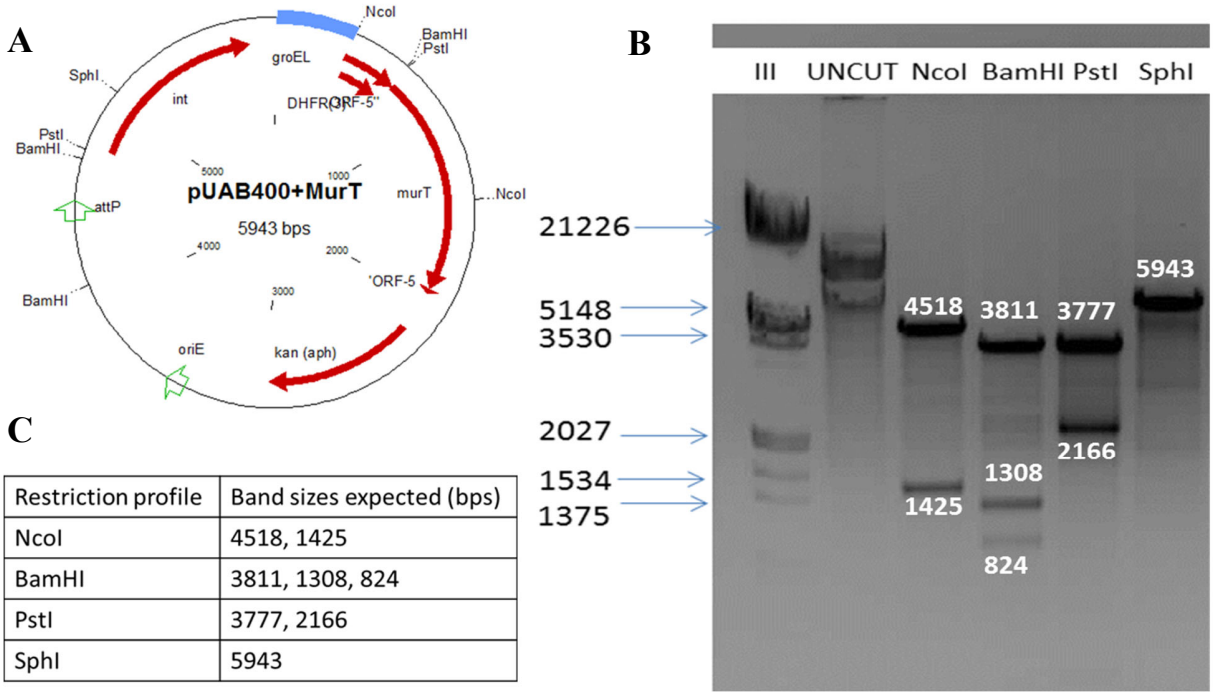

C

Restriction profile	Band sizes expected (bps)
NcoI	4518, 1425
BamHI	3811, 1308, 824
PstI	3777, 2166
SphI	5943

Figure 3.11. **pUAB400+MurT restriction profile.** (A) Plasmid map of pUAB400+MurT. (B) Agarose gel showing the DNA bands sizes expected (labeled in base pairs). (C) Table indicating the restriction enzymes used for restriction analysis of pUAB400+MurT and the DNA band sizes expected. All expected band sizes were observed.

A

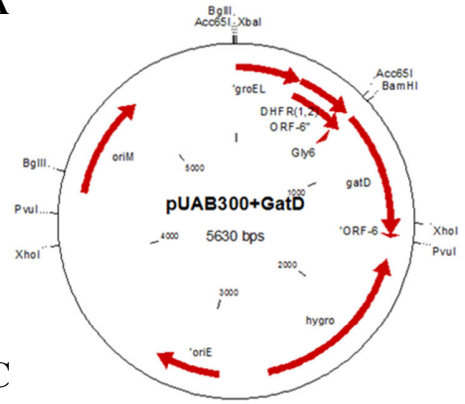

B

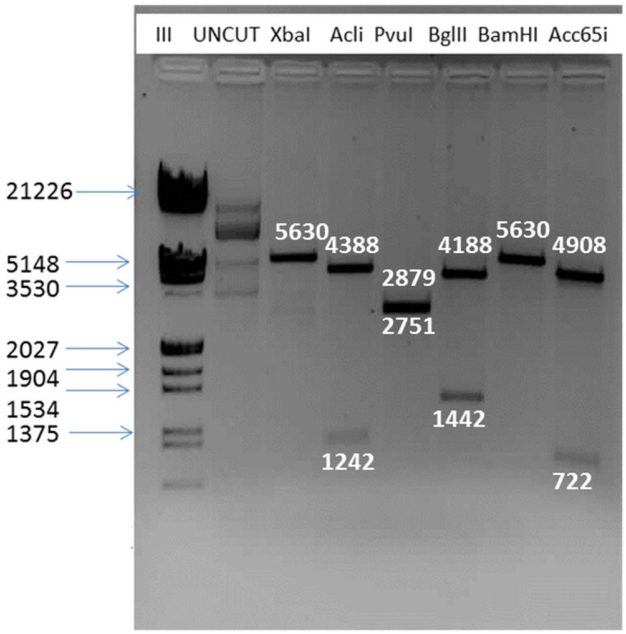

C

Restriction enzyme	Band sizes
XbaI	5630
AclI	4388, 1242
PvuI	2879, 2751
BglII	4488, 1142
BamHI	5630
Acc65i	4908, 722

Figure 3.12. **pUAB300+GatD restriction profile.** (A) Plasmid map of pUAB300+GatD. (B) Agarose gel showing the DNA bands sizes expected (labeled in base pairs). (C) Table indicating the restriction enzymes used for restriction analysis of pUAB300+GatD and the DNA band sizes expected. All expected band sizes were observed.

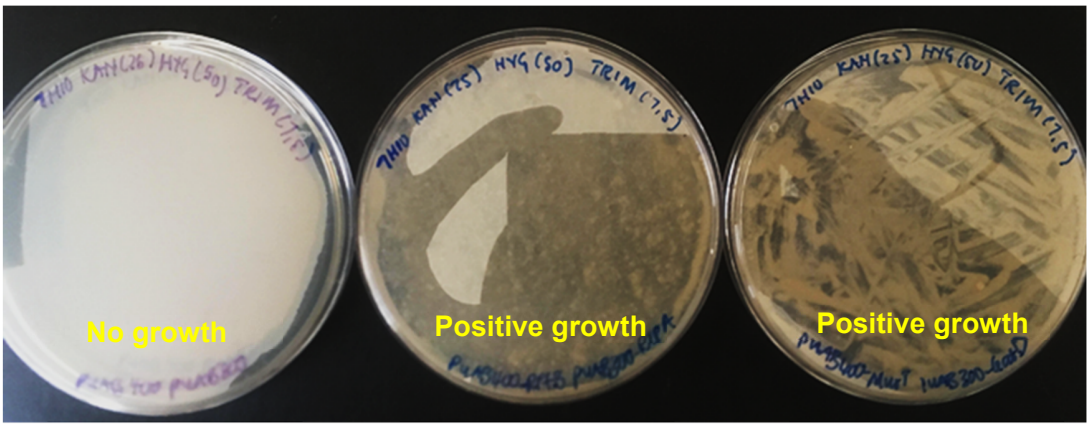

Figure 3.13. **M-PFC assay for MurT-GatD interactions.** Plasmids pUAB400+MurT and pUAB300+GatD were introduced into *M. smegmatis* to create the strain mc^{2}155::F[1,3]-MurT+F[2]-GatD. The interaction of MurT and GatD was assayed by growth of the carrier strain on trimethroprim. Growth of the carrier strain on trimethroprim is indicative of the interaction of MurT and GatD. The strain mc^{2}155::F[1,3]-RpfB+F[2]-RipA was used as a positive control and the mc^{2}155::F[1,3] +F[2] (plasmids only control) was used as the negative control.

3.5.4. MurT-GFP co-localizes with maturing peptidoglycan during cell growth

Recent studies suggest that PG remodeling/repair also involves remodeling of side-wall PG (Fig. 3.14) (83, 124). We hypothesized that incorporation of PG precursors into the side-wall for remodeling would also require prior amidation by the MurT-GatD complex. To investigate this, spatio-temporal localization of MurT-GFP during cell growth was monitored by time-lapse microscopic growth analysis of MurT-GFP cells labeled with a FDAA probe during growth. The MurT-GFP strain was labeled with TADA during time-lapse microscopy and the localization of MurT-GFP was assessed over-time.

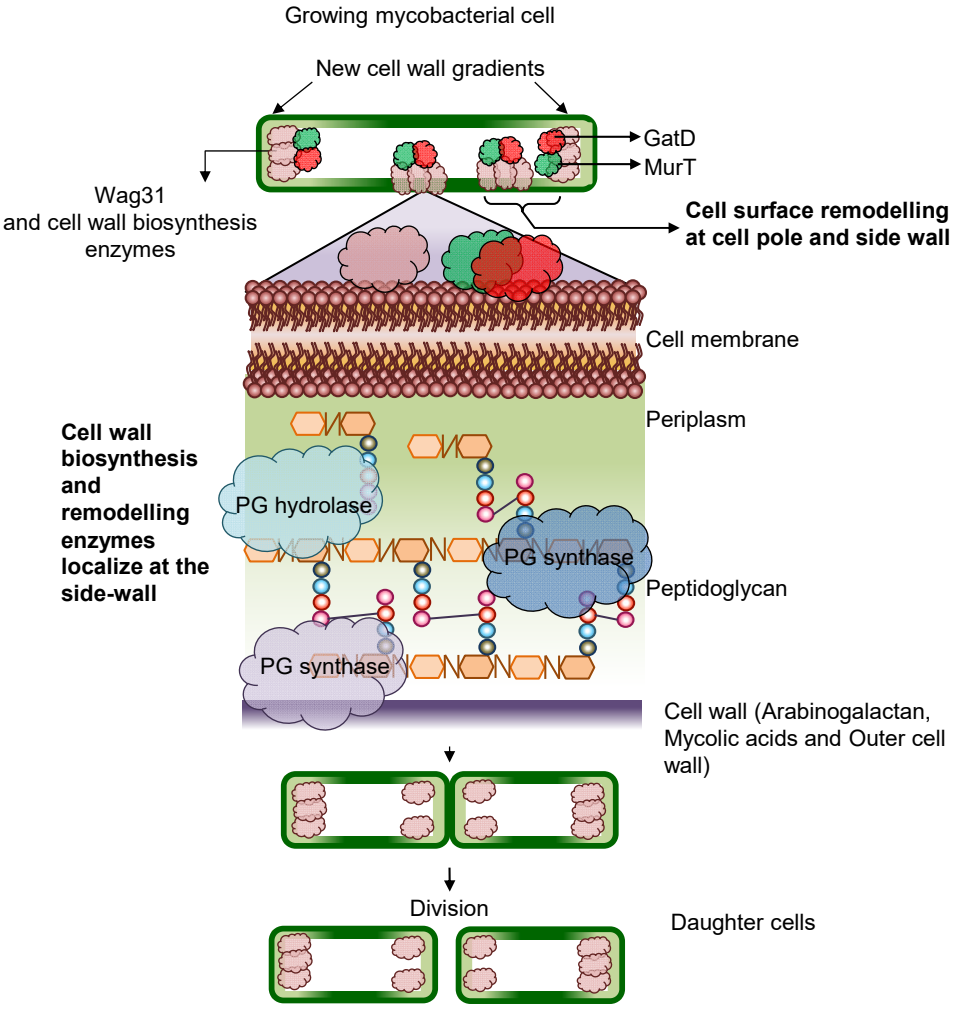

Figure 3.14. **Mycobacterial cell growth involves sidewall remodeling of maturing PG.** Cell pole elongation in mycobacteria involes the localization of Wag31 at the cell poles which recruits cell wall biosynthesis enzymes at the cell poles. During mycobacterial cell growth, sidewall PG is remodelled by PG hydrolases and PG biosynthesis enzymes, a process we propose involves PG precursor amidation prior to incorporation into mature PG.

Initial analysis revealed the labeling of the cell poles and septum with TADA and MurT-GFP localization was observed at the cell poles and cell septum. As the cells expanded the TADA label was detected at the side-wall (representing mature PG) and the MurT-GFP fluorescence signal was observed at the cell poles, septum and also at the side-wall, where it co-localized with the TADA label representing maturing PG (Fig. 3.15, Appendix 3.3). This suggested that PG remodeling at the side-wall also features cytoplasmic MurT-GatD facilitated PG precursor amidation.

TADA labeling and MurT-GFP localization

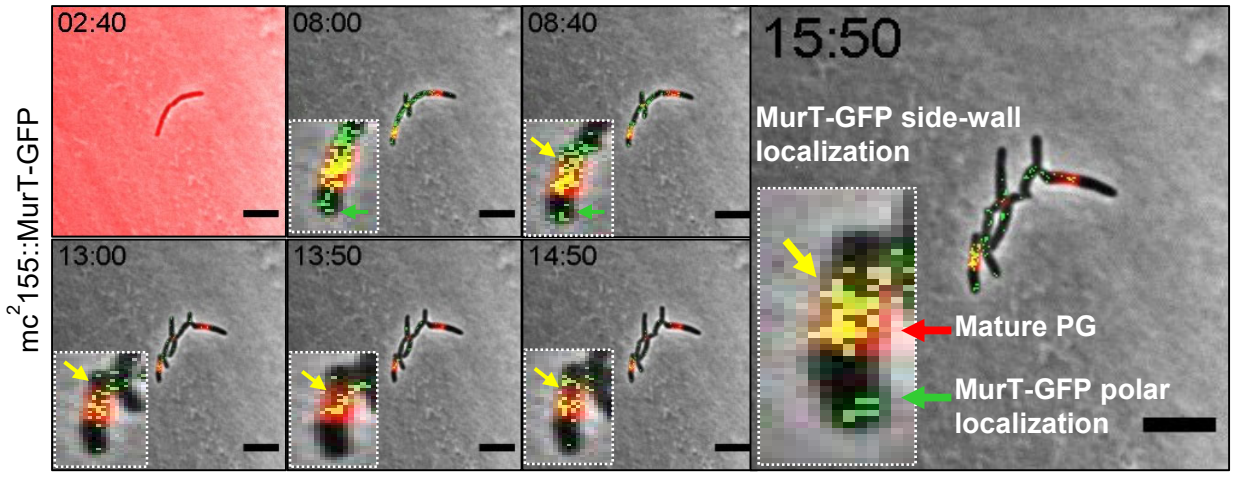

Figure 3.15**. MurT-GFP co-localizes with mature PG.** Time-lapse microscopic analysis of MurT-GFP in cells labeled with TADA (shown by red arrow)**.** MurT-GFP localizes at the cell poles (green arrows) and also with maturing PG (yellow arrrows). When MurT-GFP (green signal) localizes with TADA (red signal) labeled maturing PG a yellow (green+red) signal is detected. Scale bar is 5 µm.

3.5.5. MurT and GatD are required for PG amidation and cell growth in mycobacteria

To confirm the essentiality of the *murT-gatD* operon, we targeted *murT* (MSMEG_6276) for deletion using the two step allelic exchange method in a *M. smegmatis* strain carrying a second copy of *murT* linked downstream of a *tetO* promoter as described in section 2.1.12. This strain was generated by cloning the *murT* gene into plasmid pse100 to create plasmid pse100+murT (Fig. 3.16A) and introducing this construct into wildtype *M. smegmatis* mc^{2}155 as indicated in section 2.1.6.1. This strain was used together with wildtype mc^{2}155 to attempt to knockout the *murT* gene as described in section 2.1.12. The two-step allelic exchange method allowed the knockout of the native *murT* gene only in the presence of a second episomally expressed copy of

the *murT* gene while no *murT* mutants could be obtained from wildtype transformants (Fig. 3.16B).

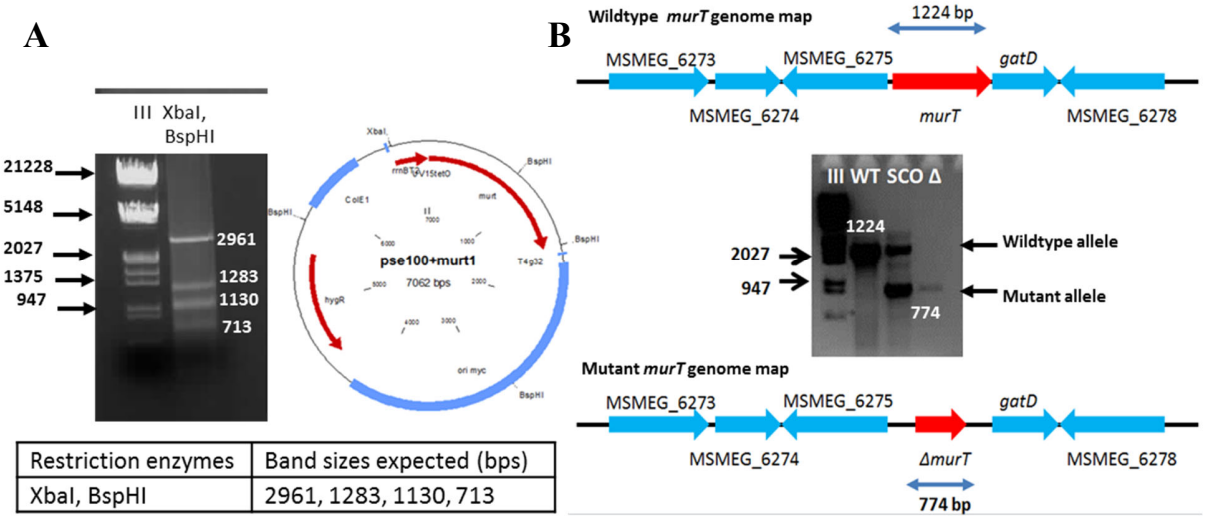

Restriction enzymes	Band sizes expected (bps)
XbaI, BspHI	2961, 1283, 1130, 713

Figure 3.16. **Knockout of *murT* from a *M. smegmatis* strain with a second episomal copy of *murT*.** (A) Restriction profile of pSE100+murT. Shown are the plasmid map of pSE100+murT, an agarose gel indicating the DNA band sizes expected and a table with restriction enzymes and band sizes expected. (B) The genome map of the wildtype and mutant *murT* alleles with an agarose gel depicting the PCR products of the wildtype and mutant *murT* alleles in the wildtype strain, the single cross-over strain and the mutant strain.

To assess the function of the MurT-GatD complex in *M. smegmatis* mc^{2}155 cells, a CRISPRi platform was used as this enzyme complex is essential for mycobacterial viability. The CRISPRi construct for depletion of MurT and GatD (plasmid PLR962+MSMEG_6276sgRNA) was generated as indicated in section 3.4.1 and restriction profiling indicated the expected profile for this construct (Fig. 3.17). The construct was then sequenced and introduced into wildtype *M. smegmatis* mc^{2}155 as indicated in section 2.1.6.1 for generation of the *M. smegmatis* MurT-GatD depletion strain (mc^{2}155::CRISPRi-MurT-GatD). Fluorescent D-amino acids (FDAAs) which are incorporated into PG during cell wall biosynthesis coupled with time-lapse microscopy were used to assess the growth and PG biosynthesis dynamics of MurT-GatD depleted cells (Fig. 3.18A). Sequential labeling of mc^{2}155::CRISPRi-MurT-GatD cells with FDAAs without CRISPRi induction showed polar incorporation of new cell wall material at the cell poles as previously demonstrated (122) and that in mycobacteria new cell wall material is not associated with old cell wall material (Fig. 3.18B, Appendix 3.4A&B)(83).

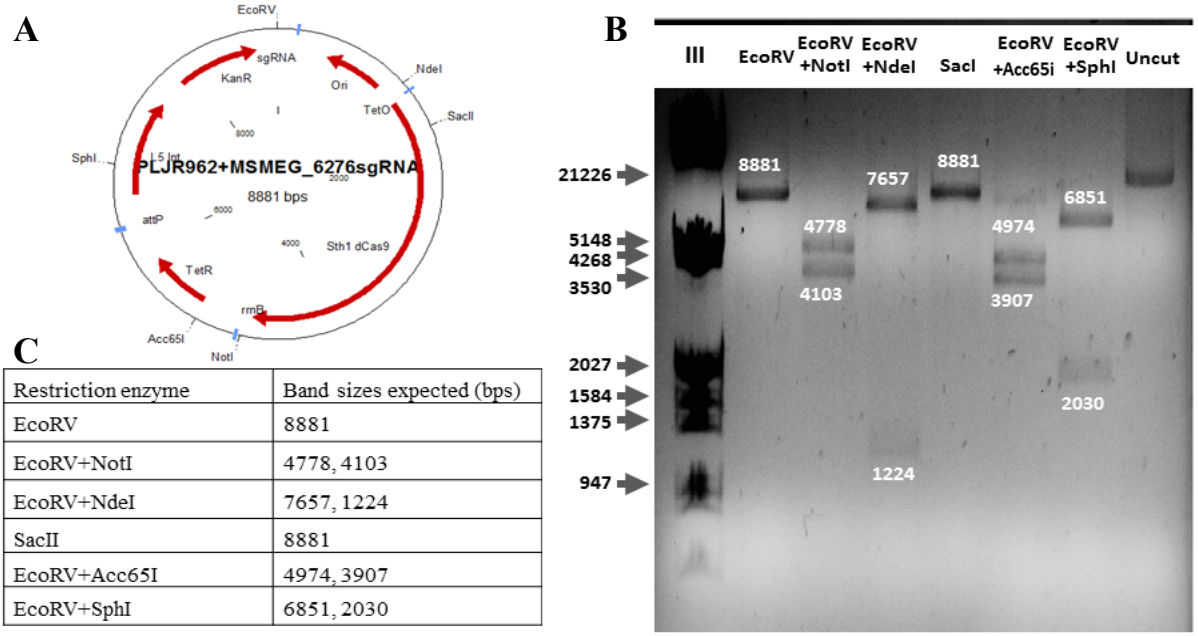

C

Restriction enzyme	Band sizes expected (bps)
EcoRV	8881
EcoRV+NotI	4778, 4103
EcoRV+NdeI	7657, 1224
SacII	8881
EcoRV+Acc65I	4974, 3907
EcoRV+SphI	6851, 2030

Figure 3.17. **Restriction profile of plasmid PLR962+MSMEG_6276sgRNA**. (A) Plasmid map of PLR962+MSMEG_6276sgRNA. (B) Agarose gel showing the DNA bands sizes expected (labeled in base pairs [bps]). (C) Table indicating the restriction enzymes used for restriction analysis of PLR962+MSMEG_6276sgRNA and the DNA band sizes expected. All expected band sizes were observed.

mc^{2}155::CRISPRi-MurT-GatD cells depleted of MurT-GatD displayed reduced cell growth upon induction of CRISPRi with ATc as expected and the cells were shorter compared to cells expressing MurT and GatD (Fig. 3.19A-D, Appendix 3.5). Polar elongation speed was determined by measuring unlabeled polar region extension over-time after labeling with FDAA with the near-old cell pole FDAA signal used as a fiducial marker (Fig 3.19E). Cells depleted of MurT-GatD displayed a reduced polar elongation speed suggestive of the role of PG amidation in regulation of cell elongation in mycobacteria (Fig 3.19F).

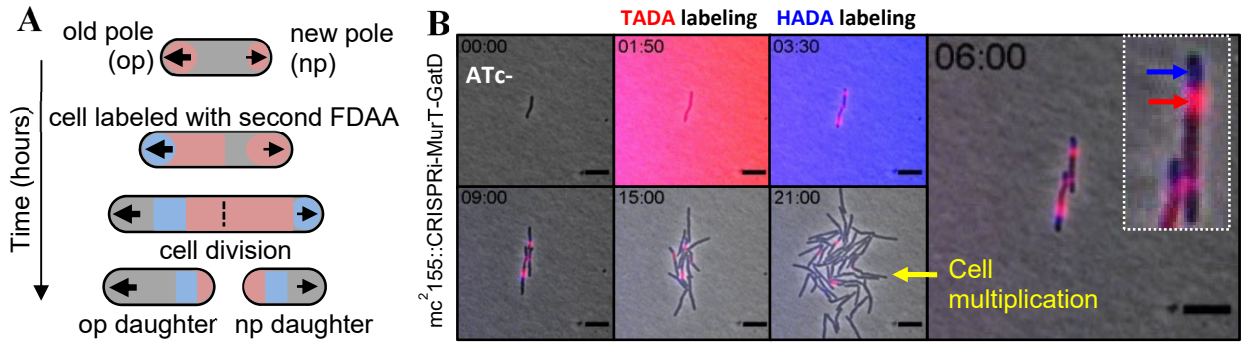

Figure 3.18. **Labeling of mc^{2}155::CRISPRi-MurT-GatD (without CRISPRi activation) with FDAAs.** (A) Schematic representation of labeling of mycobacterial cells with FDAAs for analysis of cell growth. (B) Time-lapse microscopic analysis of *M. smegmatis* CRISPRi-MurT-GatD cells without CRISPRi activation.

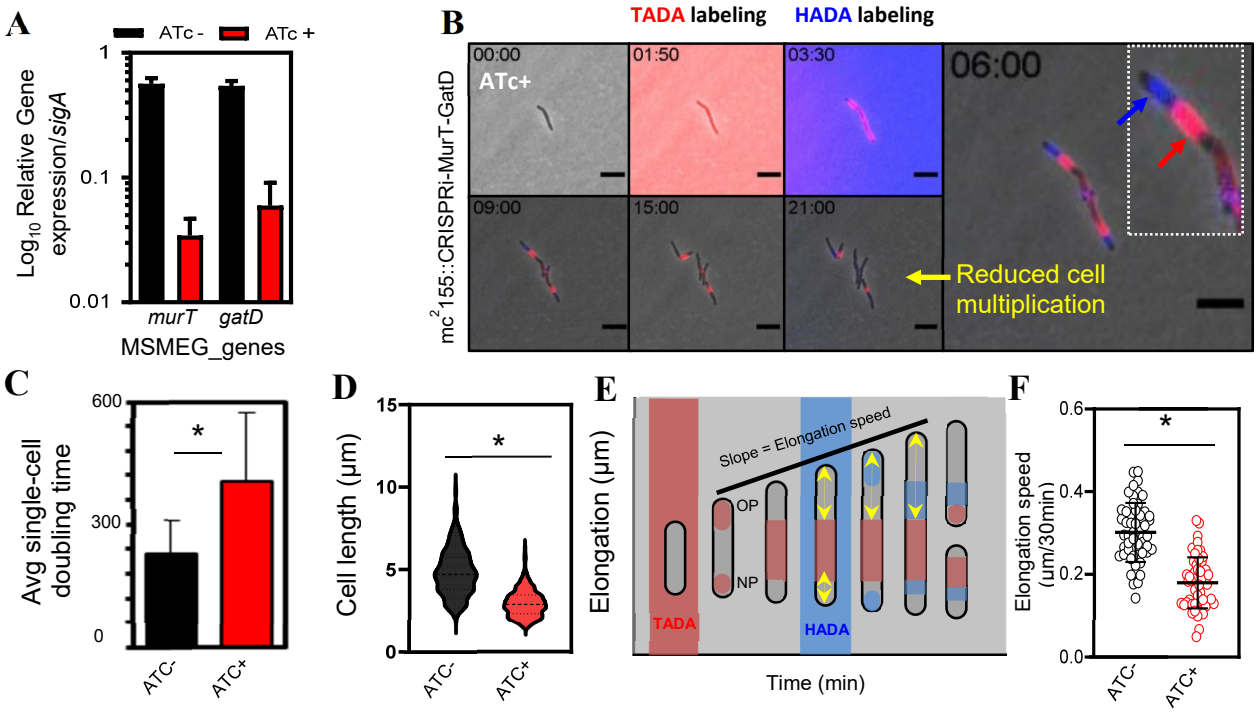

Figure 3.19. **Depletion of MurT and GatD reduces cell growth.** (A) qPCR analysis of *murT* and *gatD* expression during normal conditions or during gene knockdown conditions. Shown are the *murT* and *gatD* transcript levels normalized to *sigA*. (B) Time-lapse microscopic analysis of *M. smegmatis* CRISPRi-MurT-GatD cells with CRISPRi activation. (C) The average single-cell doubling time of cells expressing or not expressing MurT and GatD analyzed by time-lapse microscopy. Depletion of MurT and GatD increases the doubling time of the cells. (D) Violin plots showing the cell length of cells expressing MurT-GatD compared to cells depleted of MurT-GatD (n=300 per experiment). (E) Schematic representation of how cell elongation was measured in FDAA labeled cells expressing or not expressing MurT and GatD with the nearest FDAA signal to the old cell pole as fiducial marker for cell pole elongation over-time. (F) Scatter plot showing the polar elongation speed of cells expressing or not expressing MurT and GatD. Statistical analysis was conducted using Student *t*-test. *: p-value <0.05. sgRNA – short guide RNA. Scale bar is 5 µm.

3.5.6. PG cross-linking in mycobacteria requires amidation of D-glutamate in lipid II

To investigate whether depletion of MurT and GatD causes perturbed PG biosynthesis a fluorescent dipeptide probe AlkDADA was used as indicated in section 2.1.8.2 to assess PG biosynthesis in MurT-GatD depleted cells. AlkDADA is linked to a lipid II precursor to form labeled lipid II which can be detected on the cell surface by click chemistry (125). This dipeptide probe allows analysis of periplasmic PG precursor remodeling processes for incoporation into existing PG in contrast to monopeptide probes (e.g. TADA and HADA) which may also be incorporated into existing PG by periplasmic D,D-transpeptidases (DDTs) (Fig. 3.20)(126).

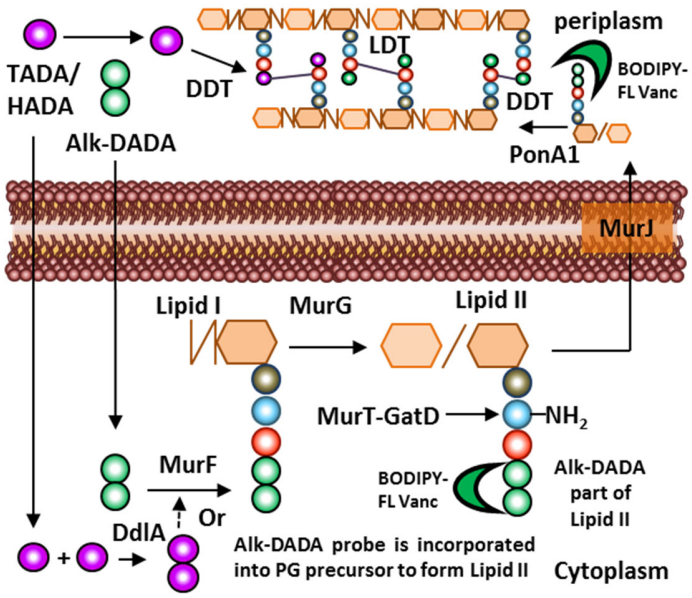

Figure 3.20. **Schematic for incorporation of Alk-DADA or monopeptide probes (TADA/HADA) during PG biosynthesis in mycobacteria.** Shown is the cytoplasmic and periplasmic processes of dipeptide (Alk-DADA) or monopeptide probe (TADA/HADA) incorporation during PG biosynthesis in mycobacteria. MurF facilitates addition of a dipeptide substrate to a PG precursor to form lipid I. D,D-transpeptidases (DDTs) can incorporate monopeptide probes into existing PG during PG remodeling processes (126). BODIPY-FL vancomycin binds the terminal D-Ala-D-Ala moiety of the PG precursors.

Cells expressing MurT-GatD displayed polar labeling with AlkDADA and reduced labeling at the side-wall indicative of insertion of the labeled PG precursors at the cell poles and remodeling of PG at the side-wall which results in a decreased signal of the label as PG 3-3 cross-links are formed (Fig. 3.21A-B) (83). Depletion of MurT-GatD caused diffused labeling of the cells suggestive of reduced PG remodeling along the side-wall. Side-wall PG remodeling involves the formation of 3-3 PG cross-links from 4-3 cross-links by LDTs. Increased AlkDADA at the side-wall of MurT-GatD depleted cells is indicative of reduced PG cross-linking or the inability of LDTs to process non-amidated PG precursors to form 3-3 cross-links (Fig. 3.21A-B). To explore this further, a fluorescent BODIPY-FL vancomycin probe – which binds the terminal D-Ala-D-Ala moiety of PG precursors at the cytoplasmic membrane to inhibit PG biosynthesis but can also bind D-Ala-D-Ala moieties in the PG sacculus (Fig. 3.20); was used as indicated in section 2.1.8.1 to probe PG cross-linking in cells depleted of MurT and GatD. As the terminal D-Ala-D-Ala moiety is lost during formation of 3-3 cross-links which predominate mature PG in mycobacteria (83), BODIPY-FL vancomycin was the ideal probe to investigate PG cross-linking by fluorescence microscopy.

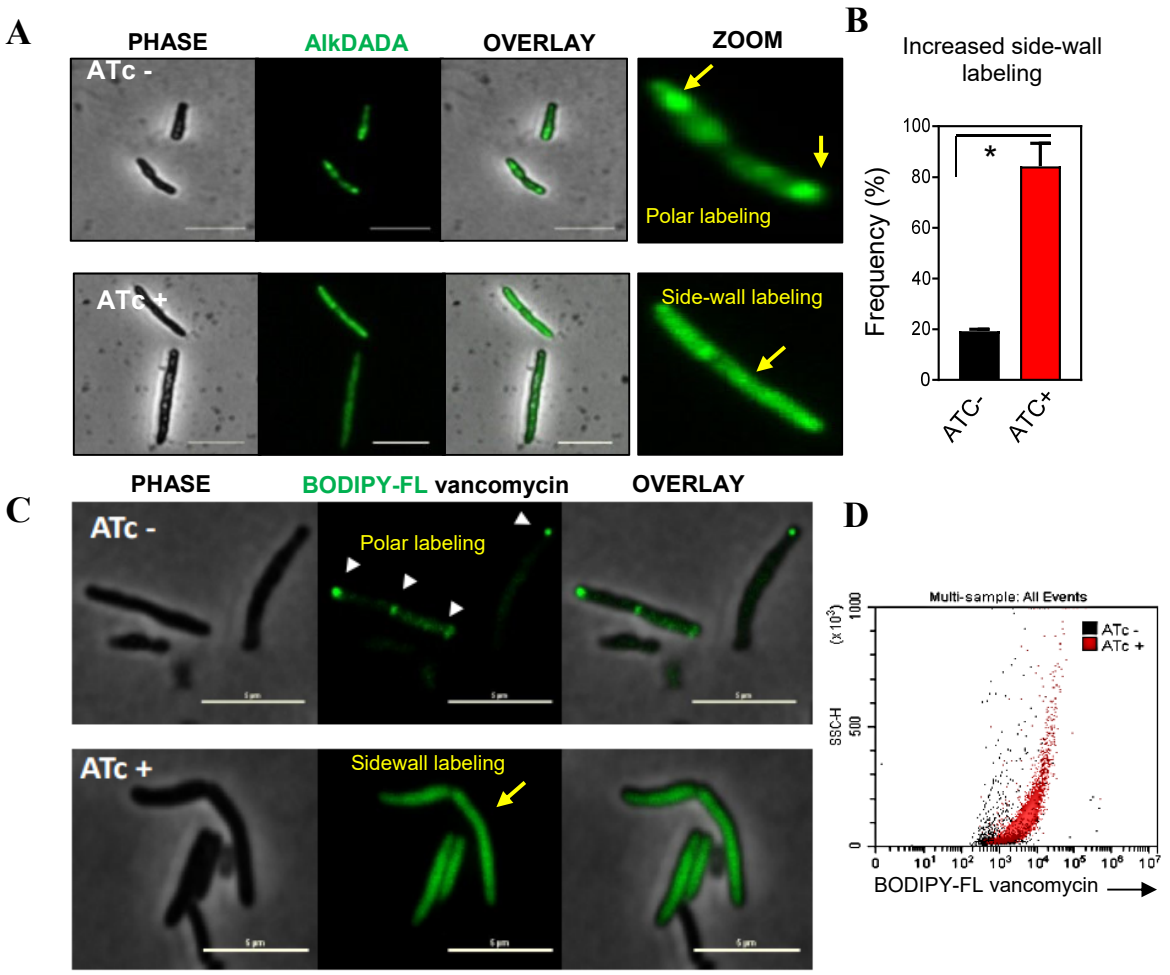

Figure 3.21. **MurT-GatD depletion causes perturbed PG remodeling**. (A) Micrographs of *M. smegmatis* CRISPRi MurT-GatD cells expressing or not expressing MurT-GatD. Inhibition of MurT-GatD expression causes increased side-wall labeling with AlkDADA. (B) Histograph showing the frequency of cells with increased side-wall AlkDADA labeling. n=100 labeled cells per experiment. (D) Schematic representation of cell wall labeling with BODIPY-FL vancomycin showing labeling of PG precursors in the periplasm. (C) Micrographs of BODIPY-FL vancomycin labeled MurT-GatD depleted cells in comparison with cells expressing tthe proteins. Inhibition of MurT-GatD expression causes increased side-wall labeling with BODIPY-FL vancomycin. n=100 labeled cells per experiment. (D) Flow cytometry quantification of BODIPY-FL vancomycin labeled MurT-GatD depleted cells in comparison to cells expressing the proteins. Statistical analysis was conducted using Student *t*-test.*:p-value <0.05. Scale bar is 5 µm.

In absence of ATc, mc^{2}155::CRISPRi-MurT-GatD cells exhibited labeling of the poles and septum. However, when the cells were depleted of MurT-GatD upon CRISPRi induction with ATc, the bacteria displayed diffused labeling with BODIPY-FL vancomycin (Fig. 3.21C-D). Because the terminal D-Ala-D-Ala is used as a substrate for PG cross-linking by PBPs, diffused labeling with BODIPY-FL vancomycin was also indicative of decreased PG-cross-linking as PG

cross-linking enzymes (LDTs and PBPs) in bacteria that express MurT and GatD have been shown to require prior PG amidation for PG-cross-linking (108). Furthermore, atomic force microscopy (AFM) was used as indicated in section 3.4.6 to assess whether reduced PG cross-linking as a result of loss of MurT-GatD function causes cell surface defects associated with decreased cell wall stifness. AFM did not reveal any detectable differences in the outer cell surface or cell wall mechanical properties in cells depleted of MurT-GatD compared to cells expressing these enzymes (Fig. 3.22).

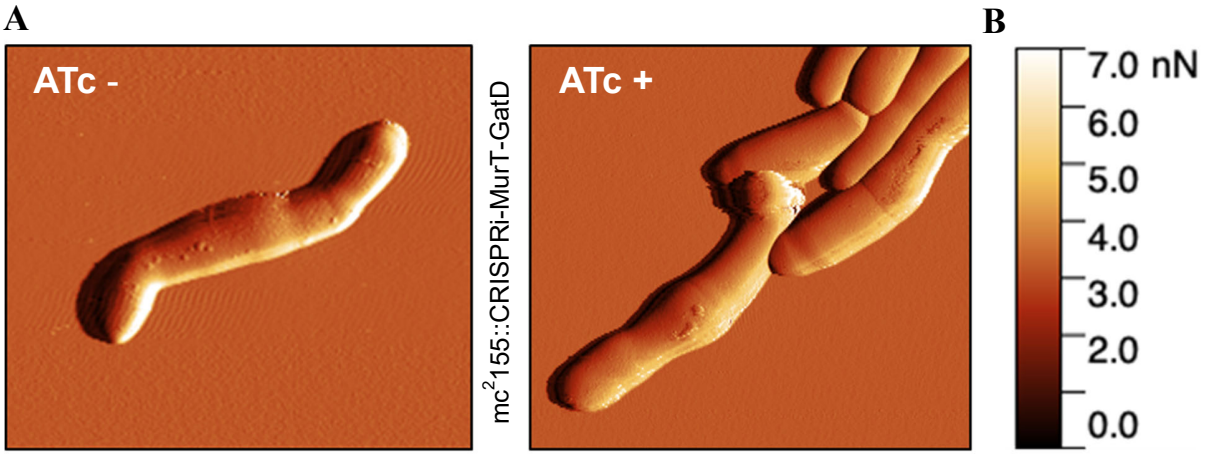

Figure 3.22. **AFM cell wall stiffness images of mc²155::CRISPRi-MurT-GatD**. (A) Three-dimentional AFM stiffness images of mc²155::CRISPRi-MurT-GatD without and with CRISPRi activation. (B) Stiffness scale for the AFM imaging experiment. MurT-GatD depletion does not change cell wall stiffness. nN: peak force unit.

We next assessed whether reduced PG-cross-linking in MurT-GatD depleted cells causes increased cell wall permeability. We tested the permeability of the cell wall upon MurT-GatD depletion by using an ethidium bromide (EtBr) diffusion assay as indicated in section 3.4.7. This assay allowed the monitoring of the fluorescence that occurs upon diffusion of EtBr into the cells and its interaction with DNA (118). This assay revealed that cells that were depleted of MurT-GatD exhibited increased cell wall permeability manifested by increased EtBr fluorescence probably reflecting reduced PG cross-linking (Fig. 3.23). Thereafter, we hypothesized that cells with reduced PG cross-linking and increased cell wall permeability as a result of MurT-GatD depletion could be more sensitive to PG targeting antimicrobials – like lysozyme.

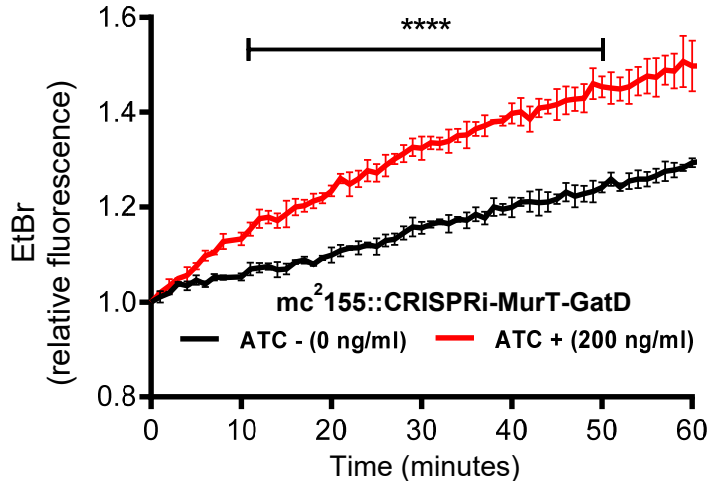

Figure 3.23. **MurT-GatD depletion causes increased cell wall permeability**. Ethidium bromide uptake into cells depleted of MurT-GatD in comparison to cells expressing the proteins shows that MurT-GatD depletion causes increased cell wall permeability. ****:p-value <0.05.

To investigate the increased susceptibility of MurT-GatD depleted cells to lysozyme, a lysozyme minimum inhibitory concentration (MIC) experiment was performed and the susceptibility of the depletion strain to lysozyme was assessed. MurT-GatD depleted cells were found to be highly sensitive to lysozyme (Fig. 3.24A). Microscopic analysis of MurT-GatD depleted cells exposed to lysozyme revealed cell lysis induced by lysozyme exposure (Fig. 3.24B).

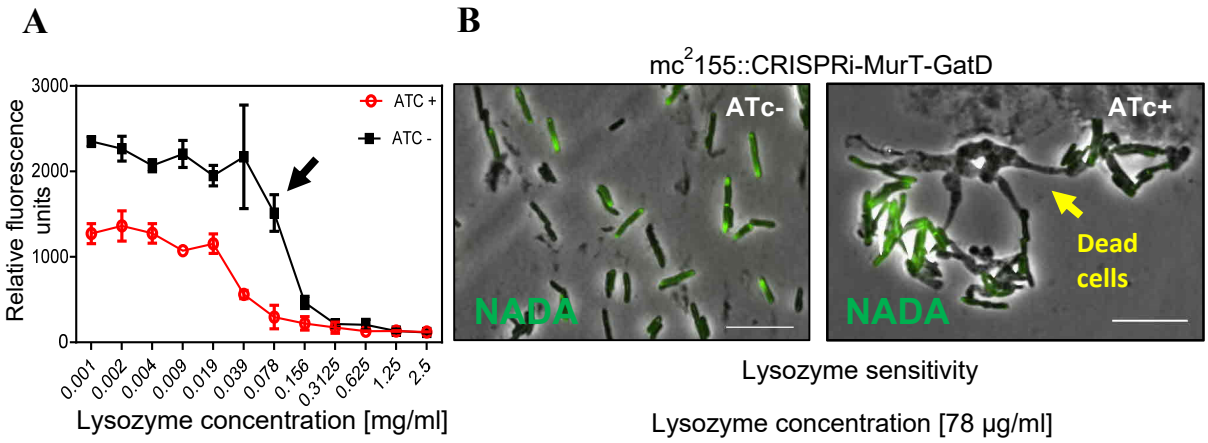

Figure 3.24. **MurT-GatD depletion causes increased sensitivity to lysozyme**. (A) Lysozyme minimum inhibitory concentration (MIC) assay for MurT-GatD depleted cells (ATc+) compared to cells expressing MurT-GatD (ATc-). (B) Micrographs of cells depleted of MurT-GatD and exposed to lysozyme (~80 µg/ml) compared to cells expressing MurT-GatD. Cells were labeled with a FDAA – NADA to check viability. Lysozyme exposure caused cell death in cells depleted of MurT-GatD. Statistical analysis was conducted using Student *t*-test. Scale bar is 5 µm.

Furthermore, the PG of lysed MurT-GatD depleted cells was extracted as described in section 3.4.8 and labeled with an amide reactive dye, Alexa Fluor 488 NHS Ester which labels primary amines (R-NH_2) to assess the level of PG amidation in these cells compared to MurT-GatD expressing cells. Analysis of the Alexa Fluor 488 NHS Ester dye signal in labeled PG from MurT depleted cells revealed a decrease in the dye signal, suggestive of a decrease in the level of PG amidation in PG from MurT-GatD depleted cells (Fig. 3.25).

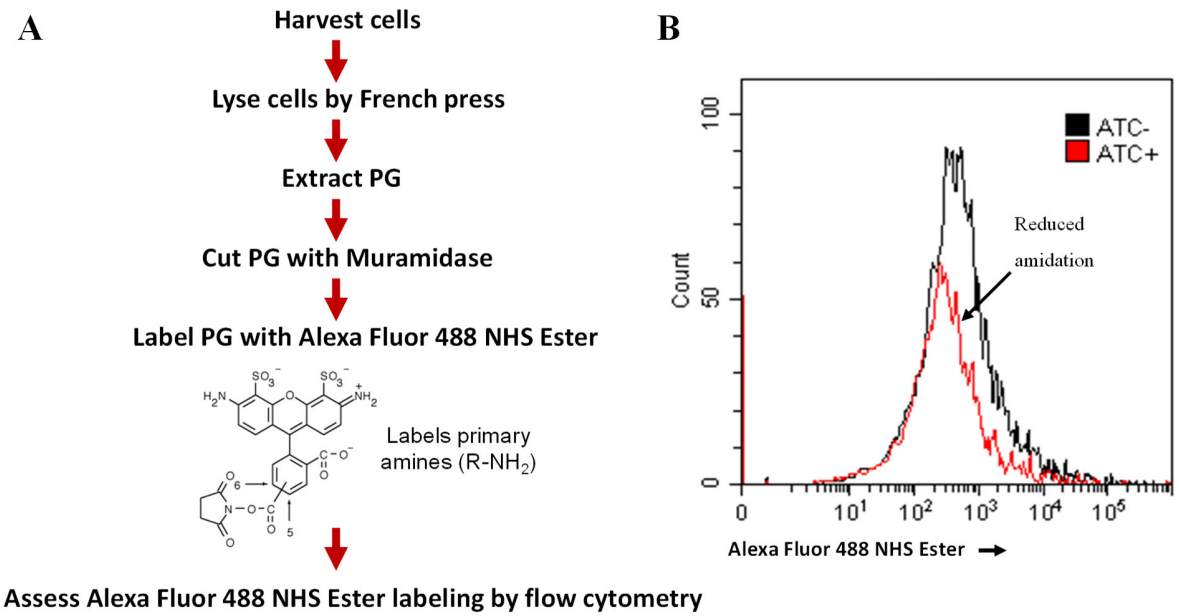

Figure 3.25. **Depletion of MurT and GatD causes reduced PG amidation**. (A) Flow chart representation of the protocol used for assessing PG amidation in MurT-GatD depleted cells by Alexa Fluor 488 NHS Ester labeling of PG in comparison with control cells (ATc-). The Alexa Fluor 488 NHS Ester labels primary amines (R-NH_2) also found in PG as a result of amidation. (B). Flow cytometry quantification of Alexa Fluor 488 NHS Ester labeled PG from MurT-GatD depleted cells in comparison to the no ATc control cells. MurT-GatD depletion causes decreased PG amidation which results in decreased labeling with Alexa Fluor 488 NHS Ester.

3.5.7. PknB regulates cell growth in response to PG amidation

PknB-like kinases have been implicated in the regulation of PG biosynthesis in most Gram-positive bacteria (127). In mycobacteria, uncross-linked PG is detected by PknB through C-terminal PASTA domains leading to the auto-phosphorylation of the N-terminal kinase at threonine residues to regulate cell growth (Fig. 3.26). In mycobacteria, PknB is essential for cell

growth and it was previously demonstrated that the extracellular PASTA domains (PASTA3 and PASTA4) of PknB are required for PknB localization at the cell poles and septum for regulation of PG biosynthesis (88, 120, 121). As PG amidation is essential for PG cross-linking, we hypothesized that in the MurT-GatD depleted strain, the PASTA domains of PknB sense uncross-linked PG and this results in the auto-phosphorylation and activation of PknB resulting in cell growth cessation in MurT-GatD depleted cells (128, 129). Furthermore, it was demonstrated that abrogation of D-isoGln interacting residues (Ser_{556} and Lys_{557} [see Fig. 3.26]) of PknB, which specifically interact with the terminal carboxyl group of D-isoGln, perturbs PknB function (130).

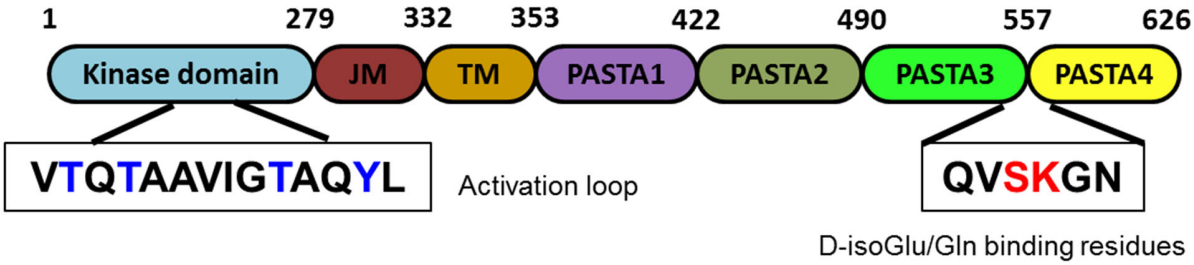

Figure 3.26. **Secondary structure of PknB.** Shown is the schematic representation of the domain structure of PknB and the D-Glu binding residues (red font) and the activation loop with threonine residues (blue font) subject to phosphorylation upon PknB activation are also shown.

To investigate whether reduced PG cross-linking as a result of MurT-GatD depletion causes increased PknB activation, phosphorylation of a FLAG-tagged PknB was assessed in MurT-GatD depleted cells. PknB (MSMEG_0028) was cloned into plasmid pFLAGEM for tagging PknB with a FLAG tag on the N-terminus as indicated in section 3.4.2 and restriction profiling of the plasmid construct indicated the expected profile for this construct (Fig. 3.27). The construct was then sequenced and introduced into the mc^2155::CRISPRi-MurT-GatD strain as indicated in section 2.1.6.1 for generation of a PknB phosphorylation reporter strain (mc^2155::CRISPRi-MurT-GatD+PknB). PknB phosphorylation status was assessed in the PknB phosphorylation reporter strain after CRISPRi induction. Cell membrane fractions of the MurT-GatD depleted cells grown at increasing concentrations of ATc (Fig. 3.28), were collected, and the protein concentration of the fractions was measured prior to western blotting of the fractions with anti-FLAG (α-FLAG) and anti-phosphothreonine (α-P-Thr) antibodies (Fig. 3.28A-B).

A

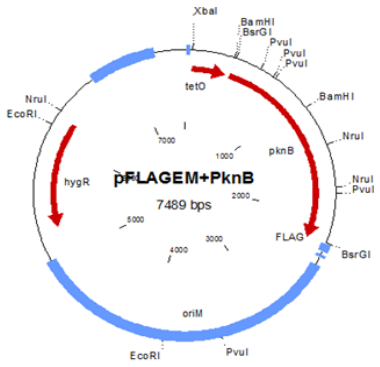

B

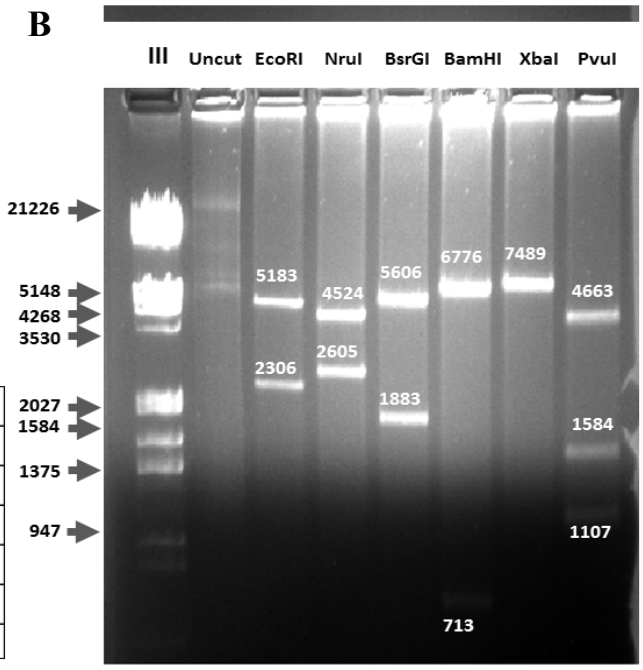

C

Restriction enzyme	Band sizes expected (bps)
EcoRI	5183, 2306
NruI	4524, 2605, 360
BsrGI	5606, 1883
BamHI	6776, 713
XbaI	7489
PvuI	4663, 1584, 1107, 117, 18

Figure 3.27. **Restriction profile of plasmid pFLAGEM+PknB**. (A) Plasmid map of pFLAGEM+PknB. (B) Agarose gel showing the DNA bands sizes expected (labeled in base pairs [bps]). (C) Table indicating the restriction enzymes used for restriction analysis of pFLAGEM+PknB and the DNA band sizes expected. All expected band sizes were observed.

A

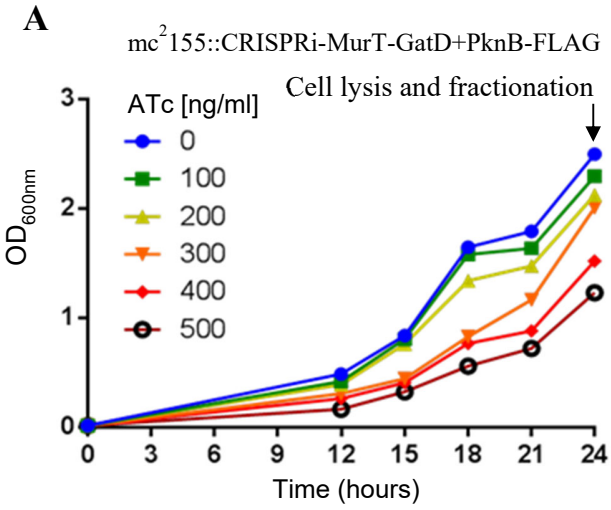

B

Sample no & [ATc] used:	Protein concentration
1 (0 ng/ml)	143 µg/ml
2 (100 ng/ml)	146 µg/ml
3 (200 ng/ml)	171 µg/ml
4 (300 ng/ml)	120 µg/ml
5 (400 ng/ml)	143 µg/ml
6 (500 ng/ml)	184 µg/ml

Figure 3.28. **Growth of the mc²155::CRISPRi-MurT-GatD+PknB-FLAG strain in increasing ATc concentration.** (A) Growth kinetics of mc²155 CRISPRi-MurT-GatD-PknB-FLAG cells grown in 0-500 ng/ml ATc. An ATc dose dependent reduction in growth of the mc²155::CRISPRi-MurT-GatD+PknB-FLAG was observed as expected. (B) Table with protein concentrations of membrane fractions extracted from cells grown in 0-500 ng/ml ATc.

MurT-GatD depletion caused increased PknB phosphorylation with high PknB phosphorylation observed in cells exposed to 200-500 ng/ml of ATc concentration for CRISPRi activation (Fig. 3.29). These results demonstrate that PknB regulates mycobacterial PG biosynthesis in response to the level of PG cross-linking.

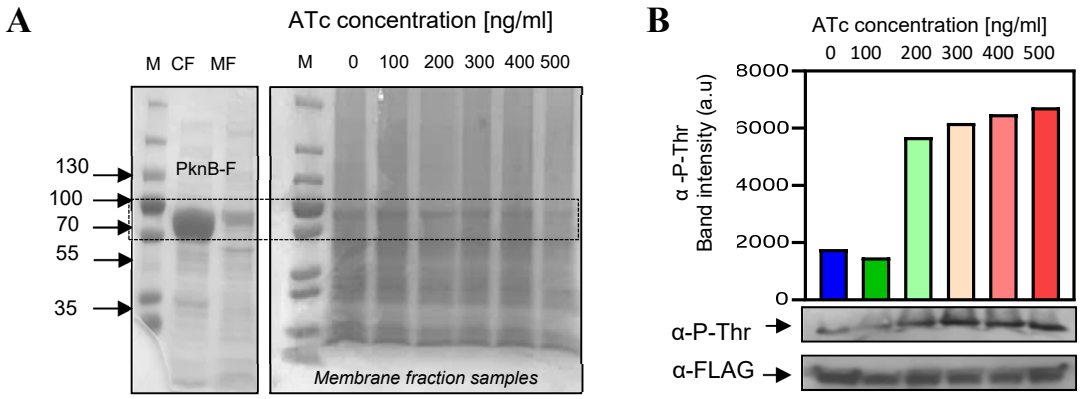

Figure 3.29. **Reduced MurT-GatD activity affects PknB activity.** (A) SDS-page gels showing expression of PknB-FLAG in the cytoplasmic fraction (CF) and presence of this protein also in the membrane fraction (MF). Membrane fractions from cells depleted of MurT-GatD were used to assess PknB phosphorylation in these cells. (B) Western blot analysis of PknB-FLAG phosphorylation from membrane fractions of MurT-GatD depleted cells. Data represents results experiment performed in triplicate. MurT-GatD depletion causes increased phosphorylation of PknB.

3.5.8. PknB localization is perturbed in MurT-GatD depleted cells

Since PknB activity is increased in MurT-GatD depleted cells, next the localization of PknB in these cells was analyzed. To assess this, wildtype PknB was linked to mRFP on the N-terminus (Fig. 3.30) by cloning the wildtype pknB allele into plasmid pMV306H+mRFP to form plasmid pMV306H+mRFP+PknB (Fig. 3.31) and the construct was sequenced and then introduced into wildtype mc^{2}155 and into the mc^{2}155::CRISPRi-MurT-GatD strain as indicated in section 2.1.6.1.

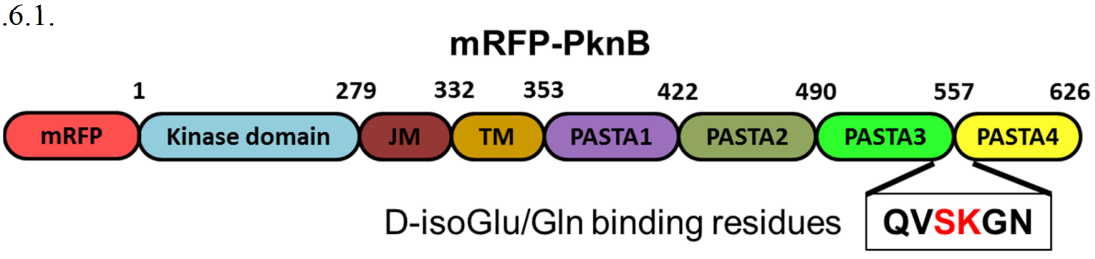

Figure 3.30. **Secondary struture of mRFP-PknB.** Shown is the schematic representation of the domain structure of PknB and the D-Glu binding residues (red font) and the activation loop with threonine residues subject to phosphorylation upon PknB activation are also shown.

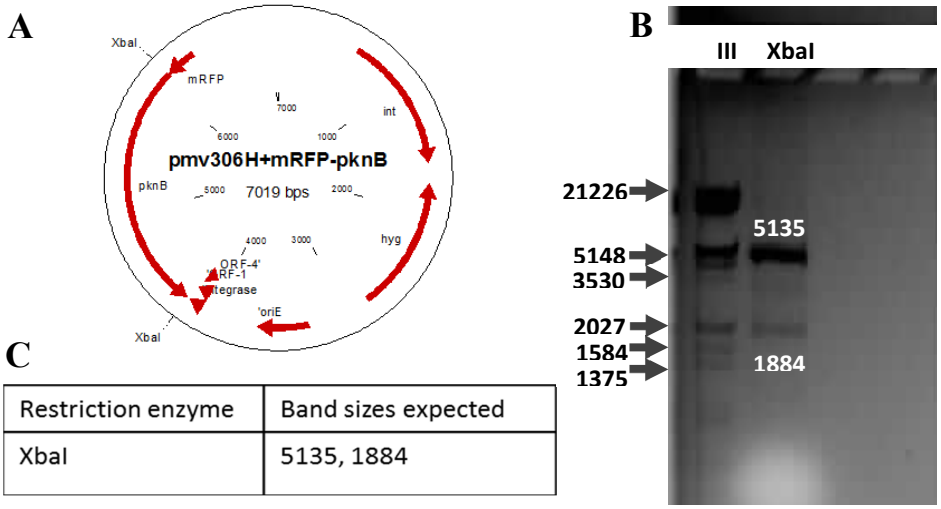

C

Restriction enzyme	Band sizes expected
XbaI	5135, 1884

Figure 3.31. **Restriction of plasmid pMV306H+mRFP-pknB**. (A) Plasmid map of pMV306H+mRFP-pknB. (B) Agarose gel showing the DNA bands sizes expected (labeled in base pairs [bps]). (C) Table indicating the restriction enzyme used for restriction analysis of pMV306H+mRFP-pknB and the DNA band sizes expected. All expected band sizes were observed.

mRFP-PknB localized at the cell poles and septum in mc2155::mRFP-PknB and mc2155::CRISPRi-MurT-GatD+mRFP-PknB without CRISPRi induction (i.e. ATc-). Upon CRISPRi induction, some cells displayed polar and septal localization, as seen with wildtype cells. However, mRFP-PknB also displayed diffused localization in MurT-GatD depleted cells (Fig. 3.32) indicative of perturbed PknB function as observed with analysis of PknB phosphorylation status.

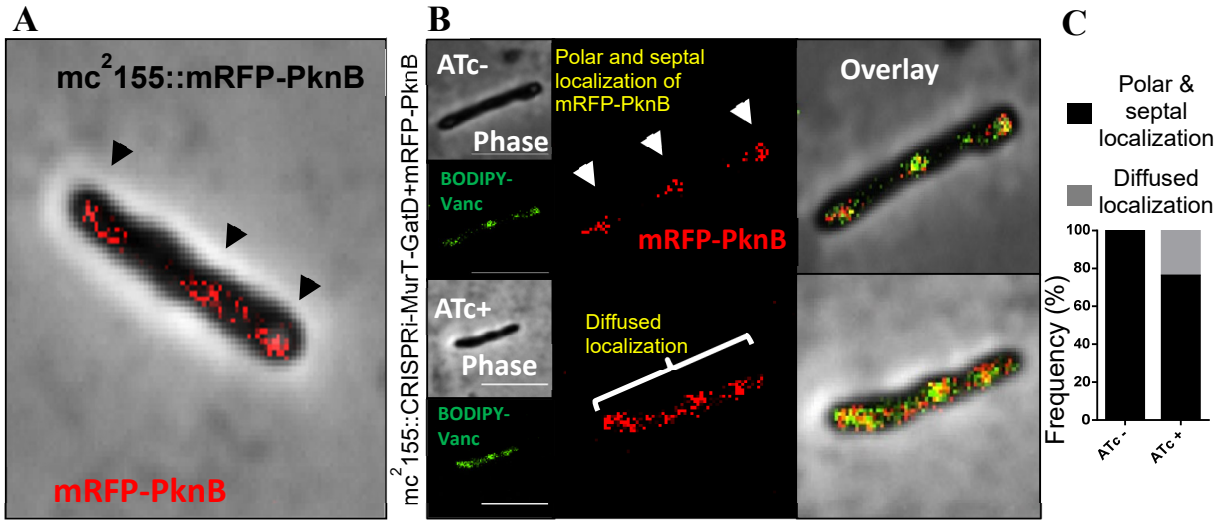

Figure 3.32. **MurT-GatD depletion causes inhibition of PG cross-linking and mis-localization of mRFP-PknB.** (A) Localization of mRFP-PknB in wildtype mc²155. mRFP-PknB localizes at the cell poles and cell septum (black arrow heads). (B) Depletion of MurT and GatD causes diffused mRFP-PknB localization. (C) Histogram showing the frequency of cells showing polar and septal or diffused mRFP-PknB localization. Scale bar is 5 µm.

3.5.9. MurT-GatD depletion causes sensitivity to β-lactam antibiotics

The importance of lipid II amidation for PG cross-linking in mycobacteria highlights a vulnerability that can be exploited for TB drug development. The reduced growth rate of mc^{2}155::CRISPRi-MurT-GatD (Fig. 3.19) and reduced PG cross-linking (Fig. 3.21) upon MurT-GatD depletion, as evidenced by diffused BODIPY-FL vancomycin labeling suggests that lipid II amidation is a rate limiting step for PG biosynthesis. We hypothesized that during limitation of amidated lipid II for PG biosynthesis, the MurT-GatD depleted cells will be sensitive to β-lactam antibiotics and result in rapid killing. To investigate the ability of β-lactams to rapidly kill MurT-GatD depleted cells, time-lapse microscopic analysis of the growth of the MurT-GatD depletion strain in the presence of a sub-lethal concentration of amoxicillin (inhibiting PBPs) and clavulanate (inhibiting β-lactamases) was performed. Amoxicillin-clavulanate treated MurT-GatD cells were unable to elongate, formed bulged cell poles and lysed (Fig. 3.33). Collectively, these results show the importance of PG amidation for mycobacterial cell growth and highlight the MurT-GatD complex as a potential drug target for TB drug development.

3.5.10. Essentiality of GatD is associated with a role in vitamin B_{12} biosynthesis

Considering that all mycobacterial LDTs (which require PG amidation for PG cross-linking) are dispensible for growth (83), the essentiality of MurT-GatD could be as a result of either MurT or GatD being also functional in additional cellular processes beyond PG amidation. Bio-informatics analysis revealed that GatD also known as CobQ2 is homologous to CobQ1 (Rv0255c), which encodes a corrin amidase required for *de novo* synthesis of the essential co-factor vitamin B_{12} (Appendix 3.6)(131). However, CobQ1 is dispensible for growth and the essentiality of GatD/CobQ2 suggests that this enzyme plays a role in both pathways (Fig. 3.34). To investigate the essentiality of GatD/CobQ2 in vitamin B_{12} biosynthesis, the mc^{2}155::CRISPRi-MurT-GatD strain which shows reduced growth upon CRISPRi activation was grown in the presence of exogenous vitamin B_{12} (i.e. Vit B_{12}+ ATc+). Reduced growth of mc^{2}155::CRISPRi-MurT-GatD upon CRISPRi activation was observed as expected (Fig. 3.35), however supplementation of growth media with exogenous vitamin B_{12} only increased the growth rate of the MurT-GatD depleted cells during the pre-exponential growth although this trend was statistically insignificant (Fig. 3.35B). This suggests that although GatD could have an

additional function in vitamin B_{12} biosynthesis, its role in PG amidation which is important for PG cross-linking is similarly important to maintain cell viability.

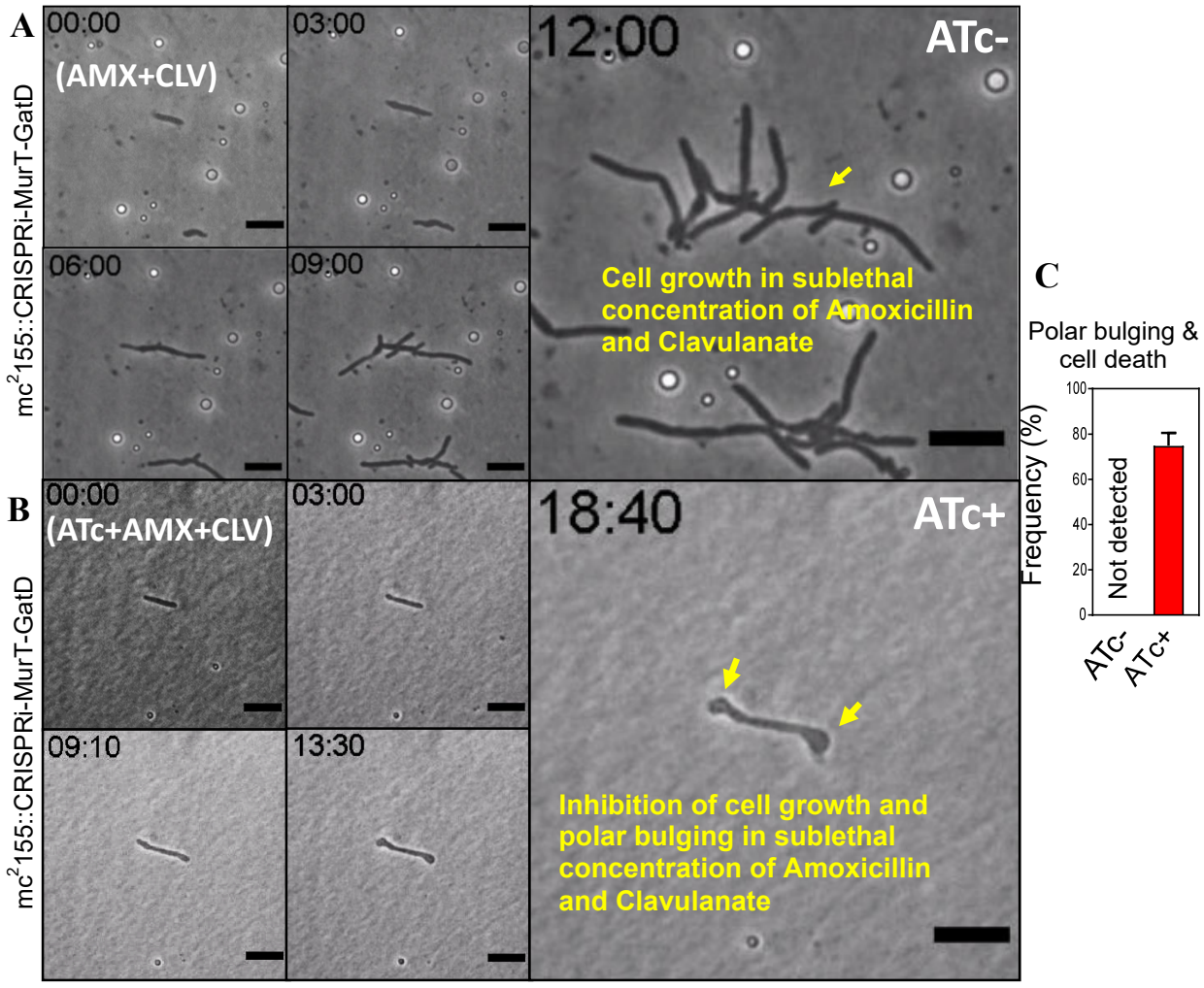

Figure 3.33. **Time-lapse microscopic analysis of amoxicilin (AMX) and clavulanate (CLV) treated MurT-GatD depletion strain cells with/without CRISPRi activation**. (A) Micrographs of amoxicilin (AMX) and clavulanate (CLV) treated MurT-GatD depletion strain cells with/without CRISPRi activation. The cells were grown in media supplemented with sublethal concentrations of amoxicillin (20 µg/ml) and clavulanate (10 µg/ml). Growth of the cells in sublethal concentrations of amoxicillin and clavulanate did not cause any morphological changes. (B) Micrographs of amoxicilin and clavulanate treated MurT-GatD depletion strain cells with CRISPRi activation (ATc+). The cells were grown in media supplemented with 200 ng/ml ATc and amoxicillin (20 µg/ml) and clavulanate (10 µg/ml). Growth of the MurT-GatD depletion cells in sublethal concentrations of amoxicillin and clavulanate caused cell pole bulging. Time-lapse microscopy of the MurT-GatD depletion cells was performed for 24 hours. Scale bar is 5 µm. (C) Histogram showing the frequency of dead cells with polar buldges, 25 time-lapse micrographs were analyzed for each experiment. Scale bar is 5 µm.

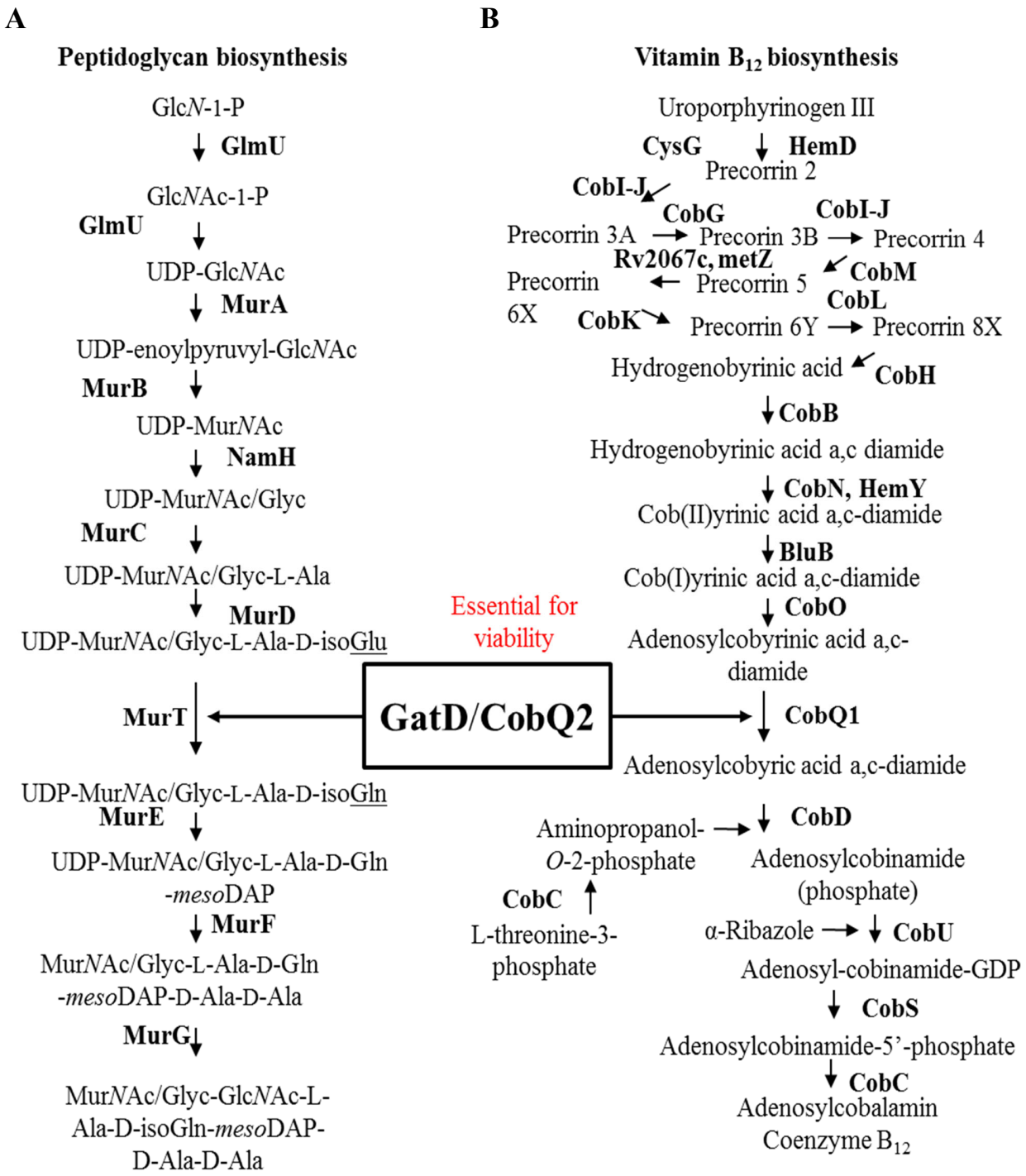

Figure 3.34. **Essentiality of GatD/CobQ2 in PG biosynthesis or Vitamin B_{12} biosynthesis.** (A) PG biosynthesis pathway in mycobacteria. (B) Vitamin B_{12} biosynthesis in mycobacteria. GatD/CobQ2 is hypothesized to play a role in both PG biosynthesis and Vitamin B_{12} biosynthesis.

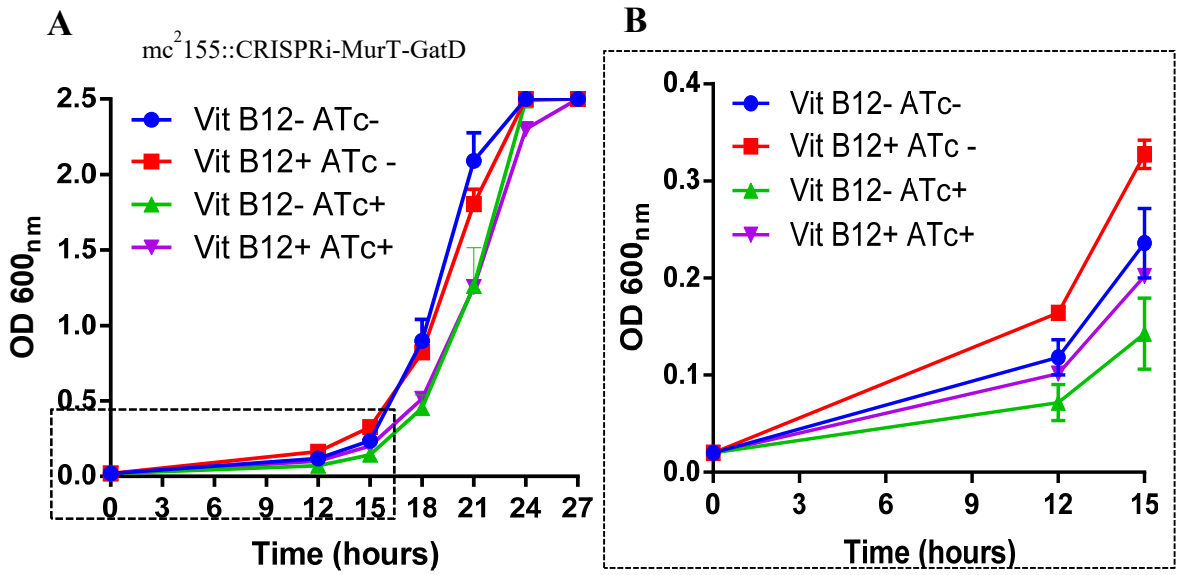

Figure 3.35. **Growth curve of mc^{2}155::CRISPRi-MurT-GatD in vitamin B_{12}.** (A) Growth kinetics of mc^{2}155::CRISPRi-MurT-GatD grown in media supplemented with vitamin B_{12} upon CRISPRi activation (Vit B_{12}+ATc+). (B) Insert of Fig. 3.35A, showing growth kinetics at 15 hours. Supplementation of mc^{2}155::CRISPRi-MurT-GatD with vitamin B_{12} rescues growth at pre-exponential phase of growth.

3.6. Discussion

β-lactam antibiotics, like penicillin, inhibit the critical cross-linking step of PG biosynthesis and have shown great success for treatment of a variety of bacterial infections (132, 133). This shows that the PG biosynthesis pathway and enzymes involved are vulnerable drug targets that can be exploited for development of new and effective antibiotics.

Recently, fluorescent probes have been used extensively to study PG biosynthesis in live bacterial cells and to elucidate previously unknown functions of enzymes enabling further idenfication of potential drug targets (95, 122, 125). These probes are monomers of PG linked to fluorescent molecules and their use by bacterial cells provides insight into the biosynthesis process of the PG polymer. With the use of fluorescent PG stem peptide mimics with amidation modifications on the second amino acid (i.e. D-Gln instead of D-Glu) of the stem peptide, we confirm that this modification is required for the PG cross-linking reaction and we further investigate the essentiality of this modification in PG biosynthesis using CRISPRi mediated depletion of the enzymes (the MurT-GatD complex) required for this process.

MurT and GatD are responsible for the amidation of the D-Glu residue in the peptide stem of PG precursors in *S. aureus*, *S. pneumoniae* and mycobacteria (80, 109-111, 119)(10-14). However, the phenotypic defects caused by loss of PG amidation due to inactivation of MurT-GatD in mycobacteria remained to be demonstrated. MurT and GatD are arranged in a bicistronic operon which is conserved in various bacterial species and in mycobacteria. Deletion of the native *murT* gene using the two step allelic exchange mutagenesis technique was only possible in the presence of a second copy of the *murT* gene, confirming the essentiality of this operon. We further use the recently developed CRISPR interference based programmable transcriptional repression platform coupled with time-lapse microscopy to confirm the essentiality of this complex for mycobacterial cell growth (113). Time-lapse microscopic analysis of MurT and GatD depleted cells demonstrated that MurT-GatD depletion causes growth cessation confirming the essentiality of the MurT-GatD complex for cell growth. It has been previously reported that PG transpeptidases required for PG cross-linking only recognize amidated PG precursors as substrates therefore, inhibition of PG precursor amidation was expected to inhibit PG cross-

linking (134). To investigate this, the MurT-GatD depleted cells were labeled with fluorescent probes (FDAAs and a vancomycin analog – BODIPY-FL vancomycin). FDAA labeled cells did not show changes in PG biosynthesis dynamics in MurT-GatD depleted cells compared to cells expressing these enzymes. Interestingly, BODIPY-FL vancomycin which binds non-cross-linked PG precursors and can be visualized by fluorescence microscopy displayed an abnormal labeling pattern in MurT-GatD depleted cells (135). The non-cross-linked PG precursors were detected all along the cell surface (i.e. diffused staining), confirming that PG cross-linking by PG transpeptidases is reduced in MurT-GatD depleted cells. However, this did not cause outer cell wall defects as analyzed by AFM.

To further study the role of MurT and GatD in mycobacteria, protein localization experiments were performed with GFP and mRFP tagged MurT and GatD, respectively. We found that MurT-GFP and mRFP-GatD co-localized at the cell poles and cell division septum and may form part of both the elongosome and divisome. These are complexes of enzymes required for synthesis of the cell wall at the poles and the cell division septum, respectively. In other species MurT interacts with GatD and activates GatD function therefore, the co-localization of MurT-GFP and mRFP-GatD suggests that mycobacterial MurT and GatD also form a complex at the sites of PG biosynthesis. To confirm this interaction, the M-PFC assay was used, confirming that indeed MurT and GatD do interact to form the amidotransferase PG amidation complex.

Recently, it was demonstrated that mycobacteria remodel and repair the side-wall during growth (83, 124). We find that time-lapse microscopic analysis of the co-localization of MurT-GFP with TADA, a monopeptide FDAA probe, during cell growth indicates that MurT-GatD also localizes with maturing PG. This mature PG can be subjected to remodeling during repair processes (124), if the cell wall has been damaged and this would require prior amidation of PG precursors facilitated by the MurT-GatD complex at this site. We also hypothesized that if the PG is loosely cross-linked, the cell wall would be more permeable. To study this, we used an ethidium bromide diffusion assay which reports on the level of permeability of the cell wall by diffusion of ethidium bromide into the cells (136). This assay revealed that depletion of MurT and GatD caused increased cell wall permeability as evidenced by the elevated accumulation of ethidium

bromide in the cells. Interestingly, non-amidated lipid II has been shown as an in-efficient substrate for the cross-linking reaction in *S. pnuemoniae* (134), supporting the notion that mycobacterial PG transpeptidases also do not recognize non-amidated PG precursors and hence cannot crosslink these. This data demonstrates that amidation of PG plays a crucial role in PG biosynthesis and maturation in mycobacteria (Fig. 3.36)

We further studied how PknB regulates PG biosynthesis in response to reduced PG cross-linking because of depletion of MurT-GatD in mycobacteria. PknB is known to regulate PG biosynthesis by sensing PG cross-linking through extracellular PASTA domains which also facilitate the localization of PknB to the cell poles and septum (137). Specifically, residues that are located in a α-helix locker between PASTA3 and PASTA4 domains of PknB bind the carboxyl terminal of D-isoGln/Glu and mDAP residues in the stem peptide of uncross-linked PG precursors and this causes auto-phosphorylation of the cytoplasmic kinase domain of PknB (130).

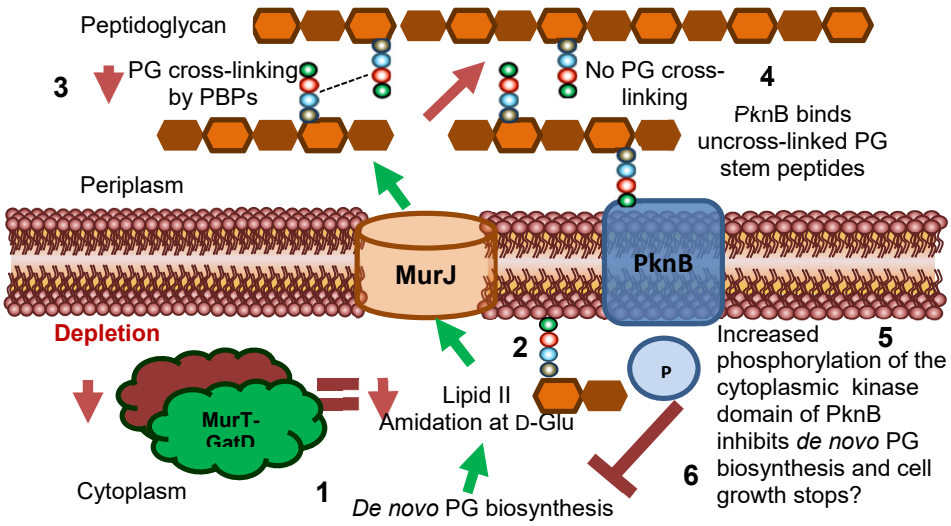

Figure 3.36**. Proposed model for the role of MurT and GatD during PG biosynthesis and cell growth in mycobacteria.** Lipid II biosynthesis involves MurT-GatD amidation of D-glutamate of the PG stem peptide. (1) Depletion of MurT-GatD causes decreased lipid II amidation at D-Glu (2) and non-amidated lipid II is not cross-linked into existing PG by PBPs (3). PknB binds uncross-linked PG stem peptides (4) and its cytoplasmic kinase domain auto-phosphorylates and causes inhibition of PG biosynthesis resulting in cessation of cell growth (6).

The activated PknB kinase domain regulates the function of PG biosynthesis enzymes including MurA, CwlM and MurJ through phosphorylation (89, 128). We confirmed that depletion of MurT and GatD causes hyper-activation of PknB. Localization experiments of mRFP-PknB in MurT-GatD depleted cells also displayed perturbed mRFP-PknB localization indicative of changes in PknB function in these cells.

We next hypothesized that cells depleted of MurT and GatD are highly dependent on PBPs to remain viable. To test this, we exposed the MurT-GatD depleted cells to a sub-lethal concentration of amoxicillin which inhibits the transpeptidase reaction of high molecular weight PBPS in the presence of clavulanate required for inhibition of β-lactamases (132, 133, 138). Cells depleted of MurT and GatD were found to be highly sensitive to amoxicillin-clavulanate, showing reduced growth, polar swelling and eventual cell lysis. These data highlight the MurT-GatD complex as a vulnerable target for inhibition of PG biosynthesis.

Recent published work demonstrated that all *M. smegmatis* LDTs known to require PG amidation for PG cross-linking are dispensible for growth while GatD is essential for viability. In this context, the essentiality of the MurT-GatD bi-enzyme complex was somewhat curious, as this complex will yield the relevant subtrate for LDT function. To further explore the issue of essentiality, we turned to the vitamin B_{12} biosynthesis pathway. There is a possible role for GatD here given the strong homology of GatD (also known as CobQ2) with CobQ1, required for synthesis an intermediate in the vitamin B_{12} biosynthesis pathway. We predicted that the eseentiality of MurT-GatD could be due an essential role that GatD plays in B_{12} biosynthesis, if this was the case, addition of vitamin B_{12} would rescue the growth defect of the depletion strain. To test this, the mc^2155::CRISPRi-MurT-GatD strain was grown in media supplemented with exogenous vitamin B_{12} upon CRISPRi. However, vitamin B_{12} supplementation only slightly complemented the loss of GatD expression. Vitamin B_{12} uptake is known to be restricted in mycobacteria depending on the cofactor requirements of the vitamin B_{12}-dependent methionine synthase (139).

Considering that MurT and GatD depletion causes reduced PG cross-linking and growth cessation, and that the mycobacterial serine/threonine protein kinase PknB is activated by uncross-linked PG precursors, we propose a model where PknB senses the level of uncross-linked PG as a result of reduced amidation caused by inactivity of MurT and GatD and regulates mycobacterial cell growth (Fig. 3.36). With this data we identify MurT and GatD as potential new drug targets for TB drug development.

3.7. Appendices

5’atgctgaccgtccgtgggcgcgccgcactggccgccggagccgccgcccgctgggcgtcccgggtcaccgggcgcggtgccggcgccatgatcggcgggctggt
cgccatgaccctggaccgttcggtcctgcggcagctcggccagggccgccggacggccatcgtgaccggcacaaacggcaaatcgaccaccaccaggatgatcgc
cgccgcgctggcgccgctgggacccgtcgcgagcaacaccgagggcgccaacatggacgccgggctggtctcggcgctcgccgccaaccgcgacgccggactcgc
ggcgctcgaagtcgacgagatgcatgtgccgcatgtgtccgatgcggtgtcgccttcggtgatcgttctgctcaatctgtcgcgtgatcagctcgatcgagtgggtga
gatcaaccacatcgagcggacgctgcgtgccggtctggcgcgtcatcccgacgcggtgatcgtcgccaactgtgacgacgtgctcatgacgtcggccgcctacgaca
accccgacgtcgtgtgggtggccgcgggcggaacctgggccaacgattcggtgagctgcccgcgcagcggcgaggtgatcgtgcgcgacgggcgcgactggtact
ccaccggcaccgacttcaagcgccccagcccgcagtggtggttcgacgagacccacatccacggacccgacgggctgtcggtgcccatggagctggccctgcccgg
caccgtcaaccggggcaatgccacgcaggccgtcgcggccgcggtggccctgggcgccgatcccgtcgcggccgtcgccgcggtctcgaccgtcgacgaggtcgcc
ggtcgctaccgcacggtgcaggtcgggccccggcacaccgcgcgggtgctgctggccaagaacccggccggctggcaggaggcgctgtcgatggtcgaccggacc
ggcgcgggcgtggtgatcgcggtcaacggccaggtgcccgacggcgaggacctgtcgtggctgtgggacgtgcggttcgaggacttctcgggtgtgcaggtggtcg
cggccggtgagcgcggcaccgatctggcggtgcgactcggctatgccgacgtcgagcacacgctggtgcacgacaccatcagcgcgatcaaatcctgcccacccgg
gcacgtcgaggtgatcgcgaactacacggcgttcctgcaactgaaccggcggctgtcatgaatgactcaccccagcaccgtgcgcatcggcctcgtgctccccgacg
tcatgggcacctacggcgacggcggcaacgccgtggtgctgcgacagcggctgcgcctgcgcgggatcgacgccgagatcgtcgagatcacgctggacgacccgg
tgcccgagtcgctggatctctacaccctcggcggcgcagaggattacgcgcagcgcctggcgaccaagcatctgatccgtcatcccggcctgcagcgcgccgccga
acgcggcgcgccgatcctcgcgatctgcgcggccatccaggtgctcgggcactggtacgagacctcggcgggtgagcgcgtcgaaggcgtcggcctgctcgacgcc
accacctctccgcaggaggcccgcaccatcggcgaggtcgcgtcccgcccgctgcccgacgggctcgaccagccgctcaccggattcgaaaaccaccgcggtgga
acacttctcggttccgacgcacgtccgctcggcgcggtcaccaagggtgcgggcaaccgtgccggcgacggtttcgacggtgccgtacagggcagtgtggtggcga
cgtacatgcacgggccgtgcctggcccgcaatccgcagttggccgaccatctgctctcccgcgtggtcggcgatctgcccccgctcgagcttcccgaggtcgaacgtt
tgcgttctgagcgcctcgccgcgccgcggcgcgtctga3’

Appendix 3.1. **Gene sequences of *murT* (MSMEG_6276, in red) and *gatD* (MSMEG_6277, in black) with the sgRNA and PAM sequences used for CRISPRi**. The PAM sequence is shown in blue font and sgRNA sequence shown by the green underlined font.

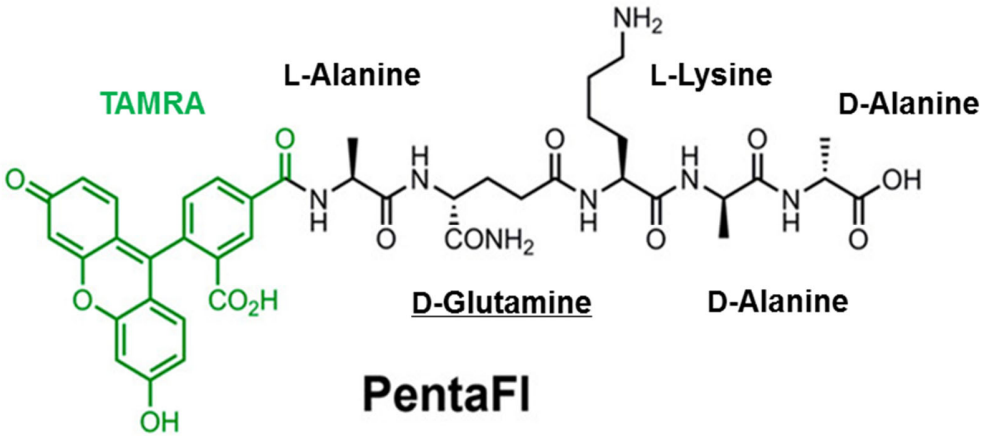

Appendix 3.2. **Chemical structure of PentaFL**. Shown is the composition of PentaFl - Tetramethylrhodamine (TAMRA)-3-amino-L-alanine-D-glutamine-L-lysine-D-alanine-D-alanine.

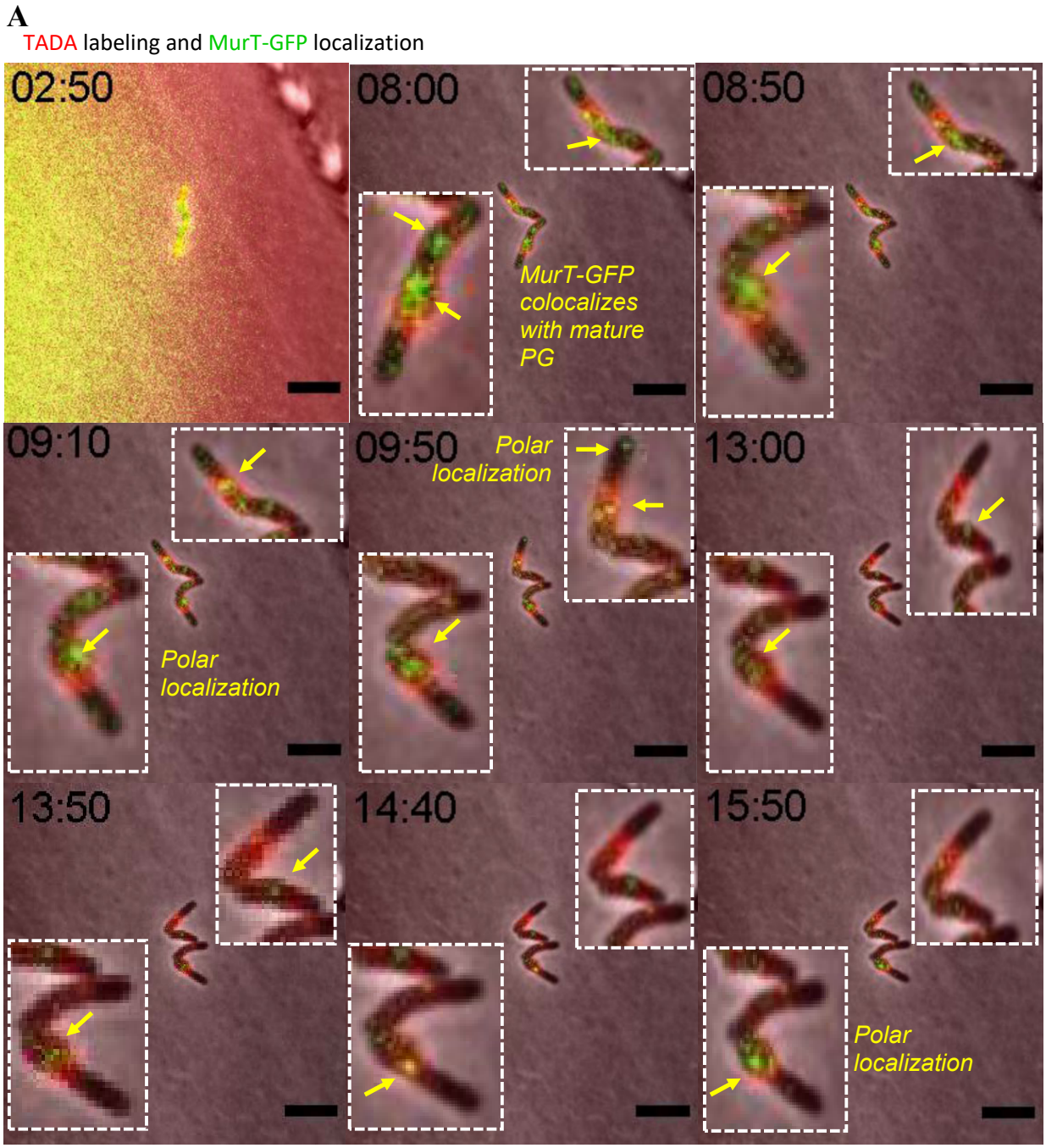

Appendix 3.3: **Time-lapse microscopic analysis of TADA labeled MurT-GFP cells**. The MurT-GFP cells were grown first in media supplemented with 1 mM TADA for 15 min. The TADA supplemented media was washed out with no-label media and time-lapse microscopy of the TADA labeled MurT-GFP cells was performed for 24 hours**.** MurT-GFP localizes at the cell poles and also with maturing PG. Scale bar is 5 µm.

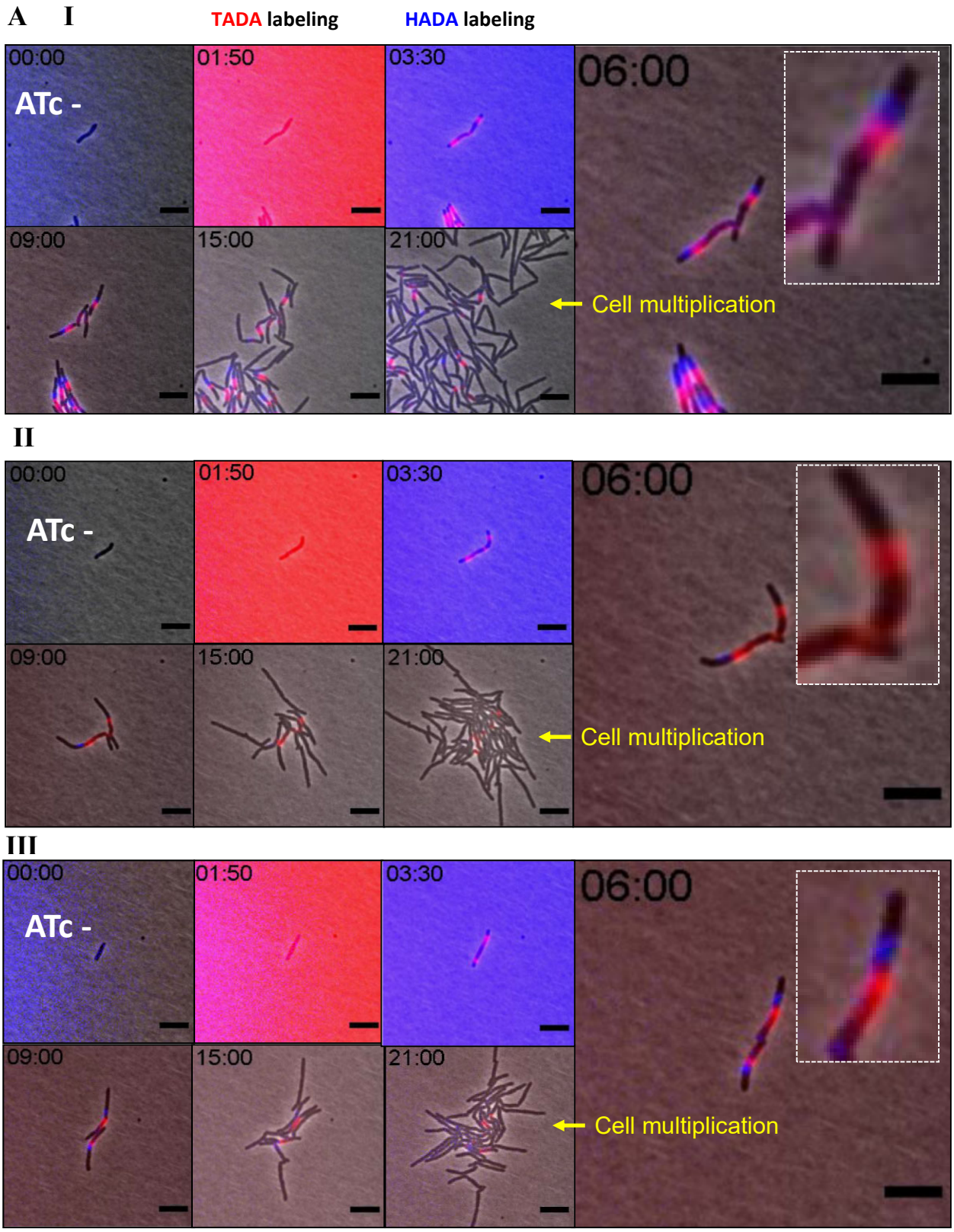
A I
TADA labeling
HADA labeling
00:00
ATc -
01:50
03:30
06:00
09:00
15:00
21:00
Cell multiplication
II
00:00
ATc -
01:50
03:30
06:00
09:00
15:00
21:00
Cell multiplication
III
00:00
ATc -
01:50
03:30
06:00
09:00
15:00
21:00
Cell multiplication

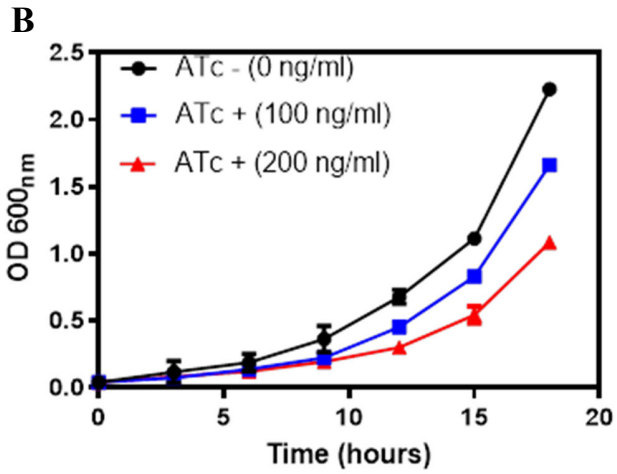

Appendix 3.4: **Micrographs of mc²155::CRISPRi-MurT-GatD without CRISPRi induction and growth analysis of mc²155::CRISPRi-MurT-GatD with/without CRISPRi induction**. (A) Time-lapse micrographs of the MurT-GatD depletion strain without CRISPRi activation (ATc-) pulse-chase labeled with FDAAs (TAMRA-D-Alanine [TADA] and HCC-D-Alanine [HADA]). The cells were grown first in no-label media only and subsequently labeled for 15 min with media supplemented with 1mM TADA. The TADA supplemented media was washed out with no-label media and the cells were later labeled for 15 min with 1 mM HADA supplemented media which was later replaced with no-label media. Scale bar is 5 µm. (B) Growth analysis of the MurT-GatD knockdown strain. Time-lapse microscopy of the TADA & HADA pulse-chase labeled cells was performed for 24 hours.

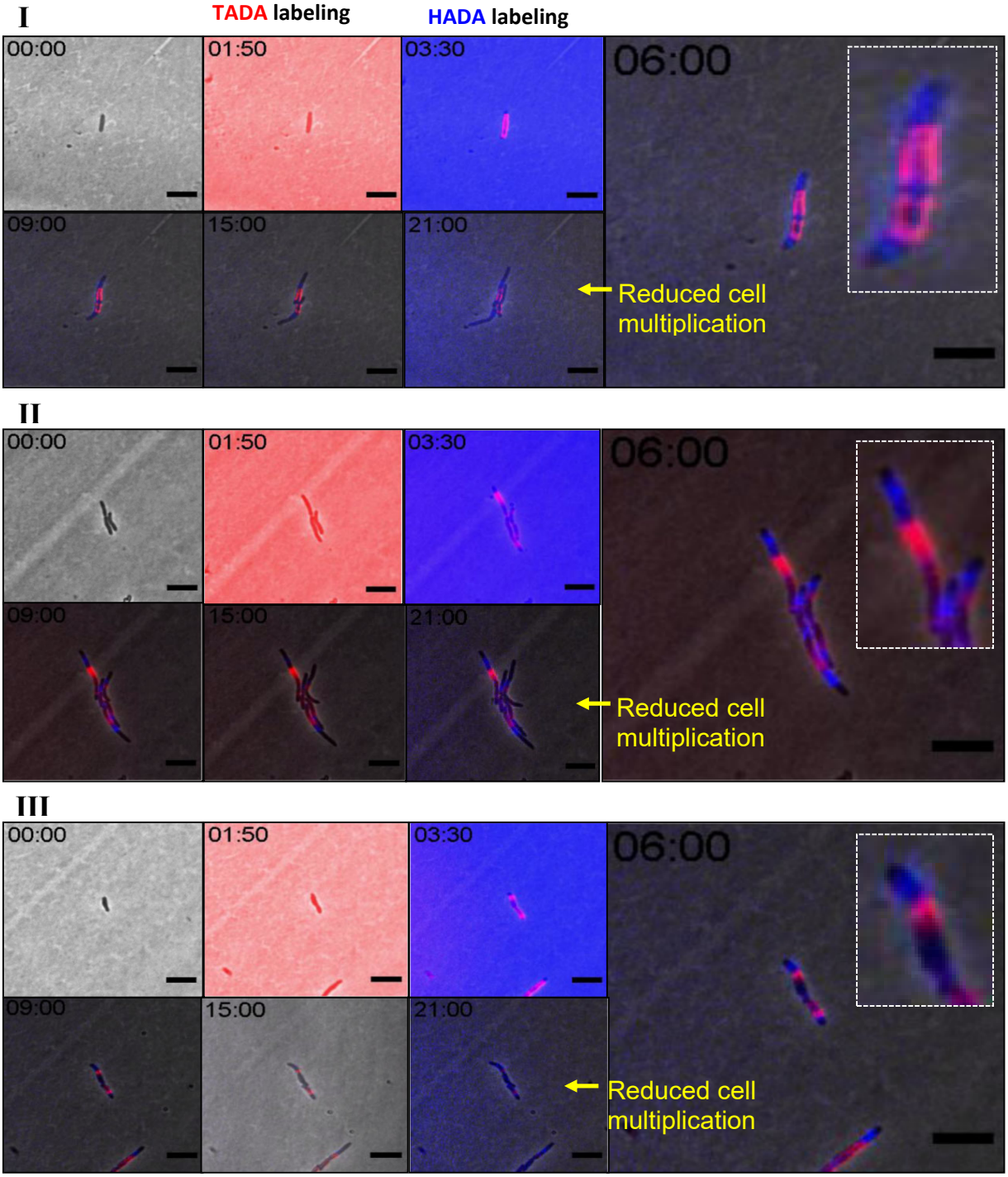

Appendix 3.5: **Time-lapse micrographs of the MurT-GatD depletion strain with CRISPRi activation (ATc+) and pulse-chase labeling with FDAAs (TAMRA-D-Alanine [TADA] and HCC-D-Alanine [HADA]).** The cells were grown first in no-label media (supplemented with 200 ng/ml ATc) and subsequently labeled for 15 min with media supplemented with 1 mM TADA and 200 ng/ml ATc. The TADA supplemented media was washed out with no-label media and the cells were later labeled for 15 min with media supplemented with 1 mM HADA and 200 ng/ml ATc which was later replaced with no-label media supplemented with 200 ng/ml ATc. Time-lapse microscopy of the TADA & HADA pulse-chase labeled MurT-GatD depletion cells was performed for 24 hours. CRISPRi mediated depletion of MurT-GatD resulted in reduced cell growth. Scale bar is 5 µm.

```
GatD/CobQ2      ------------------------------------------------------------  0
CobQ1           MTGGALLVAGTTSDAGKSMLVGGLCRLLVRKGLSVAPFKAQNMSNNSAVTVEGGEIGRAQ  60

GatD/CobQ2      ------------------------------------------------------------  0
CobQ1           AMQARAAGLAPSVRFNPILLKPGGDRTSQLVVRGQVTGSVAAADYINHRDHLAAVVADEL  120

GatD/CobQ2      ------------------------------------------------------------  0
CobQ1           SSLREDFDAVICEGAGSPAEINLRATDLANMGLARAAALPVIVVGDIDRGGLLAHLHGTV  180

GatD/CobQ2      ------------------MTHPS----------------------------------T  6
CobQ1           AVLEPADQALVSGFVVNKFRGDPSLLAPGLRQLAELTGRPTYGVIPFHDEIWLDTEDSVS  240
                                 .**                                     :

GatD/CobQ2      VRIGLVLPDVMGTYGDGGNAVVLRQRLRLRGIDA--EI----------VEITLDDPVPES  54
CobQ1           VRPGGLVGAPEPP---RGEQTLTVAAIRLPRISNSTDIEALACEPGVVVRWVTDAADLTG  297
                ** * ::          *: .:    :**  *.   :*          *. . *     .

GatD/CobQ2      LDLYTLGGAEDYAQRLATKHLIRH----PGLQRAAERGAPILAICAAIQVLGHWYET---  107
CobQ1           ADLVVIPGSKAT---VTDLRWLRERGLAAGIAAHAAAGRAVLGVCGGFQMLCSRIDDPVE  354
                 ** .: *::     ::  : :*.     *:   *  *  :*.:*..:*:*    :

GatD/CobQ2      SAGERVEGVGLLDATTSPQEARTIGEVASRPLPDGLDQPLTGFENHRGGTLLGSDARPLG  167
CobQ1           SREGRVDGLGLLDADIEFAAQK---------TLRHWETPLHGYEIHHGQVARSAETDWLG  405
                *   **:*:***** .   :             : ** *:* *:* .  .:::  **

GatD/CobQ2      AVTKGAGNRAGDGFDGAVQGSVVA-TYMHG---------PCLARNPQLADH--LLSRVVG  215
CobQ1           IGL-RRGAVYGTHWHGLLDNDALRRDWLTEVAAAAGRDGFVVADDVDVSARRDAQLDLMA  464
                      *   *  :.* ::...:   ::             :* : ::: :      ::.

GatD/CobQ2      DLPPLELPEVERLRSERLAAPRRV--------        239
CobQ1           DLIENHLDVGAILDLLEHGAPHRPTMSTALHV        496
                **   .*     *   . .**:*
```

Appendix 3.6: **Sequence alignment of GatD/CobQ2 with CobQ1.** ClustalOmega (https://www.ebi.ac.uk/Tools/msa/clustalo/) was used to align protein sequences of GatD/CobQ2 and CobQ1.

CHAPTER 4

(A Novel CRISPRi based BCG vaccine targeting the NOD-1 pathway induces protection against *Mycobacterium tuberculosis* infection in mice)

4.1. Introduction

Despite the availability of the Bacillus Calmette-Guérin (BCG) vaccine, Mtb, the causative agent of TB, remains one of the leading causes of death from a single infectious pathogen (1). TB mortality has risen for the first-time in a decade causing 1.8 million deaths in 2020 (140). BCG has reached its centenary, having first been administered in 1921 as a preventative TB vaccine to a baby born to a mother who had a few hours earlier, succumbed to TB disease (141). BCG is among the most widely administered vaccines worldwide, with approximately 154 countries having a BCG vaccination policy (142). However, BCG is only effective in preventing TB in infants and its efficacy in adolescents and adults is highly variable ranging from 0-80% (143). The failure of BCG to curb the TB epidemic highlights the need for basic understanding of BCG induced protective immune responses to enable development of a better TB vaccine (144-146).

BCG was generated by Albert Calmette and his co-worker Camille Guérin by multiple serial passages (~231 passages) of *M. bovis*, a virulent strain that causes bovine TB (141). This led to the deletion of multiple genomic regions (~16, named regions of difference [RD] 1-16) compared to Mtb that caused attenuation of BCG (147). Of particular importance to the attenuation and safety profile of BCG is the loss of a virulence protein EsxA (also known as ESAT-6), due to spontaneous deletion of a 9.5-kb RD-1 in BCG (148). The RD-1 harbors some of the genes encoding for proteins required for assembly of the ESX-1 secretion system which is essential for the secretion of key virulence proteins and for phagolysosomal escape during infection (Fig. 4.1) (149).

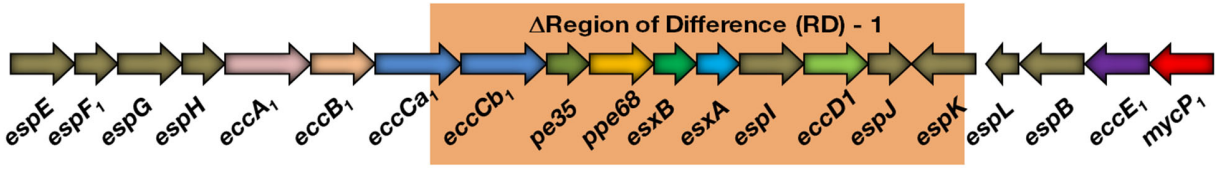

Figure 4.1. **Genetic organization of the ESX-1 secretion system**. Shown is the region of difference (RD-1) missing in BCG (in the orange box) (149).

Attempts to enhance the efficacy of BCG by re-introduction of ESX-1 from Mtb resulted in unfavourable outcomes (148). rBCG::ESX_1^{Mtb} displayed improved vaccine efficacy, however,

this strain also displayed increased virulence in murine experiments and was deemed unsafe. Further attempts involved: (I) development of a EsxA-overexpressing recombinant BCG strain, rBCG-E6 (150); (II) heterologous expression of ESX-1 from a less pathogenic mycobacterium species *M. marinum* which is related to Mtb but causes infection in fish and frogs, to create rBCG::ESX_1^{Mmar} (151) or (III) heterologous expression of Mtb EsxA in BCG designed for secretion through the ESX-5 secretion system by fusing EsxA with a ESX-5 canonical secretion signal peptide sequence to create rBCG::ESAT6-PE25SS (Table 4.1) (152). rBCG-E6 did not display improved efficacy compared to standard BCG (150). rBCG::ESX_1^{Mmar} displayed reduced virulence compared to rBCG::ESX_1^{Mtb} in murine infection experiments and also displayed improved vaccine efficacy compared to standard BCG (151). rBCG::ESAT6-PE25SS displayed increased protective efficacy compared to standard BCG, however, this strain also displayed increased immunogenecity due to ESAT-6 secretion (152).

Apart from inducing enhanced efficacy by ESX secretion system based mechanisms, other strategies to enhance BCG efficacy involve the deletion of immuno-evasive/suppressive genes from BCG or re-engineering BCG to express human pro-inflammatory cytokines, immunomodulatory bacterial toxins, or increased levels of endogenous non-protein immunomodulatory molecules like cyclic dinucleotides (153). A list of recombinant rBCG strains with such modifications is given in Table 4.1 and a brief history of genetic engineering of BCG is shown in Fig. 4.2. rBCG::ESX_1^{Mtb} is among the most effective rBCG strains ever developed (154), which demonstrated that enhancing cytosolic contact of BCG and activation of cytosolic PRRs leads to increased vaccine efficacy (155). This led to the development of candidates such as VPM1002, the most clinically advanced rBCG (156), with a urease C (*ureC*) deletion replaced by a *hly* gene encoding for listeriolysin. This enables BCG to disrupt the phagolysosomal membrane and promote release of phagolysosomal content to the cytosol. Although there is no evidence that VPM1002 reaches the cytosol itself (141), this vaccine displays increased immunogenicity and efficacy, highlighting that increased activation of cytosolic PRRs enhances BCG efficacy.

Table 4.1. **A list of recombinant BCG vaccines**. The list contains rBCG strains with deletions in immunosuppressive/evasive genes, rBCGs expressing human pro-inflammatory cytokines, immunomodulatory bacterial toxins, or increased levels of endogenous non-protein immunomodulatory molecules.

Strain name	Description	Ref
rBCG::ESX_1^{Mtb}	rBCG with the RD1 gene cluster inserted (Rv3861–Rv3885). Expresses ESAT-6 and CFP10	(157)
rBCG:ESX_1^{Mmar}	rBCG with the insertion of the esx1 locus of *Mycobacterium marinum*	(151)
rBCG E6	BCG over-expressing ESAT-6	(150)
rBCG::ESAT6-PE25SS	rBCG with ESAT-6 fused with the canonical ESX-5 secretion system signal sequence – secretes ESAT-6 through ESX-5	(152)
rBCG-Rv2212	rBCG expressing Rv2212, an adenylyl cyclase from Mtb	(158)
rBCG:CysVac2	rBCG expressing CysVac2, a fusion protein of Ag85A & CysD	(159)
rBCG85C5	rBCG overexpressing Ag85A and C5 peptide of CFP-10	(160)
rBCG/PhoPR	rBCG overexpressing PhoP-PhoR	(161)
rBCGΔureC::hly (pMPIIB01)	rBCG ΔureC:hly expressing the latency antigens Rv2659c, Rv3407, and Rv1733c	(162)
rBCG-Ag85B-ESAT-6-TNFα	rBCG expressing the fusion protein Ag85B-ESAT-6-TNF-α	(163)
rBCG 30	rBCG over-expressing antigen 85B (Ag85B)	(164)
rBCG(mbtB30)	rBCG over-expressing Ag85B, with disrupted synthesis of the siderophore mycobactin	(165)
rBCG-1173:A	rBCG expressing Ag85A	(166)
rBCG::AXB	Cocktail of rBCGs expressing Ag85A, Ag85B and latency antigen HspX	(167)
(H)PE-ΔMPT64-rBCG	rBCG expressing MPT64 fused to the PE domain of the PE_PGRS33	(168)
AERAS-422 (AFRO-1)	rBCG expressing Ag85A, Ag85B and TB10.4	(169)
rBCG-LTAK63lo	rBCG expressing LTAK63, a detoxified form of *E. coli* heat labile toxin	(170)
rBCG-disA-OE	rBCG overexpressing the di-adenylate cyclase DisA and releases high levels of the STING agonist c-di-AMP	(171)
rBCG-Sec^{DFG}	rBCG overexpressing Mtb SecDFG involved in the Sec Pathway responsible for exporting extracellular proteins	(172)
rBCG:ESAT-L28A/L29S	rBCG expressing mutated ESAT-6 (ESAT-L28A/L29S)	(154)
rBCG Ag85B-ESAT-6-IFN-γ	rBCG expressing the fusion protein Ag85B-ESAT-6-IFN-γ	(173)
sapM::Tn BCG	sapM transposon mutant of BCG that abolishes its expression	(174)

rBCG Δzmp1	rBCG deficient in gene zmp1, a putative Zn2+ metalloprotease	(175)
rBCG ΔureC:hlyΔpdx1/ VPM1002Δpdx1	rBCG ΔureC:hly deficient in pyridoxine synthase, required for synthesis of the essential vitamin B6	(176)
rBCG ΔureC::hlyΔnuoG	rBCG ΔureC:hly with deletion of nuoG, an anti-apoptotic gene	(177)
rBCGΔBCG1419c	rBCG deficient in gene BCG1419c	(178)
rBCG-ΔUT	Urease-deficient rBCG	(179)
rBCG-DHTM	rBCG-ΔUT expressing fusion protein of HSP70 and MMPII	(180)
rBCG-PEST	Urease-deficient rBCG expressing fusion protein of Mtb HSP70 and MMPII)with PEST sequence in both ends of HSP70-MMPII fusion protein	(181)
AERAS-401 (rBCG1331 ΔureC:ΩpfoAG137Q)	rBCG with the ureC gene replaced with the PfoAG137Q gene for perfringolysin O	(169)
rBCG(MCP-3)	rBCG expressing MCP-3 (monocyte chemotactic protein 3)	(182)
rBCGi	rBCG expressing Ipr1 (intracellular pathogen resistance 1)	(183)
rBCG::BAX	rBCG-expressing pro-apoptotic protein BAX	(184)
rBCG ΔureC:hly_hIL7 and rBCG ΔureC ::hly_hIL18	rBCG ΔureC:hly expressing human IL-7 or human IL-18	(185)
rBCG-IL-4, rBCG-IL-6, rBCG-GMCSF, rBCG-IFN-γ, rBCG-IL-2, rBCG-IL-18	rBCGs expressing murine interleukin (IL)-4, IL-6, GM-CSF, IFN-γ, and IL-2	(186)
rBCG-Ag85B-IL-15	rBCG expressing a fusion protein of Ag85B and IL-15	(187)
rBCG2	rBCG expressing Ag85B, CFP10 and IL-12	(188)
rBCG::IL-12p70-ESAT-6	rBCG expressing a fusion protein of the human IL-12p70 and ESAT-6	(189)
rBCG::Ag85B-IL-15	rBCG expressing a fusion protein of the human IL-15 and Ag85B	(187)
rBCG::CMX	rBCG expressing a fusion protein (CMX) composed of immunodominant epitopes from Ag85C, MPT51, and HspX	(190)
rBCG::Mkan85B	rBCG expressing the Ag85B protein of *M. kansasii* (Mkan85B)	
rBCG::CRISPRi-AftC	CRISPRi based rBCG designed for the truncation of the anti-inflammatory cell wall associated lipoglycan – lipoarabinomannan (LAM) into the pro-inflammatory lipomannan derivative (LM) by repression of AftC expression	(191)

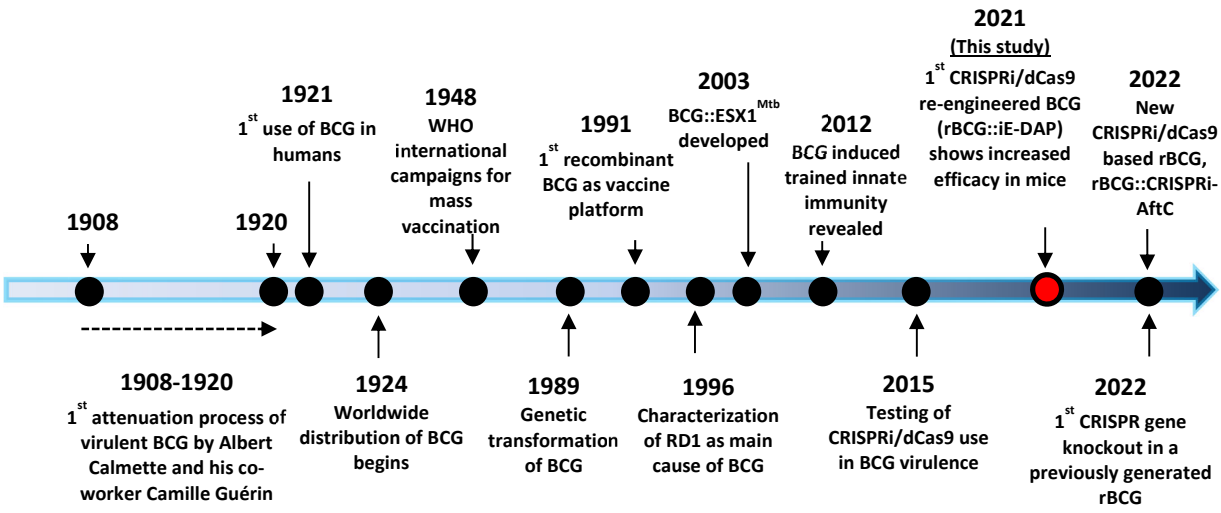

Figure 4.2. **Time-line showing the key events for rBCG development since the development of the BCG vaccine in 1921**. Experimental attenuation of BCG started from 1908 to 1920 by serial passaging of a virulent strain of *M. bovis* by Albert Calmette and Camille Guérin (192). In 1921, BCG was used to immunize a baby against TB infection for the 1st time (192). In 1924, global distribution of BCG began (193). In 1948, campaigns for international mass vaccinations were introduced by the WHO (194). In 1989, genetic transformation of BCG was reported (195). The first rBCG strain for proof of concept of a rBCG as a vaccine platform was reported in 1991 (196). In 1996, characterization of the RD-1 region as the main cause of BCG attenuation was reported (197). Proof of increased efficacy against TB infection for a rBCG was shown with the development of the BCG::ESX_1^{Mtb} strain in 2003 (157). In 2012, BCG induced trained innate immunity was revealed (198). In 2015, a CRISPR/dCas9 platform was tested for applicability in BCG (199). In 2022, a CRISPR gene knockout platform was used for generation of an antibiotic unmarked auxotrophic BCG strain and the CRISPRi platform was used for generation of rBCG::CRISPRi-AftC (191, 200). In this study we show that rBCG::iE-DAP improves protection againt Mtb H37Rv infection in a mouse model of TB infection.This figure was adapted from Lazaro et al. 2021 (153).

Recombinant BCG strains re-engineered to activate innate cytosolic PRRs show enhanced efficacy (156, 171, 201). For example, rBCG-disA-OE, a rBCG strain overexpressing the diadenylate cyclase DisA causing high release of the STING agonist cyclic-di-AMP, displayed increased efficacy in a guinea pig infection model showing that increased cytosolic PRR signaling increases BCG efficacy (171). This spurred the need to uncover mechanisms through which BCG masks potential PRR ligands to suppress cytosolic PRR signaling as a strategy to improve BCG efficacy.

4.2. BCG induced correlates of protection against TB infection beyond T helper-1 responses

BCG vaccination induces the development of T-helper type 1 (Th1) CD4+ memory lymphocytes, CD8+ T cell responses, Th17 responses, activation of natural killer (NK) cells, antibodies, IFN-γ-negative T cell responses and trained innate immune responses among other immune responses (Fig. 4.3) (202-204). CD4+ T cell responses are critical for protective immunity against TB disease (205, 206), however, a clinical study of the MVA85A vaccine, a viral vectored TB vaccine candidate inducing high CD4+ T cell responses failed to show efficacy in late-stage clinical development (207). This highlights that other aspects of the anti-tuberculous immune response remain to be targeted and activated by new TB vaccines to enhance vaccine efficacy (Fig 4.4) (155, 208, 209).

In this chapter, an overview of other aspects of BCG induced immunity beyond CD4+ T cell responses is discussed and rBCG strains enhancing these immune responses that correlate with protective immunity are highlighted. Finally the NOD-1 pathway is identified as a target for development of a novel rBCG vaccine. We show that vaccination of mice with a novel rBCG; rBCG::iE-DAP designed to target the NOD-1 pathway improves protection againt Mtb H37Rv infection in a mouse model of TB infection.

4.3. Role of CD8+T cells in BCG induced immunity

BCG vaccination induces limited activation of CD8+ T cells and this contributes to the insufficient efficacy of BCG (210). However, studies have identified a role of CD8+ T cell responses against Mtb infection (Fig. 4.4), prompting the need for development of CD8+ T cell activating TB vaccines (211). Post-BCG vaccination, dendritic cells with internalized BCG, drive the activation of CD8+ T cells through major histocompatibility complex (MHC) class I cross-presentation of antigens (212). Murine studies with BCG show that mycobacteria specific CD8+ T cells accumulate in the lung after BCG immunization and correlated with protection against Mtb infection (213). Subcutaneous vaccination of mice with rBCG::ABX and BCGΔBCG1419c induced protection against Mtb infection, which correlated with increased antigen specific CD4+ T cells and CD8+ T cells (214, 215). Other rBCGs, including rBCG2, rBCG::IL-12p70-ESAT-6 and rBCG::Ag85B-IL-15 expressing human cytokines in addition to

mycobacterial antigens were also shown to induce increased activation of CD8+ T cells, this correlated with increased vaccine efficacy (187-189). BCG::ESX_1^{Mmar} was also shown to increase CD8+ T cell responses, showing that BCG efficacy can be enhanced by increased cytosol access and activation of CD8+ T cell responses (151). VPM1002 was designed to also access the host cytosol and increase availability of mycobacterial antigens to the MHC-class I pathway (216). This led to increased activation of CD8+ T cells by VPM1002 and is an attribute of the increased efficacy of this vaccine candidate (156).

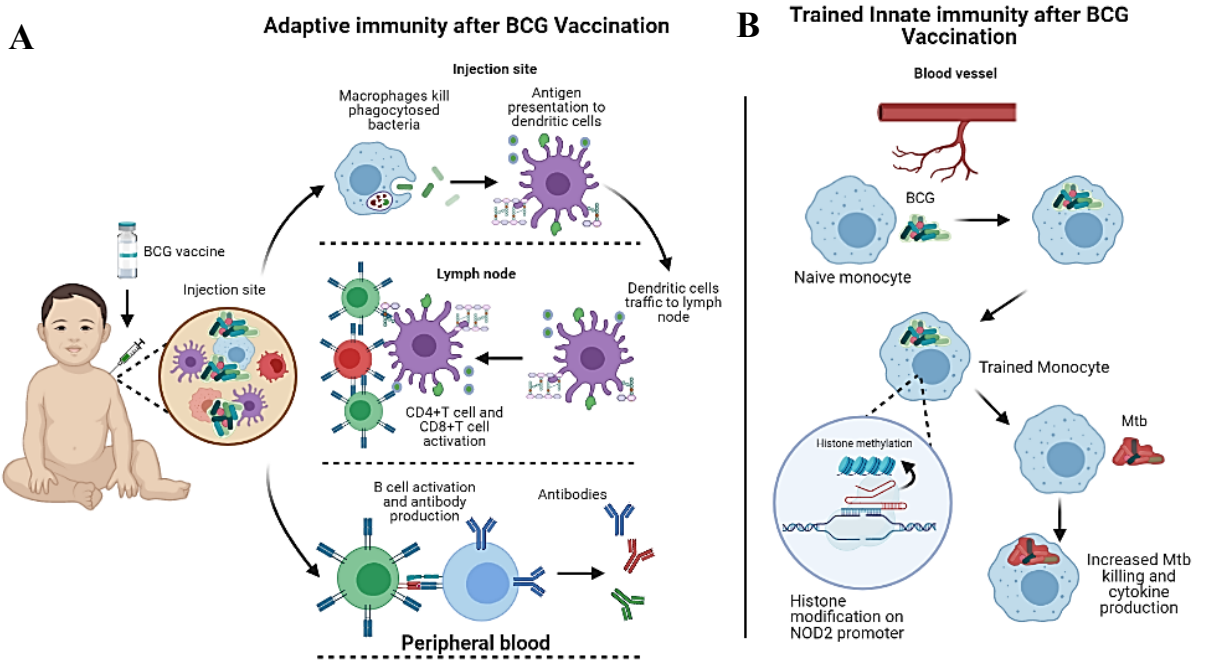

Figure 4.3. **Immune responses induced by BCG vaccination at the site of injection, lymph nodes and peripheral blood.** Shown are the adaptive immune responses (A) and trained innate immune responses (B) elicited after BCG vaccination. After BCG vaccination at the injection site, macrophages, monocytes and dendritic cells internalize BCG (which replicate for a limited amout of time at the injection) and kill the bacteria for presentation of BCG antigens. Activated dendritic cells with BCG antigens presented by macrophages migrate to the lymph nodes for activation of naïve CD4+ T cells and CD8+ T cells. Activated T cells enter peripheral blood where they activate naïve B cells which differentiate into antibody producing plasma cells. BCG also induces trained innate immune responses in macrophages. Naïve macrophages that phagocytose BCG are trained by exposure to BCG and possess epigenetic and metabolic modifications through BCG activation of the NOD-2 PRR. Trained macrophages are more bactericidal to Mtb upon exposure at a later stage. Image created with Biorender.com.

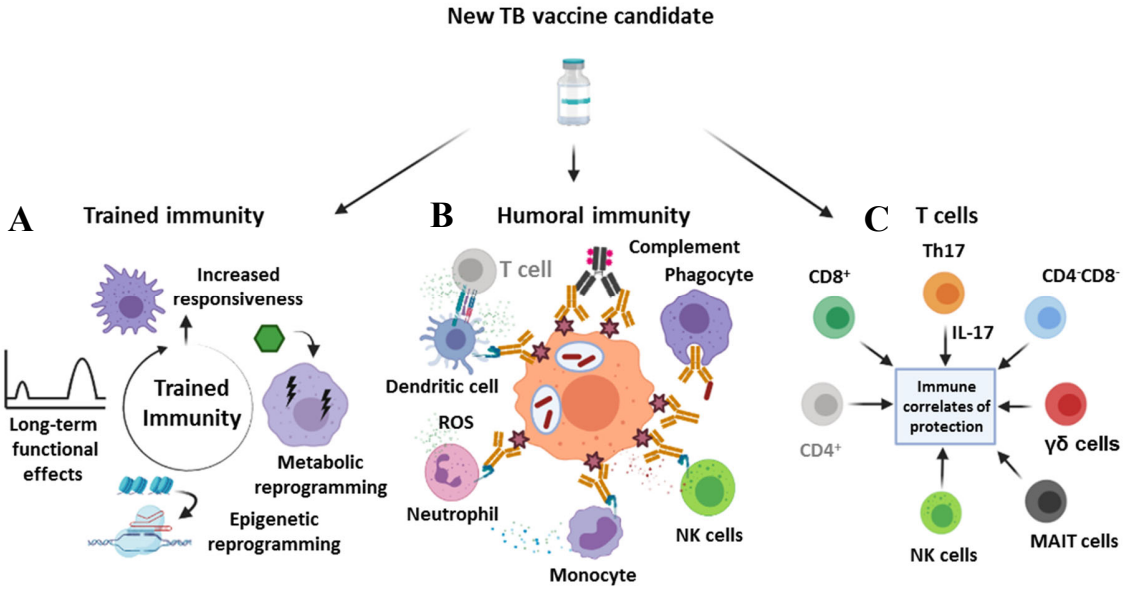

Figure 4.4. **Targets of the host immune system for new TB vaccine candidates**. Shown are the immune correlates of TB vaccine mediated protection, namely: (A) trained innate immune responses, (B) humoral immunity and T cell mediated responses. Image created with Biorender.com

4.4. Role of Th17 responses in BCG induced immunity

The quest for identification of correlates of protection against TB infection has also identified Th17 cells as a cell type associated with protective immunity induced by BCG vaccination (Fig. 4.4) (217, 218). Th17 cells are derived from naive CD4+ T cells upon activation by myeloid-derived macrophages. BCG vaccination induces a sub-optimal Th17 response and this has been attributed to the lack of the RD-1 region or access of BCG to the host cytosol as re-introduction of RD-1 in BCG resulted in promotion of protective Th17 dependent responses (219). TB vaccine candidates inducing Th17 responses, together with others employing novel IL-17 response-inducing adjuvants, are of interest in TB vaccine development as increased Th17 and IL-17 responses during the early phase of infection correlate with vaccine mediated protection against Mtb infection (220).

Vaccination of mice with VPM1002 resulted in production of increased Th17 responses in the lungs of mice following Mtb infection, which correlated with protection against infection (156). Similarly, vaccination of mice with BCG-CMX resulted in increased Th1, Th17 and

polyfunctional T cells with higher protective efficacy against Mtb infection (190). Another example of the protective role of IL-17 signaling after vaccination was shown by vaccination of mice with rBCG-LTAK63lo. This resulted in production of higher levels of Th1 cytokines in conjunction with IL-17 in the lungs of vaccinated mice, which in turn provided better protection against Mtb infection compared to mice vaccinated with standard BCG (221). In other murine studies, vaccination with BCGΔBCG1419c reduced production of pro-inflammatory cytokines such as TNFα and IL-17 at later stages of infection. This is correlated with enhanced vaccine efficacy as reduced pro-inflammatory cytokines at later stages of infection may possibly dampen disease associated inflammation to reduce lung pathology (178).

4.5. Role of Natural Killer cells in BCG induced immunity

Natural killer (NK) cells are another cell type that has attracted attention for TB vaccine development (Fig. 4.4) (208). NK cells are cytotoxic granular lymphocytes which possess non-MHC-restricted cytotoxic activity against microbes and infected host cells (222). NK cells can bind pathogens and exert this cytolytic activity by bactericidal molecules including perforin, granulysin and granzymes and also exert cytotoxicity on infected host cells lacking expression of MHC-class I molecules on the cell surface (222). NK cells can bind and kill extracellular Mtb directly and also recognize and lyse Mtb-infected immune cells (223). The concept that NK cells could have features of immunologic memory has highlighted the need to develop and test NK cell activating TB vaccines (224). BCG vaccination has been shown to induce expansion of NK cells with memory-like features and characterized by increased cytokine production upon re-exposure to Mtb (225). These NK cells were found to contribute to vaccine-induced protection against Mtb infection and were able to proliferate and contribute to Mtb growth control upon adoptive transfer into Mtb infected mice (225). In humans, BCG vaccination has been shown to induce trained innate immune responses in NK cells, characterized by increased pro-inflammatory responses (226). BCG-reactive NK cells with memory-like features are induced by BCG vaccination in infants and BCG revaccination of latently TB infected adults induced the production of long-lived memory-like NK cells, which may be targeted for TB vaccine development (227).

4.6. Role of humoral anti-TB immunity in BCG induced immunity

Early studies on the role of humoral immunity in protection against TB infection have suggested that neither B-cells nor antibodies could confer protection against TB disease (228). An example of this was demonstrated by a study on the depletion of B-cells in a cynomolgus macaque model of TB infection, showing no difference in overall disease pathology between B-cell depleted animals and healthy animals when challenged with Mtb (229). However, analysis of individual granulomas from these animals demonstrated changes in T-cell responses and cytokine levels. This was accompanied by increased bacterial burdens in B-cell depleted animals, a finding which was also observed in mice lacking B-cells or mice with B-cells unable to secrete antibodies (229-231). Interestingly, there is emerging evidence that antibodies can play a role in protection against TB (Fig. 4.4).

BCG vaccination-induced humoral responses have been correlated with protective immunity against TB (232). BCG-revaccination studies in human clinical trials and animal challenge studies demonstrated increased production of anti-mycobacterial specific antibodies (233, 234). Additionally, rhesus macaques that received repeated BCG endobronchial instillation produced high titers of purified Mtb protein derivative (PPD)-specific antibodies (235). This suggested that BCG vaccination could result in generation of protective antibodies that in turn could be amplified by subsequent vaccination. An example of this was demonstrated in a study assessing the contribution of humoral immunity in a rhesus model of intravenous (IV) BCG vaccination in which sterilizing immunity against TB infection had been observed (236). This study demonstrated the broad production of protective antibody responses in the blood and broncho-alveolar lavage fluid (BAL) from animals that received IV BCG compared to animals that received aerosol or intradermal BCG vaccination. Among the antibody subtypes analyzed, IgM titers in the plasma and BAL highly correlated with protection against TB. Furthermore, *in vitro* experiments demonstrated the efficacy of a LAM-specific synthetic IgM antibody in inhibiting Mtb growth (236).

Recombinant BCG vaccines (VPM1002 and BCGΔ*ureC*::*hly*Δ*nuoG*) induced increased production of Mtb-specific antibodies compared with BCG (216, 237). Furthermore,

immunization of mice with a derivative of VPM1002 - BCGΔ*ureC*::*hly*Δ*nuoG*, (designed to enhance apoptosis of infected macrophages by deletion of the anti-apoptotic virulence gene *nuoG* from VPM1002), induced increased antibody production compared to VPM1002 and BCG (238). These studies demonstrated that BCG can be engineered to induce humoral anti-TB responses.

4.7. Role of BCG induced trained innate immunity against Mtb infection

BCG induced trained immunity has been suggested as a correlate of protection implicated in early clearance of TB infection independent of Th1 responses (155). BCG induced trained immunity has also been associated with reduced all cause neonatal mortality (239). While the immune responses responsible are now being investigated, monocytes derived from BCG-vaccinated new-borns and TB resistors have been shown to display a trained phenotype and epigenetic modifications causing increased cytokine production correlating with the ability of these cells to control Mtb growth *in vitro* (240, 241). These studies highlighted the unexpected ability of innate cells to possess memory-like features that could be exploited for TB vaccine development.

BCG induced trained innate immunity has emerged as an avenue that remains to be targeted for development of novel TB vaccines (155). In murine studies, intravenous administration of BCG reprograms hematopoietic stem cells (HSCs) to produce trained macrophages with epigenetic and metabolic modifications that confer significantly better protection against Mtb infection when compared to naïve macrophages (242). Additionally, pulmonary BCG administration has been shown to induce memory-like features in AMs enabling them to control Mtb growth upon challenge (243). In another study, epigenetically programmed mouse-lung macrophages displayed pro-inflammatory responses associated with Mtb growth control (244). Furthermore, macrophages isolated from BCG vaccinated individuals could control Mtb growth and these macrophages displayed an altered DNA methylation pattern with increased production of cytokines (245). BCG induced trained innate immunity is associated with epigenetic modifications (e.g. H3K4me3, trimethylation of histone 3 at lysine 4 or H3K2Ac, acetylation of histone 3 at lysine 2, causing increased gene transcription) on the promoter region of immune

associated genes, including the gene coding for the NOD-2 receptor (246, 247). Furthermore, analysis of BCG induced immune responses in previously BCG-naive adult individuals 8 months post vaccination revealed BCG-induced differential methylation of immune genes, including a NOD-2-like receptor signaling pathway. This was suggestive of induction of NOD-2 dependent epigenetic modulation for development of BCG induced protection (248). NOD-1 and NOD-2 both bind released PG fragments during bacterial infection (249). Recombinant BCG vaccines able to epigenetically prime transcription of PRRs, including both NOD-1 and NOD-2, could enhance induction of trained innate immune responses (250, 251).

The recombinant BCG vaccine, rBCG disA-OE, which induced increased protection against Mtb infection in a murine TB study (171), has been shown to induce enhanced trained innate immune responses (252). This provides support for the concept that anti-TB trained innate immune responses can be enhanced by novel TB vaccines. TB vaccine candidates designed to modulate the epigenetics of innate immune cells and prime these cells for enhanced responses upon Mtb infection through trained immunity will enable the study of effective innate immune responses for protection against TB infection. Herein, we present a novel rBCG, rBCG::iE-DAP designed to activate the NOD-1 pathway to enhance protective immune responses against Mtb infection.

The aims and objectives of this chapter are outlined in the next sections.

4.8. Hypothesis

Reduced expression of MurT and GatD in BCG causes decreased PG amidation, increased activation of NOD-1 and NOD-2 and an enhanced development of anti-tuberculous immune responses effective against virulent Mtb infection.

4.9. Aim

The aim of this section is to determine the effect of MurT-GatD depletion in BCG and to determine the ability of a recombinant BCG strain (depleted of MurT and GatD enzymes) to induce the development of protective immunity against Mtb infection in mice.

4.10. Objectives

1. Construction of a rBCG strain depleted of MurT and GatD enzymes.
2. Assess the phenotypic effects of MurT-GatD depletion in BCG.
3. Assess the ability of rBCG trained macrophages to provide better protection against virulent Mtb when compared to macrophages trained with standard BCG.
4. Assess the activation of rBCG::iE-DAP in Bone Marrow Derived Macrophages (BMDMs) and induction of cytokine expression by rBCG::iE-DAP compared to BCG by ELISA.
5. Assess rrBCG::iE-DAP activation *in vitro* and in mice-aerosol infections with Doxycyline.
6. Analysis of the efficacy of rBCG::iE-DAP vaccination compared to BCG against Mtb infection in a mouse model of TB infection.
7. Analysis of the mouse lung pathology after vaccination with rBCG::iE-DAP+Dox compared to WT BCG post Mtb infection.

4.11. Materials and Methods

4.11.1. Bacterial strains and Culture conditions

4.11.1.1. Growth conditions for *E. coli* DH5α and derivative strains

E. coli DH5α and derivative strains were grown in Luria-Bertani broth (LB) or on Luria-Bertani agar (LA) at 37ºC with supplementation of the media with appropriate antibiotics. The antibiotic concentration used was as follows: Kanamycin (Kan): 50 µg/ml. Liquid cultures were grown at 37ºC with shaking at a 100 rpm.

4.11.1.2. Growth conditions for Mycobacterial and derivative strains

M. bovis BCG, Mtb H37Rv and the recombinant BCG::CRISPRi MurT-GatD strain were grown at 37ºC in Middlebrook 7H9 broth supplemented with OADC enrichment, 0.5% glycerol, 0.05% Tween 80 and appropriate antibiotics (hereafter referred to as Middlebrook 7H9 broth) or on Middlebrook 7H11 agar supplemented with OADC enrichment and 0.5% glycerol and appropriate antibiotics. Antibiotic concentration used is Kan: 50 µg/ml.

4.11.2. Construction of a recombinant BCG::CRISPRi strains

The programmable mycobacterial CRISPRi system for repression of gene transcription was used as previously described by Rock et al. 2017, to generate the recombinant BCG::CRISPRi strain – rBCG::iE-DAP (14). Briefly, the CRISPRi system utilizes a catalytically-inactivated anhydrotetracycline/doxycycline (ATc/Dox)-inducible CRISPRi dCas9 from *S. thermophiles* which is directed by a ATc-inducible short-guide RNA (sgRNA) to specific target genes to prevent transcription initiation or elongation (113). The sgRNA for *murT-gatD* targeting was designed with the CRISPRi sgRNA design tool - https://pebble.rockefeller.edu/. The sgRNA oligos (Top and Bottom oligos [Table A2]) were annealed and cloned into BsmBI-digested CRISPRi vector PLJR965 in proximity to the dCas9 handle to assemble the sgRNA. The resulting plasmid was introduced into *M. bovis* BCG by electroporation as described in section 2.6.1.1.

4.11.3. Quantitative real-time PCR (qPCR)

qPCR was performed using Sso Fast Evagreen Supermix (BioRad) as per manufacturer's instructions. Briefly, 20 µl reactions were set up, each containing 10 µl Evagreen Supermix, 0.75

µl forward primer (10 µM), 0.75 µl reverse primer (10 µM), 2 µl cDNA and nuclease-free water. All reactions were incubated in the CFX96 Real-Time PCR detection system (BioRad) using the following parameters: 98 °C for 2 min followed by 39 cycles consisting of three steps – 98 °C for 5 sec, 60 °C for 5 sec and 72 °C for 5 sec with SYBR Green quantification at the end of each cycle. Melt curve analysis was conducted from 65 °C with a gradual increase in 0.5 °C increments every 0.05 sec to 95 °C with SYBR Green quantification conducted continuously throughout this stage. The raw data was analyzed using the Biorad CFX Manager 3.0 Software (BioRad).

4.11.4. Mammalian cell culture and infection

For cell-based *in vitro* infection assays, the human monocyte U937 cell line (obtained as a gift from the Council for Scientific and Industrial Research [CSIR] of South Africa) and BMDMs extracted from the bone marrow (BM) of 6-8 weeks old female wildtype BALB/c mice were cultivated in RPMI-Glutamax (Cat. 61870-036, Fischer Scientific) supplemented with 10% heat inactivated fetal bovine serum (FBS) (Cat. 10082147, Fischer Scientific) at 37ºC with 5% CO_2. BMDMs were generated as previously described by Toda et al., (253). Briefly, for differentiation of BM cells into macrophages, BM cells were seeded in BMDM differentiation media (RPMI-Glutamax supplemented with 10% FBS and 10% L929-conditioned media) and differentiated for 6 days. Non-adherent cells were washed out with warm BMDM differentiation media and adherent macrophages were used for *in vitro* infection assays.

4.11.5. *In vitro* training of human monocyte U937 cell lines

In vitro training of monocytes was performed according to the model by Bekkering et al, 2016 (254) and Pan et al. (255). Briefly, U937 monocytes (1×10^6/mL) were transferred into a 24-well plate and cells were incubated with either culture medium only as a negative control or MDP, LPS, heat killed WT BCG or heat killed rBCG::CRISPRi strains at 37 °C, and 5% CO_2 for 24 h. Cells were washed twice with 1 mL of warm PBS and then incubated for 2 days in RPMI with 10% FBS and penicillin streptomycin in the presence of 25 nM phorbol 12-myristate 13-acetate (PMA) (which induces the differentiation of monocytes to macrophages). After washing twice with 1 mL of warm PBS, the differentiated macrophages were infected with Mtb H37Rv at MOI:1 and incubated for 24h. After 24 h, cells were lysed and bacterial load was enumerated by plating for CFU counts.

4.11.6. Enzyme-linked immunosorbent assay (ELISA)

Sandwiched ELISA was performed for cytokine (TNF-α and IL-6) measurement in culture supernatants. Culture supernatants were used immediately after harvest for ELISA. Sandwiched ELISAs (R&D systems) were performed as per manufacturer's recommendations.

4.11.7. BCG infection of WT/SCID BALB/c mice and CFU enumeration

The Johns Hopkins University animal care and use committee (protocol number: M020M20) was followed to determine the lung bacillary burden or virulence of wildtype (WT) and rBCG::iE-DAP strains 6-8 week-old female wildtype BALB/c mice or BALB/c SCID. The mice were infected using the aerosol route in a Glasscol inhalation exposure system (Glasscol). The inoculum implanted in the lungs at day 1 (n = 3 mice per group) in female BALB/c mice was determined by plating the whole-lung homogenate on 7H11-selective plates containing Carbenicillin (50 mg/ml), Trimethoprim (20 mg/ml), Polymyxin B (25 mg/ml) and Cycloheximide (10 mg/ml). Doxycycline was administered at a determined dose for CRISPRi activation by daily oral gavage *in vivo*. following infection, mice lungs were harvested (n = 5 animals/group), homogenized in sterile PBS and plated on 7H11-selective plates at different dilutions. The 7H11-selective plates were incubated at 37 °C and single colonies were enumerated at 10 days, week 4 and 8.

4.11.8. Mouse immunization and determination of vaccine protective efficacy and lung histopathology analysis

To test the efficacy of rBCG::iE-DAP, BALB/c mice (n = 10 per group) were immunized intradermally with 10^5 CFU/100 µL of WT BCG or rBCG::iE-DAP strains. Mice were sham immunized with saline and Dox was administered by daily oral gavage to the Saline+Dox (n=5), WT BCG+Dox (n=5) and the rBCG::iE-DAP+Dox (n=5) groups for 6 weeks. Mice were weighed once per week to monitor the effect of Dox administration on the health of the mice. Mice were challenged with ~100 CFU of Mtb H37Rv strain by the aerosol route 6 weeks post immunization in a Glasscol inhalation exposure system (Glasscol). Lungs and spleens from infected animals were harvested at week 4 and week 8 post Mtb infection for analysis of lung bacterial burden by plating the whole-lung homogenate on 7H11-selective plates containing Carbenicillin (50 mg/ml), Trimethoprim (20 mg/ml), Polymyxin B (25 mg/ml) and Cycloheximide (10 mg/ml). For histopathology, vertical halves of the left lung were fixed in 10% buffered formalin and sections of 5 µm in thickness from formalin fixed and paraffin embedded

tissues were cut onto glass slides and stained with H&E for histopathological examination.

4.11.9. Scanning electron microscopy (SEM) and transmission electron microscopy (TEM)

SEM and TEM were used to study the cell surface morphologies of the WT BCG and rBCG strains. The bacteria were immobilized to poly-l-lysine charged coverslips for 30 min and processed for SEM. Similarly, for TEM, bacterial suspensions were fixed and embedded in Spurr's resin. The immobilized bacteria were rinsed with phosphate buffered saline (PBS), and fixed in 2.0% paraformaldehyde, 2.0% glutaraldehyde in 1× PBS with 3 mM $MgCl_2$, pH 7.2 for 1 hour at room temperature. This was followed by 3 cycles of 10 minutes washes in sodium cacodylate buffer with 3% sucrose, samples were post-fixed in 0.8% potassium ferrocyanide, 1% OsO_4 and 3mM $CaCl_2$ in 0.1 M sodium for 1 hour on ice in the dark. Samples were then rinsed in sodium cacodylate buffer and slowly rocked at 4ºC overnight. After a brief water rinse (2 x 5 min), bacteria were placed in 2% uranyl acetate for 1 hour at room temperature in the dark. The samples were dehydrated through a graded series of ethanol to 100% EtOH, then a 1:1 solution of ethanol:Hexamethyldisiloxazne (HMDS) (Polysciences) followed by pure HMDS. Coverslips were dried in a desiccator overnight and then attached to aluminum stubs via carbon sticky tabs (TedPella Inc.), and coated with 20 nm of AuPd with a Denton Vacuum Desk III sputter coater. Stubs were viewed and digital images captured on a Leo 1530 field emission SEM operating at 1 kV. For TEM, equal volumes of 2× fixative (as described above) were added to bacterial suspensions and rocked for 10 minutes at room temperature. Samples were centrifuged, supernatant removed and 1× fixative added carefully to not disturb the pellet. All subsequent steps were identical to the protocol described above up for SEM to the final 100% ethanol step. Bacterial cells were transferred to propylene oxide, and gradually infiltrated with Spurr's low viscosity resin (Polysciences): propylene oxide. After 3 changes in 100% Spurr's resin, pellets were cured at 60ºC for two days. Sections were cut on a Reichert Ultra cut E with a Diatome Diamond knife. 80 nm sections were picked up on formvar coated 1 × 2 mm copper slot grids and stained with tannic acid and uranyl acetate followed by lead citrate. Grids were viewed on a Phillips CM 120 TEM operating at 80 kV and digital images captured with an AMT 8 K × 8 K CCD camera.

4.12. Results

4.12.1. Generation of rBCG::iE-DAP

The BCG vaccine expresses immune evasion proteins, lipids or molecules also found in Mtb that limit its efficacy (256). Transposon mutagenesis screens have been used successfully to identify non-essential immunomodulatory proteins that limit the efficacy of the BCG vaccine, including SapM; inactivation of which resulted in the development of the sapM::Tn BCG candidate vaccine (257, 258). However, essential mycobacterial immunomodulatory proteins remain to be studied to evaluate their role in modulating BCG vaccine efficacy. CRISPRi has been tested successfully in BCG for the study of essential genes (199). We targeted the *murT-gatD* genes in BCG (see Appendix 4.1) with CRISPRi to develop rBCG::iE-DAP designed for depletion of MurT-GatD expression which results in reduced PG amidation aimed at activating the NOD-1 pathway for enhancing BCG PRR signaling during vaccination. The PAM sequence and sgRNA oligos used are listed in Table A2 and shown in Appendix 4.1. The CRISPRi construct for depletion of MurT-GatD was generated as indicated in section 4.11.2 and restriction profiling of this construct indicated the expected profile (Fig. 4.5).

A

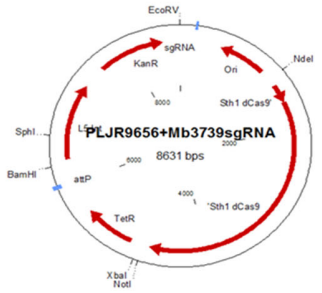

C

Restriction enzyme	Band sizes expected (bps)
EcoRV	8631
EcoRV+NotI	4778, 3853
EcoRV+NdeI	7407, 1224
EcoRV+XbaI	4826, 3805
BamHI	8631
EcoRV+SphI	6601, 2030

B

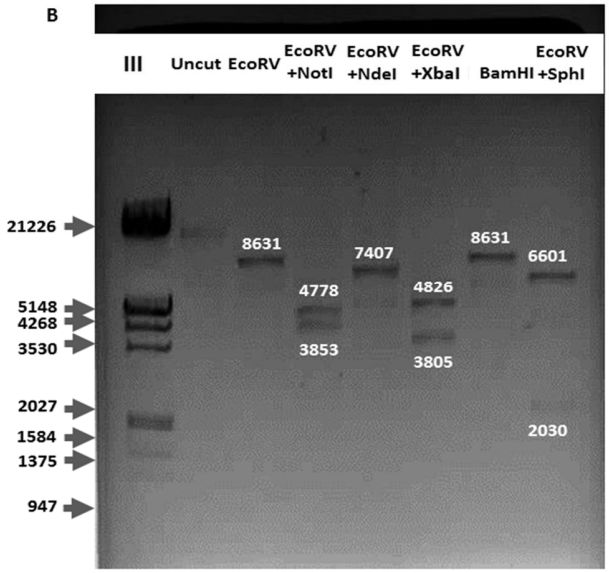

Figure 4.5. **Restriction profile of plasmid PLR965+Mb3739sgRNA**. (A) Plasmid map of PLR965+Mb3739sgRNA. (B) Agarose gel showing the DNA bands sizes expected (labeled in base pairs [bps]). (C) Table indicating the restriction enzymes used for restriction analysis of PLR965+Mb3739 sgRNA and the DNA band sizes expected. All expected band sizes were observed.

The construct was then introduced into *M. bovis* BCG pasteur as indicated in section 2.1.6.1 for generation of rBCG::iE-DAP, designed for inhibition of MurT-GatD PG amidation activity (Figure 4.6A-B). Following ATc induction of the CRISPRi system, the relative mRNA levels of the full length *murT* transcript were a ca. 1000-fold lower in rBCG::iE-DAP compared with the induced rBCG strain (Figure 4.6B, Appendix 4.2).

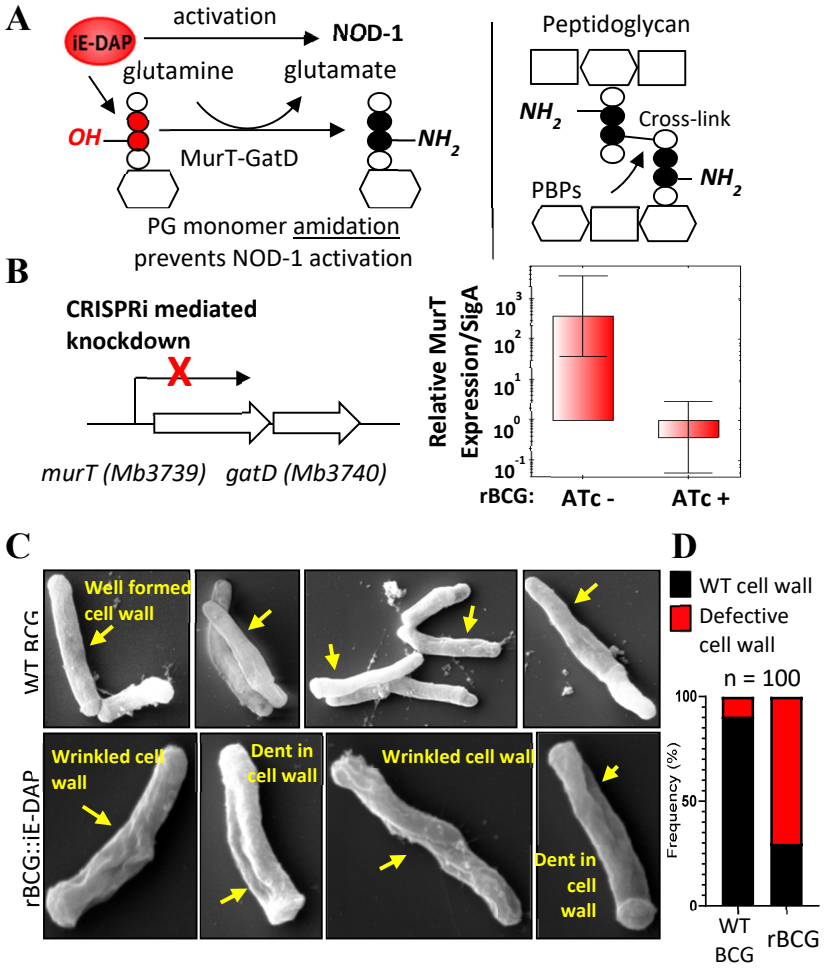

Figure 4.6: **Phenotypic characterization of rBCG::iE-DAP.** (A) Schematic representation of MurT-GatD mediated PG precursor amidation. (B) qPCR data for CRISPRi depletion of MurT-GatD in rBCG-CRISPRi-MurT-GatD. CRISPRi activation with ATc (200 ng/ml) resulted in inhibition of *murT* expression. (C) Scanning electron micrographs of WT BCG ((n=45 micrographs, 100 cells counted) and rBCG::iE-DAP grown in media supplemented with 200 ng/ml ATc. Depletion of MurT-GatD in rBCG-CRISPRi-MurT-GatD (n=48 micrographs, 100 cells counted) causes outer cell wall defects (wrinkled and dents in the cell wall). (D) Frequency of cells with cell wall defects.

Scanning and transmission electron microscopy was performed as described in section 4.11.9 to assess whether depletion of MurT-GatD causes perturbations in bacterial cell wall morphology. As shown in Fig. 4.6C, SEM revealed a well-formed typical mycobacterial outer cell wall structure in WT BCG whereas rBCG::iE-DAP cells displayed a wrinkled outer-cell wall structure or dents in the outer cell wall indicative of altered cell wall biosynthesis upon MurT-GatD depletion. Quantification of SEM fields revealed a 70% increase in the frequency of bacilli with cell-wall defects in rBCG::iE-DAP relative to the WT BCG (Fig. 4.6D). Similarly, as shown in Fig. 4.7A and appendix 4.3, TEM revealed a typical multi-layered mycobacterial cell wall outline with visible layers in WT BCG in comparison to the defective cell wall structure in rBCG::iE-DAP without a clear cell wall outline and layers. Upon counting individual cells by TEM, we observed a 65% increase in the frequency of wall defects in rBCG::iE-DAP compared with the WT BCG strain (Fig. 4.7B). Consistent with this, the rBCG::iE-DAP strain displayed increased sensitivity to cell wall targeting antibiotics (Fig. 4.7C and Appendix 4.4).

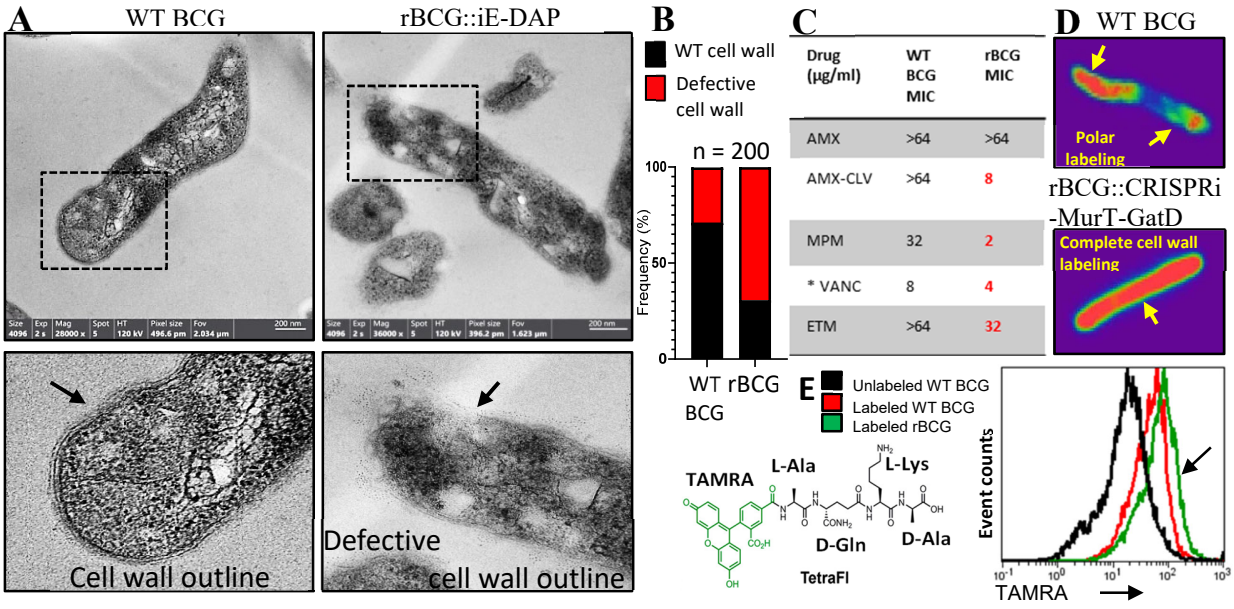

Figure 4.7: **Transmission electron microscopy and phenotypic characterization of rBCG::iE-DAP.** (A) Transmission electron micrographs of WT BCG and rBCG::iE-DAP grown in media supplemented with 200 ng/ml ATc. Depletion of MurT-GatD causes cell wall defects. (B) Frequency of cells with cell wall defects. (C) Minimum inhibitory concentration of antibiotics targeting cell wall biosynthesis against WT BCG and rBCG::iE-DAP grown in media supplemented with 200 ng/ml ATc. AMX: Amoxicillin, CLV: Clavulanate, MPM: Meropenem, VANC: Vancomycin and ETM: Ertapenem. Depletion of MurT-GatD in rBCG::iE-DAP causes increased sensitivity to cell wall targeting antibioics. (D) MurT-GatD depleted cells labeled with fluorescent BODIPY-FL vancomycin reveals side-wall labeling. (E) Flow cytometry analysis of WT BCG and rBCG-::iE-DAP cells labeled with a PG amidation reporter probe (TAMRA-L-Ala-D-glutamine-L-Lys-D-Ala [TetraFL]). Depletion of MurT-GatD causes increased labeling with the PG amidation reporter probe indicative of reduced PG amidation in the MurT-GatD depleted cells.

Microscopic imaging of the MurT-GatD depleted cells labeled with a fluorescent PG dye BODIPY FL-vancomycin, which specifically labels uncross-linked PG, showed complete labeling of the cells with this dye in contrast to cell pole labeled WT BCG cells (Fig. 4.7D). This phenotype (similar to that seen in Chapter 3 with *M. smegmatis*) was suggestive of reduced PG cross-linking in rBCG::iE-DAP (grown in ATc containing media), resulting in the cell wall defects observed through electron microscopy and the increased sensitivity to cell wall targeting antibiotics. Labeling of the MurT-GatD depleted cells with a fluorescent PG-amidation reporter chemical-probe (TetraFl-1) which has amide groups required for incorporation into PG showed increased labeling of the cells with this probe indicative of reduced PG-amidation upon MurT-GatD depletion as during PG biosynthesis in the periplasmic space of the bacterial cell wall, amidated PG precursor are incorporated rapidly into existing PG (Fig. 4.7E) (82).

4.12.2. rBCG::iE-DAP *in vitro* trained macrophages control Mtb H37Rv growth

To study the efficacy of rBCG::iE-DAP we first tested the ability of this strain to train monocytes *in vitro* and assessed the Mtb bactericidal activity of trained macrophages in an *in vitro* monocyte training assay (254). rBCG::iE-DAP is designed to express non-amidated PG components (i.e. iE-DAP) which is expected to activate NOD-1 (Fig. 4.8A). U937 monocytes were trained with heat-killed rBCG::iE-DAP vs WT BCG, and LPS (derived from *E. coli*), MDP (murein dipeptide derived from *E. coli*) and RPMI were included as control (Fig. 4.8B). MDP was particularly included as a control as this molecule has been shown to activate the NOD-2 PRR and induce trained innate immune responses in macrophages (259). rBCG::iE-DAP trained macrophages displayed increased control of Mtb H37Rv compared to WT BCG trained macrophages (Fig. 4.8C). Given these encouraging results, we next moved to primary cells to further test the rBCG::iE-DAP strain in mouse BMDMs and in mouse immunization models of TB to assess the efficacy of rBCG::iE-DAP as a TB vaccine candidate.

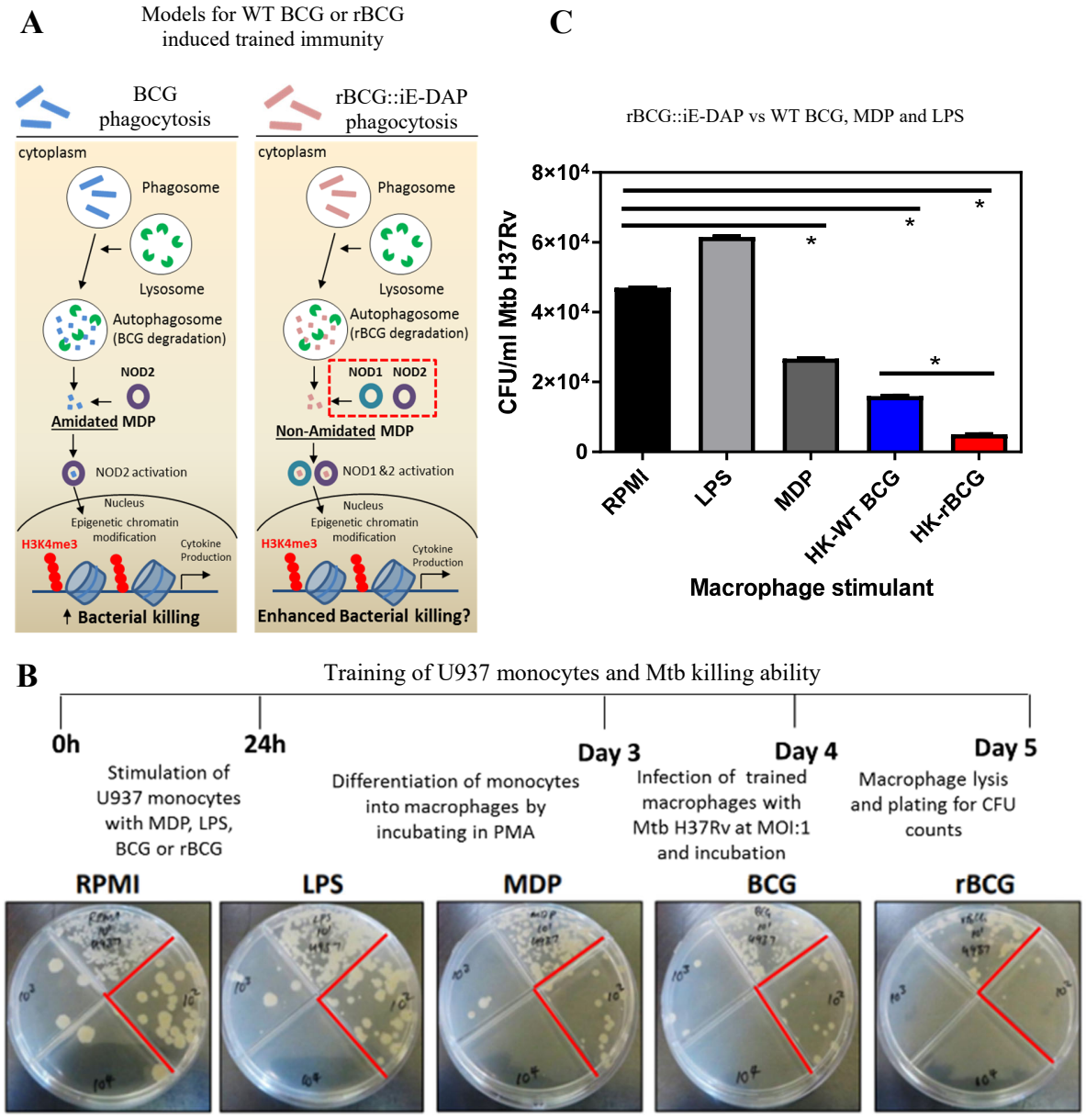

Figure 4.8. **rBCG::iE-DAP enhances the Mtb H37Rv killing ability of macrophages derived from trained U937 monocytes**. (A) Schematic diagram depicting the models of WT BCG and rBCG induced training of monocytes. CRISPRi mediated depletion of MurT-GatD in rBCG::iE-DAP is hypothesized to reduce PG amidation leading to both NOD-1 and NOD-2 activation. (B) Model for training of U937 cells with heat-killed (HK) rBCG vs WT BCG, LPS and MDP, RPMI only was used as control. (C) Macrophages derived from HK-rBCG-trained monocytes were able to control Mtb H37Rv growth significantly different from macrophages derived from HK-WT BCG, LPS, MDP trained/stimulated monocytes and non-stimulated macrophages (RPMI control). Statistical analysis was conducted using the Student *t*-test *: p-value: <0.01.

4.12.3. rBCG::iE-DAP is responsive to anhydrotetracycline activation and causes increased TNFα expression in BMDMs

To test the hypothesis that inhibition of MurT-GatD expression in rBCG::iE-DAP improves the immunogenicity of the recombinant strain, we infected IFNγ activated BMDMs with rBCG::iE-DAP and supplemented the growth media with increasing concentrations of ATc to assess activation of the CRISPRi system *ex vivo*. Growth of the strain was recorded by plating for rBCG::iE-DAP CFU counts at day 3 and day 5 post-infection. At day 3 lower bacterial counts were observed with all ATc concentrations tested for activating CRISPRi, contributing to growth inhibition by activated BMDMs and a dose dependent inhibition of growth of rBCG::iE-DAP was observed at day 5, with 500 ng/ml ATc resulting in a ~3 fold difference in growth inhibition of rBCG::iE-DAP in comparison to WT BCG and rBCG::iE-DAP without ATc supplementation (Fig 4.9A).

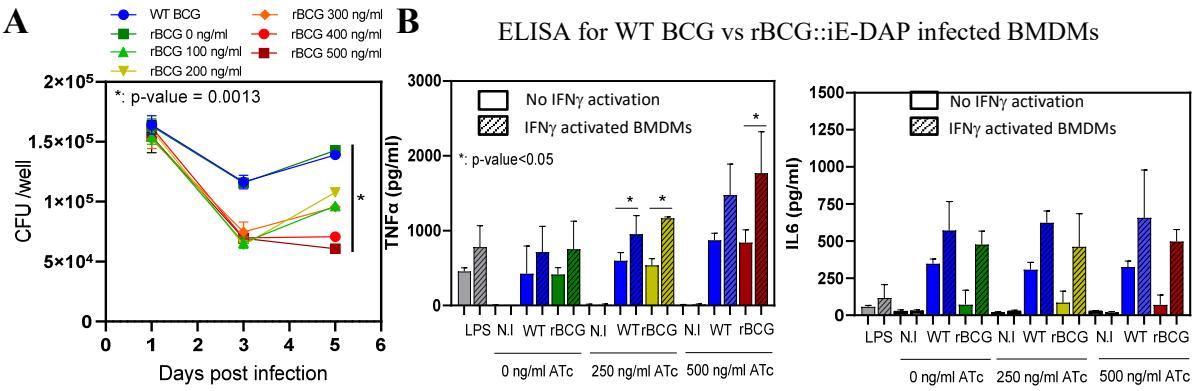

Figure 4.9. **Survival of rBCG-CRISPRi-MurT-GatD in IFNγ activated BMDMs and analysis of pro-inflammatory cytokine release.** (A) IFNγ activated BMDMs (1×10^6 cells) were infected at MOI: 1 with WT BCG and rBCG-CRISPRi-MurT-GatD. ATc was added to culture media for induction of CRISPRi in rBCG-CRISPRi-MurT-GatD at 100 ng/ml – 500 ng/ml and growth of the strains was assessed after 3 and 5 days. Supplementation of culture media with 400-500 ng/ml ATc resulted in significantly reduced growth of rBCG-CRISPRi-MurT-GatD on day 5 in comparison to WT BCG. (B) Secreted TNFα and IL-6 levels from non-activated and IFNγ-activated BMDMs infected with WT BCG and rBCG-CRISPRi-MurT-GatD at MOI 1:20. No difference in IL-6 secretion was observed. Increased TNFα secretion was observed from rBCG-CRISPRi-MurT-GatD infected IFNγ-activated BMDMs cultured in media supplemented with 500 ng/ml ATc. LPS was used as a control.

Next, we performed ELISA experiments to assess cytokine expression as described in section 4.11.6. We assessed the expression of the pro-inflammatory cytokines TNFα and IL-6 as rBCG::iE-DAP is designed to express the NOD-1 ligand iE-DAP and potentially induce

increased NF-κB activation, leading to increased pro-inflammatory cytokine expression (249). Activation of rBCG::iE-DAP by supplementation of growth media with ATc resulted in a dose dependent increase in TNFα expression but not IL-6 expression in comparison to WT BCG (Fig. 4.9B). These results demonstrate that rBCG::iE-DAP is responsive to activation *ex vivo* and signals for increased pro-inflammatory cytokine expression.

4.12.4. rBCG::iE-DAP activation *in vitro* and in mice-aerosol infections with doxycyline

Doxycycline (Dox), a tetracycline analog, is used in TB *in vivo* models for temporal regulation of the ATc responsive mycobacterial gene expression system (260). The CRISPRi platform used in rBCG::iE-DAP is also based on a Dox-responsive TetR-*tetO* unit (113). rBCG::iE-DAP was grown in an increasing range of Dox concentrations to assess the activation of CRISPRi *in vitro*. In comparison to the WT BCG control which displayed some sensitivity to Dox during growth in liquid broth as Dox is an antibiotic, activation of CRISPRi in rBCG::iE-DAP with Dox resulted in a dose dependent inhibition of growth of rBCG::iE-DAP, confirming that the MurT-GatD enzymes are essential for growth (Fig. 4.10A-D). To test the activation of rBCG::iE-DAP *in vivo*, and to determine the minimum effective Dox dose, we aerosol infected BALB/c mice with ~100 CFU of rBCG::iE-DAP as indicated in section 4.11.7 and Dox was administered for 10 days by oral gavage at doses ranging from 0.125 - 1 mg/kg/day. A 1 mg/kg/day Dox administration resulted in a significant reduction in growth of rBCG::iE-DAP in the lungs (Fig. 4.10E-F).

To assess retention of the CRISPRi plasmid (PLR965+Mb3739sgRNA, which has a kanamycin [Kan] resistance cassette) by rBCG::iE-DAP *in vivo*, we also plated lung homogenates on media with Kan and found that rBCG::iE-DAP bacilli from the lungs of the aerosol infected mice formed similar CFU counts on both media with or without Kan (Fig. 4.10F, right panel). These results demonstrate long term retention of the CRISPRi plasmid by rBCG::iE-DAP during *in vivo* conditions.

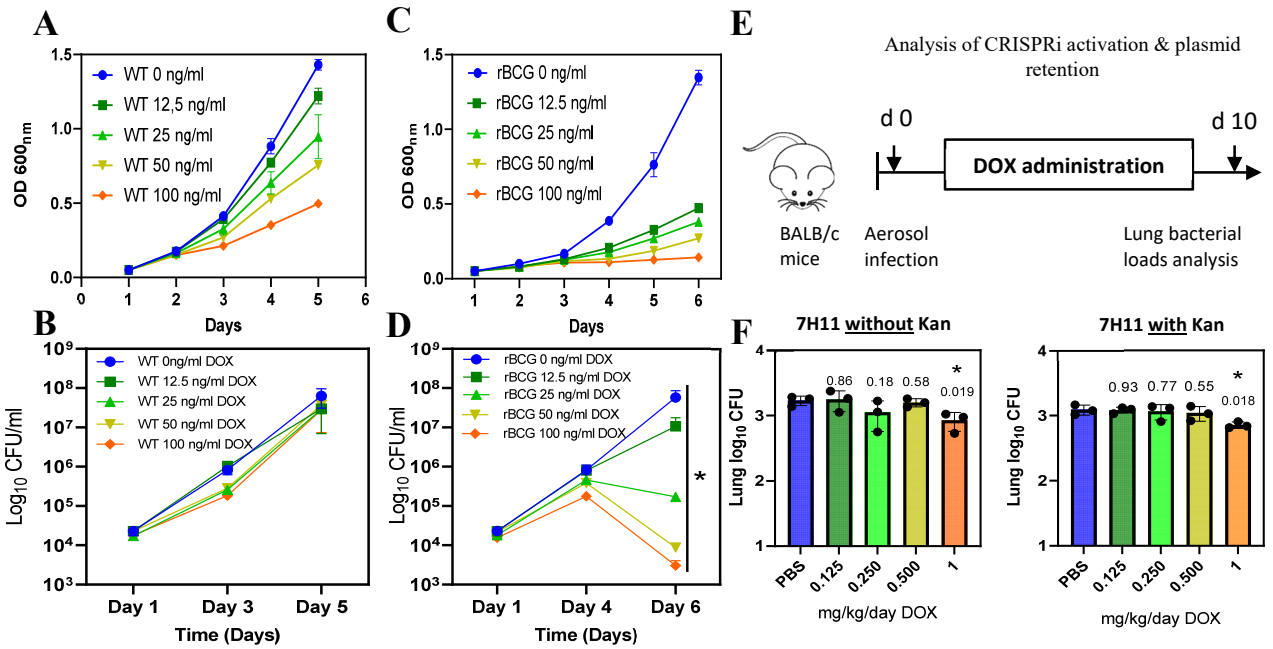

Figure 4.10. **rBCG::iE-DAP activation *in vitro* and in mice-aerosol infections with doxycycline**. (A-D) *In vitro* growth rates of WT BCG by OD_{600nm} (A) and CFU counting (B) and of rBCG::iE-DAP by OD_{600nm} (C) and CFU counting (D) in complete 7H9 medium at varying concentrations of Dox. (E) Determination of the Dox concentration for activation of rBCG::iE-DAP *in vivo*. Mice were aerosol infected with ~2.5 log_{10} CFU of rBCG and Dox (at doses of 0.125-1 mg/kg/day) - administered by oral gavage for 10 days. (F) CFU counts from the experiment shown in panel-E. A dose of 1 mg/kg/day Dox resulted in reduced growth of rBCG::iE-DAP indicative of sufficient activation of the CRISPRi system. Lung homogenates were plated on both 7H11 with and without kanamycin (25 µg/ml) to assess the loss of the CRISPRi plasmid during *in vivo* growth. There was no difference in the growth of recovered bacteria on media containing kanamycin, indicating the presence of the CRISPRi plasmid in recovered bacteria. Statistical analysis was conducted using the Student t-test. *: p-value: <0.05.

We further evaluated the long term efficacy of 1 mg/kg/day Dox for rBCG::iE-DAP activation at 4 weeks and 8 weeks post aerosol infection of mice and found that recovered rBCG::iE-DAP bacilli formed small colonies on solid agar in comparison to WT BCG recovered from infected mice also exposed to 1 mg/kg/day Dox dose, indicative of the long term efficacy of Dox *in vivo* for CRISPRi activation (Fig. 4.11A-F). Although the total CFU was slightly higher for rBCG::iE-DAP+Dox compared to WT BCG, the appearance of small colonies was indicative of the sensitivity of rBCG::iE-DAP to Dox. Genomic DNA was extracted from small colonies (SC) and big colonies (BC) as described in section 2.1.3.1.1 and a PCR was performed for verification of the presence of the CRISPRi plasmid as described in section 2.1.4.1.2. PCR amplification of the dCas9 ORF (encoding the dead endonuclease dCas9 used in the CRISPRi platform) demonstrated the presence of the dCas9 allele in all colonies analyzed (Fig. 4.11G).

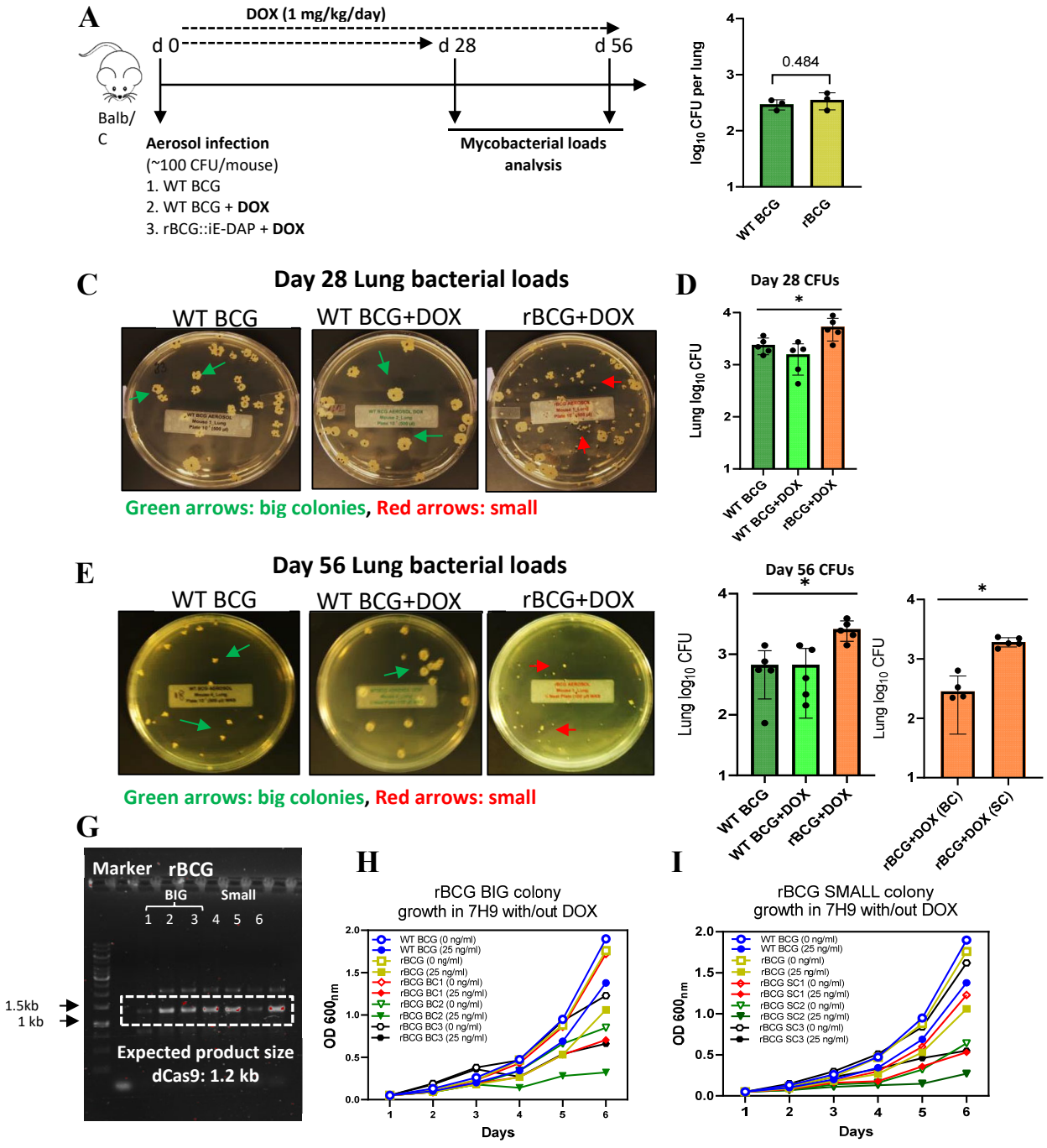

Figure 4.11. **Efficacy of 1 mg/kg/day dose of doxycycline for CRISPRi activation.** (A) Schematic representation of mice aerosol infection with WT BCG and rBCG::iE-DAP and analysis of the efficacy of 1 mg/kg/day dose of doxycycline for CRISPRi-MurT-GatD activation *in vivo*. (B) Day 1 implantation of WT BCG and rBCG::iE-DAP in the lungs of aerosol infected mice. (C-F) Day 28 and Day 56 Lung bacterial loads of WT BCG and rBCG::iE-DAP aerosol infected mice. (G) PCR amplication of dCas9 in recovered Big (BC) or Small (SC) rBCG::iE-DAP colonies. (H&I) Growth kinetics of big and small colonies of rBCG::iE-DAP in liquid broth supplemented with Doxycycline. Statistical analysis was conducted using Student *t*-test. *: p-value: <0.01.

The rBCG::iE-DAP SCs and BCs were then regrown in the presence of Dox and all displayed reduced growth rate in liquid broth supplemented with Dox, while the WT strain displayed only slight sensitivity to Dox (Fig 4.11H-I). These results showed that 1 mg/kg/day Dox is effective for rBCG::iE-DAP activation *in vivo* (261).

4.12.5. Analysis of rBCG::iE-DAP attenuation in SCID mice

Aerosol infection experiments and long term (4-8 week) *in vivo* activation of rBCG::iE-DAP with Dox resulted in the recovery of rBCG::iE-DAP bacilli that form small colonies on solid agar (Fig. 4.11C&E), suggestive of a persisting phenotype *in vivo*. To further explore this phenotype, we aerosol infected female SCID (severe combined immunodeficiency) mice with a low dose (~100 CFU) of WT BCG and rBCG::iE-DAP, and included Dox receiving groups (i.e. WT BCG+Dox and rBCG::iE-DAP+Dox) (Fig. 4.12A&B).

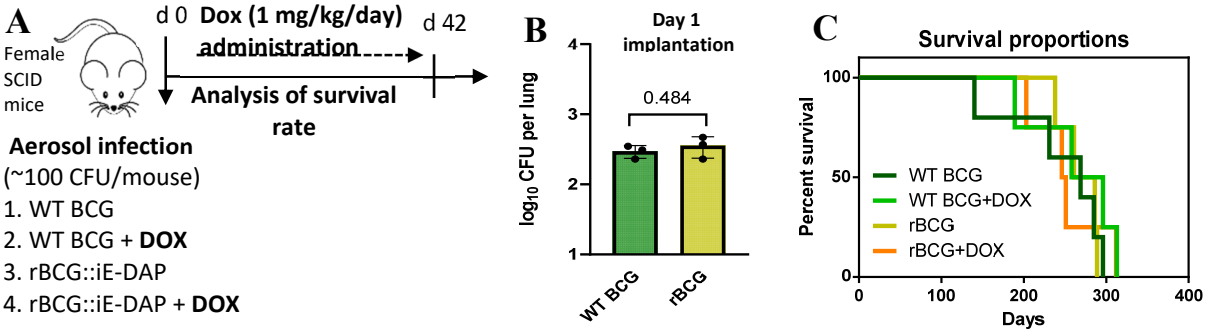

Figure 4.12: **Analysis of rBCG::iE-DAP strain attenuation**. (A) Schematic representation of SCID mice aerosol infection with WT BCG and rBCG::iE-DAP for analysis of strain attenuation. rBCG::iE-DAP activation *in vivo* was achieved by administration of Dox at 1 mg/kg/day. SCID mice (n = 5 per group) were aerosol infected with ~100 colony-forming units (CFUs)/mouse of WT BCG or rBCG::iE-DAP, a WT BCG + Dox group was included as a control. (B) Day 1 implantation of WT BCG and rBCG::iE-DAP in the lungs of aerosol infected SCID mice. (C) Percent survival of SCID mice following low-dose challenge with WT BCG and rBCG compared to WT BCG+Dox or rBCG+Dox groups.

WT BCG infected mice displayed early decreased survival as expected, followed by the WT BCG+Dox group of mice (Fig. 4.12C). Although rBCG::iE-DAP infected mice, either receiving Dox or not, displayed slight increased survival, this data was not signicantly different from WT BCG infected mice. This suggested that rBCG::iE-DAP upon CRISPRi activation is not more attenuated than WT BCG and does not cause more disease in SCID mice compared to WT BCG.

4.12.6. rBCG::iE-DAP induces better protection against *Mycobacterium tuberculosis* infection in mice compared to WT BCG

To assess the protective efficacy of rBCG::iE-DAP against Mtb infection in comparison to the standard BCG vaccine, we immunized groups of BALB/c mice (n=5 per group) intradermally with WT BCG or rBCG::iE-DAP (Fig. 4.13A). rBCG::iE-DAP immunized mice received a Dox dose by oral gavage at 1 mg/kg/day for activation of CRISPRi *in vivo* and we also included a Saline+Dox group, WT BCG group, WT-BCG+Dox group and a rBCG::iE-DAP without Dox group as controls for the vaccination experiment (Fig. 4.13A). The immunized mice receiving Dox were weighed weekly for 6 weeks prior to challenge with Mtb H37Rv to assess the effect of daily Dox administration on the health of the mice. We assessed the percentage weight change of mice receiving Dox in comparison to no-Dox groups and found that the percentage weight change of WT BCG immunized mice receiving Dox was significantly different from WT BCG immunized mice without Dox treatment (Fig. 4.13B). The WT BCG+Dox group collectively displayed a drop of ~5% in weight compared to the WT BCG group. However, the rBCG::iE-DAP immunized group receiving Dox did not display significant weight change compared to all groups (Fig. 4.13B). Importantly, the Saline+Dox, WT BCG+Dox and rBCG::iE-DAP+Dox groups were similar in weight at 6 weeks pre-challenge with Mtb H37Rv.

After 6 weeks, the immunized mice were challenged with ~100 CFU of Mtb H37Rv via the aerosol route and bacterial burden were determined in lungs and spleens at 4 and 8 weeks post challenge (Fig. 4.13A). At 4 weeks post challenge, mice were sacrificed to assess lung pathology (the lungs were also weighed) and bacterial burden in the lungs and spleens which were also weighed. The WT BCG+Dox group displayed lower lung weights, the WT-BCG and rBCG::iE-DAP without Dox-treatment groups displayed similar lung weights while the Saline+Dox and rBCG::iE-DAP+Dox groups displayed increased lung weights indicative of increased lung inflammation, as we expect an enhanced immune response in the rBCG::iE-DAP+Dox (Fig. 4.13C). The Saline+Dox group displayed increased spleen weights compared to the other groups indicative of increased disseminated infection (Fig. 4.13D). Analysis of lung bacterial burden at week 4 revealed that rBCG::iE-DAP+Dox was superior to WT BCG and WT BCG+Dox in protecting against Mtb H37Rv challenge in the lungs (Fig. 4.13E).

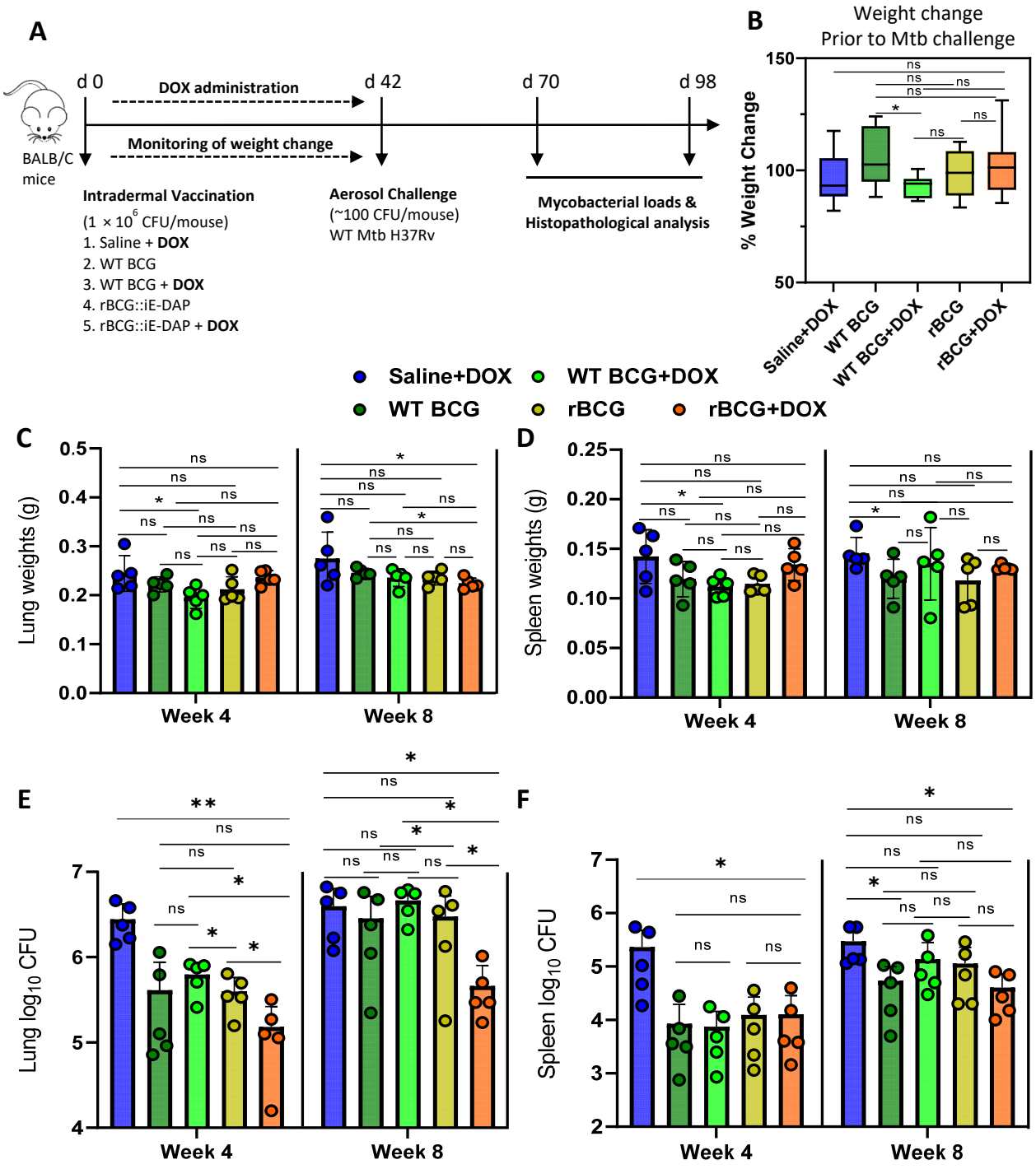

Figure 4.13: **Efficacy of rBCG::iE-DAP in comparison to standard WT BCG for protection against Mtb H37Rv infection in mice**. (A) Schematic representation of the mouse immunization and Mtb H37Rv challenge protocol. (B) Percentage weight change at week 6 (d42) immediately prior to Mtb challenge. (C-D) Lung and spleen weights at week 4 and week 8 post-challenge with Mtb. (E-F) Lung and spleen bacterial burdens at week 4 and week 8 post-challenge with Mtb. rBCG::iE-DAP+Dox was superior to WT BCG or WT BCG+Dox in controlling Mtb H37Rv growth in the lungs at week 4 and week 8 post challenge with Mtb. * :p-value <0.05, **: p-value <0.01.

At week 8 post challenge, the rBCG::iE-DAP+Dox group displayed reduced lung weights compared to BCG + Dox indicative of control of bacterial burden and analysis of lung bacterial burden demonstrated again that rBCG::iE-DAP+Dox was superior to WT BCG or WT BCG+Dox in controlling Mtb H37Rv growth in the lung which both displayed waning efficacy in this model (Fig. 4.13C&E). In the spleen rBCG::iE-DAP+Dox displayed similar efficacy to WT BCG in control of infection compared to the Saline+Dox group (Fig.4.13F).

4.12.7. Histopathological analysis of lung pathology after vaccination with rBCG::iE-DAP+Dox compared to WT BCG post Mtb Infection

Histopathological analysis of hematoxylin and eosin (H&E) stained lung samples from the vaccinated and Mtb challenged mice indicated that rBCG::iE-DAP+Dox immunized mice presented with substantially early increased lung inflammation compared to WT BCG+Dox vaccinated mice, although the percentage inflamed area of the analyzed lung sections was statistically non-significant (Fig. 4.14A&B). At week 8 also, rBCG::iE-DAP+Dox immunized mice presented with slightly more granulomatous and inflamed proportions of lung area compared to WT BCG+Dox and the rBCG::iE-DAP group without Dox - immunized mice, suggestive of sustained inflammation for control of infection (Fig. 4.14C&D). The increased early inflammation in rBCG::iE-DAP+Dox immunized mice is reflective of early induction of anti-tuberculous immune responses which were able to control growth early before establishment of infection and the sustained inflammation at week 8 is suggestive of enhanced immune responses during chronic disease, which enable control of disease progression as rBCG::iE-DAP+Dox displayed efficacy at week 8 while WT BCG induced protection waned.

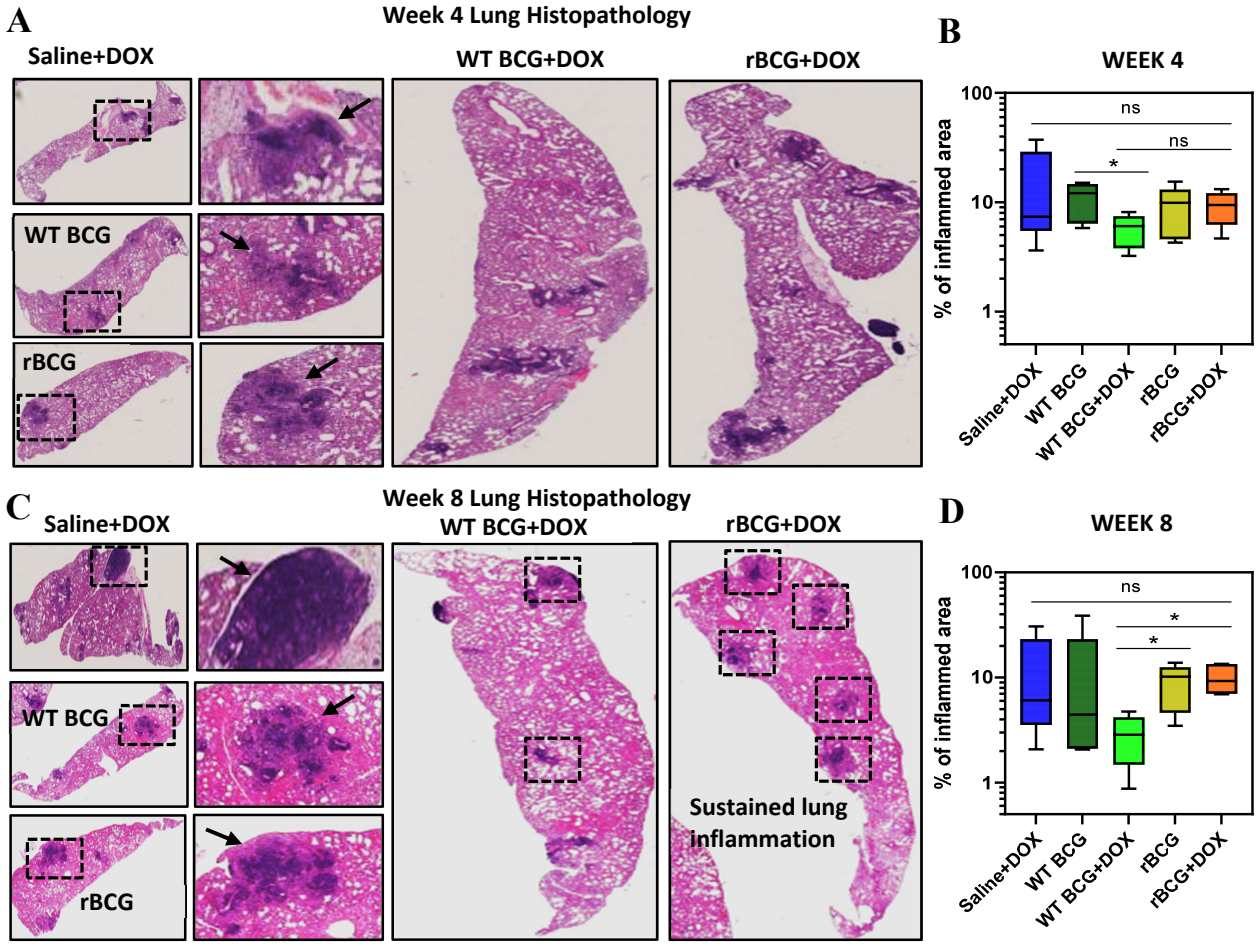

Figure 4.14. **Histopathological analysis of lung samples**. (A) Histological Hematoxylin and Eosin (H&E) staining of lung samples at week 4 post Mtb challenge. (B) Analysis of percentage of inflamed area (indicated with black arrows) from each mouse lung per immunized group (n=5 per group), shows that rBCG::iE-DAP+Dox immunized mice present with early lung inflammation compared to WT BCG+Dox. (C) Histological Hematoxylin and Eosin (H&E) staining of lung samples at week 8 post Mtb H37Rv infection. (D) Analysis of percentage of inflamed area from each mouse lung (n=5 per group), shows that rBCG::iE-DAP+Dox immunized mice present with sustained lung inflammation compared to WT BCG and WT BCG+Dox. The percentage inflamed area was evaluated using ImageJ software (NIH) and plotted as whisker boxplots (whiskers represent minimum and maximum values) and a Student *t*-test was used for statistical analysis. * :p-value <0.05.

4.13. Discussion

The BCG vaccine has been in use for a century to date for vaccination at birth and is effective at preventing TB in infants. However, BCG does not provide sufficient protection against TB infection in adults and has failed to eradicate the TB pandemic (202). This has spurred the need to develop next-generation TB vaccine candidates with novel modes of action to replace BCG (262). However, BCG remains the gold-standard for TB vaccine development (143). BCG possesses a number of immune evasion mechanisms similar to those used by Mtb during infection. These can be targeted for deletion to enhance its efficacy (5, 256). For example, rBCG strains further attenuated by deletion of immune evasion genes such as *sapM* (258), *nuoG* (238) or *zmp1* (263) have been developed and these show enhanced immunogenicity and efficacy against Mtb infection. PtpB, a mycobacterial phospholipid phosphatase inhibiting host pyroptosis during infection has also recently been identified as a target to improve BCG efficacy (264). Immune evasion genes that are also essential for BCG viability remain to be studied for development of next generation rBCG strains with enhanced efficacy.

Gene regulation platforms, including CRISPRi are being used to study the role of essential genes in BCG (113, 199). For example genes encoding for essential enzymes involved in the biosynthesis of potent immune-modulating cell wall lipids such as trehalose dimycolate, di- and triacylglycerols, PDIMs and phenolic glycolipids are potential targets of gene regulation platforms such as CRISPRi to study their role in limiting BCG efficacy. Selective chemical removal of these lipids from BCG (i.e. delipidation of BCG) has shown the ability to increase BCG efficacy in preventing Mtb infection in mice (265). Gene regulation platforms, including CRISPRi are ideal platforms to study the effect of such essential immunomodulatory BCG enzymes that can be targeted to enhance BCG efficacy. Indeed, recently a CRISPRi based rBCG (rBCG::CRISPRi-AftC) designed for the truncation of the anti-inflammatory cell wall associated LAM into the pro-inflammatory lipomannan derivative (LM) upon CRISPRi mediated depletion of the enzyme arabinofuranosyltransferase C (AftC, required for addition of D-arabinan branches on LM) was shown to enhance the immunogenicity of BCG by upregulating the expression of TNFα, a major pro-inflammatory cytokine (191).

We targeted essential genes (*murT-gatD*) required for PG amidation in BCG with the recently developed CRISPRi platform (113) to create rBCG::iE-DAP designed to activate the NOD-1 pathway by expression of non-amidated PG fragment (iE-DAP). Phenotypic characterization of rBCG::iE-DAP post CRISPRi activation with SEM and TEM revealed changes in the outer cell wall surface and structure of the cell wall in rBCG::iE-DAP, respectively. These data were consistent with the essentiality of MurT-GatD during PG biosynthesis. Changes in the cell wall structure were also associated with increased sensitivity to cell wall targeting antibiotics (amoxicillin+clavulanate, meropenem, vancomycin and ertapenem), confirming the essentiality of MurT-GatD mediated amidation of PG fragments for cell wall biosynthesis as previously described in mycobacteria and other bacterial species (80, 109, 119). PG amidation by the MurT-GatD complex is required for PG cross-linking by penicillin binding proteins and LDTs in mycobacteria (108). Considering this, we further analyzed the level of PG cross-linking in rBCG::iE-DAP by labeling the cells with BODIPY-FL vancomycin, a fluorescent vancomycin derivative binding uncross-linked nascent PG monomers (266). We found that transcriptional repression of MurT-GatD expression in rBCG::iE-DAP was associated with complete cell wall labeling. This was indicative of reduced PG cross-linking in rBCG::iE-DAP. To probe for the reduction of PG amidation in rBCG::iE-DAP, we used a previously developed amidation reporter probe, TetraFl (82) to label MurT-GatD depleted cells. This probe was used in Chapter 3 and similarly, here it showed increased labeling in rBCG::iE-DAP indicative of reduced amidation upon transcriptional repression of MurT-GatD expression.

We next tested rBCG::iE-DAP in an *in vitro* monocyte training assay (254) to assess the efficacy of this strain in training innate responses of macrophages. BCG induces a NOD-2 dependent trained immunity in monocytes resulting in epigenetic and metabolic reprogramming of monocytes which differentiate into macrophages with increased bactericidal properties (198, 267). We therefore tested rBCG::iE-DAP trained macrophages for their *in vitro* Mtb killing ability and found that in contrast to WT BCG trained macrophages, rBCG::iE-DAP trained macrophages displayed enhanced Mtb killing ability as measured by CFU counts 24 hours post infection. We further show that rBCG::iE-DAP is responsive to activation in BMDMs using ATc and also in a mouse aerosol infection model for at least 8 weeks post infection using a minimal

Dox dose, as Dox was previously shown to have immunomodulatory effects (261). To investigate whether expression of iE-DAP in rBCG::iE-DAP for activation of innate immune responses would cause increased pathogenicity of the recombinant BCG, we aerosol infected female SCID mice and administered Dox to the mice for 8 weeks, and assessed the survival of the mice over time compare to WT BCG infected mice. This revealed that rBCG::iE-DAP was similarly attenuated as WT BCG and did not cause increased disease in infected mice. Furthermore, *in vitro* work revealed that activation of rBCG::iE-DAP in BMDMs resulted in increased TNFα expression, as measured by ELISA providing evidence that expression of iE-DAP in rBCG::iE-DAP enhances immunogenecity of BCG. These results provided a framework for the investigation of rBCG::iE-DAP in *in vivo* or mouse model experiments as a potential TB vaccine candidate.

In this study, we have demonstrated that intradermal vaccination of mice with rBCG::iE-DAP and administration of Dox for 6 weeks for CRISPRi mediated repression of MurT-GatD expression resulted in superior protection from Mtb challenge in the lungs of the immunized mice compared to the WT BCG vaccine. Similar bacterial control was observed in the spleens of immunized mice. Our vaccination experiments also included a WT BCG+Dox control group to rule out the role of Dox mediated immunomodulatory effects in enhancing WT BCG vaccine efficacy post Mtb challenge when compared with rBCG::iE-DAP+Dox efficacy. Administration of Dox to WT BCG vaccinated mice (i.e. WT BCG+Dox group) did not enhance WT BCG vaccine efficacy against Mtb challenge when compared to the WT BCG without Dox control group, while rBCG::iE-DAP+Dox shows increased protection at both 4 and 8 weeks post Mtb challenge.

Histopathological analysis of lung sections from the immunized and Mtb challenged mice shows that rBCG::iE-DAP+Dox induces early immune infiltration to the lung compared to WT BCG+Dox and this is maintained until 8 weeks post infection providing early and sustained protection against Mtb challenge. Interestingly, analysis of vaccine induced correlates of protection in an IV model of BCG vaccination in peripheral blood of rhesus macaques which showed the development of sterilizing immunity against TB infection (268), revealed induction

of an early innate transcriptional immune response to IV BCG as a correlate of BCG induced protection against TB infection (269). This work demonstrated that next generation TB vaccines designed to induce early innate immune responses against TB infection could have increased efficacy. The immune correlates of protection induced by rBCG::iE-DAP are the subject of our future studies. Because we used a CRISPRi platform to create rBCG::iE-DAP, the next step would be to use alternative genome editing strategies or plaforms to create a ΔMurT-GatD rBCG using suppressor screens. Furthermore, to verify the results of this study a NOD-1 deficient mouse model would be useful. In conclusion, this work shows that MurT-GatD can be targeted to develop a new TB vaccine candidate.

4.14. Appendices

5'gtggtaaccacccgggcacgcctggccctagccgccggcgcgggcgcacgctgggcgtcgcgggtcaccggtcgcggcgccggagcgatgatcggcggtctggtcgc
catgaccctggaccgctcgatcctgcgccaactcgggatgggccggcgcaccgtcgtcgtcaccggcaccaacggcaagtcgaccaccacacggatgaccgcggccgc
gctgggcacgttgggagccgtggccaccaacgccgagggcgccaacatggacgccggcctggtggccgcgctcgccgctcaccgcgacgccgagctggcggtgctgga
agtcgacgagatgcacgtaccgcacatctccgatgccgtcgatcccgccgtcgtcgtcttgctcaacctctcccgagaccagctggaccgggtcggcgagatcaacgtcat
cgaacgcacactgcgggccgggctggcccggcaccccgacgctgtcgtggtcgccaactgcgacgacgtgctgatgacctcggccgcctacgacagccccaacgtcgttt
gggtggctgccggcggcgcgtggtcaaacgattcggtcagctgcccgcgcagcagcgaggtcatcgttcgcaaggccccctctcaggaagaccactggtactccaccgg
cgccgacttcaagcggcccgccccgcactggtggttcgacgacgccacgctgtatgggcccgacgggctggcgctgccgatgcggctggcactgccaggctcggtgaatc
gcggcaacgccgcccaagccgtggccgccgcagtcgccctcggcgccgatccggctgtggccgtcgccgccgtctgccaggtcgacgaggtcgccggacgctaccggac
cgttcgtatcggcgcgcaccaagcccggatcctgctggccaaaaacccggccggctggcaggaagcgctggcgatggtcgacaagcatgcagacggggtggtcatcgc
ggtcaacgggcgggttcctgacggcgaggacctgtcctggttgtgggacgtgcgcttcgagcacttcgagacgacccgagtggtagccgctggggagcgcggcaccgatt
tggcggttcgcctcggatatgcaggcgtcgagcacaccctggtgcacgacaccgtggccgccatcgcctcatgcccacccgggcgggtggaggtcgtcgccaactacacc
gcgttcctgcagctgcaacgagcattggcgcgtcgtggctgagtggtgcggatcgggctcgtgctgcccgacgtgatgggcacctacggcgacggcggcaacgccgtggt
gctacgacagcggctgctgctgcgcggcatcgccgccgagatcgtcgagatcacgctggccgatccggtgccggattcgctggacctctacacgctgggcggagcggag
gactacgcgcagcggctggccacccggcacctacgtcgatatccgggcctgcaacgcgcggcgggccggggtgctccagtattggcgatctgcgcggccatccaggtgct
tgggcactggtacgagacgtcgtcgggagaccgggtcgacggcgtggggttgctggatgtgaccacgtcaccgcaggatgcgcgcaccatcggcgagttggtcagcaag
ccgttgctggccggtttgacccaacccttgaccggttttgagaaccaccgcggcggcaccgtcctcgggcccggaacgtcgcccttgggcgcggtggtcaagggagccgg
caaccgggccggcgacggttttgatggcgcggttgcgggcagcgtggtcgcgacctacatgcacgggccgtgcctggcccgcaacccggagcttgccgacctgctgctga
gcaaggtggttggtgagctggcgccgctggatttgcccgaggtggacctgctgcgccgcgaacggctatccgcgcgttag3'

Appendix 4.1. **Gene sequences of MurT (Mb3739, in red) and GatD (Mb3740, in black) with the sgRNA and PAM sequences used for CRISPRi**. The PAM sequence is shown in blue font and sgRNA sequence shown by the green underlined font.

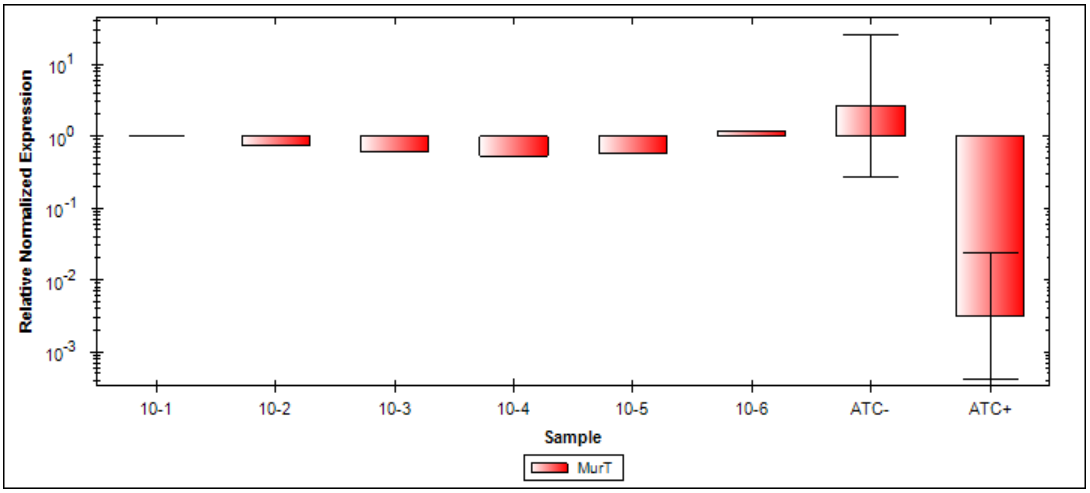

Appendix 4.2. **qPCR data of MurT expression from rBCG::iE-DAP** (ATc- vs ATc+ samples) compared to WT BCG (10^{-1}-10^{-6} diluted genomic DNA standard samples). MurT expression was normalized to SigA expression. A 1000 fold decrease in *murT* expression in the rBCG::iE-DAP ATc+ samples compared to the ATc- samples. The experiment was performed with three biological repeats.

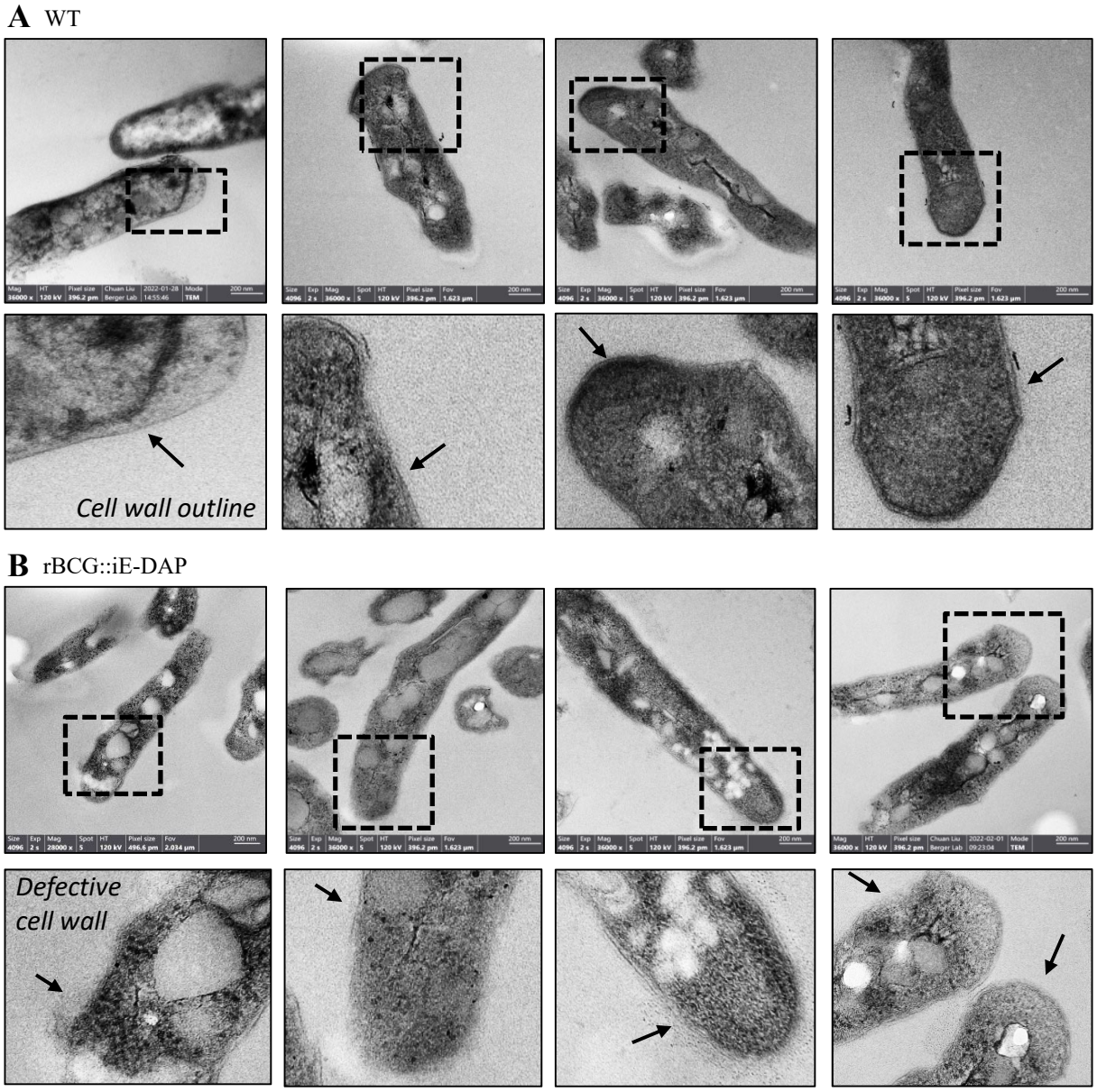

Appendix 4.3. **TEM reveals defective cell wall of rBCG-CRISPRi-MurT-GatD**. Transmission electron micrographs of WT BCG (A) and rBCG-CRISPRi-MurT-GatD (B) grown in media supplemented with 200 ng/ml ATc. Depletion of MurT-GatD causes cell wall defects.

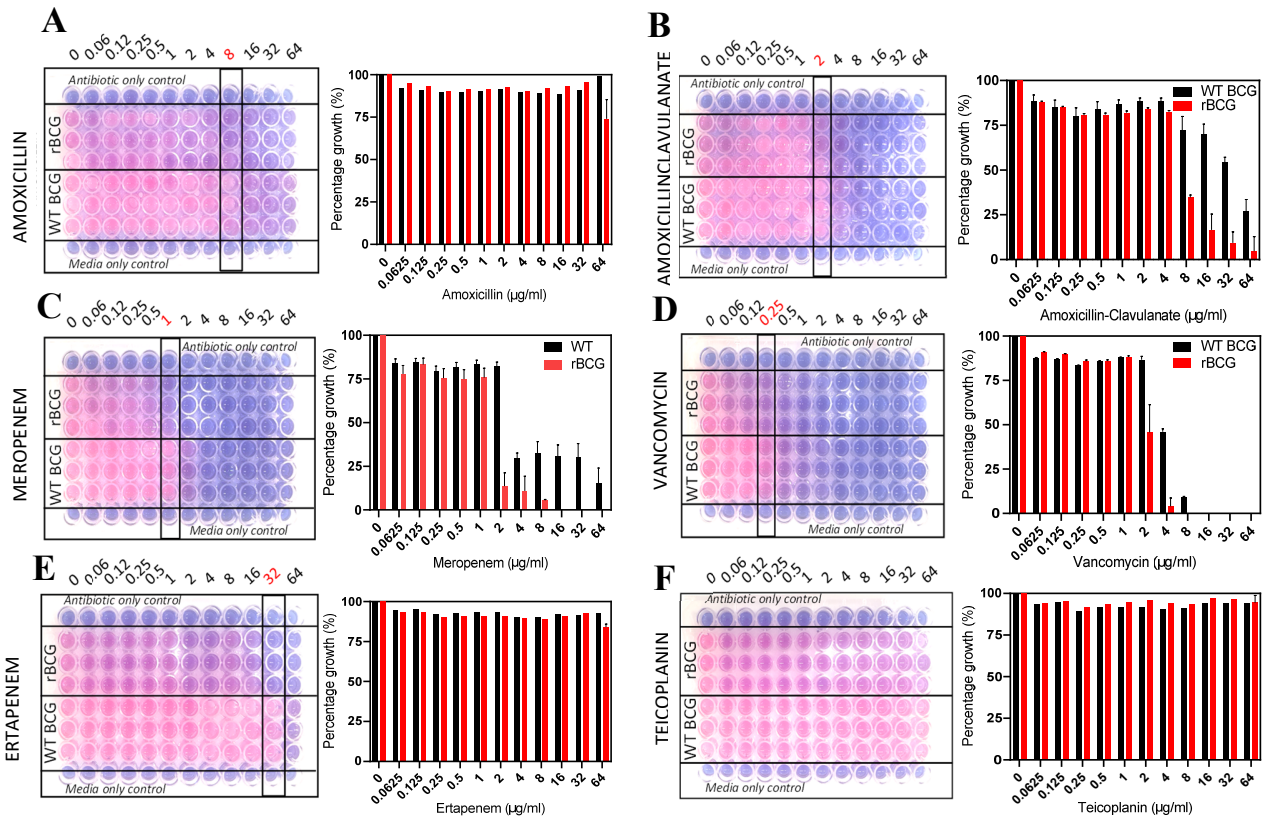

Appendix 4.4. **MIC experiments for WT BCG and rBCG::iE-DAP (both grown in media supplemented in 200 ng/ml ATc) with cell wall targeting antibiotics (A-F).** rBCG::iE-DAP is more susceptible to amoxicillin-clavulanate, meropenem and vancomycin.

Table A1. **List of plasmids created and/or used in this study.**

Plasmids	Description	Source/Ref
1. pMV306H	Genetic complementation vector, which integrates at the attB site in the mycobacterial genome. Hyg^R	H. Boshoff
2. pTweety	Genetic complementation vector, which integrates at the tRNA site in the mycobacterial genome. Kan^R	(270)
3. pMV306H+GFP	Derivative of pMV306H carrying a green fluorescence protein sequence (GFP). Hyg^R	CBTBR
4. pTweety+mRFP	Derivative of pTweety carrying a red fluorescence protein sequence (mRFP). Kan^R	CBTBR
5. pUAB400	*E. coli* - Mycobacterial shuttle plasmid carrying mDH fragment 3. Kan^R	(114)
6. pUAB300	*E. coli* - Mycobacterial shuttle plasmid carrying the mDHFR fragment 1 and 2, together with a glycine linker. Hyg^R	(114)
7. pUAB400+MurT	Derivative of pUAB400 carrying the wild type allele of *murT*. Kan^R	This study
8. pUAB300+GatD	Derivative of pUAB400 carrying the wild type allele of *gatD* Kan^R	This study
9. pUAB300+RipA	Derivative of pUAB300 carrying the wild type allele of *ripA*. Hyg^R	CBTBR
10. pUAB400+RpfB	Derivative of pUAB400 carrying the wild type allele of *rpfB*. Kan^R	CBTBR
11. pse100	*E. coli*-mycobacterial episomal shuttle vector containing origins of *E. coli* (pMB1) and mycobacteria (pAL500) and a multiple cloning site flanked by two transcriptional terminators. Hyg^R	(271)
12. pse100+MurT	Derivative of pse100 carrying a wildtype MurT allele	This study
13. p2NIL	*E. coli* cloning vector. Kan^R	(104)
14. pMurT-KO	Derivative of p2NIL carrying the delta-*murT* deletion allele and the *lacZ* and *sacB* genes. Kan^R	This study
15. PLR962	CRISPRi plasmid optimized for *M. smegmatis*. Kan^R	(113)
16. PLR965	CRISPRi plasmid optimized for Mtb or BCG. Kan^R	(113)
17. PLR962+MSMEG_6276 sgRNA	PLR962 derivative with a sgRNA for inhibition of MSMEG_6276 transcription. Kan^R	This study
18. PLR965+Mb_3739 sgRNA	PLR965 derivative with a sgRNA for inhibition of MSMEG_6276 transcription. Kan^R	This study
19. pMV306H+MurT-GFP	Derivative of pMV306H carrying a wildtype *murT* allele tagged with GFP. This plasmid expresses a MurT-GFP fusion protein. Hyg^R	This study
20. pTweety+mRFP-GatD	Derivative of pTweety+mRFP carrying a wildtype *gatD* allele tagged with GFP. This plasmid expresses a MurT-GFP fusion protein. Kan^R	This study
21. pFLAGEM	*E. coli*-mycobacterial episomal shuttle vector carrying the 3× FLAG epitope sequence and a Tet-operator. Hyg^R	CBTBR
22. pFLAGEM+PknB	Derivative of pFLAGEM carrying the wildtype *pknB* allele. Hyg^R	This study

Table A2. **List of strains generated with CRISPRi, target genes, PAM sequences and sgRNA targeting sequences.**

CRISPRi Strain	Gene Name	PAM Sequence	sgRNA Targeting Sequence and primers for cloning (5'-3')
1. mc^{2}155::CRISPRi-MurT-GatD	MSMEG_6276-MSMEG_6277 Operon	TGAGCAG	GAGCTGATCACGCGACAGAT Primers Fwd: GAGCTGATCACGCGACAGAT Rev: ATCTGTCGCGTGATCAGCTC
2. rBCG::iE-DAP	Mb3739-Mb3740 Operon	TGAGCAA	AGCTGGTCTCGGGAGAGGT Primers Fwd: AGCTGGTCTCGGGAGAGGT Rev: ACCTCTCCCGAGACCAGCT

Table A3. **List of bacterial strains created and/or used in this study.**

Strain	Description	Source/Ref
1. *E. coli*	*SupE44 ΔlacU169 hsdR17 recA1 endA1 gyrA96 thi-1*	Promega, Madison, WI
2. mc^{2}155	High frequency transformation mutant of *M.smegmatis* ATCC 607	ATCC
3. Mtb H37Rv (s)	Mtb wildtype parent strain	CBTBR
4. *M. bovis* BCG	*M. bovis* BCG parent strain. Strep^R	CBTBR
5. mc^{2}155::pse100+MurT	Derivative of mc^{2}155 carrying the pse100+MurT plasmid. Hyg^R	This study
6. ΔMurT::pse100+MurT	Derivative of mc^{2}155::pse100+MurT with a deletion of the wildtype MurT allele. Hyg^R	This study
7.mc^{2}155::pUAB400+MurT + pUAB300+GatD	Derivative of mc^{2}155 carrying plasmids pUAB300+GatD and pUAB400+MurT. Kan^R Hyg^R Trim^R	This study
8. mc^{2}155::RipA+RpfB	Derivative of mc^{2}155 carrying plasmids pUAB300+RipA and pUAB400+RpfB. Kan^R Hyg^R Trim^R	CBTBR
9. mc^{2}155::pUAB400 + pUAB300	Derivative of mc2155 carrying plasmids pUAB300 and pUAB400. KanR Hyg^R	CBTBR
10. *M. smegmatis* CRISPRi-MurT-GatD	Derivative of mc^{2}155 carrying the CRISPRi-MurT-GatD knockdown plasmid. Constructed by electroporation of plasmid PLR962+ MSMEG_6276sgRNA into mc^{2}155. Kan^R	This study
11. rBCG::iE-DAP	Derivative of *M. bovis* BCG carrying the CRISPRi-MurT-GatD knockdown plasmid. Constructed by electroporation of plasmid PLR965+Mb3739sgRNA into *M. bovis* BCG. Kan^R	This study
12. mc^{2}155:: MurT-GFP	Derivative of mc^{2}155 expressing a GFP tagged wild type allele of MurT at the *attB* site. Constructed by electroporation of plasmid pMV306H+MurT-GFP into mc^{2}155. Hyg^R	This study
13. mc^{2}155:: MurT-GFP+mRFP-GatD	Derivative of mc^{2}155::MurT-GFP expressing a mRFP tagged wild type allele of GatD at the *tRNA* site. Constructed by electroporation of plasmid pTweety+mRFP-GatD into mc^{2}155::MurT-GFP. Hyg^R	This study

	and Kan^R	
14. *M. smegmatis* CRISPRi-MurT-GatD+ pFLAGEM+PknB	Derivative of mc^2155::CRISPRi-MurT-GatD expressing a FLAG tagged wildtype allele of PknB episomally. Constructed by electroporation of plasmid pFLAGEM+PknB into mc^2155:: CRISPRi-MurT-GatD. Hyg^R and Kan^R	This study

Culture media contents

Luria-Bertani Agar (LA)

5g yeast extract, 10g tryptone, 10g NaCl, 1.5g agar, 1000 ml H_2O

Luria-Bertani Broth (LB)

5g yeast extract, 10g tryptone, 10g NaCl, 1000 ml H_20

Middlebrook 7H9

4.7 g Difco Middlebrook 7H9 powder, 2 ml glycerol, 900 ml H_2O, 10 ml 100× glucose-salt, 2 ml Tween80

Middlebrook 7H10

19 g Difco Middlebrook 7H10 powder, 5 ml glycerol, 900 ml H_2O, 10 ml 100× glucose-salt

100× Glucose-salt

Glucose salt 10 g glucose, 4.25 g NaCl, 500 ml H_2O

Tween80 (25 %)

10 ml Tween80 dissolved in 40 ml dH2O then sterilized by filtration

Media was sterilized by autoclaving at 121 °C for 20 min

Solutions

DNA manipulation solutions

1 M Tris-HCl

60.56 g Tris, pH 8.0 with HCl, 500 ml H_2O final volume

0.5 M EDTA 18.6 g powder, pH 8.0 with NaOH, H_2O

Solution I

50 nM glucose, 25 mM Tris-HCl, 10 mM EDTA, pH 8.0

Solution II

0.2 M NaOH, 1.0 % SDS

Solution III

5 M potassium acetate, 11.5 ml glacial acetic acid, 88.5 H_20, pH 4.8

TE buffer

1 ml 1 M Tris-HCl, 2 ml 0.5 M EDTA

TAE buffer

242 g Tris base, 100 ml 0.5 M EDTA, 57.1 ml glacial acetic acid, pH 8.0, 1000 ml final volume H_2O

Chloroform: Isoamyl alcohol

24 ml chloroform, 1 ml isoamyl alcohol

Sodium acetate

3M sodium acetate dissolved in H_2O (autoclaved)

CTAB/NaCl

4.1 % NaCl, 10 % N-cetyl-N, N, N-trimethyl ammonium bromide dissolved in H_2O (filter sterilized)

CHAPTER 5

(Summary: Conclusion, limitations and future studies)

5.1. Conclusion

The WHO declared TB a pandemic three decades ago (272). This resulted in the development of effective therapies in the form of drug regimens and development of next generation TB vaccines. However, the rapid emergence and global spread of DR-TB, with some strains being resistant to even newly developed drugs like BDQ, necessitates a deeper understanding of the physiology of Mtb to identify novel drug targets and an understanding of the interactions between Mtb and host cells, to aid the development of new vaccines. In this thesis, we use the model organism, *M. smegmatis* mc^2155 to characterize the role of the essential MurT-GatD complex in PG amidation and cross-linking; and we identify this enzyme complex as a target for development of new anti-TB drugs (Fig. 5.1). Synthetic inhibitory compounds against the *E. coli* murein peptide ligase (Mpl) which shares a similar tertiary structure with mycobacterial MurT have been developed (273). This suggests that MurT is a druggable target. We also propose that the essentiality of GatD is associated with a role in vitamin B_{12}, an essential co-factor for mycobacterial cell viability. The identified roles of both enzymes in essential cell growth pathways as shown in this work highlight the need to target such enzymes for development of new drugs against TB.

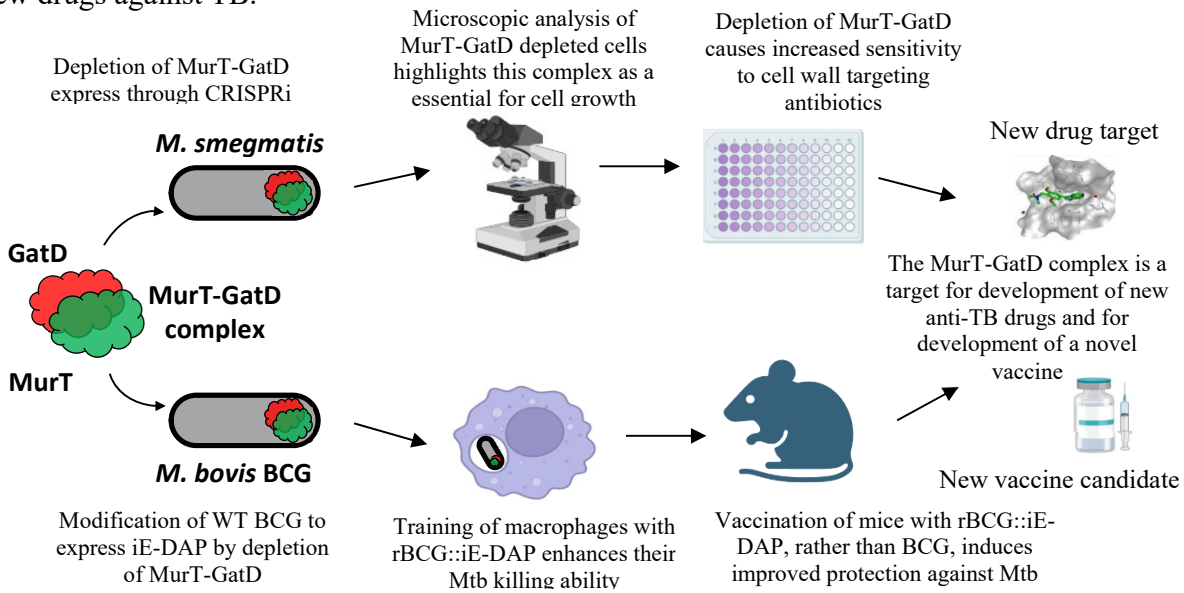

Figure 5.1. **The MurT-GatD complex is a new drug target and a target for development of a new TB vaccine.** *M. smegmatis* was used as a model to study the role of the MurT-GatD complex in mycobacterial cell wall biosynthesis. Depletion of MurT-GatD causes increased sensitivity to cell wall targeting antibiotics. *M. bovis* BCG was re-egineered with CRISPRi to reduce MurT-GatD expression causing expression of iE-DAP, a NOD-1 ligand. rBCG::iE-DAP trained macrophages and mice vaccinated with rBCG::iE-DAP control Mtb growth better than WT BCG trained macrophages and vaccinated mice.

We further identify the MurT-GatD enzyme complex as a target for development of a novel rBCG based vaccine by exploiting the role of this enzyme complex in modification of PG to evade immune signaling during infection. A CRISPRi re-engineered rBCG strain – rBCG::iE-DAP, was able to induce enhanced Mtb killing properties in an *in vitro* macrophage training experiment and also displays increased efficacy against Mtb infection in a mouse model of TB infection (Fig. 5.1). However, the essentiality of this enzyme complex necessitates the development of innovative ways to develop a marker-less and complete gene deletion whole-cell vaccine using the BCG vaccine as a platform.

5.2. Limitations

Several limitations in this work included firstly, the lack of antibodies targeting MurT or GatD which would be essential to confirm the depletion of these proteins by western blotting. Secondly, this work was limited by the lack of liquid chromatographic techniques linked to mass spectrometry to biochemically characterize the PG profile of these MurT-GatD depleted cells. However, this was resolved by the use of synthetic fluorescent PG amidation reporter probes to assay the level of amidation in the cells.

5.3. Future studies

(I) Potential future studies for this work include the design and synthesis of MurT or GatD inhibitory compounds. For example, compounds that would block the interaction of MurT and GatD would be effective at inhibiting the activity of these enzymes. This would validate the MurT-GatD as potential TB drug targets.

(II) The immune responses induced by rBCG::iE-DAP are the subject of future studies to identify the immune correlates of protection induced by this vaccine candidate. Furthermore, preclinical studies of this vaccine candidate in other animal models including guinea pigs, rabbit or macaque models of TB infection would further confirm the efficacy of this candidate.

(III) The efficacy of rBCG::iE-DAP against clinical relevant strains of Mtb would also support further development of this candidate as a future TB vaccine.

References

1. **WHO**. 2022. Global tuberculosis report 2022. https://www.who.int/publications/i/item/9789240061729.

2. **Gupta RK, Lucas SB, Fielding KL, Lawn SD**. 2015. Prevalence of tuberculosis in post-mortem studies of HIV-infected adults and children in resource-limited settings: a systematic review and meta-analysis. AIDS **29**:1987.

3. **Pai M, Kasaeva T, Swaminathan S**. 2022. Covid-19's devastating effect on tuberculosis care—a path to recovery. New England Journal of Medicine **386**:1490-1493.

4. **Pai M, Behr M, Dowdy D, Dheda K, Divangahi M, Boehme C, Raviglione M**. 2016. Tuberculosis. Nature Reviews Disease Primers, 2, 16076, p doi: 10.1038/nrdp.2016.76.

5. **Chandra P, Grigsby SJ, Philips JA**. 2022. Immune evasion and provocation by *Mycobacterium tuberculosis*. Nature Reviews Microbiology:1-17.

6. **Cohen SB, Gern BH, Delahaye JL, Adams KN, Plumlee CR, Winkler JK, Sherman DR, Gerner MY, Urdahl KB**. 2018. Alveolar macrophages provide an early Mycobacterium tuberculosis niche and initiate dissemination. Cell host microbe **24**:439-446. e4.

7. **Ravesloot-Chávez MM, Van Dis E, Stanley SA**. 2021. The innate immune response to *Mycobacterium tuberculosis* infection. Annual Review of Immunology **39**:611-637.

8. **Rothchild AC, Olson GS, Nemeth J, Amon LM, Mai D, Gold ES, Diercks AH, Aderem A**. 2019. Alveolar macrophages generate a noncanonical NRF2-driven transcriptional response to *Mycobacterium tuberculosis* in vivo. Science immunology **4**:eaaw6693.

9. **Augenstreich J, Briken V**. 2020. Host cell targets of released lipid and secreted protein effectors of *Mycobacterium tuberculosis*. Frontiers in Cellular Infection Microbiology **10**:595029.

10. **Ehlers S, Schaible UE**. 2013. The granuloma in tuberculosis: dynamics of a host–pathogen collusion. Frontiers in immunology **3**:411.

11. **Flynn JL, Chan J**. 2022. Immune cell interactions in tuberculosis. Cell **185**:4682-4702.

12. **Zumla A, Nahid P, Cole ST**. 2013. Advances in the development of new tuberculosis drugs and treatment regimens. Nature reviews Drug discovery **12**:388-404.

13. **Conradie F, Diacon AH, Ngubane N, Howell P, Everitt D, Crook AM, Mendel CM, Egizi E, Moreira J, Timm J**. 2020. Bedaquiline, pretomanid and linezolid for treatment

of extensively drug resistant, intolerant or non-responsive multidrug resistant pulmonary tuberculosis. The New England Journal of Medicine **382**:893.

14. **Ma Z, Lienhardt C, McIlleron H, Nunn AJ, Wang X**. 2010. Global tuberculosis drug development pipeline: the need and the reality. The Lancet **375**:2100-2109.

15. **Berg K**. 1949. The toxic effect of streptomycin on the eighth cranial nerve histological investigations a preliminary report. Annals of Otology, Rhinology Laryngology **58**:448-456.

16. **Martin D, Spring F, Dempsey T, Goodacre C, Seymour D**. 1948. p-Aminosalicylic acid in the treatment of tuberculosis. Nature **161**:435-435.

17. **Kerantzas CA, Jacobs Jr WR**. 2017. Origins of combination therapy for tuberculosis: lessons for future antimicrobial development and application. MBio **8**:e01586-16.

18. **Thomas J, Baughn C, Wilkinson R, Shepherd R**. 1961. A new synthetic compound with antituberculous activity in mice: Ethambutol (dextro-2, 2′-(ethylenediimino)-di-1-butanol). American Review of Respiratory Disease **83**:891-893.

19. **WHO**. 2017. Guidelines for treatment of drug-susceptible tuberculosis and patient care (2017 update). https://apps.who.int/iris/bitstream/handle/10665/255052/9789241550000-eng.pdf.

20. **Dorman SE, Nahid P, Kurbatova EV, Phillips PP, Bryant K, Dooley KE, Engle M, Goldberg SV, Phan HT, Hakim J**. 2021. Four-month rifapentine regimens with or without moxifloxacin for tuberculosis. New England Journal of Medicine **384**:1705-1718.

21. **Lange C, Dheda K, Chesov D, Mandalakas AM, Udwadia Z, Horsburgh Jr CR**. 2019. Management of drug-resistant tuberculosis. The Lancet **394**:953-966.

22. **Conradie F, Diacon AH, Ngubane N, Howell P, Everitt D, Crook AM, Mendel CM, Egizi E, Moreira J, Timm J**. 2020. Treatment of highly drug-resistant pulmonary tuberculosis. New England Journal of Medicine **382**:893-902.

23. **Thwaites G, Nahid P**. 2020. Triumph and Tragedy of 21st Century Tuberculosis Drug Development. The New England journal of medicine **382**:959-960.

24. **Jacobson KR, Tierney DB, Jeon CY, Mitnick CD, Murray MB**. 2010. Treatment outcomes among patients with extensively drug-resistant tuberculosis: systematic review and meta-analysis. Clinical infectious diseases **51**:6-14.

25. **Cerrone M, Bracchi M, Wasserman S, Pozniak A, Meintjes G, Cohen K, Wilkinson RJ**. 2020. Safety implications of combined antiretroviral and anti-tuberculosis drugs. Expert opinion on drug safety **19**:23-41.

26. **Isralls S, Baisley K, Ngam E, Grant AD, Millard J**. 2021. QT interval prolongation in people treated with bedaquiline for drug-resistant tuberculosis under programmatic conditions: a retrospective cohort study. Open forum infectious diseases **8**:ofab413.

27. **Kirby BJ, Collier AC, Kharasch ED, Whittington D, Thummel KE, Unadkat JD**. 2011. Complex drug interactions of HIV protease inhibitors 1: inactivation, induction, and inhibition of cytochrome P450 3A by ritonavir or nelfinavir. Drug metabolism disposition **39**:1070-1078.

28. **Dulberger CL, Rubin EJ, Boutte CC**. 2020. The mycobacterial cell envelope—a moving target. Nature Reviews Microbiology **18**:47-59.

29. **Abrahams KA, Besra GS**. 2018. Mycobacterial cell wall biosynthesis: a multifaceted antibiotic target. Parasitology **145**:116-133.

30. **Vilchèze C**. 2020. Mycobacterial Cell Wall: A Source of Successful Targets for Old and New Drugs. Applied Sciences **10**:2278.

31. **Shaku M, Ealand C, Kana BD**. 2020. Cell surface biosynthesis and remodeling pathways in mycobacteria reveal new drug targets. Frontiers in Cellular Infection Microbiology **10**:603382.

32. **Patel H, Karpoormath R, Palkar M**. 2020. Exploring MDR-TB inhibitory potential of 4-amino quinazolines as *Mycobacterium tuberculosis N*-acetylglucosamine-1-phosphate uridyltransferase (GlmU MTB) inhibitors. Chemistry & Biodiversity **17**:e2000237.

33. **Belete TM**. 2022. Recent progress in the development of novel mycobacterium cell wall inhibitor to combat drug-resistant tuberculosis. Microbiology Insights **15**:11786361221099878.

34. **Bensen D, Rodriguez S, Nix J, Cunningham M, Tari L**. 2012. Structure of MurA (UDP-*N*-acetylglucosamine enolpyruvyl transferase) from *Vibrio fischeri* in complex with substrate UDP-*N*-acetylglucosamine and the drug fosfomycin. Acta Crystallographica Section F: Structural Biology and Crystallization Communications **68**:382-385.

35. **Babajan B, Chaitanya M, Rajsekhar C, Gowsia D, Madhusudhana P, Naveen M, Chitta SK, Anuradha C**. 2011. Comprehensive structural and functional characterization of *mycobacterium tuberculosis* UDP-NAG enolpyruvyl transferase (Mtb-MurA) and prediction of its accurate binding affinities with inhibitors. Interdisciplinary Sciences: Computational Life Sciences **3**:204-216.

36. **Kumar P, Saumya KU, Giri R, Dynamics**. 2020. Identification of peptidomimetic compounds as potential inhibitors against MurA enzyme of *Mycobacterium tuberculosis*. Journal of Biomolecular Structure **38**:4997-5013.

37. **Rani J, Silla Y, Borah K, Ramachandran S, Bajpai U**. 2020. Repurposing of FDA-approved drugs to target MurB and MurE enzymes in *Mycobacterium tuberculosis*. Journal of Biomolecular Structure and Dynamics **38**:2521-2532. doi: .

38. **Hervin V, Arora R, Rani J, Ramchandran S, Bajpai U, Agrofoglio LA, Roy V**. 2020. Design and synthesis of various 5′-Deoxy-5′-(4-substituted-1, 2, 3-triazol-1-yl)-uridine analogues as inhibitors of *Mycobacterium tuberculosis* Mur ligases. Molecules **25**:4953.

39. **Story-Roller E, Lamichhane G**. 2018. Have we realized the full potential of β-lactams for treating drug-resistant TB? IUBMB life **70**:881-888.

40. **de Chiara C, Homšak M, Prosser GA, Douglas HL, Garza-Garcia A, Kelly G, Purkiss AG, Tate EW, de Carvalho LPS**. 2020. D-Cycloserine destruction by alanine racemase and the limit of irreversible inhibition. Nature Chemical Biology **16**:686-694.

41. **Prosser GA, de Carvalho LPS**. 2013. Reinterpreting the mechanism of inhibition of *Mycobacterium tuberculosis* D-alanine: D-alanine ligase by D-cycloserine. Biochemistry **52**:7145-7149. doi: .

42. **Gold B, Smith R, Nguyen Q, Roberts J, Ling Y, Lopez Quezada L, Somersan S, Warrier T, Little D, Pingle M**. 2016. Novel cephalosporins selectively active on nonreplicating *Mycobacterium tuberculosis*. Journal of medicinal chemistry **59**:6027-6044.

43. **Lopez Quezada LA, Smith R, Lupoli T, Edoo Z, Li X, Gold B, Roberts J, Ling Y, Park SW, Nguyen Q**. 2020. Activity-based protein profiling reveals that cephalosporins selectively active on nonreplicating *Mycobacterium tuberculosis* bind multiple protein families and spare peptidoglycan transpeptidases. Frontiers in Microbiology **11**:1248.

44. **Carette X, Platig J, Young DC, Helmel M, Young AT, Wang Z, Potluri L-P, Moody CS, Zeng J, Prisic S**. 2018. Multisystem analysis of *Mycobacterium tuberculosis* reveals kinase-dependent remodeling of the pathogen-environment interface. MBio **9(2)**:e02333-17.

45. **Kumar P, Arora K, Lloyd JR, Lee IY, Nair V, Fischer E, Boshoff HI, Barry III CE**. 2012. Meropenem inhibits D,D-carboxypeptidase activity in *M ycobacterium tuberculosis*. Molecular microbiology **86**:367-381.

46. **Chu J, Vila-Farres X, Inoyama D, Gallardo-Macias R, Jaskowski M, Satish S, Freundlich JS, Brady SF**. 2018. Human microbiome inspired antibiotics with improved β-lactam synergy against MDR *Staphylococcus aureus*. ACS infectious diseases **4**:33-38.

47. **Siricilla S, Mitachi K, Wan B, Franzblau SG, Kurosu M**. 2015. Discovery of a capuramycin analog that kills nonreplicating *Mycobacterium tuberculosis* and its synergistic effects with translocase I inhibitors. The Journal of antibiotics **68**:271-278.

48. **Huszár S, Singh, V., Polčicová, A., Baráth, P., Barrio, M.B., Lagrange, S., Leblanc, V., Nacy, C.A., Mizrahi, V. and Mikušová, K.,**. 2017. *N*-Acetylglucosamine-1-phosphate transferase, WecA, as a validated drug target in *Mycobacterium tuberculosis*. Antimicrobial agents and chemotherapy **61(11)**:e01310-17.

49. **Degiacomi G, Belardinelli JM, Pasca MR, Rossi ED, Riccardi G, Chiarelli LR**. 2020. Promiscuous targets for antitubercular drug discovery: The paradigm of DprE1 and MmpL3. Applied Sciences **10**:623.

50. **Zhang L, Zhao, Y., Gao, Y., Wu, L., Gao, R., Zhang, Q., Wang, Y., Wu, C., Wu, F., Gurcha, S.S., and Veerapen, N.,**. 2020. Structures of cell wall arabinosyltransferases with the anti-tuberculosis drug ethambutol. Science **368(6496)**:pp.1211-1219. .

51. **Senior SJ, Illarionov PA, Gurcha SS, Campbell IB, Schaeffer ML, Minnikin DE, Besra GS**. 2003. Biphenyl-based analogues of thiolactomycin, active against *Mycobacterium tuberculosis* mtFabH fatty acid condensing enzyme. Bioorganic & medicinal chemistry letters **13**:3685-3688.

52. **Faion L, Djaout K, Frita R, Pintiala C, Cantrelle F-X, Moune M, Vandeputte A, Bourbiaux K, Piveteau C, Herledan A**. 2020. Discovery of the first *Mycobacterium tuberculosis* MabA (FabG1) inhibitors through a fragment-based screening. European Journal of Medicinal Chemistry **200**:112440.

53. **Grzegorzewicz AE, Eynard N, Quémard A, North EJ, Margolis A, Lindenberger JJ, Jones V, Korduláková J, Brennan PJ, Lee RE**. 2015. Covalent modification of the *Mycobacterium tuberculosis* FAS-II dehydratase by Isoxyl and Thiacetazone. ACS infectious diseases **1**:91-97.

54. **Dessen A, Quemard A, Blanchard JS, Jacobs WR, Sacchettini JC**. 1995. Crystal structure and function of the isoniazid target of *Mycobacterium tuberculosis*. Science **267**:1638-1641.

55. **Holas O, Ondrejcek P, Dolezal M**. 2015. *Mycobacterium tuberculosis* enoyl-acyl carrier protein reductase inhibitors as potential antituberculotics: development in the past decade. Journal of enzyme inhibition and medicinal chemistry **30**:629-648.

56. **Martínez-Hoyos M, Perez-Herran E, Gulten G, Encinas L, Álvarez-Gómez D, Alvarez E, Ferrer-Bazaga S, García-Pérez A, Ortega F, Angulo-Barturen I**. 2016. Antitubercular drugs for an old target: GSK693 as a promising InhA direct inhibitor. EBioMedicine **8**:291-301. doi: .

57. **Abrahams KA, Chung C-w, Ghidelli-Disse S, Rullas J, Rebollo-López MJ, Gurcha SS, Cox JA, Mendoza A, Jiménez-Navarro E, Martínez-Martínez MS**. 2016. Identification of KasA as the cellular target of an anti-tubercular scaffold. Nature communications **7**:1-13.

58. **Veeravarapu H, Malkhed V, Mustyala KK, Vadija R, Malikanti R, Vuruputuri U, Muthyala MKK**. 2020. Structure-based drug design, synthesis and screening of MmaA1 inhibitors as novel anti-TB agents. Molecular Diversity **24**:1-16.

59. **Lehmann J, Cheng TY, Aggarwal A, Park AS, Zeiler E, Raju RM, Akopian T, Kandror O, Sacchettini JC, Moody DB**. 2018. An antibacterial β-lactone kills *Mycobacterium tuberculosis* by disrupting mycolic acid biosynthesis. Angewandte Chemie International Edition **57**:348-353.

60. **Wilson R, Kumar P, Parashar V, Vilchèze C, Veyron-Churlet R, Freundlich JS, Barnes SW, Walker JR, Szymonifka MJ, Marchiano E**. 2013. Antituberculosis thiophenes define a requirement for Pks13 in mycolic acid biosynthesis. Nature chemical biology **9**:499-506.

61. **Zhang W, Lun S, Wang S-H, Jiang X-W, Yang F, Tang J, Manson AL, Earl AM, Gunosewoyo H, Bishai WR**. 2018. Identification of novel coumestan derivatives as polyketide synthase 13 inhibitors against *Mycobacterium tuberculosis*. Journal of medicinal chemistry **61**:791-803.

62. **Cox JA, Abrahams KA, Alemparte C, Ghidelli-Disse S, Rullas J, Angulo-Barturen I, Singh A, Gurcha SS, Nataraj V, Bethell S**. 2016. THPP target assignment reveals EchA6 as an essential fatty acid shuttle in mycobacteria. Nature microbiology **1**:1-10.

63. **Dupont C, Chen Y, Xu Z, Roquet-Banères F, Blaise M, Witt A-K, Dubar F, Biot C, Guérardel Y, Maurer FP**. 2019. A piperidinol-containing molecule is active against *Mycobacterium tuberculosis* by inhibiting the mycolic acid flippase activity of MmpL3. Journal of Biological Chemistry **294**:17512-17523.

64. **Xu Z, Meshcheryakov VA, Poce G, Chng S-S**. 2017. MmpL3 is the flippase for mycolic acids in mycobacteria. Proceedings of the National Academy of Sciences **114**:7993-7998.

65. **Warrier T, Tropis M, Werngren J, Diehl A, Gengenbacher M, Schlegel B, Schade M, Oschkinat H, Daffe M, Hoffner S**. 2012. Antigen 85C inhibition restricts *Mycobacterium tuberculosis* growth through disruption of cord factor biosynthesis. Antimicrobial agents and chemotherapy **56**:1735-1743.

66. **Adewumi AT, Elrashedy A, Soremekun OS, Ajadi MB, Soliman ME**. 2022. Weak spots inhibition in the *Mycobacterium tuberculosis* antigen 85C target for antitubercular drug design through selective irreversible covalent inhibitor-SER124. Journal of biomolecular structure dynamics **40**:2934-2954.

67. **Świerzko AS, Bartłomiejczyk MA, Brzostek A, Łukasiewicz J, Michalski M, Dziadek J, Cedzyński M**. 2016. Mycobacterial antigen 85 complex (Ag85) as a target for ficolins and mannose-binding lectin. International Journal of Medical Microbiology **306**:212-221.

68. **Kremer L, Guérardel Y, Gurcha SS, Locht C, Besra GS**. 2002. Temperature-induced changes in the cell-wall components of *Mycobacterium thermoresistibile*. Microbiology **148**:3145-3154.

69. **Zhang R, Pan YT, He S, Lam M, Brayer GD, Elbein AD, Withers SG**. 2011. Mechanistic analysis of trehalose synthase from *Mycobacterium smegmatis*. Journal of Biological Chemistry **286**:35601-35609.

70. **Thanna S, Sucheck SJ**. 2016. Targeting the trehalose utilization pathways of *Mycobacterium tuberculosis*. MedChemComm **7**:69-85.

71. **Syson K, Stevenson CE, Rashid AM, Saalbach G, Tang M, Tuukkanen A, Svergun DI, Withers SG, Lawson DM, Bornemann S**. 2014. Structural insight into how *Streptomyces coelicolor* maltosyl transferase GlgE binds α-maltose 1-phosphate and forms a maltosyl-enzyme intermediate. Biochemistry **53**:2494-2504.

72. **Jankute M, Cox, J.A., Harrison, J. and Besra, G.S.,**. 2015. Assembly of the mycobacterial cell wall. nnual review of microbiology **69**:pp.405-423.

73. **Zhao X, Yu H, Yu S, Wang F, Sacchettini JC, Magliozzo RS**. 2006. Hydrogen Peroxide-mediated isoniazid activation catalyzed by *Mycobacterium tuberculosis* catalase−peroxidase (KatG) and its S315T mutant. Biochemistry **45**:4131-4140.

74. **Vannelli TA, Dykman A, de Montellano PRO**. 2002. The antituberculosis drug ethionamide is activated by a flavoprotein monooxygenase. Journal of Biological Chemistry **277**:12824-12829.

75. **Aggarwal A, Parai MK, Shetty N, Wallis D, Woolhiser L, Hastings C, Dutta NK, Galaviz S, Dhakal RC, Shrestha R**. 2017. Development of a novel lead that targets *M. tuberculosis* polyketide synthase 13. Cell **170**:249-259. e25.

76. **Alderwick LJ, Harrison, J., Lloyd, G.S. and Birch, H.L.,**. The mycobacterial cell wall—peptidoglycan and arabinogalactan. Cold Spring Harbor perspectives in medicine **5(8)**:p.a021113. doi: .

77. **Kolly GS, Mukherjee R, Kilacsková E, Abriata LA, Raccaud M, Blaško J, Sala C, Dal Peraro M, Mikušová K, Cole ST**. 2015. GtrA protein Rv3789 is required for arabinosylation of arabinogalactan in *Mycobacterium tuberculosis*. Journal of bacteriology **197**:3686-3697.

78. **Harrison J, Lloyd, G., Joe, M., Lowary, T.L., Reynolds, E., Walters-Morgan, H., Bhatt, A., Lovering, A., Besra, G.S. and Alderwick, L.J.,**. 2016. Lcp1 is a phosphotransferase responsible for ligating arabinogalactan to peptidoglycan in *Mycobacterium tuberculosis*. MBio **7(4)**:e00972-16.

79. **Raymond JB, Mahapatra S, Crick DC, Pavelka MS**. 2005. Identification of the *namH* gene, encoding the hydroxylase responsible for the *N*-glycolylation of the mycobacterial peptidoglycan. Journal of Biological Chemistry **280**:326-333. doi: .

80. **Münch D, Roemer T, Lee SH, Engeser M, Sahl HG, Schneider T**. 2012. Identification and *in vitro* analysis of the GatD/MurT enzyme-complex catalyzing lipid II amidation in *Staphylococcus aureus*. PLoS pathogens **8**:e1002509.

81. **Levefaudes M, Patin D, de Sousa-d'Auria C, Chami M, Blanot D, Hervé M, Arthur M, Houssin C, Mengin-Lecreulx D**. 2015. Diaminopimelic acid amidation in corynebacteriales: new insights into the role of LtsA in peptidoglycan modification. Journal of Biological Chemistry **290**:13079-13094.

82. **Pidgeon SE, Apostolos AJ, Nelson JM, Shaku M, Rimal B, Islam MN, Crick DC, Kim SJ, Pavelka MS, Kana BDaP, Marcos M**. 2019. L,D-Transpeptidase Specific Probe Reveals Spatial Activity of Peptidoglycan Cross-Linking. ACS chemical biology **14**:2185-2196.

83. **Baranowski C, Welsh MA, Sham L-T, Eskandarian HA, Lim HC, Kieser KJ, Wagner JC, McKinney JD, Fantner GE, Ioerger TR**. 2018. Maturing *Mycobacterium smegmatis* peptidoglycan requires non-canonical crosslinks to maintain shape. Elife **7**:e37516.

84. **Kahan FM, Kahan JS, Cassidy PJ, Kropp H**. 1974. The mechanism of action of fosfomycin (phosphonomycin). Annals of the New York Academy of Sciences **235**:364-386.

85. **De Smet KA, Kempsell KE, Gallagher A, Duncan K, Young DB**. 1999. Alteration of a single amino acid residue reverses fosfomycin resistance of recombinant MurA from *Mycobacterium tuberculosis*. Microbiology **145**:3177-3184.

86. **Kumar P, Chauhan V, Silva JRA, Lameira J, d'Andrea FB, Li S-G, Ginell SL, Freundlich JS, Alves CN, Bailey S**. 2017. *Mycobacterium abscessus* L,D-transpeptidases are susceptible to inactivation by carbapenems and cephalosporins but not penicillins. Antimicrobial agents and chemotherapy **61**:e00866-17.

87. **Bellinzoni M, Wehenkel AM, Durán R, Alzari PM**. 2019. Novel mechanistic insights into physiological signaling pathways mediated by mycobacterial Ser/Thr protein kinases. Genes & Immunity **20**:383-393.

88. **Mir M, Asong J, Li X, Cardot J, Boons G-J, Husson RN**. 2011. The extracytoplasmic domain of the *Mycobacterium tuberculosis* Ser/Thr kinase PknB binds specific muropeptides and is required for PknB localization. PLoS pathogens **7**:e1002182.

89. **Turapov O, Forti F, Kadhim B, Ghisotti D, Sassine J, Straatman-Iwanowska A, Bottrill AR, Moynihan PJ, Wallis R, Barthe P**. 2018. Two faces of CwlM, an essential PknB substrate, in *Mycobacterium tuberculosis*. Cell reports **25**:57-67. e5.

90. **Arora D, Chawla Y, Malakar B, Singh A, Nandicoori VK**. 2018. The transpeptidase PbpA and noncanonical transglycosylase RodA of *Mycobacterium tuberculosis* play important roles in regulating bacterial cell lengths. Journal of Biological Chemistry **293**:6497-6516. doi: .

91. **Kieser KJ, Boutte CC, Kester JC, Baer CE, Barczak AK, Meniche X, Chao MC, Rego EH, Sassetti CM, Fortune SM**. 2015. Phosphorylation of the peptidoglycan synthase PonA1 governs the rate of polar elongation in mycobacteria. PLoS Pathog **11**:e1005010.

92. **Kieser KJ, Rubin EJ**. 2014. How sisters grow apart: mycobacterial growth and division. Nature Reviews Microbiology **12**:550-562.

93. **Hett EC, Rubin EJ**. 2008. Bacterial growth and cell division: a mycobacterial perspective. Microbiology and Molecular Biology Reviews **72**:126-156.

94. **Machowski EE, Senzani S, Ealand C, Kana BD**. 2014. Comparative genomics for mycobacterial peptidoglycan remodelling enzymes reveals extensive genetic multiplicity. BMC microbiology **14**:75. doi: .

95. **Botella H, Vaubourgeix J, Lee MH, Song N, Xu W, Makinoshima H, Glickman MS, Ehrt S**. 2017. *Mycobacterium tuberculosis* protease MarP activates a peptidoglycan hydrolase during acid stress. The EMBO journal **36**:536-548.

96. **Senzani S, Li D, Bhaskar A, Ealand C, Chang J, Rimal B, Liu C, Kim SJ, Dhar N, Kana B**. 2017. An Amidase_3 domain-containing *N*-acetylmuramyl-L-alanine amidase is required for mycobacterial cell division. Scientific reports **7**:1-16. doi: .

97. **Wu KJ, Boutte, C.C., Ioerger, T.R. and Rubin, E.J.,** . 2019. *Mycobacterium smegmatis* HtrA blocks the toxic activity of a putative cell wall amidase. Cell reports **27(8)**:pp.2468-2479. doi: .

98. **Johnson JW, Fisher JF, Mobashery S**. 2013. Bacterial cell-wall recycling. Annals of the New York Academy of Sciences **1277**:54. doi: .

99. **Moynihan PJ, Cadby IT, Veerapen N, Jankute M, Crosatti M, Mukamolova GV, Lovering AL, Besra GS**. 2019. The hydrolase LpqI primes mycobacterial peptidoglycan recycling. Nature communications **10**:1-11. doi: .

100. **Uehara T, Park J**. 2008. Peptidoglycan Recycling. EcoSal Plus **3**.

101. **Reith J, Mayer C**. 2011. Peptidoglycan turnover and recycling in Gram-positive bacteria. Applied microbiology and biotechnology **92**:1.

102. **Ahangar MS, Furze CM, Guy CS, Cooper C, Maskew KS, Graham B, Cameron AD, Fullam E**. 2018. Structural and functional determination of homologs of the

Mycobacterium tuberculosis N-acetylglucosamine-6-phosphate deacetylase (NagA). Journal of Biological Chemistry **293**:9770-9783. doi: .

103. **Irazoki O, Hernandez S, Cava F**. 2019. Peptidoglycan muropeptides: release, perception and functions as signalling molecules. Frontiers in microbiology **10**:500.

104. **Gordhan BG, Parish T**. 2001. Gene Replacement using Pretreated DNA. Methods Mol Med **54**:77-92.

105. **Vollmer W, Blanot D, De Pedro MA**. 2008. Peptidoglycan structure and architecture. FEMS microbiology reviews **32**:149-167. doi:.

106. **Mahapatra S, Crick DC, McNeil MR, Brennan PJ**. 2008. Unique structural features of the peptidoglycan of *Mycobacterium leprae*. Journal of bacteriology **190**:655-661.

107. **Lavollay M, Arthur M, Fourgeaud M, Dubost L, Marie A, Veziris N, Blanot D, Gutmann L, Mainardi J-L**. 2008. The peptidoglycan of stationary-phase Mycobacterium tuberculosis predominantly contains cross-links generated by L, D-transpeptidation. Journal of bacteriology **190**:4360-4366.

108. **Ngadjeua F, Braud E, Saidjalolov S, Iannazzo L, Schnappinger D, Ehrt S, Hugonnet JE, Mengin-Lecreulx D, Patin D, Ethève-Quelquejeu M**. 2018. Critical Impact of Peptidoglycan Precursor Amidation on the Activity of L, D-Transpeptidases from *Enterococcus faecium* and *Mycobacterium tuberculosis*. Chemistry–A European Journal **24**:5743-5747.

109. **Liu X, Gallay C, Kjos M, Domenech A, Slager J, van Kessel SP, Knoops K, Sorg RA, Zhang JR, Veening JW**. 2017. High-throughput CRISPRi phenotyping identifies new essential genes in *Streptococcus pneumoniae*. Molecular systems biology **13**:931.

110. **Nöldeke ER, Muckenfuss LM, Niemann V, Müller A, Störk E, Zocher G, Schneider T, Stehle T**. 2018. Structural basis of cell wall peptidoglycan amidation by the GatD/MurT complex of Staphylococcus aureus. Scientific reports **8**:1-15.

111. **Morlot C, Straume D, Peters K, Hegnar OA, Simon N, Villard A-M, Contreras-Martel C, Leisico F, Breukink E, Gravier-Pelletier C**. 2018. Structure of the essential peptidoglycan amidotransferase MurT/GatD complex from *Streptococcus pneumoniae*. Nature communications **9**:1-12.

112. **Nelson JM**. 2018. Characterizing Bacterial Cell Wall Synthesis Through the Use of Fluorescent Stem Peptide Mimics.

113. **Rock JM, Hopkins FF, Chavez A, Diallo M, Chase MR, Gerrick ER, Pritchard JR, Church GM, Rubin EJ, Sassetti CM**. 2017. Programmable transcriptional repression in mycobacteria using an orthogonal CRISPR interference platform. Nature microbiology **2**:1-9.

114. **Singh A, Mai D, Kumar A, Steyn AJ**. 2006. Dissecting virulence pathways of *Mycobacterium tuberculosis* through protein–protein association. Proceedings of the National Academy of Sciences **103**:11346-11351.

115. **Hett EC, Chao MC, Steyn AJ, Fortune SM, Deng LL, Rubin EJ**. 2007. A partner for the resuscitation-promoting factors of *Mycobacterium tuberculosis*. Molecular microbiology **66**:658-668.

116. **Dhar N, Manina G**. 2015. Single-cell analysis of mycobacteria using microfluidics and time-lapse microscopy, p 241-256, Mycobacteria Protocols, vol 1285. Springer.

117. **Eskandarian HA, Odermatt PD, Ven JX, Hannebelle M, Nievergelt AP, Dhar N, McKinney JD, Fantner GE**. 2017. Division site selection linked to inherited cell surface wave troughs in mycobacteria. Nature microbiology **2**:1-6.

118. **Rodrigues L, Ramos J, Couto I, Amaral L, Viveiros M**. 2011. Ethidium bromide transport across *Mycobacterium smegmatis* cell-wall: Correlation with antibiotic resistance. BMC microbiology **11**:1-10.

119. **Maitra A, Nukala S, Dickman R, Martin LT, Munshi T, Gupta A, Shepherd AJ, Arnvig KB, Tabor AB, Keep NH**. 2021. Characterization of the MurT/GatD complex in *Mycobacterium tuberculosis* towards validating a novel anti-tubercular drug target. JAC-antimicrobial resistance **3**:dlab028.

120. **Sassetti CM, Boyd DH, Rubin EJ**. 2003. Genes required for mycobacterial growth defined by high density mutagenesis. Molecular microbiology **48**:77-84.

121. **DeJesus MA, Gerrick ER, Xu W, Park SW, Long JE, Boutte CC, Rubin EJ, Schnappinger D, Ehrt S, Fortune SM**. 2017. Comprehensive essentiality analysis of the *Mycobacterium tuberculosis* genome via saturating transposon mutagenesis. MBio **8**:e02133-16.

122. **Aldridge BB, Fernandez-Suarez M, Heller D, Ambravaneswaran V, Irimia D, Toner M, Fortune SM**. 2012. Asymmetry and aging of mycobacterial cells lead to variable growth and antibiotic susceptibility. Science **335**:100-104.

123. **Meniche X, Otten R, Siegrist MS, Baer CE, Murphy KC, Bertozzi CR, Sassetti CM**. 2014. Subpolar addition of new cell wall is directed by DivIVA in mycobacteria. Proceedings of the National Academy of Sciences **111**:E3243-E3251.

124. **Garcia-Heredia A, Pohane AA, Melzer ES, Carr CR, Fiolek TJ, Rundell SR, Lim HC, Wagner J, Morita YS, Swarts BM**. 2018. Peptidoglycan precursor synthesis along the sidewall of pole-growing mycobacteria. bioRxiv:292607.

125. **Liechti G, Kuru E, Hall E, Kalinda A, Brun Y, VanNieuwenhze M, Maurelli A**. 2014. A new metabolic cell-wall labelling method reveals peptidoglycan in *Chlamydia trachomatis*. Nature **506**:507-510.

126. **Kuru E, Radkov A, Meng X, Egan A, Alvarez L, Dowson A, Booher G, Breukink E, Roper DI, Cava F**. 2019. Mechanisms of incorporation for D-amino acid probes that target peptidoglycan biosynthesis. ACS Chemical Biology **14**:2745-2756.

127. **Pereira SF, Goss L, Dworkin J**. 2011. Eukaryote-like serine/threonine kinases and phosphatases in bacteria. Microbiology Molecular Biology Reviews **75**:192-212.

128. **Turapov O, Loraine J, Jenkins CH, Barthe P, McFeely D, Forti F, Ghisotti D, Hesek D, Lee M, Bottrill AR**. 2015. The external PASTA domain of the essential serine/threonine protein kinase PknB regulates mycobacterial growth. Open biology **5**:150025.

129. **Yeats C, Finn RD, Bateman A**. 2002. The PASTA domain: a β-lactam-binding domain. Trends in biochemical sciences **27**:438-440.

130. **Kaur P, Rausch M, Malakar B, Watson U, Damle NP, Chawla Y, Srinivasan S, Sharma K, Schneider T, Jhingan GD**. 2019. LipidII interaction with specific residues of *Mycobacterium tuberculosis* PknB extracytoplasmic domain governs its optimal activation. Nature communications **10**:1231.

131. **Gopinath K, Moosa A, Mizrahi V, Warner DF**. 2013. Vitamin B12 metabolism in Mycobacterium tuberculosis. Future microbiology **8**:1405-1418.

132. **Diacon AH, van der Merwe L, Barnard M, von Groote-Bidlingmaier F, Lange C, García-Basteiro AL, Sevene E, Ballell L, Barros-Aguirre D**. 2016. β-Lactams against Tuberculosis--New Trick for an Old Dog? The New England journal of medicine **375**:393.

133. **Hugonnet J-E, Tremblay LW, Boshoff HI, Barry CE, Blanchard JSJS**. 2009. Meropenem-clavulanate is effective against extensively drug-resistant *Mycobacterium tuberculosis*. **323**:1215-1218.

134. **Zapun A, Philippe J, Abrahams KA, Signor L, Roper DI, Breukink E, Vernet T**. 2013. In vitro reconstitution of peptidoglycan assembly from the Gram-positive pathogen *Streptococcus pneumoniae*. ACS chemical biology **8**:2688-2696.

135. **Malin JJ, de Leeuw E**. 2019. Therapeutic compounds targeting Lipid II for antibacterial purposes. Infection Drug Resistance **12**:2613.

136. **Senzani S, Li D, Bhaskar A, Ealand C, Chang J, Rimal B, Liu C, Kim SJ, Dhar N, Kana B**. 2017. An Amidase_3 domain-containing *N*-acetylmuramyl-L-alanine amidase is required for mycobacterial cell division. Scientific reports **7**:1-16.

137. **Barthe P, Mukamolova GV, Roumestand C, Cohen-Gonsaud M**. 2010. The structure of PknB extracellular PASTA domain from *Mycobacterium tuberculosis* suggests a ligand-dependent kinase activation. Structure **18**:606-615.

138. **Dhar N, Dubée V, Ballell L, Cuinet G, Hugonnet J-E, Signorino-Gelo F, Barros D, Arthur M, McKinney JD**. 2015. Rapid cytolysis of *Mycobacterium tuberculosis* by faropenem, an orally bioavailable β-lactam antibiotic. Antimicrobial agents chemotherapy **59**:1308-1319.

139. **Kipkorir T, Mashabela GT, De Wet TJ, Koch A, Dawes SS, Wiesner L, Mizrahi V, Warner DF**. 2021. De novo cobalamin biosynthesis, transport, and assimilation and cobalamin-mediated regulation of methionine biosynthesis in *Mycobacterium smegmatis*. Journal of bacteriology **203**:e00620-20.

140. **WHO**. 2021. Tuberculosis deaths rise for the first time in more than a decade due to the COVID-19 pandemic. https://www.who.int/news/item/14-10-2021-tuberculosis-deaths-rise-for-the-first-time-in-more-than-a-decade-due-to-the-covid-19-pandemic. Accessed Accessed 18 October.

141. **Kaufmann SH**. 2021. Vaccine development against tuberculosis over the last 140 years: failure as part of success. Frontiers in Microbiology:2813.

142. **Zwerling A, Behr MA, Verma A, Brewer TF, Menzies D, Pai M**. 2011. The BCG World Atlas: a database of global BCG vaccination policies and practices. PLoS medicine **8**:e1001012.

143. **Martinez L, Cords O, Liu Q, Acuna-Villaorduna C, Bonnet M, Fox GJ, Carvalho ACC, Chan P-C, Croda J, Hill PC**. 2022. Infant BCG vaccination and risk of pulmonary and extrapulmonary tuberculosis throughout the life course: a systematic review and individual participant data meta-analysis. The Lancet Global Health **10**:e1307-e1316.

144. **Andersen P, Scriba TJ**. 2019. Moving tuberculosis vaccines from theory to practice. Nature Reviews Immunology **19**:550-562.

145. **Sher A, Flynn JL**. 2021. Sterilizing immunity: New opportunities for rational TB vaccine design. The Journal of Experimental Medicine **218**.

146. **Scriba TJ, Netea MG, Ginsberg AM**. Key recent advances in TB vaccine development and understanding of protective immune responses against *Mycobacterium tuberculosis*, p 101431. *In* (ed), Elsevier,

147. **Brosch R, Gordon SV, Pym A, Eiglmeier K, Garnier T, Cole ST**. 2000. Comparative genomics of the mycobacteria. International journal of medical microbiology **290**:143-152.

148. **Brosch R, Gordon SV, Garnier T, Eiglmeier K, Frigui W, Valenti P, Dos Santos S, Duthoy S, Lacroix C, Garcia-Pelayo C**. 2007. Genome plasticity of BCG and impact on vaccine efficacy. Proceedings of the National Academy of Sciences **104**:5596-5601.

149. **Gröschel MI, Sayes F, Simeone R, Majlessi L, Brosch R**. 2016. ESX secretion systems: mycobacterial evolution to counter host immunity. Nature Reviews Microbiology **14**:677-691.

150. **Rao V, Dhar N, Tyagi A**. 2003. Modulation of host immune responses by overexpression of immunodominant antigens of *Mycobacterium tuberculosis* in bacille Calmette–Guerin. Scandinavian journal of immunology **58**:449-461.

151. **Gröschel MI, Sayes F, Shin SJ, Frigui W, Pawlik A, Orgeur M, Canetti R, Honoré N, Simeone R, van der Werf TS**. 2017. Recombinant BCG expressing ESX-1 of *Mycobacterium marinum* combines low virulence with cytosolic immune signaling and improved TB protection. Cell reports **18**:2752-2765.

152. **Heijmenberg I, Husain A, Sathkumara HD, Muruganandah V, Seifert J, Miranda-Hernandez S, Kashyap RS, Field MA, Krishnamoorthy G, Kupz A**. 2021. ESX-5-targeted export of ESAT-6 in BCG combines enhanced immunogenicity & efficacy against murine tuberculosis with low virulence and reduced persistence. Vaccine **39**:7265-7276.

153. **Marques-Neto LM, Piwowarska Z, Kanno AI, Moraes L, Trentini MM, Rodriguez D, Silva JL, Leite LC**. 2021. Thirty years of recombinant BCG: new trends for a centenary vaccine. Expert Review of Vaccines **20**:1001-1011.

154. **Bottai D, Frigui W, Clark S, Rayner E, Zelmer A, Andreu N, de Jonge MI, Bancroft GJ, Williams A, Brodin P**. 2015. Increased protective efficacy of recombinant BCG strains expressing virulence-neutral proteins of the ESX-1 secretion system. Vaccine **33**:2710-2718.

155. **Khader SA, Divangahi M, Hanekom W, Hill PC, Maeurer M, Makar KW, Mayer-Barber KD, Mhlanga MM, Nemes E, Schlesinger LS**. 2020. Targeting innate immunity for tuberculosis vaccination. The Journal of clinical investigation **129**:3482-3491.

156. **Nieuwenhuizen NE, Kulkarni PS, Shaligram U, Cotton MF, Rentsch CA, Eisele B, Grode L, Kaufmann SH**. 2017. The recombinant Bacille Calmette–Guérin vaccine VPM1002: ready for clinical efficacy testing. Frontiers in immunology **8**:1147.

157. **Pym AS, Brodin P, Majlessi L, Brosch R, Demangel C, Williams A, Griffiths KE, Marchal G, Leclerc C, Cole STJNm**. 2003. Recombinant BCG exporting ESAT-6 confers enhanced protection against tuberculosis. **9**:533-539.

158. **Pedroza-Roldán C, Marquina-Castillo B, Mata-Espinosa D, Barrios-Payán J, de Jesús Aceves-Sánchez M, Pando RH, Flores-Valdez MA**. 2018. BCG constitutively expressing the adenylyl cyclase encoded by Rv2212 increases its immunogenicity and reduces replication of *M. tuberculosis* in lungs of BALB/c mice. Tuberculosis **113**:19-25.

159. **Counoupas C, Pinto R, Nagalingam G, Britton WJ, Triccas JA**. 2018. Protective efficacy of recombinant BCG over-expressing protective, stage-specific antigens of *Mycobacterium tuberculosis*. Vaccine **36**:2619-2629.

160. **Khan A, Bakhru P, Saikolappan S, Das K, Soudani E, Singh CR, Estrella JL, Zhang D, Pasare C, Ma Y**. 2019. An autophagy-inducing and TLR-2 activating BCG vaccine induces a robust protection against tuberculosis in mice. npj Vaccines **4**:1-19.

161. **Ahn SK, Tran V, Leung A, Ng M, Li M, Liu J**. 2018. Recombinant BCG overexpressing phoP-phoR confers enhanced protection against tuberculosis. Molecular Therapy **26**:2863-2874.

162. **Reece ST, Nasser-Eddine A, Dietrich J, Stein M, Zedler U, Schommer-Leitner S, Ottenhoff TH, Andersen P, Kaufmann SH**. 2011. Improved long-term protection against *Mycobacterium tuberculosis* Beijing/W in mice after intra-dermal inoculation of recombinant BCG expressing latency associated antigens. Vaccine **29**:8740-8744.

163. **Shen H, Wang C, Yang E, Xu Y, Liu W, Yan J, Wang F, Wang H**. 2010. Novel recombinant BCG coexpressing Ag85B, ESAT-6 and mouse TNF-α induces significantly enhanced cellular immune and antibody responses in C57BL/6 mice. Microbiology immunology **54**:435-441.

164. **Gillis TP, Tullius MV, Horwitz MA**. 2014. rBCG30-induced immunity and cross-protection against *Mycobacterium leprae* challenge are enhanced by boosting with the Mycobacterium tuberculosis 30-kilodalton antigen 85B. Infection Immunity **82**:3900-3909.

165. **Tullius MV, Harth Gn, Masleša-Galić Sa, Dillon BJ, Horwitz MA**. 2008. A replication-limited recombinant *Mycobacterium bovis* BCG vaccine against tuberculosis designed for human immunodeficiency virus-positive persons is safer and more efficacious than BCG. Infection immunity **76**:5200-5214.

166. **Dai F-Y, Wang J-F, Gong X-L, Bao L**. 2017. Immunogenicity and protective efficacy of recombinant Bacille Calmette-Guerin strains expressing mycobacterium antigens Ag85A, CFP10, ESAT-6, GM-CSF and IL-12p70. Human Vaccines Immunotherapeutics **13**:1425-1432.

167. **Li G, Liu G, Song N, Kong C, Huang Q, Su H, Bi A, Luo L, Zhu L, Xu Y**. 2015. A novel recombinant BCG-expressing pro-apoptotic protein BAX enhances Th1 protective immune responses in mice. Molecular Immunology **66**:346-356.

168. **Sali M, Di Sante G, Cascioferro A, Zumbo A, Nicolo C, Dona V, Rocca S, Procoli A, Morandi M, Ria F**. 2010. Surface expression of MPT64 as a fusion with the PE domain of PE_PGRS33 enhances *Mycobacterium bovis* BCG protective activity against *Mycobacterium tuberculosis* in mice. Infection immunity **78**:5202-5213.

169. **Sun R, Skeiky YA, Izzo A, Dheenadhayalan V, Imam Z, Penn E, Stagliano K, Haddock S, Mueller S, Fulkerson J**. 2009. Novel recombinant BCG expressing perfringolysin O and the over-expression of key immunodominant antigens; pre-clinical characterization, safety and protection against challenge with *Mycobacterium tuberculosis*. Vaccine **27**:4412-4423.

170. **Carvalho Dos Santos C, Rodriguez D, Kanno Issamu A, Cezar De Cerqueira Leite L, Pereira Nascimento I**. 2020. Recombinant BCG expressing the LTAK63 adjuvant induces increased early and long-term immune responses against Mycobacteria. Human vaccines immunotherapeutics **16**:673-683.

171. **Dey RJ, Dey B, Singh AK, Praharaj M, Bishai W**. 2020. Bacillus Calmette-Guerin overexpressing an endogenous stimulator of interferon genes agonist provides enhanced protection against pulmonary tuberculosis. The Journal of infectious diseases **221**:1048-1056.

172. **Nisa A, Counoupas C, Pinto R, Britton WJ, Triccas JA**. 2022. Characterization of the Protective Immune Responses Conferred by Recombinant BCG Overexpressing Components of *Mycobacterium tuberculosis* Sec Protein Export System. Vaccines **10**:945.

173. **Xu Y, Zhu B, Wang Q, Chen J, Qie Y, Wang J, Wang H, Wang B, Wang H**. 2007. Recombinant BCG coexpressing Ag85B, ESAT-6 and mouse-IFN-γ confers effective protection against *Mycobacterium tuberculosis* in C57BL/6 mice. FEMS Immunology Medical Microbiology **51**:480-487.

174. **Festjens N, Vandewalle K, Houthuys E, Plets E, Vanderschaeghe D, Borgers K, Van Hecke A, Tiels P, Callewaert N**. 2019. SapM mutation to improve the BCG vaccine: Genomic, transcriptomic and preclinical safety characterization. Vaccine **37**:3539-3551.

175. **Khatri B, Whelan A, Clifford D, Petrera A, Sander P, Vordermeier HM**. 2014. BCG Δzmp1 vaccine induces enhanced antigen specific immune responses in cattle. Vaccine **32**:779-784.

176. **Gengenbacher M, Vogelzang A, Schuerer S, Lazar D, Kaiser P, Kaufmann SH**. 2014. Dietary Pyridoxine Controls Efficacy of Vitamin B6-Auxotrophic Tuberculosis Vaccine Bacillus Calmette-Guérin ureC:: hly pdx1 in Mice. mBio.

177. **Gengenbacher M, Nieuwenhuizen N, Vogelzang A, Liu H, Kaiser P, Schuerer S, Lazar D, Wagner I, Mollenkopf H-J, Kaufmann SH**. 2016. Deletion of nuoG from the vaccine candidate Mycobacterium bovis BCG Δ ureC:: hly improves protection against tuberculosis. MBio **7**:e00679-16.

178. **Aceves-Sánchez MdJ, Flores-Valdez MA, Pedroza-Roldán C, Creissen E, Izzo L, Silva-Angulo F, Dawson C, Izzo A, Bielefeldt-Ohmann H, Segura-Cerda CA**. 2021. Vaccination with BCGΔBCG1419c protects against pulmonary and extrapulmonary TB and is safer than BCG. Scientific Reports **11**:1-14.

179. **Mukai T, Tsukamoto Y, Maeda Y, Tamura T, Makino M**. 2014. Efficient activation of human T cells of both CD4 and CD8 subsets by urease-deficient recombinant *Mycobacterium bovis* BCG that produced a heat shock protein 70-*M. tuberculosis*-derived major membrane protein II fusion protein. Clinical Vaccine Immunology **21**:1-11.

180. **Makino M**. 2013. Development of a novel recombinant BCG for tuberculosis vaccine. Nihon Hansenbyo Gakkai Zasshi= Japanese Journal of Leprosy: Official Organ of the Japanese Leprosy Association **82**:107-110.

181. **Tsukamoto Y, Maeda Y, Tamura T, Mukai T, Mitarai S, Yamamoto S, Makino M**. 2016. Enhanced protective efficacy against tuberculosis provided by a recombinant urease deficient BCG expressing heat shock protein 70-major membrane protein-II having PEST sequence. Vaccine **34**:6301-6308.

182. **Ryan AA, Spratt JM, Britton WJ, Triccas JA**. 2007. Secretion of functional monocyte chemotactic protein 3 by recombinant *Mycobacterium bovis* BCG attenuates vaccine virulence and maintains protective efficacy against *M. tuberculosis* infection. Infection immunity **75**:523-526.

183. **Wang Y, Yang C, He Y, Zhan X, Xu L**. 2016. Ipr1 modified BCG as a novel vaccine induces stronger immunity than BCG against tuberculosis infection in mice. Molecular Medicine Reports **14**:1756-1764.

184. **Li G, Liu G, Song N, Kong C, Huang Q, Su H, Bi A, Luo L, Zhu L, Xu YJMI**. 2015. A novel recombinant BCG-expressing pro-apoptotic protein BAX enhances Th1 protective immune responses in mice. **66**:346-356.

185. **Rao M, Vogelzang A, Kaiser P, Schuerer S, Kaufmann SH, Gengenbacher M**. 2013. The tuberculosis vaccine candidate Bacillus Calmette-Guérin Δ ureC:: hly coexpressing human interleukin-7 or-18 enhances antigen-specific T cell responses in mice. PloS one **8**:e78966.

186. **Murray PJ, Aldovini A, Young RA**. 1996. Manipulation and potentiation of antimycobacterial immunity using recombinant bacille Calmette-Guerin strains that secrete cytokines. Proceedings of the National Academy of Sciences **93**:934-939.

187. **Tang C, Yamada H, Shibata K, Maeda N, Yoshida S, Wajjwalku W, Ohara N, Yamada T, Kinoshita T, Yoshikai Y**. 2008. Efficacy of recombinant bacille Calmette-Guérin vaccine secreting interleukin-15/antigen 85B fusion protein in providing protection against *Mycobacterium tuberculosis*. The Journal of infectious diseases **197**:1263-1274.

188. **Chen Y-Y, Lin C-W, Huang W-F, Chang J-R, Su I-J, Hsu C-H, Cheng H-Y, Hsu S-C, Dou H-Y**. 2017. Recombinant bacille Calmette–Guerin coexpressing Ag85b, CFP10, and interleukin-12 elicits effective protection against *Mycobacterium tuberculosis*. Journal of Microbiology, Immunology and Infection **50**:90-96.

189. **Deng Y, Bao L, Yang X**. 2011. Evaluation of immunogenicity and protective efficacy against *Mycobacterium tuberculosis* infection elicited by recombinant *Mycobacterium bovis* BCG expressing human Interleukin-12p70 and Early Secretory Antigen Target-6 fusion protein. Microbiology immunology **55**:798-808.

190. **Costa ACd, Costa-Junior AdO, Oliveira FMd, Nogueira SV, Rosa JD, Resende DP, Kipnis A, Junqueira-Kipnis AP**. 2014. A new recombinant BCG vaccine induces specific Th17 and Th1 effector cells with higher protective efficacy against tuberculosis. PLoS One **9**:e112848.

191. **Madduri BT, Allen L, Taylor SC, Besra GS, Alderwick LJ**. 2022. Enhanced immunogenicity of *Mycobacterium bovis* BCG through CRISPRi mediated depletion of AftC. The Cell Surface **8**:100088.

192. **Calmette A**. 1931. Preventive vaccination against tuberculosis with BCG. SAGE Publications.

193. **Oettinger T, Jørgensen M, Ladefoged A, Hasløv K, Andersen P**. 1999. Development of the *Mycobacterium bovis* BCG vaccine: review of the historical and biochemical evidence for a genealogical tree. Tubercle lung disease **79**:243-250.

194. **WHO**. 1954. Mass BCG vaccination campaigns: 1948-1951/reports prepared by the Tuberculosis Research Office, World Health Organization.

195. **Lugosi L, Jacobs Jr W, Bloom B**. 1989. Genetic transformation of BCG. Tubercle **70**:159-170.

196. **Stover C, De La Cruz V, Fuerst T, Burlein J, Benson L, Bennett L, Bansal G, Young J, Lee M, Hatfull G**. 1991. New use of BCG for recombinant vaccines. Nature **351**:456-460.

197. **Mahairas GG, Sabo PJ, Hickey MJ, Singh DC, Stover CK**. 1996. Molecular analysis of genetic differences between *Mycobacterium bovis* BCG and virulent *M. bovis*. Journal of bacteriology **178**:1274-1282.

198. **Kleinnijenhuis J, Quintin J, Preijers F, Joosten LA, Ifrim DC, Saeed S, Jacobs C, van Loenhout J, de Jong D, Stunnenberg HG**. 2012. Bacille Calmette-Guerin induces NOD2-dependent nonspecific protection from reinfection via epigenetic reprogramming of monocytes. Proceedings of the National Academy of Sciences **109**:17537-17542.

199. **Choudhary E, Thakur P, Pareek M, Agarwal N**. 2015. Gene silencing by CRISPR interference in mycobacteria. Nature communications **6**:1-11.

200. **Moraes L, Trentini MM, Fousteris D, Eto SF, Chudzinski-Tavassi AM, de Cerqueira Leite LC, Kanno AI**. 2022. CRISPR/Cas9 approach to generate an auxotrophic BCG strain for unmarked expression of LTAK63 adjuvant: A tuberculosis vaccine candidate. Frontiers in Immunology **13**.

201. **Pym AS, Brodin P, Majlessi L, Brosch R, Demangel C, Williams A, Griffiths KE, Marchal G, Leclerc C, Cole ST**. 2003. Recombinant BCG exporting ESAT-6 confers enhanced protection against tuberculosis. Nature medicine **9**:533-539.

202. **Dockrell HM, Butkeviciute E**. 2022. Can what have we learnt about BCG vaccination in the last 20 years help us to design a better tuberculosis vaccine? Vaccine **40**:1525-1533.

203. **Singh S, Saavedra-Avila NA, Tiwari S, Porcelli SA**. 2022. A century of BCG vaccination: Immune mechanisms, animal models, non-traditional routes and implications for COVID-19. Frontiers in immunology **13**.

204. **Rozot V, Nemes E, Geldenhuys H, Musvosvi M, Toefy A, Rantangee F, Makhethe L, Erasmus M, Bilek N, Mabwe S**. 2020. Multidimensional analyses reveal modulation of adaptive and innate immune subsets by tuberculosis vaccines. Communications biology **3**:1-12.

205. **Derrick SC, Yabe IM, Yang A, Morris SL**. 2011. Vaccine-induced anti-tuberculosis protective immunity in mice correlates with the magnitude and quality of multifunctional CD4 T cells. Vaccine **29**:2902-2909.

206. **Caruso AM, Serbina N, Klein E, Triebold K, Bloom BR, Flynn JL**. 1999. Mice deficient in CD4 T cells have only transiently diminished levels of IFN-γ, yet succumb to tuberculosis. The Journal of Immunology **162**:5407-5416.

207. **Macleod M**. 2018. Learning lessons from MVA85A, a failed booster vaccine for BCG. BMJ **360**.

208. **Nemes E, Khader SA, Swanson RV, Hanekom WA**. 2020. Targeting unconventional host components for vaccination-induced protection against TB. Frontiers in immunology:1452.

209. **Jeyanathan M, Yao Y, Afkhami S, Smaill F, Xing Z**. 2018. New tuberculosis vaccine strategies: taking aim at un-natural immunity. Trends in immunology **39**:419-433.

210. **Flynn JL, Goldstein MM, Triebold KJ, Koller B, Bloom BR**. 1992. Major histocompatibility complex class I-restricted T cells are required for resistance to *Mycobacterium tuberculosis* infection. Proceedings of the National Academy of Sciences **89**:12013-12017.

211. **Turner J, Frank AA, Orme IM**. 2002. Old mice express a transient early resistance to pulmonary tuberculosis that is mediated by CD8 T cells. Infection immunity **70**:4628-4637.

212. **Lin PL, Flynn JL**. CD8 T cells and Mycobacterium tuberculosis infection, p 239-249. *In* (ed), Springer,

213. **Basile JI, Liu R, Mou W, Gao Y, Carow B, Rottenberg ME**. 2020. Mycobacteria-specific T cells are generated in the lung during mucosal BCG immunization or infection with *Mycobacterium tuberculosis*. Frontiers in immunology **11**:566319.

214. **Yuan X, Teng X, Jing Y, Ma J, Tian M, Yu Q, Zhou L, Wang R, Wang W, Li L**. 2015. A live attenuated BCG vaccine overexpressing multistage antigens Ag85B and HspX provides superior protection against *Mycobacterium tuberculosis* infection. Applied microbiology biotechnology **99**:10587-10595.

215. **Flores-Valdez MA, Pedroza-Roldán C, Aceves-Sánchez MdJ, Peterson EJ, Baliga NS, Hernández-Pando R, Troudt J, Creissen E, Izzo L, Bielefeldt-Ohmann H**. 2018. The BCGΔBCG1419c vaccine candidate reduces lung pathology, IL-6, TNF-α, and IL-10 during chronic TB infection. Frontiers in Microbiology **9**:1281.

216. **Kaufmann SH, Cotton MF, Eisele B, Gengenbacher M, Grode L, Hesseling AC, Walzl G**. 2014. The BCG replacement vaccine VPM1002: from drawing board to clinical trial. Expert review of vaccines **13**:619-630.

217. **Ravn P, Boesen H, Pedersen BK, Andersen P**. 1997. Human T cell responses induced by vaccination with *Mycobacterium bovis* bacillus Calmette-Guérin. The Journal of Immunology **158**:1949-1955.

218. **Choi H-G, Kwon KW, Choi S, Back YW, Park H-S, Kang SM, Choi E, Shin SJ, Kim H-J**. 2020. Antigen-specific IFN-γ/IL-17-co-producing CD4+ T-cells are the determinants for protective efficacy of tuberculosis subunit vaccine. Vaccines **8**:300.

219. **Chatterjee S, Dwivedi VP, Singh Y, Siddiqui I, Sharma P, Van Kaer L, Chattopadhyay D, Das G**. 2011. Early secreted antigen ESAT-6 of *Mycobacterium tuberculosis* promotes protective T helper 17 cell responses in a toll-like receptor-2-dependent manner. PLoS pathogens **7**:e1002378.

220. **Franco AR, Peri F**. 2021. Developing new anti-tuberculosis vaccines: focus on adjuvants. Cells **10**:78.

221. **Nascimento IP, Rodriguez D, Santos CC, Amaral EP, Rofatto HK, Junqueira-Kipnis AP, Gonçalves ED, D'Império-Lima MR, Hirata MH, Silva CL**. 2017. Recombinant BCG expressing LTAK63 adjuvant induces superior protection against *Mycobacterium tuberculosis*. Scientific reports **7**:1-11.

222. **Abebe F**. 2021. Immunological basis of early clearance of *Mycobacterium tuberculosis* infection: the role of natural killer cells. Clinical Experimental Immunology **204**:32-40.

223. **Allen M, Bailey C, Cahatol I, Dodge L, Yim J, Kassissa C, Luong J, Kasko S, Pandya S, Venketaraman V**. 2015. Mechanisms of control of *Mycobacterium tuberculosis* by NK cells: role of glutathione. Frontiers in Immunology **6**:508.

224. **Kupz A, Zedler U, Stäber M, Perdomo C, Dorhoi A, Brosch R, Kaufmann SH**. 2016. ESAT-6–dependent cytosolic pattern recognition drives noncognate tuberculosis control in vivo. The Journal of clinical investigation **126**:2109-2122.

225. **Venkatasubramanian S, Cheekatla S, Paidipally P, Tripathi D, Welch E, Tvinnereim AR, Nurieva R, Vankayalapati R**. 2017. IL-21-dependent expansion of memory-like NK cells enhances protective immune responses against *Mycobacterium tuberculosis*. Mucosal immunology **10**:1031-1042.

226. **Kleinnijenhuis J, Quintin J, Preijers F, Joosten LA, Jacobs C, Xavier RJ, van der Meer JW, van Crevel R, Netea MG**. 2014. BCG-induced trained immunity in NK cells: role for non-specific protection to infection. Clinical immunology **155**:213-219.

227. **Suliman S, Geldenhuys H, Johnson JL, Hughes JE, Smit E, Murphy M, Toefy A, Lerumo L, Hopley C, Pienaar B**. 2016. Bacillus Calmette–Guerin (BCG) revaccination of adults with latent *Mycobacterium tuberculosis* infection induces long-lived BCG-reactive NK cell responses. The Journal of Immunology **197**:1100-1110.

228. **Li H, Javid B**. 2018. Antibodies and tuberculosis: finally coming of age? Nature Reviews Immunology **18**:591-596.

229. **Phuah J, Wong EA, Gideon HP, Maiello P, Coleman MT, Hendricks MR, Ruden R, Cirrincione LR, Chan J, Lin PL**. 2016. Effects of B cell depletion on early *Mycobacterium tuberculosis* infection in cynomolgus macaques. Infection immunity **84**:1301-1311.

230. **Maglione PJ, Xu J, Chan J**. 2007. B cells moderate inflammatory progression and enhance bacterial containment upon pulmonary challenge with *Mycobacterium tuberculosis*. The Journal of Immunology **178**:7222-7234.

231. **Torrado E, Fountain JJ, Robinson RT, Martino CA, Pearl JE, Rangel-Moreno J, Tighe M, Dunn R, Cooper AM**. 2013. Differential and site specific impact of B cells in the protective immune response to *Mycobacterium tuberculosis* in the mouse. PloS one **8**:e61681.

232. **Tanner R, Villarreal-Ramos B, Vordermeier HM, McShane H**. 2019. The humoral immune response to BCG vaccination. Frontiers in immunology **10**:1317.

233. **Nemes E, Geldenhuys H, Rozot V, Rutkowski KT, Ratangee F, Bilek N, Mabwe S, Makhethe L, Erasmus M, Toefy A**. 2018. Prevention of M. tuberculosis infection with H4: IC31 vaccine or BCG revaccination. New England Journal of Medicine **379**:138-149.

234. **Husain AA, Warke SR, Kalorey DR, Daginawala HF, Taori GM, Kashyap RS**. 2015. Comparative evaluation of booster efficacies of BCG, Ag85B, and Ag85B peptides based vaccines to boost BCG induced immunity in BALB/c mice: a pilot study. Clinical Experimental Vaccine Research **4**:83-87.

235. **Dijkman K, Sombroek CC, Vervenne RA, Hofman SO, Boot C, Remarque EJ, Kocken CH, Ottenhoff TH, Kondova I, Khayum MA**. 2019. Prevention of tuberculosis infection and disease by local BCG in repeatedly exposed rhesus macaques. Nature medicine **25**:255-262.

236. **Irvine EB, O'Neil A, Darrah PA, Shin S, Choudhary A, Li W, Honnen W, Mehra S, Kaushal D, Gideon HP**. 2021. Robust IgM responses following intravenous vaccination with Bacille Calmette–Guérin associate with prevention of *Mycobacterium tuberculosis* infection in macaques. Nature immunology **22**:1515-1523.

237. **Grode L, Ganoza CA, Brohm C, Weiner 3rd J, Eisele B, Kaufmann SH**. 2013. Safety and immunogenicity of the recombinant BCG vaccine VPM1002 in a phase 1 open-label randomized clinical trial. Vaccine **31**:1340-1348.

238. **Gengenbacher M, Nieuwenhuizen N, Vogelzang A, Liu H, Kaiser P, Schuerer S, Lazar D, Wagner I, Mollenkopf H, Kaufmann S**. 2016. Deletion of nuoG from the vaccine candidate *Mycobacterium bovis* BCG ΔureC:: hly improves protection against tuberculosis. mBio **7**:e00679-16.

239. **Aaby P, Roth A, Ravn H, Napirna BM, Rodrigues A, Lisse IM, Stensballe L, Diness BR, Lausch KR, Lund N**. 2011. Randomized trial of BCG vaccination at birth to low-birth-weight children: beneficial nonspecific effects in the neonatal period? Journal of Infectious Diseases **204**:245-252.

240. **Curtis N**. 2019. BCG vaccination and all-cause neonatal mortality. The Pediatric Infectious Disease Journal **38**:195-197.

241. **Verrall AJ, Schneider M, Alisjahbana B, Apriani L, van Laarhoven A, Koeken VA, van Dorp S, Diadani E, Utama F, Hannaway RF**. 2020. Early clearance of *Mycobacterium tuberculosis* is associated with increased innate immune responses. The Journal of infectious diseases **221**:1342-1350.

242. **Kaufmann E, Sanz J, Dunn JL, Khan N, Mendonça LE, Pacis A, Tzelepis F, Pernet E, Dumaine A, Grenier J-C**. 2018. BCG educates hematopoietic stem cells to generate protective innate immunity against tuberculosis. Cell **172**:176-190. e19.

243. **Mata E, Tarancon R, Guerrero C, Moreo E, Moreau F, Uranga S, Gomez AB, Marinova D, Domenech M, Gonzalez-Camacho F**. 2021. Pulmonary BCG induces lung-resident macrophage activation and confers long-term protection against tuberculosis. Science Immunology **6**:eabc2934.

244. **Pisu D, Huang L, Narang V, Theriault M, Lê-Bury G, Lee B, Lakudzala AE, Mzinza DT, Mhango DV, Mitini-Nkhoma SC**. 2021. Single cell analysis of *M. tuberculosis* phenotype and macrophage lineages in the infected lung. Journal of Experimental Medicine **218**:e20210615.

245. **Joosten SA, van Meijgaarden KE, Arend SM, Prins C, Oftung F, Korsvold GE, Kik SV, Arts RJ, van Crevel R, Netea MG**. 2018. Mycobacterial growth inhibition is associated with trained innate immunity. The Journal of clinical investigation **128**:1837-1851.

246. **Arts RJ, Moorlag SJ, Novakovic B, Li Y, Wang S-Y, Oosting M, Kumar V, Xavier RJ, Wijmenga C, Joosten LA**. 2018. BCG vaccination protects against experimental viral infection in humans through the induction of cytokines associated with trained immunity. Cell host microbe **23**:89-100. e5.

247. **Katzmarski N, Domínguez-Andrés J, Cirovic B, Renieris G, Ciarlo E, Le Roy D, Lepikhov K, Kattler K, Gasparoni G, Händler K**. 2021. Transmission of trained immunity and heterologous resistance to infections across generations. Nature Immunology **22**:1382-1390.

248. **Singhania A, Dubelko P, Kuan R, Chronister WD, Muskat K, Das J, Phillips EJ, Mallal SA, Seumois G, Vijayanand P**. 2021. CD4+ CCR6+ T cells dominate the BCG-induced transcriptional signature. EBioMedicine **74**:103746.

249. **Caruso R, Warner N, Inohara N, Núñez G**. 2014. NOD1 and NOD2: signaling, host defense, and inflammatory disease. Immunity **41**:898-908.

250. **Lee J-Y, Hwang E-H, Kim D-J, Oh S-M, Lee K-B, Shin SJ, Park J-HJI**. 2016. The role of nucleotide-binding oligomerization domain 1 during cytokine production by macrophages in response to Mycobacterium tuberculosis infection. **221**:70-75.

251. **Fritz JH, Le Bourhis L, Sellge G, Magalhaes JG, Fsihi H, Kufer TA, Collins C, Viala J, Ferrero RL, Girardin SE**. 2007. Nod1-mediated innate immune recognition of peptidoglycan contributes to the onset of adaptive immunity. Immunity **26**:445-459.

252. **Singh AK, Praharaj M, Lombardo KA, Yoshida T, Matoso A, Baras AS, Zhao L, Srikrishna G, Huang J, Prasad PJNc**. 2022. Re-engineered BCG overexpressing cyclic di-AMP augments trained immunity and exhibits improved efficacy against bladder cancer. **13**:1-16.

253. **Toda G, Yamauchi T, Kadowaki T, Ueki K**. 2021. Preparation and culture of bone marrow-derived macrophages from mice for functional analysis. STAR protocols **2**:100246.

254. **Bekkering S, Blok BA, Joosten LA, Riksen NP, van Crevel R, Netea MG**. 2016. In vitro experimental model of trained innate immunity in human primary monocytes. Clinical Vaccine Immunology **23**:926-933.

255. **Pan W, Hao S, Zheng M, Lin D, Jiang P, Zhao J, Shi H, Yang X, Li X, Yu Y**. 2020. Oat-derived β-glucans induced trained immunity through metabolic reprogramming. Inflammation **43**:1323-1336.

256. **Ernst JD**. 2018. Mechanisms of M. tuberculosis immune evasion as challenges to TB vaccine design. Cell host microbe **24**:34-42.

257. **Borgers K, Vandewalle K, Van Hecke A, Michielsen G, Plets E, van Schie L, Vanmarcke S, Schindfessel L, Festjens N, Callewaert N**. 2020. Development of a Counterselectable Transposon To Create Markerless Knockouts from an 18,432-Clone Ordered *Mycobacterium bovis Bacillus Calmette*-Guérin Mutant Resource. Msystems **5**:e00180-20.

258. **Festjens N, Vandewalle K, Houthuys E, Plets E, Vanderschaeghe D, Borgers K, Van Hecke A, Tiels P, Callewaert N**. 2019. SapM mutation to improve the BCG vaccine: Genomic, transcriptomic and preclinical safety characterization. Vaccine **37**:3539-3551.

259. **Mourits VP, Koeken VA, De Bree LCJ, Moorlag SJ, Chu WC, Xu X, Dijkstra H, Lemmers H, Joosten LA, Wang Y**. 2020. BCG-induced trained immunity in healthy individuals: the effect of plasma muramyl dipeptide concentrations. Journal of Immunology Research **2020**.

260. **Gengenbacher M, Zimmerman MD, Sarathy JP, Kaya F, Wang H, Mina M, Carter C, Hossen MA, Su H, Trujillo C**. 2020. Tissue distribution of doxycycline in animal models of tuberculosis. Antimicrobial agents chemotherapy **64**:e02479-19.

261. **Miow QH, Vallejo AF, Wang Y, Hong JM, Bai C, Teo FS, Wang AD, Loh HR, Tan TZ, Ding Y**. 2021. Doxycycline host-directed therapy in human pulmonary tuberculosis. The Journal of clinical investigation **131**.

262. **Dockrell HM, McShane H**. 2022. Tuberculosis vaccines in the era of Covid-19–what is taking us so long? EBioMedicine **79**:103993.

263. **Sander P, Clark S, Petrera A, Vilaplana C, Meuli M, Selchow P, Zelmer A, Mohanan D, Andreu N, Rayner E**. 2015. Deletion of zmp1 improves *Mycobacterium bovis* BCG-mediated protection in a guinea pig model of tuberculosis. Vaccine **33**:1353-1359.

264. **Chai Q, Yu S, Zhong Y, Lu Z, Qiu C, Yu Y, Zhang X, Zhang Y, Lei Z, Qiang L**. 2022. A bacterial phospholipid phosphatase inhibits host pyroptosis by hijacking ubiquitin. Science **378**:eabq0132.

265. **Moliva JI, Hossfeld AP, Sidiki S, Canan CH, Dwivedi V, Beamer G, Turner J, Torrelles JB**. 2019. Selective delipidation of *Mycobacterium bovis* BCG enables direct pulmonary vaccination and enhances protection against *Mycobacterium tuberculosis*. Mucosal immunology **12**:805-815.

266. **Miao L, Liu W, Qiao Q, Li X, Xu Z**. 2020. Fluorescent antibiotics for real-time tracking of pathogenic bacteria. J Pharm Anal **10**:444-451.

267. **Blok BA, Arts RJ, van Crevel R, Benn CS, Netea MG**. 2015. Trained innate immunity as underlying mechanism for the long-term, nonspecific effects of vaccines. Journal of leukocyte biology **98**:347-356.

268. **Darrah PA, Zeppa JJ, Maiello P, Hackney JA, Wadsworth MH, Hughes TK, Pokkali S, Swanson PA, Grant NL, Rodgers MA**. 2020. Prevention of tuberculosis in macaques after intravenous BCG immunization. Nature **577**:95-102.

269. **Liu YE, Darrah PA, Zeppa JJ, Kamath M, Laboune F, Doueck DC, Maiello P, Roederer M, Flynn JL, Seder RA**. 2022. Blood transcriptional correlates of BCG-induced protection against tuberculosis in rhesus macaques. BioRxiv.

270. **Pham TT, Jacobs-Sera D, Pedulla ML, Hendrix RW, Hatfull GF**. 2007. Comparative genomic analysis of mycobacteriophage Tweety: evolutionary insights and construction of compatible site-specific integration vectors for mycobacteria. Microbiol **153**:2711-2723.

271. **Guo XV, Monteleone M, Klotzsche M, Kamionka A, Hillen W, Braunstein M, Ehrt S, Schnappinger D**. 2007. Silencing essential protein secretion in *Mycobacterium smegmatis* by using tetracycline repressors. Journal of bacteriology **189**:4614-4623.

272. **Snider Jr DE, Raviglione M, Kochi A**. 1994. Global burden of tuberculosis. Tuberculosis: pathogenesis, protection,control:1-11.

273. **Hervé M, Kovač A, Cardoso C, Patin D, Brus B, Barreteau H, Mengin-Lecreulx D, Gobec S, Blanot D**. 2013. Synthetic tripeptides as alternate substrates of murein peptide ligase (Mpl). Biochimie **95**:1120-1126.

annotated-Thesis%202023%20Moagi%20Shaku_Final.docx (1).pdf

ORIGINALITY REPORT

6%	6%	5%	0%
SIMILARITY INDEX	INTERNET SOURCES	PUBLICATIONS	STUDENT PAPERS

PRIMARY SOURCES

1	core.ac.uk Internet Source	3%
2	www.ncbi.nlm.nih.gov Internet Source	2%
3	www.nature.com Internet Source	1%
4	Moagi Shaku, Christopher Ealand, Ofentse Matlhabe, Rushil Lala, Bavesh D. Kana. "Peptidoglycan biosynthesis and remodeling revisited", Elsevier BV, 2020 Publication	1%

Exclude quotes	On	Exclude matches	< 1%
Exclude bibliography	On		

UNIVERSITY OF THE WITWATERSRAND JOHANNESBURG	HUMAN RESEARCH ETHICS COMMITTEE (MEDICAL)

Office of the Deputy Vice-Chancellor (Research & Post Graduate Affairs)

TO: Mr M Shaku
School: Pathology
Department: CoE in Biomedical TB
NHLS
de Korte Street
E-mail: shakumoagi@gmail.com

CC: Supervisor: Professor B Kana <Bavesh.Kana@nhls.ac.za>
and <HREC-Medical.ResearchOffice@wits.ac.za>

FROM: Iain Burns
Human Research Ethics Committee (Medical)
Tel: 011 717 1252

E-mail: Iain.Burns@wits.ac.za

DATE: 13/02/2018

REF: *R14/49*

PROTOCOL NO: W-CBP-180213-01 *(This is your ethics application study reference number. Please quote this reference number in all correspondence relating to this study)*

PROJECT TITLE: *Peptidoglycan recycling enzymes in Mycobacterium tuberculosis as new drug targets for tuberculosis*

Please find attached the Clearance Certificate for the above project. I hope it goes well and that an article in a recognized publication comes out of it. This will reflect well on your professional standing and contribute to the Government funding of the University.

MSWorks2000/Iain0007/ClearScanWaiver.wps

UNIVERSITY OF THE
WITWATERSRAND
JOHANNESBURG

HUMAN RESEARCH ETHICS COMMITTEE (MEDICAL)

13/02/2018

Ref: W-CBP-180213-01

TO WHOM IT MAY CONCERN:

Waiver: This certifies that the following research does not require clearance from the Human Research Ethics Committee (Medical).

Investigator: Mr M Shaku
Student No. (if appropriate): 1099419

Supervisor: Professor B Kana

School: Pathology
Department: CoE in Biomedical TB
NHLS
de Korte Street

Project title: *Peptidoglycan recycling enzymes in Mycobacterium tuberculosis as new drug targets for tuberculosis*

Reason: Laboratory gene manipulation.
No human participants will be involved in the study.

Professor CB Penny
Chairperson: Human Research Ethics Committee (Medical)

Copy – HREC (Medical) Secretariat: Zanele Ndlovu and Rhulani Mkansi.

Research Office Secretariat:
Physical address: Phillip Tobias Building, 3rd Floor, Office 302, Corner York Road and Princess of Wales Terrace, Parktown, Johannesburg 2193.
Postal address: Private Bag 3, Wits 2050
Tel Nos. +27 (0)11-717-1234/2656/2700/1252
Office E-mail: HREC-Medical.ResearchOffice@wits.ac.za.
Website:http://www.wits.ac.za/research/about-our-research/ethics-and-research-integrity/

JOHNS HOPKINS
UNIVERSITY

Animal Care and Use Committee

1620 McElderry Street
Reed Hall, Room B122
Baltimore, Maryland 21205-1911
(443) 287-3738 / FAX (443) 287-3747
www.jhu.edu/animalcare

Dr. William Bishai
Department of Medicine

Dear Dr. Bishai:

On 01/22/2020, the Johns Hopkins University Animal Care and Use Committee (ACUC) approved the following research protocol for which you are the Principal Investigator. A copy of the approved protocol is attached.

Protocol Number: MO20M20

TITLE: Mouse model of tuberculosis-virulence testing by aerosol infection (replaces MO17M62)

The approval period is for three (3) years. The ACUC office will send a notice reminding you to submit the 3rd year replacement protocol. This notice will be sent out 90 days prior to the expiration date. Please use this protocol number when placing an order with Research Animal Resources (RAR) (formerly known as Animal Services). They can be contacted by calling 5-3713. Note: Approval of this protocol does not guarantee University space for housing animals.

You may request modifications to this protocol by submitting the appropriate amendment form (i.e., Change in Animal Number, Change in Personnel, or Change in Procedures) to the ACUC office for review and approval. Copies of all our forms can be found on our website www.jhu.edu/animalcare. For guidance on protocol modifications that require amendments, please refer to the reverse side of this letter. If the locations for outside housing or procedures change, please submit a Change in Location Form, also available on the website.

Sincerely,

Nancy A. Ator

Nancy A. Ator, PhD
Chair, Animal Care and Use Committee

Johns Hopkins University Animal Care and Use Committee (ACUC)

PROTOCOL FORM

Release Date: **01/24/2014, minor revision 5/20/2015, 2/28/2019**

For ACUC Use Only

☐ Original ☑ Revision

PROTOCOL #: M020M20

DATE REC'D: orig 1/2/20, rev: 1/22/20

EXPIRATION DATE: 1/22/23

☑ Logged ☑ Database

BSL: 2 3 ABSL: 2 3

New Protocol? ____ Yes X No

3rd Year Replacement of Protocol#: **MO17M62** 2/16/20

Do you currently have animals housed on this protocol? X Yes No

PROTOCOL TITLE: "Mouse model of tuberculosis-virulence testing by aerosol infection"

---

1. PRINCIPAL INVESTIGATOR (PI): Faculty member responsible for design and implementation of the research.

LAST NAME: Bishai **FIRST:** William **M. INITIAL:** R **DEGREE (S):** MD, PhD

Title: Professor **School:** Medicine **Dep't/Div:** Infectious Diseases

Campus Mail Address:

Campus: E. Baltimore **Building:** CRB2 **Room Number:** 108

Phone: 410-955-3507 **Fax:** 410-614-8173 **E-mail:** wbishai@jhmi.edu

2. PRIMARY CO-INVESTIGATOR, if applicable: Person who is delegated authority when the PI is unavailable.

LAST NAME: Lun **FIRST:** Shichun **M. INITIAL:** ____ **DEGREE (S):** PhD

Title: Res. Assoc. **School:** Medicine **Dep't/Div:** Infectious Diseases

Campus Mail Address:

Campus: E. Baltimore **Building:** CRB2 **Room Number:** 103

Phone: 410-955-7170 **Fax:** 410-614-8173 **E-mail:** slun1@jhmi.edu

3. ADMINISTRATIVE CONTACT *(to whom the ACUC office may release protocol information if requested)*

Name: Geltruda Demczuk **Phone:** 443-287-4141 **Fax:** 410-614-8173 **E-mail:** geltrouda@jhmi.edu

4a. ANIMAL REQUIREMENTS: A separate protocol form is required for each species. List rodent strains separately. See questions 13 and 17a to list numbers of animals that will be needed.

Genus/Species or Common Name	Strain and/or Stock	Sex	Source (e.g., commercial, another investigator, in-house breeding)	Indicate age and/or weight required
Mouse	Balb/C and C57BL/6	Female	Charles River	4-8 wk 18-25 grams
Mouse	Kramnik (C3H3B/FeJ)	Female	Jackson Labs	3-8 wks 18-25 gm
Mouse	B6-sst1S	Female	Bred in-house	4-8 wk 18-25 gm

4b. Number of rats or mice that might be used from the euthanasia racks per year: **0**

These are cages of animals that have been marked for euthanasia that may be used for training, practice, or tissue harvest using procedures approved in this protocol. The use of these animals must be completed the same day they are taken. Your name will be added to a list of approved users and you will be sent complete instructions if you are not already approved.

5. ANIMAL RESOURCES HOUSING: What is the range (lowest # to highest #) of the number of animals you predict to be housed and cared for in central facilities at any given time? 50-400

6. SATELLITE HOUSING: Will any animals be housed outside an Animal Resources facility for more than 12 hours if the species is covered by USDA regulations or for more than 24 hours if not? ____ **Yes** X **No**

The ACUC website, web.jhu.edu/animalcare, contains a formulary for rodent drug doses and ACUC-approved guidelines for many procedures. If you are following these, you can cite them as the method to be used instead of listing all the information in the form.

**If "Yes", complete the Satellite Housing Form (web.jhu.edu/animalcare) and submit as an attachment to this protocol.

7. **PROCEDURAL KEYWORD CHECKLIST:** *Please read each carefully and check all of the following that apply.* ***Provide requested details in the answer to question 14 unless another question number is indicated.*** (Note: This list is not meant to be exhaustive. It is possible that no items will be checked).

	Antibody production – Indicate if polyclonal or monoclonal antibodies will be produced. Tell whether ascites will be used.*
	Behavioral studies – Methods and apparatus to be used for the purpose of explaining what the animals will experience.*
X	**Breeding colony - Note**: If breeding mice, you will need to complete the "Mouse Breeding Colony Form" that is on the website.*
	Caging – Special caging requirements (e.g., wire bottom, metabolic). Give reasons.
	Dietary manipulation (i.e., testing the effects of manipulating the content of food or fluid)
	Environmental manipulation – Describe any non-standard environmental manipulation (e.g., altered light cycle, temperature and/or humidity outside normal range)
X	**Euthanize and harvest tissue ONLY—NO other procedures in this protocol, including pre-treatments.**
	Food or fluid regulation – Give durations and information on monitoring weight/hydration status, as applicable.* *Does not apply to pre-anesthetic food restriction.* See question 14f.
	Imaging (X-ray, MR, CT, PET scan, ultrasound, etc.) – Include frequency for individual animals if more than once.
X	**Infectious disease** – See question 19.
	Irradiation– Describe expected effects on animals after the procedure and duration of effects.
	Human embryonic stem cells- Must also submit application to JHU ISCRO (http://eiscro.jhu.edu)
	Non-survival surgery– Describe in 14a
	Paralyzing agents (e.g., during surgery) – Must be used in conjunction with anesthesia and must describe the methods used to determine depth of anesthesia. Also indicate that the animal will be on a ventilator.
	Restraint (other than by hand or briefly) – Indicate the method, rationale, procedures for habituation, durations, and monitoring.*
X	**Recombinant or synthetic nucleic acids, potentially infectious agents/pathogens, biological toxins or human-derived materials.** - See question 19.
	Stress - As the topic of study (e.g. cold exposure, restraint, forced exercise, uncontrollable aversive stimuli). Provide rationale and explain why this particular method is being used.
	Survival surgery - See question 15*.
	Teaching – Type of class(es) or students.
	Toxicology or study of effects of chronic drug delivery– Indicate classes or specific substances to be used; give route(s), sites, and frequencies of administration. Give expected untoward effects and their duration, if known.
	Tumors - Experimentally induced or transplanted – Indicate expected maximum size and plan for monitoring. If xenografts, identify source.*

***See guidelines at:** web.jhu.edu/animalcare

8. **LOCATIONS OF PROCEDURES TO BE PERFORMED ON LIVE ANIMALS:** If procedures will be performed in an Animal Resources facility, indicate "AR" in place of the room number.

Procedures performed on live animals:	Building(s)	Room Number(s)	Campus
Survival surgery (Major & Minor)			
Non-survival surgery or euthanize and harvest	CRB2	ABSL-2ABSL-3	E. Baltimore
Behavioral testing			
Imaging			
CO_2 Euthanasia			
Other (specify):			

In answering the questions below, please use terminology that will be understood by a non-specialist. Spell out abbreviations on first use.

9. **OBJECTIVE(S):** Briefly explain the overall purpose of the project.

To identify new drug treatments for tuberculosis. The hypothesis is that drugs which are effective against tuberculosis infection in mice may prove useful in higher mammals and potentially in humans

The ACUC website web.jhu.edu/animalcare contains a formulary for rodent drug dose and ACUC-approved guidelines for many procedures. If you are following these, you can cite them as the method to be used instead of listing all the information in the form.

10. IMPORTANCE OF RESEARCH: What is the relevance of this work for human or animal health, the advancement of knowledge, or the good of society?

The current treatment for tuberculosis involves a regimen of several drugs over a period of six months or more. Many side effects may occur or compliance is not maintained. Multdrug resistant TB is also an increasing problem worldwide and new drugs are needed to treat it more effectively.

It would be extremely beneficial to find a vaccine against TB to prevent infection and the spread of the disease. The current BCG vaccine is not very effective. Through genetic studies to identify virulence genes, it may be possible to develop such a vaccine, which would be more effective than what is currently available. In addition, the identification of virulence genes would help in developing more effective drug regimens against TB.

11. RATIONALE FOR ANIMAL USE: Why are live animals necessary for this study? *Include the reason a non-animal approach such as mathematical models or computer simulation cannot be used.*

Tissue culture models of evaluating the virulence of a recombinant M. tuberculosis strain are unreliable because they fail to mimic the full array of host cell and humoral immunity against the pathogen. Hence, there are no adequate alternatives to virulence testing to circumvent the use of animals.

12. SPECIES SELECTION: Explain why you selected this species as opposed to another.

Mice are the optimal species for drug assessment against tuberculosis because they are susceptible to infection, sustain reproducible infections, are relatively inexpensive, and are well-characterized in the literature.

13. NUMBERS OF ANIMALS AND RATIONALE: **Explain how many animals (or range of animals) are needed for each experimental condition (e.g., group size) and estimate the total number of animals for the 3 years covered by this protocol (e.g., numbers of groups or experiments). State how you determined that this number per experimental condition is appropriate (e.g., power analysis, previous studies, FDA request, etc.).** Use a table showing experimental and control groups if it aids communication. If the total number of animals will not match up with the total for question 17a, please explain.

For evaluation of virulence. *M. tuberculosis* recombinant strains will be tested in BALB/c, C57BL/6, C3HeB/FeJ (Kramnik), and B6-sst1S mice, **a total of 1560 mice per year (1200 category D, 360 category E)** are requested as explained below.

A. For colony forming unit (CFU) organ burden studies (1200 mice requested per year). We seek to test **8 putative M. tuberculosis virulence genes per year** under this protocol by CFU organ burden study.

25 mice are infected in groups of 5 animals and are sacrificed at 5 time points (2, 4, 8, 12, and 16 weeks) following infection (5 mice x 5 time-points = **25 mice**). There will be 3 bacterial strains tested for each bacterial gene to be tested for virulence: wild-type strain, mutant, and complemented mutant requiring **75 mice** per bacterial gene to be evaluated. **In my experience with mouse TB models over the years, 5 animals per group is sufficient to obtain statistical significance for organ CFU differences of 0.2 log10 units or more.**

For each putative *M. tuberculosis* virulence gene to be evaluated, 2 species of mice will be used. Therefore, a total of **150 mice** per putative bacterial virulence gene are required. Rationale for 2 mouse species: The two mouse species to be tested are: **#1** Wild type mice which form cellular granulomas (either BALB/c or C57BL/6). And **#2** mice with mutation of the sst1 gene which form necrotic granulomas (either C3HeB/FeJ [Kramnik] or B6-sst1S mice). C3HeB/FeJ (Kramnik) mice which are commercially available have the sst1S mutation in the sst1 gene as well as a number of other mutations which confer additional susceptibility to M. tb. B6-sst1S mice (which are not commercially available but which have been provided to us by Dr. Igor Kramnik) represent > 10 back-crosses with of C57BL/6 mice and C3HeB/FeJ (Kramnik) mice leading to the B6-sst1S strain which is congenic with C57BL/6 except for harboring the sst1S locus. We breed B6-sst1S mice in-house.

We anticipate that **eight** putative M. tuberculosis virulence genes will be tested per year requiring a total of **1200 mice** (8 bacterial genes to be evaluated x 150 mice = 1200 mice).

The 8 putative *M. tuberculosis* virulence gene mutants to be tested in Year 1 are listed in the Appendix after section 14a. Based on our findings in Year 1, we anticipate making complemented strains and double mutants that will require testing of an additional 8 recombinant strains in Year 2, and an additional 8 in Year 3.

B. For time-to-death studies (360 mice requested per year). We seek to test **5 putative M. tuberculosis virulence genes per year** under this protocol by time-to-death study.

For further evaluation of the role of a bacterial gene in virulence, we are requesting an additional mice for time-to-death studies. In this assay, groups of **12 mice** will be infected with a specific bacterial strain and held to determine the survival time of the infected animals. Statistically, 12 mice per group are appropriate and have been used by our lab and others extensively in the literature. A minimum of **3 bacterial strains** (wild-type, mutant, and complemented mutant) are needed to test one putative bacterial virulence gene. Therefore, we require **36 mice** for each putative bacterial virulence gene (3 strains x 12 mice per group = 36 mice). We plan on testing 5 putative bacterial virulence genes per year in wild type mice (BALB/c or C57BL/6), requiring **180 mice** (5 bacterial genes x 36 mice = 180 mice). And we plan on testing the same 5 putative bacterial virulence genes per year in mice which form necrotic granulomas (C3HeB/FeJ [Kramnik] or B6-sst1S), requiring another **180 mice**.

Thus, we are requesting a **total of 360 mice** per year for these time-to-death studies.

In the design of the proposed studies, the numbers and species of animals have been carefully considered. It is our contention that this proposal reflects the numbers and species appropriate to answer the questions posed.

14a. DESCRIBE THE PROPOSED PROCEDURES: Provide a description of all procedures to be carried out on living animals. **See prompts in question 7 for details of specific procedures to include. For survival surgeries, state which surgeries will be performed but save details of surgery and post-operative care for question 15. For non-survival surgeries, include details here. Save method of euthanasia for question 16d.** ***Further Guidance: a) Blood sampling-*** *include sites, quantities and frequencies of collection.* ***b) Pharmacological assessments*** *– include names of drugs or identify groups by chemical class and/or mechanism of action. Provide the basis on which dose ranges will be determined if specific doses are not known. Indicate possible routes of administration.* ***c)*** *Use ranges for the durations of experimental conditions and other parameters unless these are not likely to change.* ***d)*** *Think ahead to minimize the need to submit amendments later if the possibility of other procedures or modifications of parameters is likely.* **Make sure it will be clear which procedures are being done to each animal or group of animals and the likely sequence.**

Experimental Protocol

Infection Protocol
Aerosol infection: Mice will be infected by exposure to virulent *M. tuberculosis* bacilli by the aerosol route. Up to 100 mice are placed in a Glas-Col aerosol machine unit, which is housed in a special animal prep room in the ABSL-3 facility. The mice are exposed to a uniform mist containing the bacilli of interest for approximately 30 minutes. After mice are exposed to the bacilli, the infectious mist is removed through the HEPA filtered exhaust outlet, and multiple passes of fresh HEPA-filtered air are circulated through the chamber to remove un-inhaled bacteria. The mice are removed from the aerosol chamber and placed in micro-isolator cages.

Tissue Colony Forming Units Protocol
At day 1 and weeks 2, 4, 8, 12, and 16 post-infection, specified mice will be sacrificed with isoflurane **in a 1 liter beaker**. A piece of gauze is placed in a beaker and 1 ml of isoflurane is placed under the gauze and the beaker sealed with aluminum foil so that the beaker becomes saturated with the fumes. **A grate is placed over the gauze to prevent mice from coming in contact with the isoflurane. Alternatively, the isoflurane-soaked gauze will be placed into an opened 50 mL conical tube, and placed in the beaker to prevent mouse physical contact with the isoflurane.** Mice are placed in the beaker until breathing has ceased. The animal is removed, and the chest and abdomen are sterilized with 70% ethanol. The chest cavity and abdomen are opened with sterile instruments, and the lungs and spleen removed. These tissues will be homogenized in TenBroeck tissue grinders. Homogenates of the tissues will be diluted and plated on bacteriologic agar and placed in an incubator. Four weeks following plating, *M. tuberculosis* colony counts will be determined for the organs of each mouse. Confirmation of death will be the opening of the abdomen and the chest cavity and removal of vital organs.

Time to Death Study Protocol
For further evaluation of the virulence of M. tuberculosis strains, we are requesting an additional 36 mice per strain tested as described above. After infection the mice will be retained to assess the survival of mice infected with a particular recombinant bacterial strain. Statistically, 12 mice per strain are appropriate and have been used by our lab and others

for publication.

As the tuberculosis infection proceeds the animals will have weight loss, ruffled fur, hunched appearance, and other moribund signs. If the animals survive extensively in a moribund state, we will add water packs for easier access to water and broken biscuits and extra bedding to the floor of the cage. Any mice that do not develop signs of tuberculosis will be observed for up to one year.

Mouse time to death studies are a standard experimental approach to quantifying the virulence of Mycobacterium tuberculosis mutants and strains. The endpoint of the study is death. The approach has been used by many institutions including NIH and Harvard.

References:

Domenech P et al, J Bacterial, 2009, 191(2): 477-85.
Barczak AK et al, J Infect Dis, 2005, 192(4): 600-5.
Domenech P et al, Infect Immun, 2005, 73(6): 3492-501.
Domenech P et al, J Biol Chem, 2004, 279(20), 21257-65.
Chackerian AA et al, Tuberculosis, 2003, 83(5): 279-85.
Karnath AB et al, Infect Immun, 2003, 71(7): 412-8.

B. Duplication

Evaluations of the putative virulence genes to be studied have not been reported in the literature and to the best of our knowledge are not being tested in other laboratories for efficacy against tuberculosis. Hence this work is not duplicative.

Appendix:

Below is a list of the putative M. tuberculosis virulence genes we plan to test in year 1 of this protocol:

1	Rv3248c[ab]	sahH	P9WGV3	intermediary metabolism and respiration	Probable adenosylhomocysteinase SahH
2	Rv0462[abc]	lpdC	P9WHH9	intermediary metabolism and respiration	Dihydrolipoamide dehydrogenase LpdC
3	Rv3841[abc]	bfrB	P9WNE5	intermediary metabolism and respiration	Bacterioferritin BfrB
4	Rv1876[ab]	bfrA	P9WPQ9	intermediary metabolism and respiration	Probable bacterioferritin BfrA
5	Rv2467[a]	pepN	L7N655	intermediary metabolism and respiration	Probable aminopeptidase N PepN
6	RV1164[a]	narI	O06562	intermediary metabolism and respiration	Probable respiratory nitrate reductase NarI
7	Rv1293[a]	lysA	P9WIU7	intermediary metabolism and respiration	Diaminopimelate decarboxylase LysA
8	Rv0984[ac]	moaB2	O53897	intermediary metabolism and respiration	Possible pterin-4-alpha-carbinolamine dehydratase MoaB2

14b. WILL ALL DRUGS USED FOR SEDATION, ANESTHESIA, ANALGESIA OR EUTHANASIA NAMED IN THIS PROTOCOL (Questions 14a, 15, 16d) BE "PHARMACEUTICAL GRADE"? ******See "Non-pharmaceutical Grade Drug Policy" at web.jhu.edu/animalcare for full definitions of "pharmaceutical grade" and exceptions and for JHU requirements on preparation and storage.**__X___ Yes _____ No _____ Not applicable.** Formulations used for these purposes must be those sold for clinical use (i.e., "pharmaceutical grade") unless an alternative formulation is necessary due to (1) scientific considerations or (2) non-availability of the preferred compound in a clinical use formulation that can be used unaltered (e.g., without dilution). **If the answer above is "No", state below the name of any drugs for these purposes that may not be pharmaceutical grade and your reason for using the non-pharmaceutical grade version.**

14c. WILL ALL DRUGS/CHEMICALS USED AS RESEARCH TOOLS OR THE SUBJECT OF INVESTIGATION BE "PHARMACEUTICAL GRADE"? _____ Yes _____ No ___X_ Not applicable. If **"No"**, state below the name or class of the compound and the reason that non-pharmaceutical grade is necessary. **Reasons could include: (1) non-availability in a clinical use formulation or in one that could be used unaltered; or clinical use formulation is not suitable for desired mode of delivery (e.g., is a pill); (2) scientific considerations (e.g., lack of suitable vehicle control, presence of preservatives, necessity of manipulating concentration, comparability with previous studies), (3) use of drugs provided by NIH drug supply program.** ****See "Non-pharmaceutical Grade Drug Policy" at* web.jhu.edu/animalcare *for full policy and requirements for preparation and storage.****

Not applicable

14d. MULTIPLE SURVIVAL SURGERIES: If you indicated in 14a that a survival surgery (i.e., any procedure involving an incision) will occur, state whether any animal will undergo more than one survival surgery (i.e., involving separate periods of anesthesia and recovery). This includes any surgeries yet to be fully described in #15. **_____ Yes _____ No __X___ Not applicable**. If **"Yes"**, the order and the interval (or range of intervals) between them should be stated. Below, provide the scientific justification for multiple survival surgeries in the same animal. (Note: Neither cost savings alone nor reduction of the number of animals needed is considered adequate.)

Not applicable

14e. BREEDING: Will **animals** be bred at JHU under this protocol? ___X___ **Yes** _____ **No**

If **"Yes"** provide a rationale below for why breeding is needed for this protocol and for the planned number of breeders indicated in Question 17a.

If breeding **mice,** complete the **Mouse Breeding Colony Form** (web.jhu.edu/animalcare).

If breeding **species other than mice,** provide details below (i.e., projected number of offspring per year; breeding age range; weaning age; genotyping, if applicable; special care; etc.):

We seek to evaluate putative M. tuberculosis virulence genes in the B6-sst1S mouse. This strain is congenic with C57BL/6 except for a mutation in the sst1 gene. In contrast to WT mice, the sst1S mutation leads to necrotic granulomas following M. tb infection. Necrotic granulomas are a hallmark of human TB, hence the B6-sst1S mouse is a highly valuable mouse strain. **B6-sst1S mice are not commercially available.** We received them from Dr Igor Kramnik at BU in 2017 under an MTA and have had a breeding colony since then.

14f. FOOD OR FLUID REGULATION: Refers to regulation of food/fluid as a necessary component of an experimental design (*e.g., "scheduled access" where the animal is given unrestricted access to food/fluid for one or more periods of time each day or "restricted access" where amount of food/fluid per day is controlled).* This does not refer to restriction before anesthesia (i.e., pre-operative). Will food or fluid be regulated? **____ Yes __X__ No.**
If **"Yes"**, a justification and description will need to be provided below if not already included in 14a. See **"Food and Fluid Regulation"** guideline (web.jhu.edu/animalcare) for a list of the specific information you will need to include when answering this question.

15. SURVIVAL SURGERY: *(If more than one type will be performed fill out a separate question 15 for each one.)*
Name of Surgical Procedure: _____

Not applicable

15a. MAJOR OPERATIVE PROCEDURE? Will this surgery penetrate and expose a major body cavity or cause substantial impairment of physical or physiologic function? ____ Yes __X__ No

15b. Pre-anesthetic agents (e.g. sedatives to permit handling, intubation). *Name, dose, and route.*

Not applicable

The ACUC website web.jhu.edu/animalcare contains a formulary for rodent drug dose and ACUC-approved guidelines for many procedures. If you are following these, you can cite them as the method to be used instead of listing all the information in the form.

15c. Pre-emptive analgesia (i.e., analgesia given prior to the surgical procedure). *Name, dose, and route.*

Not applicable

15d. Anesthesia. *Name, dose, and route.* Also state the method that will be used to assure the animal is anesthetized prior to initial incision and during the surgical procedure.

No anesthesia will be used

15e. Will a neuromuscular blocking agent (paralytic) (i.e., one that prevents respiration) be used at any point in the procedure? ____ Yes ___X__ No If **"Yes"**, state name, dose, route and frequency of administration of paralytic agent(s). What parameter(s) will be used to determine that the animal remains anesthetized?

15f. Describe intra-operative procedures including: intubation, IV fluid delivery, monitoring, surgical procedure, method of wound closure, etc. Must be aseptic technique including assurance regarding the use of gown, gloves, mask, and sterilized instruments. Include name, dose, and route of any intra-operative analgesia, antibiotic or other drug. DO NOT REPEAT INFORMATION ALREADY PROVIDED ABOVE.

Not applicable

15g. Describe first 24 hours of post-operative care. Include frequency of monitoring, supportive care, and analgesia.

Not applicable

15h. Describe post-operative care procedures after the first 24 hours, including plan for frequency of monitoring by laboratory personnel, suture removal, further analgesia, special feeding, etc.

Not applicable

16a. PLANNED ENDPOINT/EUTHANASIA: State the timepoint or other criterion in the experiment at which euthanasia will occur for each animal or experimental group if the study goes as planned. If this has been provided in 14a, please refer reader back to that section. Save method of euthanasia for 16d.

For CFU organ burden studies, mice will be euthanized at predetermined time points prior to obtaining serum or organ specimens for bacterial counts. The method is described in 14a. Death will be verified by opening of the chest cavity and removal of lungs. In addition, any mouse developing a moribund appearance (inactivity, ruffled fur, visible weight loss) or manifesting unusual behavior will be euthanized.

For time to death studies mice will be held after infection until death occurs. The endpoint in this study is (i) death or (ii) survival greater or equal to one year (this occurs rarely with highly attenuated M.tb mutants). Control animals are those infected with wild type M. tuberculosis (usually strain H37Rv or CDC1551) and the genetically complemented mutant strain. With control infection, the animals generally die first (time to death is typically 30-70 days depending on the inoculum) because they are infected with fully virulent bacilli. The death endpoint is essential, since there would be no other way to determine the survival after infection. Animals cannot be euthanized early when they become moribund because in this study living one day longer is statistically important. As the tuberculosis infection proceeds the animals will have weight loss, ruffled fur, hunched appearance, and other moribund signs. If the animals survive extensively in a moribund state, we will add water packs for easier access to water and broken biscuits and extra bedding to the floor of the cage for all animals in the group.

16b. If euthanasia is not required by the study, or for particular animals, indicate the possible disposition of the animals (e.g., adoption, transfer to another study). Note: At the discretion of the Attending Veterinarian, animals may be adopted out without specific inclusion of that option in the protocol.

Not applicable. The endpoint will always be euthanasia in the CFU study because the animals will be infected with

M. tuberculosis and cannot be re-used in anyway. In the time-to-death study, animals surviving beyond one year will be euthanized as well because they are M.tb-infected and cannot be re-used in any way.

16c. Give the health conditions and/or criteria under which early euthanasia or withdrawal of an animal from the study will be considered. These include, but are not limited to, general signs of distress such as hunched posture, lethargy, anorexia, dehydration, rough hair coat etc. and/or those that are directly related to the experimental procedures (e.g. tumor ulceration, dislodged/unrepairable headcap, etc.).

Any mouse developing a moribund appearance (inactivity, ruffled fur, visible weight loss) or manifesting unusual behavior will be euthanized unless being held for the Time to Death studies.

16d. Which method(s) of euthanasia will be used by laboratory personnel? State how death will be verified before disposal (give two methods if euthanasia is other than decapitation). *See JHU's Euthanasia Guideline at web.jhu.edu/animalcare for suggested methods.*

Mice will be anesthetized with isoflurane. piece of gauze is placed in a beaker and 1 ml of isoflurane is placed under the gauze and the beaker sealed with aluminum foil so that the beaker becomes saturated with the fumes. Mice are placed in the beaker until breathing has ceased. Confirmation of death will be the opening of the abdomen and the chest cavity and removal of vital organs.

17a. PAIN/DISTRESS: Indicate in the table below the number of animals that will fall in each Pain/Distress category. In *addressing pain and distress, please consider all aspects of the study (e.g., surgery, phenotype of the animal, induced disease, tumor burden, behavioral procedures).* For protocols that involve more than one procedure, place animals in the category that pertains to the greatest degree of pain, distress and/or discomfort to which the animal will be exposed. *Do not count an animal more than once*. The total number of animals entered must agree with the total animals in question 13 unless the discrepancy is explained there. The total should not include the number in answer to question 4b (euthanasia rack). ***Use of anesthesia for rodent tail snips or purely for restraint (e.g., for imaging) does not require placement in Category D.***

Categories	Examples	Total Number of Animals for 3 Years (Entered into ACUC database at time of protocol approval)
B—Breeding - number of males and females to be used for breeding	e.g., breeding only, no other procedures	120
C—Procedures cause momentary, slight, or no pain/distress in absence of analgesia or anesthesia	e.g., injections, euthanasia, blood collection, brief restraint, imaging	3600 (1200 x 3)
D—Procedures potentially are painful but anesthetics and/or analgesics are given	e.g., surgery, blood collection by invasive routes	
E—Procedures involve pain/distress that will not be alleviated by drugs	e.g., toxicity studies, pain or stress studies, some disease models	1080 (360 x 3)

****** Answer 17b and c below only if any animals fall into Category D or E. ******

17b. Which procedure(s) or other elements in this protocol fit the definition of Category D and/or E as given in the chart above?

The Time to Death studies would place them in Category E. The mice are held for time to death to determine survival after infection.

17c. Are there alternative methods to those named in 17b that could be used that would produce less pain and distress and achieve the same experimental purpose? EITHER state approaches that might seem to be reasonable alternatives to the ones in 17b and explain why they will not accomplish the experimental objective with less pain/distress OR carry out a Keyword/Literature Search. DO NOT DO BOTH.

The ACUC website web.jhu.edu/animalcare contains a formulary for rodent drug dose and ACUC-approved guidelines for many procedures. If you are following these, you can cite them as the method to be used instead of listing all the information in the form.

If you choose the first approach, state the reasons you can be confident that you have relevant and up-to-date information on the topic. Reasons could include: 1) consultation with an expert in the research area (give name/qualifications), 2) regular attendance at scientific meetings (names of organizations), 3) regular attention to the scientific literature on the topic (cite sample journal names), and/or 4) personal experience with the alternative method.

Approach 1.

I am an expert in the research area of animal models of TB. I attend TB Keystone, ICAAC, ASM Microbe, and ATS meetings regularly. I review and contribute to the TB animal model literature regularly (250 co-authored papers in PubMed, ~10-12 per year), and I have personal experience with alternatives to animal model testing, namely cell-based models. Please see details below.

In short, cell-based models of TB infection are short-term: cells can only be propagated for 5-8 days post infection. The treatment of human TB takes 6 months or more, and sterilization of all tissues is a key parameter. Sterilization cannot be tested in cell-based models. A second key issue is that M. tuberculosis achieves a persister state during treatment of humans and animals. This persister state cannot be modeled in cells.

To determine the survival of mice after infection, a time to death study is done where 12 mice are held for each strain tested with the endpoint being death. There would be no other way to determine the survival after infection. Animals cannot be euthanized early when they become moribund because in this study living one day longer is statistically important. In addition we have evidence from previous studies that death in Kaplan Meier is sometimes in two bursts and that in between the mice appear moribund but don't die. Please see graph below.

At -day 38 after infection the H37Rv infected mice were very sick and appeared that they would die in a few days. However, half of those mice died at - day 125 to day 179 after infection. The whiB3 infected mice were also sick early but the last day of death was day 231. The whiB6 infected mice also appeared quite sick early like the H37Rv but the last day of death was day 363. In the table below one can see that the H37Rv mice were dying early but then recovered and some lived until day 179. Due to the appearance of these bursts in survival, it would not be reliable to euthanize the mice before the endpoint of death.

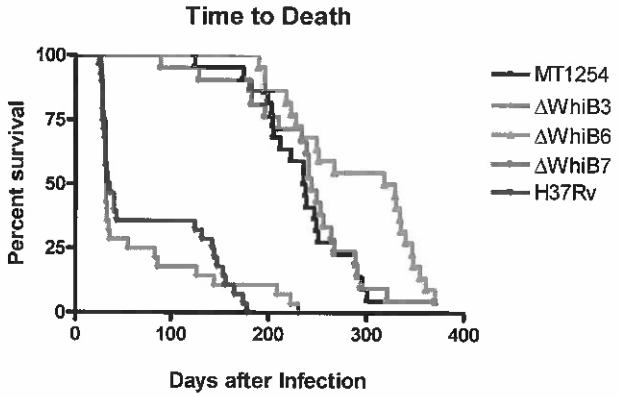

This is an accepted method in the field of tuberculosis research as shown in the numerous scientific literature sited below.

Domenech P et al, J Bacterial, 2009, 191(2): 477-85.
Lun S et al, J Biol Chem, 2007, 282(25): 18348-56.
Agarwal N et al, Infect Immun, 2007, 75(1):452-61.
Barczak AK et al, J Infect Dis, 2005, 192(4): 600-5.
Domenech P et al, Infect Immun, 2005, 73(6): 3492-501.
Domenech P et al, J Biol Chem, 2004, 279(20), 21257-65.
Chackerian AA et al, Tuberculosis, 2003, 83(5): 279-85.
Karnath AB et al, Infect Immun, 2003, 71(7): 412-8.

If you do a Keyword/Literature search provide the following information:

Date (day, month, year) search was performed: _____

Years covered by search: _____

Keywords used in search: These must be in relation to alternatives to the procedure(s) named in 17b, not in relation to use of animals.

Number of hits: _____

Databases searched (check all that apply):
____ MEDLINE /PUBMED ____ AWIC ____ TOXLINE ___ AGRICOLA ____ Other (describe)

Did the literature search reveal one or more alternatives that cause less pain/distress than the methods proposed but accomplish the same scientific purpose? ____ **Yes** ___ **No** If **"Yes"**, explain why the alternative is not being used.

18. ENVIRONMENTAL ENRICHMENT: Requests for exemption from the JHU program. See *http://web.jhu.edu/animalcare/links.html* for detailed information on the JHU Environmental Enrichment/Social Housing program for all species. *Unless an exemption is approved, the animals under this protocol will be included in the campus-wide plan for this species.*

ALL SPECIES:

a. **Most animals will be provided toys and/or other non-food enrichment items (such as nesting material for mice). Are you seeking an exemption for scientific reasons from such enrichment for any portion of the work covered in this protocol? _____ Yes __X___ No If "Yes", explain below.**

b. **Most animals (other than mice and rats) are periodically provided edible enrichment. Are you seeking an exemption for scientific reasons for any portion of the work covered in this protocol? ____Yes _____No __X___ Not Applicable. If "Yes", explain below.**

c. **Will you be providing edible or other enrichment beyond or in place of that provided by central facilities for your animals? _____ Yes __X___ No If "Yes", state how. NOTE: Nylabones and plastic cylinders and huts for rats or mice may be chosen at any time as per the JHU Enrichment Program without explicit approval in this protocol.**

d. **Most animals will be routinely housed in pairs or groups with others of their species. Are you seeking an exemption for scientific reasons from JHU's social housing plan for this species for any portion of the work covered in this protocol? _____ Yes __X__ No If "Yes", explain below.** Note: The Attending Veterinarian may exempt your animals from social housing for health or other well-being concerns even if you do not seek an exemption for scientific reasons.

DOGS:

e. **If this protocol covers dogs, are you seeking an exemption for scientific reasons from JHU's exercise program? _____ Yes _____ No __X__ Not Applicable. If** "Yes", **state reason.**

19. BIOHAZARDOUS, RADIOACTIVE, OR CHEMICALLY HAZARDOUS AGENTS USED IN ANIMALS.
Use of certain recombinant or synthetic nucleic acids, infectious or other biohazardous agents requires approval from Health, Safety & Environment's Institutional Biosafety Office/Committee (410-955-5918).

Type of Hazardous Agent	Yes	No	Name of Agent	Current Approval Date*	Biosafety Regis. # or Radiation Safety #
BIOHAZARDS:					
Recombinant or synthetic nucleic acids	X		Recombinant DNA #1 Recombinant DNA #2	3/1/2019 to 2/28/2020 1/1/2019 to 1/31/2020	DN1803090102 DN9501270425
Bacteria, parasites virus or viral-based vectors or other pathogens	X		Mycobacterium tuberculosis	8/1/2019 to 8/31/2020	**P9902170220**
Human tissues or cell lines					
RADIOACTIVE COMPOUNDS					
CHEMICALS (e.g., lead, MPTP) that render the animal's waste toxic				Not applicable	Not applicable

***If Biosafety Committee approval is pending, attach a copy of the IBC application.**

NOTE: If it is determined that an animal given the agent(s) named above has the potential to be hazardous to people (e.g., through exposure to its urine or feces), you are required to label the cage, rack, or room door with an appropriate card at the time of initial exposure and for the duration of hazardous effect. Instructions for biohazards will be included with the Approval Letter for this protocol.

20. TRAINING & QUALIFICATIONS: Provide specific information on training and/or experience that qualifies each person to perform the procedures involving the species of animal in this protocol. Make additional copies of these pages as necessary.

If any individuals listed below have not previously been included on an approved protocol at JHU they must complete the online Animal Care and Use training course (link is found on our website web.jhu.edu/animalcare or through *My Learning* (http://www.hopkinsmedicine.org/interactive_learning/my_learning/) and enroll in the Animal Exposure Surveillance Program (AESP) before the protocol can be approved (contact Occupational Health at 410-955-6211). Or the person can be removed and added after protocol approval via personnel amendment.

The AESP certificate of enrollment for these individuals must be supplied to the ACUC Office before final approval of the protocol may be granted.

Note: For protocols used only for Teaching/Training trainees do not need to be listed in question 20.

Role:	**Principal Investigator**			
Last Name:	Bishai	First Name:	William	M. Initial: R

1) *Degree(s) held. MD/PhD*

2) *Specialty and/or major for each degree listed above. Biochemistry, Pharmacology, Micro & Mol Genetics, Internal Medicine, Infectious Diseases*

3) *List procedures this person will be performing (can state "all" if appropriate). all*

4) *Describe the person's experience with the procedures and the species in this protocol. 30+ years*

5) *If training and/or supervision of this person is necessary, who will be providing it? NA*

ACUC office use: AESP __✓__ OLT __✓__ MG

Role:	**Primary Co-investigator (person delegated authority when PI is unavailable)**			
Last Name:	Lun	First Name:	Shichun	M. Initial:
Department:	Medicine	Phone Number:	410-955-7170	
JHU Address:	1550 Orleans Street	Bldg & Room:	CRB2, Room 103	
Email Address:	Slun1@jhmi.edu			

1) *Degree(s) held. PhD*

2) *Specialty and/or major for each degree listed above. Genetics and Microbiology*

3) *List procedures this person will be performing (can state "all" if appropriate). all*

4) *Describe the person's experience with the procedures and the species in this protocol. 30+ years of experience*

5) *If training and/or supervision of this person is necessary, who will be providing it? NA*

ACUC office use: AESP __✓__ OLT __✓__ MG

Role:	☐ **Co-Investigator** ☐ **Fellow** X **Student** ☐ **Faculty** ☐ **Staff** ☐ **Outside Collaborator** (Check all that apply.)			
Last Name:	Krug	First Name:	Stefanie	M. Initial:
Department:	Medicine	Phone Number:	2-8230	
JHU Address:	1550 Orleans Street	Bldg & Room:	CRB2, Room 176	

The ACUC website web.jhu.edu/animalcare contains a formulary for rodent drug dose and ACUC-approved guidelines for many procedures. If you are following these, you can cite them as the method to be used instead of listing all the information in the form.

Email Address:

1) ***Degree(s) held. BS***

2) ***Specialty and/or major for each degree listed above. Liberal Arts, Biology***

3) ***List procedures this person will be performing (can state "all" if appropriate). all***

4) ***Describe the person's experience with the procedures and the species in this protocol. Extensive experience with mouse handling and husbandry, infecting, treating and sacrificing***

5) ***If training and/or supervision of this person is necessary, who will be providing it? NA***

ACUC office use: AESP ✓ OLT ✓ JM6

Role: ☐ **Co-Investigator** X **Fellow** ☐ **Student** ☐ **Faculty** ☐ **Staff** ☐ **Outside Collaborator** (Check all that apply.)

Last Name:	Bullen	First Name:	Cynthia	M. Initial:
Department:	Medicine	Phone Number:	2-8230	
JHU Address:	1550 Orleans Street	Bldg & Room:	CRB2, Room 176	
Email Address:	cshrum1@jhmi.edu			

1) ***Degree(s) held. BA, PhD***

2) ***Specialty and/or major for each degree listed above. Biochemistry, Molecular & Cell Biology/HIV Biology***

3) ***List procedures this person will be performing (can state "all" if appropriate). all***

4) ***Describe the person's experience with the procedures and the species in this protocol. 4+ years of TB-infections with mice.***

5) ***If training and/or supervision of this person is necessary, who will be providing it? NA***

ACUC office use: AESP ✓ OLT ✓ JM6

Role: ☐ **Co-Investigator** ☐ **Fellow** X**Student** ☐ **Faculty** ☐ **Staff** ☐ **Outside Collaborator** (Check all that apply.)

Last Name:	Praharaj	First Name:	Monali	M. Initial:
Department:	Pathology	Phone Number:	2-8230	
JHU Address:	1550 Orleans St.	Bldg & Room:	CRB2, Room 176	

The ACUC website web.jhu.edu/animalcare contains a formulary for rodent drug dose and ACUC-approved guidelines for many procedures. If you are following these, you can cite them as the method to be used instead of listing all the information in the form.

Email Address: mprahar1@jhu.edu

1) *Degree(s) held. PhD*

2) *Specialty and/or major for each degree listed above. Immunology*

3) *List procedures this person will be performing (can state "all" if appropriate). all*

4) *Describe the person's experience with the procedures and the species in this protocol. Extensive experience on mouse model with 12+ years of experience on mouse handling, surgery oral gavaging etc.*

5) *If training and/or supervision of this person is necessary, who will be providing it? NA*

ACUC office use: AESP ✓ OLT ✓ VM

Role: ☐ Co-Investigator X Fellow ☐ Student ☐ Faculty ☐ Staff ☐ Outside Collaborator (Check all that apply.)

Last Name: Rohilla First Name: Akshay M. Initial:

Department: Medicine Phone Number: 2-8230

JHU Address: 1550 Orleans St. Bldg & Room: CRB2, Room 176

Email Address: arohill1@jhmi.edu

1) *Degree(s) held. PhD*

2) *Specialty and/or major for each degree listed above. Biochemistry, Tuberculosis*

3) *List procedures this person will be performing (can state "all" if appropriate). all*

4) *Describe the person's experience with the procedures and the species in this protocol. 13+ years of experience handling small animals (mice, guinea pigs) infectious samples, M. tuberculosis culturing, infection, blood drawing, performing necropsy, immunization*

5) *If training and/or supervision of this person is necessary, who will be providing it? NA*

ACUC office use: AESP ✓ OLT ✓ VM

Role: ☐ Co-Investigator X Fellow ☐ Student ☐ Faculty ☐ Staff ☐ Outside Collaborator (Check all that apply.)

The ACUC website web.jhu.edu/animalcare contains a formulary for rodent drug dose and ACUC-approved guidelines for many procedures. If you are following these, you can cite them as the method to be used instead of listing all the information in the form.

Last Name:	Singh	First Name:	Alok	M. Initial:
Department:	Medicine	Phone Number:	2-8230	
JHU Address:	1550 Orleans St.	Bldg & Room:	CRB2, Room 176	
Email Address:	Asingh51@jhmi.edu			

1) ***Degree(s) held. PhD***

2) ***Specialty and/or major for each degree listed above. Infectious Diseases, Immunology***

3) ***List procedures this person will be performing (can state "all" if appropriate). all***

4) ***Describe the person's experience with the procedures and the species in this protocol. 2+ years' experience in small animal handling, necropsy, infection***

5) ***If training and/or supervision of this person is necessary, who will be providing it? NA***

ACUC office use: AESP ✓ OLT ✓ ✓VG

Role: ☐ **Co-Investigator** X **Fellow** ☐ **Student** ☐ **Faculty** ☐ **Staff** ☐ **Outside Collaborator** (Check all that apply.)

Last Name:	Parveen	First Name:	Sadiya	M. Initial:
Department:	Medicine	Phone Number:	2-8230	
JHU Address:	1550 Orleans St.	Bldg & Room:	CRB2, Room 176	
Email Address:	sparvee2@jhmi.edu			

1) ***Degree(s) held. PhD***

2) ***Specialty and/or major for each degree listed above. Biochemistry***

3) ***List procedures this person will be performing (can state "all" if appropriate). all***

4) ***Describe the person's experience with the procedures and the species in this protocol. 12+ years experience working with mouse model of experimental tuberculosis, dissection, infection, operations, aseptic techniques, breeding, surgeries, etc.***

5) ***If training and/or supervision of this person is necessary, who will be providing it? NA***

The ACUC website web.jhu.edu/animalcare contains a formulary for rodent drug dose and ACUC-approved guidelines for many procedures. If you are following these, you can cite them as the method to be used instead of listing all the information in the form.

ACUC office use: AESP ✓ OLT ✓ AK

Role: ☐ Co-Investigator X Fellow ☐ Student ☐ Faculty ☐ Staff ☐ Outside Collaborator (Check all that apply.)

Last Name:	Kumar	First Name:	Amit	M. Initial:
Department:	Medicine	Phone Number:	2-8230	
JHU Address:	1550 Orleans St.	Bldg & Room:	CRB2, Room 176	
Email Address:	akumar60@jhmi.edu			

1) ***Degree(s) held. PhD***

2) ***Specialty and/or major for each degree listed above. Biochemistry***

3) ***List procedures this person will be performing (can state "all" if appropriate). all***

4) ***Describe the person's experience with the procedures and the species in this protocol. 12+ years experience working with mouse model of experimental tuberculosis, dissection, infection, operations, aseptic techniques, breeding, surgeries, etc.***

5) ***If training and/or supervision of this person is necessary, who will be providing it? NA***

ACUC office use: AESP ✓ OLT ✓ AK

Role: ☐ Co-Investigator ☐ Fellow ☐ Student ☐ Faculty X Staff ☐ Outside Collaborator (Check all that apply.)

Last Name:	Lisok	First Name:	Ala	M. Initial:
Department:	Medicine	Phone Number:	2-8230	
JHU Address:	1550 Orleans St.	Bldg & Room:	CRB2, Room 176	
Email Address:	Alisok1@jhmi.edu			

The ACUC website web.jhu.edu/animalcare contains a formulary for rodent drug dose and ACUC-approved guidelines for many procedures. If you are following these, you can cite them as the method to be used instead of listing all the information in the form.

1) *Degree(s) held. BA*

2) *Specialty and/or major for each degree listed above. Liberal arts*

3) *List procedures this person will be performing (can state "all" if appropriate). all*

4) *Describe the person's experience with the procedures and the species in this protocol. 15+ years experience working with mouse models including dissection, infection, operations, aseptic techniques, breeding, surgeries, etc.*

5) *If training and/or supervision of this person is necessary, who will be providing it? Will receive TB-specific training from Dr. Lun and Ms Krug.*

ACUC office use: AESP √ OLT √ MG

21. ASSURANCES: Signature verifies that you accept these responsibilities.

a) I assume responsibility for compliance with Johns Hopkins University, United States Department of Agriculture and/or Public Health Service requirements, as applicable, for work carried out under this protocol.

b) I assume responsibility for providing each member of the laboratory who will perform procedures under this protocol with a final version of the approved protocol and require that they follow the procedures described.

c) I assure that all individuals carrying out procedures described in this protocol will be experienced or trained appropriately in the procedures each will perform.

d) I understand that amendments for significant changes, as defined in the JHU ACUC Guidelines, must be approved by the JHU ACUC prior to their implementation. Exceptions may be authorized for clinical reasons on a one-time basis by a Research Animal Resources (RAR) veterinarian.

e) I certify that I have determined that the research to be conducted under this protocol is not unnecessarily duplicative of previously reported research.

f) I understand that no work can begin unless I have received approval from the Animal Care and Use Committee.

Principal Investigator's Signature: William Rice **Date:** 31-Dec-2019

IACUC Chair's Signature: Nancy A. Afton **Date:** 1/22/20

Please submit to the JHU ACUC office (please do not staple):
Reed Hall B122, East Baltimore Campus
If you prefer to fax, please use only the last five numbers if dialing within Hopkins (7-3747). Use the entire number only if faxing from outside of Hopkins (443-287-3747).

To email send to: acuc@jhmi.edu

If you fax the protocol and choose also to mail the original, please put a cover sheet on the original indicating that the protocol previously was faxed so that it is not logged in as a new submission.
Thank you.

The ACUC website web.jhu.edu/animalcare contains a formulary for rodent drug dose and ACUC-approved guidelines for many procedures. If you are following these, you can cite them as the method to be used instead of listing all the information in the form.

Johns Hopkins University Animal Care and Use Committee

MOUSE BREEDING COLONY FORM

Release Date: 5/12, revised 11/12, 3/14, 8/17

For ACUC office use only	
3rd Year Renewal:	M020 M20
Date Received:	1/2/20
Compliance approval:	GD
☑ Logged	☑ Database

Protocol Number
(if 3rd year renewal): MO17M62

Protocol Title: "Mouse model of tuberculosis-virulence testing by aerosol infection"

Principal Investigator: William Bishai

Office Phone: 410-955-3507 Fax: 410-614-8173 E-mail: wbishai@jhmi.edu

The purpose of this form is to identify investigator mouse production plans.

- ***It does not guarantee additional cage space.***
- ***For help filling out this form, contact the ACUC Office at 443-287-3738***

Guidance

- ***See the Mouse Breeding Guidelines at the ACUC website, www.jhu.edu/animalcare***
- ***Attend the monthly Mouse Breeding Seminar, the schedule is available at the ACUC website (Optional)***

1. Strain and/or Stock and Estimated Numbers for Three Years or Remainder of the Protocol Approval Period: *(fill in the table; expand the table for multiple strains/stocks)*

Strain and/or stock	Estimated # male breeders	Estimated # female breeders	Estimated # of offspring born: # of pups not litters	Estimated # or % of offspring to be used
B6-sst1S	**20**	**20**	**100**	**50%**

2. Indicate what will be done with Retired Breeders and Excess Offspring: *(check all that apply)*

Do not leave dependent pups marked for euthanasia without a lactating dam.

a. **Euthanasia**
   _X___ Euthanized as described in question 16 of the parent protocol
   ____ Marked to be euthanized by Animal Resources using the Technical Request for Euthanasia Form
   ____ Other: ***(describe)***

b. **Provide animals to another protocol.** ***(This requires submission of the RAR Animal Transfer Request Form)***
   ____ Mice will be bred with the purpose of providing mice to other protocol(s)
   ____ Excess mice due to good production or unneeded genotypes may be given to other PIs as available.

3. Breeding Plan(s): What is the age range during which the animals will be bred? __2 to 8 months of age____

Breeding schemes should include only one male unless option # 8 in question 3b. is selected and includes a justification.

a. **BREEDING SCHEME: (*check all that apply*)**
   _X___ Monogamous (one male and one female per cage)
   ____ Trio (one male and two females per cage)*
   ____ Polygamous (one male and more than two more females per cage)*

   *In question 3b. indicate how the cage population will be managed if there could be 2 litters in one cage. Options 3., 6., and 7. address this.

b. **BREEDING MANAGEMENT - to prevent overcrowding or welfare concerns:** ***(check all that apply)*** **See the Overcrowded Cage Policy at the ACUC website, *www.jhu.edu/animalcare***

1. _X__ Females pregnant from postpartum estrus will have their weanling age pups weaned concurrent with the delivery of the next litter
2. _X__ Males will be removed from the cage once females are confirmed pregnant
3. _X__ Pregnant females will be moved to their own cages prior to parturition
4. ___ Males will be rotated through the females cages
5. ___ Females will not be bred again until their offspring are weaned
6. ___ When 2 females, each with a litter are in 1 cage, one female & litter will be moved to her own cage
7. ___ Offspring will be used before weaning
8. ___ Other breeding cage management options, include special conditions due to atypical breeding/offspring production: ***(describe)***

4. IDENTIFICATION: *(check all that apply)*

____ Some or all offspring will be individually identified _X___ Individual identification is not necessary
____ Ear punch ____ Ear tag ____ Toe tattoo ____ Other***(describe)***

Toe clip ____ ***(provide justification)***
Toe-clipping should be used only when no other identification method is feasible. It may be an acceptable method for neonatal mice up to 7 days of age if the identification and genotyping can be combined. For additional requirements, see the ACUC *Toe Clipping Policy* on the ACUC website.

5. GENOTYPING (*recommended* before weaning): *(check all methods that may be used)*

____ Genotyping will be performed for some or all __X__ Genotyping is not necessary

Tissue will be obtained from the following source: ____ **Tail*** ____ **Ear** ____ **Other:** ***(describe)***

*Will the amount of tail tissue exceed 5 mm? ____ **Yes** ____ **No**
If "Yes", ***(indicate amount needed and provide justification)***

*Bleeding will be stopped by: __ **Pressure** __**Cauterization** __**Styptic powder** __ **Other:** ***(describe)***

*When the tail tissue is collected, could animals be greater than 21 days old? ___ **Yes** ___ **No**
If "Yes", even occasionally, the mice must be anesthetized or receive topical analgesic.
(list the anesthesia or analgesia that will be used)

This does not require placement in Pain Category D. See the JHU Guidelines for Tail Biopsy at the ACUC website, ***www.jhu.edu/animalcare***

6. WEANING SCHEDULE: *(check all that apply)*

Litters of females that are pregnant due to post-partum estrus *must* be weaned at 21 days of age unless option #8 "Other breeding cage management" is described in section 3b of this form.

_X__ 21 days of age
___ >21 – 28 days of age
___ >28 days of age: ***(justify delayed weaning and maximum age)***

7. SPECIAL HUSBANDRY REQUIREMENTS:

__X_ Special care is not required
___ Special care is required for some or all: ***(describe: e.g., food on floor, alternate water source etc.)***

8. CONSIDERATION OF PHENOTYPE:

If using genetically engineered animals, might the phenotype result in a change in appearance or a functional deficit? ____ **Yes** __X__ **No** ____ **Unknown**

If **"Yes"**, ***(describe)***

If **"Unknown"**, ***(describe plan for monitoring animals to detect possible impairments)***

William Rice

31-Dec-2019

PI Signature: _____ Date: _____

ACUC Chair Signature: Nancy A. Aker Date: 1/22/20